MULTI-RATE OBSERVERS FOR MODEL-BASED PROCESS MONITORING

A Dissertation

by

CHEN LING

Submitted to the Office of Graduate and Professional Studies of
Texas A&M University
in partial fulfillment of the requirements for the degree of

DOCTOR OF PHILOSOPHY

Chair of Committee,	Costas Kravaris
Committee Members,	M. Nazmul Karim
	Yossef A. Elabd
	Suman Chakravorty
Head of Department,	M. Nazmul Karim

May 2019

Major Subject: Chemical Engineering

ABSTRACT

Very often, critical quantities related to safety, product quality and economic performance of a chemical process cannot be measured on line. In an attempt to overcome the challenges caused by inadequate on-line measurements, state estimation provides an alternative approach to reconstruct the unmeasured state variables by utilizing available on-line measurements and a process model. Chemical processes usually possess strong nonlinearities, and involve different types of measurements. It remains a challenging task to incorporate multiple measurements with different sampling rates and different measurement delays into a unified estimation algorithmic framework.

This dissertation seeks to present developments in the field of state estimation by providing the theoretical advances in multi-rate multi-delay observer design. A delay-free multi-rate observer is first designed in linear systems under asynchronous sampling. Sufficient and explicit conditions in terms of maximum sampling period are derived to guarantee exponential stability of the observer, using Lyapunov's second method. A dead time compensation approach is developed to compensate for the effect of measurement delay. Based on the multi-rate formulation, optimal multi-rate observer design is studied in two classes of linear systems where optimal gain selection is performed by formulating and solving an optimization problem. Then a multi-rate observer is developed in nonlinear systems with asynchronous sampling. The input-to-output stability is established for the estimation errors with respect to measurement errors using the Karafyllis-Jiang vector small-gain theorem. Measurement delay is also accounted for in the observer design using dead time compensation. Both the multi-rate designs in linear and nonlinear systems provide robustness with respect to perturbations in the sampling schedule.

Multi-rate multi-delay observer is shown to be effective for process monitoring in polymerization reactors. A series of three polycondensation reactors and an industrial gas-phase polyethylene reactor are used to evaluate the observer performance. Reliable on-line estimates are obtained from the multi-rate multi-delay observer through simulation.

Dedicated to my loving family.

To my parents, Longjuan Shan and Wenmin Ling,

and to my grandma, Lanbao Feng,

for their love and support.

ACKNOWLEDGMENTS

The past five years at Texas A&M University has been an unforgettable journey. When it finally comes to an end, I took a look back and the memories of the days and nights in the graduate school flashed through my mind. All the help, support and love that I received have made it possible for me to pursue a PhD from the Artie McFerrin Department of Chemical Engineering at Texas A&M University.

This dissertation would not have been possible without the guidance of my advisor, Professor Costas Kravaris. I definitely owe a great deal of thanks for the time and supervision he has devoted to preparing me as an independent researcher. I entered the PhD program in 2013 from a polymer background with a specific goal of contributing to the field of polymer materials. However, things do not always go as planned. While I was frustrated and almost hopeless, Professor Kravaris, who was still in Greece at that time and planned to join Texas A&M in 2014, kindly took me as his first PhD student here without hesitation, even though we only communicated over a few emails and I didn't have any knowledge about system theory. Only after a few years that I worked with him and learned the developments in the field of process system engineering, did I realize that I am blessed to have the privilege of working with one of the most brilliant minds in chemical engineering and calling him my advisor. It was an extremely pleasant experience to work under the supervision of Professor Kravaris which I will treasure for the rest of my life. There are many memories with joy and gratitude that I can keep talking for days. Professor Kravaris is extremely kind, supportive and patient. He offered me great freedom and helped me in everyway he can. I couldn't have asked for a better advisor. He was always available whenever I went to his office for a "quick" discussion, which usually ended up with a one hour long discussion about my research update, his course, life in academia, etc. He is not only an advisor, but also a friend who I can talk with about everything. In the past five years, I have witnessed his passion for teaching, research and educating students. The inspiration, encouragement and trust he placed pushed me towards excellence in research and helped me become a better man. He has influenced me in both my personal and professional life

which helped shape who I am today and will certainly shape my future career (you can think of this as the effect of a stabilizing controller on a nonlinear system with uncertainties and disturbances). If I could go back and select my advisor again, I would definitely make the same choice.

I am also grateful for the helpful feedback that I received from the members of my dissertation committee, Professor M. Nazmul Karim, Professor Yossef A. Elabd, Professor Suman Chakravorty and Professor Alexander Parlos. Professor Karim and Professor Jayaraman offered me tremendous help especially in my first year before my advisor formally joined the department. They treated me as if I was a student of their groups and offered lots of help to make sure that the transition would go as smoothly as possible. I am thankful to Professor Elabd for his willingness to collaborate that provided me a great opportunity to test the observer algorithms on their lab-scale polymerization reactors. Participating in the proposal writing which eventually got funded by the NSF was one of the most rewarding moments in my PhD study. I cannot express my gratitude enough to Professor Chakravorty. I knew him at his graduate course on optimal estimation where I learned a great deal. The lecture notes and course project helped me get through several job interviews and landed a job in autonomous driving where state estimation plays an important role. I would like to thank for his kindness and being in my committee because of the last-minute change of committee members. I appreciated his availability for students and responsiveness to my emails. I was overjoyed to see a reply from Professor Chakravorty a couple of minutes after I sent it out, which made it much easier to schedule my dissertation defense. I thank him for the fruitful discussions we had about research and career opportunities in automation. He is a remarkable mentor.

I am very fortunate and grateful to know Dr. M. Nicolas Cruz Bournazou and Professor Iasson Karafyllis and have the opportunity to learn from them. Nico visited our group in 2015 when I just started research. Words cannot describe how delighted I was to have a senior member in the office who I could always count on a discussion with to get insights. He was very patient and taught me how to write efficient MATLAB codes, which made a great impact on my coding styles for the rest of my doctoral studies. Professor Kravaris introduced Professor Karafyllis to me over Skype when I had a difficult time to understand the mathematics in his papers. He explained those complicated

concepts word by word to ensure that I could understand. He also pointed me in the right direction and some chapters of this dissertation would not have been possible without his support. Moreover, I would like to extend my gratitude to Professor Nikolaos Kazantzis, who I've never met in person, but the work presented in this dissertation is very relevant to his previous work. If I have completed anything in my PhD, it is by standing on the shoulders of these researchers. During my PhD, I took a few courses that guided me to the realm of dynamic systems. I would like to thank my instructors Professor Aniruddha Datta, Professor Garng M. Huang and Professor Suman Chakravorty. Ashley Henley, Vickie Garcia and Toni Alvarado, who are vital to the operation of the department, offered invaluable assistance and support throughout the course of my PhD.

I had an incredible internship experience at Genentech in 2017. I am grateful for having Geeta Singh and Dr. Victor Saucedo as my mentors who I learned communication and multitasking skills, how to collaborate and move a project forward in a company, etc. from. The internship experience greatly helped me build up my self-confidence and made me think about the impact of the projects and research from a practical perspective. Dr. Xiaohong Cui offered tremendous help when I was looking for an internship and I attribute the internship opportunity to her.

Lastly, I move to friends and family. Their company brought more and more laughter and joy into my life that made my PhD journey so special. Having been in four offices, there are too many people to mention explicitly. I am thankful for everyone I crossed path with who made this journey enjoyable. The members in our research group were spread out and sit in different offices. Because of this, I especially treasured every moment when we gathered together including Zhaoyang Duan, Joshiba A. Venkidasalapathy, Sunjeev Venkateswaran, Mengxi Yu and Qiancheng Liu. Zhaoyang is one of my closest friends and of course a part of my best memories which will never fade away. Patrick Lathrop was an excellent collaborator who I enjoyed working with. I would like to thank him for taking the lead and making effective plans during our discussions. I have been extremely fortunate to be part of the tennis club and the workout group. I thank Ishan Bajaj, Doga Demirhan, Abhinav Narasingam and Patrick for teaching me tennis which becomes one of my favorite sports. I thank Dr. Robert Browne and Dr. Jose L. Gomez Ballesteros for pushing me hard in the gym and

helping me stay motivated. I look fondly at all of the professional and personal interactions I have had with Professor Joseph Sang-Il Kwon, Dr. Xinghua Pan, Chiranjivi Botre, Chi Zhang, Rui Sun, Zhuoran Zhang, Tzu-Ling Chen, Yifei Yang, Wen Zhu, Dr. Yanpu Zhang, Yue Sun, Edna Méndez, Yuhe Tian, Dr. Nandita Kohli, Ravi Chawla, Duanduan Han, Dr. Ruochong Fei, Dr. Yizhi Hong, Dr. Zhe Han, Ling Zhu and Yujing Fan. Furthermore, I take this opportunity to thank my excellent and caring roommates including Yingyezhe Jin, Zhuoer Sun, Jingyao Wang, Yixi Chen and Azhar Ali whose friendship has helped me grow tremendously. It is truly a blessing to be surrounded by so many great friends and I wish you success in all your future endeavors.

Finally, my family has always been my inspiration to reach great heights. I am grateful for their constant support and unconditional love in any situation. My parents, Longjuan Shan and Wenmin Ling, have sacrificed greatly to support me in the pursuit of dreams. Even though we are separated by distance, I feel that we are even closer to each other than before. They always believe in me even through the most difficult moments of my PhD. My loving grandma, Lanbao Feng, by whom I was raised and to whom I owe everything, supported my decisions and increased my motivation. I appreciate the influence she has had on my life and I wish I could have spent more time with her. Thank you to my family who has helped shape me into the man I am today. I love you so much!

CONTRIBUTORS AND FUNDING SOURCES

Contributors

This work was supported by a dissertation committee consisting of Professor Costas Kravaris and Professors M. Nazmul Karim and Yossef A. Elabd of the Department of Chemical Engineering and Professor Suman Chakravorty of the Department of Aerospace Engineering.

All work for the dissertation was completed by the student independently.

Funding Sources

Graduate study was supported in part from the National Science Foundation through the grant CBET-1706201.

NOMENCLATURE

LTI	Linear time-invariant
EKF	Extended Kalman filter
UKF	Unscented Kalman filter
EnKF	Ensemble Kalman filter
MHE	Moving horizon estimation
PCA	Principal component analysis
PLS	Partial least squares
PET	Polyethylene terephthalate
BHET	Bis(2-hydroxyethyl) terephthalate
EG	Ethylene glycol
DP	Degree of polymerization
CSTR	Continuous stirred-tank reactor
DEG	Diethylene glycol
PDE	Partial differential equations
LBT	Lower block triangular
LMI	Linear matrix inequality
ISS	Input-to-state stability
IOS	Input-to-output stability
UIOS	Uniform input-to-output stability
BIC	Boundedness-Implies-Continuation

TABLE OF CONTENTS

Page

LIST OF FIGURES

FIGURE Page

LIST OF TABLES

TABLE Page

1. INTRODUCTION

Process system engineering is a discipline that develops theoretical approaches, computational techniques, and computer-aided tools for modeling, design, optimization, and control of complex engineering systems. State estimation, as a branch of the discipline, uses computational algorithms to reconstruct the state or a functional of the state of a dynamic system and thus, places less reliance on hardware sensors needed in a system. As a result, the cost of device installation and maintenance is greatly reduced. In addition, it is very rare in practice that all the state variables are available via direct on-line[1] measurements, especially in chemical processes. In most cases, there is a substantial need for accurate estimation of the unmeasurable state variables in real time, which may be used in process monitoring, model-based controller synthesis, and early detection of operational problems [4]. State estimation, as a soft sensor technique, opens up possibilities to tackle the aforementioned tasks by using available on-line measurements and a process model. However, a chemical process usually involves different types of measurements, and it remains a challenging and critical task to incorporate multiple measurements with different sampling rates and different measurement delays into the same estimator design, in a unified algorithmic framework.

To this extent, this dissertation presents developments in the field of state estimation by providing the theoretical advances in multi-rate multi-delay state observer design, and several simulation case studies with focus on polymerization reactors, which are selected as the application area of the theoretical developments.

1.1 Background and Motivation

The increasingly competitive chemical industry urges innovative smart manufacturing of products in large quantities, with desired quality, and in a cost-effective and sustainable manner. Energy-efficient operations can often be realized by integration of process design, mathematical modeling, optimization, and process control. The objective of control is to address problems of process stabi-

[1] *On line* means that the techniques have been designed for continuous operation in a production process or at least appear qualified for such use in the foreseeable future [3].

lization and regulation as well as enhancement of the stability properties and system performance. However, the implementation of feedback control laws in a plant often requires the availability of all state variables for direct on-line measurements. In practice, despite the fact that some physical variables (e.g., temperature, pressure, flow rate, liquid level) can be directly measured on line, critical variables related to safety, product quality, and economic performance of a chemical process usually cannot be measured on line. For example, product quality indices (e.g., molecular weight, melt index, tear strength, elastic modulus) cannot be measured in real time because of the complicated and slow measurement techniques needed or simply the technical limitations to measure the quality indices until the final product is formulated or used [5]. Hence, it is extremely difficult to control and monitor product quality without efficient and reliable on-line measurements.

Polymerization reactors belong to a class of processes where control and monitoring of product quality are limited by the lack of reliable and robust on-line polymer characterization instruments. Some product quality measurements (e.g., melt viscosity, polymer structure properties, mechanical strength) may be available from off-line lab analysis, during the course or at the end of a reaction. However, infrequent sampling and large measurement delays, caused by the off-line analysis, often prevent operators from making decisions that maintain high product quality and safe operation in a timely manner. Consequently, there is a desperate need for the development of new on-line sensors for product quality monitoring [6, 7]. Comprehensive literature surveys of recent advances in the development of on-line hardware sensors for monitoring polymerization reactions were presented in [3, 8], which provided guidance to both academia and industry on the selection of sensors for different applications. Although technological advancements in electronics and materials have led to a new generation of sensor products, the development of on-line sensor technology is still slow due to its multi-disciplinary requirements (e.g., statistics, mathematical modeling, polymer chemistry, electronics, instrumentation) and the complex nature of polymerization systems. Apart from the developments in sensors, efforts have been made to find the qualitative and quantitative relationships between the difficult-to-measure polymer properties (e.g., drawing behavior, mechanical strength) and the easier-to-measure fundamental polymer properties (e.g., composition, density, re-

fractive index, molecular weight) [9–15]. In many cases, the relationships are based on experience without theoretical justification, and thus could be very application-specific.

In an attempt to overcome some of the problems caused by inadequate on-line measurements, state estimation methods have gained a lot of attentions because of low cost, ease of implementation, and reliability of estimation. In a state-space representation, state variables are those variables that uniquely describe the state of a system at any given time. In other words, the state of a system can be uniquely determined once all the state variables are known to us. State estimation is a type of soft sensor that utilizes computational algorithms to reconstruct the unmeasured state variables by using available on-line measurements and a process model. Effective control and monitoring of a polymerization reactor can be achieved if reliable real-time information on the state variables are available. As previously mentioned, a representative mathematical model of the process is required to perform the estimation task, as the model describes the quantitative relationships among all the state variables. A significant amount of studies have been carried out in the area of modeling and simulation of polymerization reactors in the last forty years. Ray [16] and Kiparissides [17] gave a broad overview of different polymerization processes and mathematical modeling approaches. Because of the complexity in polymerization mechanisms and the presence of different lengths of polymer chains in the reaction mixture, detailed models generally contain too many state variables. Moreover, the dynamics described by ordinary (or partial) differential equations are highly coupled and nonlinear in nature.

Obviously, mechanism models are too complex to be used in process control and optimization applications. To guarantee solvable solutions and avoid heavy computational burden, it is desirable to develop and use dynamic models that are simple in mathematical structure, yet capable of adequately capturing the essential process characteristics. It was presented in [18] that the method of moments can be applied in a batch solution polymerization to reduce the original infinite number of differential equations to a tractable set of fewer nonlinear differential equations, which became favorable for control and optimization purpose. Other representative pieces of work from the literature can be found in [19–24], where simplified polymerization models were adopted to develop

feasible control strategies.

There are many survey papers in the literature which reviewed the principal difficulties and the applications of advanced control and estimation techniques in polymerization reactors [6,7,25–28]. Since early 1980's, a lot of efforts have been made to design and employ nonlinear state estimators in free radical polymerization reactors, as the commercial on-line size exclusion chromatography and other advanced measurements became available. The extended Kalman filter (EKF) has been widely used in chemical processes (including polymerization reactors) and achieved good performance [20,29–41]. However, the EKF has its inherent disadvantages: (i) the error convergence and stability properties are difficult to analyze mathematically; (ii) it is computationally demanding as the covariance matrix and the states need to be integrated at each time step; (iii) it could even fail to converge because of the local linearization approximation, unless a good initial guess of the states is provided [42–44].

Apart from the EKF, observer methods provide an alternative approach to estimate the unmeasured state variables, where the convergence properties can be established mathematically in most studies. Several observer design methods have been proposed and implemented in polymerization reactors [45–49], including high-gain observers [50, 51]. The results in [49] clearly demonstrated the promise of using a nonlinear observer over the EKF in a solution homo-polymerization reactor. Although temperature and density are usually sampled frequently and are available without delay, most of the product quality measurements have relatively low sampling rates and significant output delays. Despite the slow sampling rate and measurement delay, the measurements that provide important quality information on the products, must be incorporated in an intelligent manner together with the fast-sampled measurements, to make the entire system observable as well as improve the estimation accuracy [52].

1.2 Literature Review

Several studies within the literature have investigated state estimation methods for various systems, e.g., linear and nonlinear systems, continuous-time and sampled-data systems, deterministic and stochastic processes. In general, most soft sensors can be classified into two classes, namely,

model-based and data-driven. The model-based soft sensor is developed based on the knowledge of a first-principle model that captures the evolution of physical and chemical phenomena in the process. The data-driven soft sensor has recently gained in popularity in the process industry with increasing amount of available data and rapid growth of computing power. This section will highlight some of these studies with focus on the model-based methods.

1.2.1 Model-Based Soft Sensors

A wide variety of approaches for model-based state estimation in linear and nonlinear systems have been proposed in the literature. Some commonly used methods are summarized in Table 1.1. This section will provide a brief overview of Bayesian filters, state observers, and moving horizon estimators as well as their applications in chemical processes. Proper techniques should be selected for estimator design and implementation according to the estimator properties and the features of particular applications.

	Linear Systems	Nonlinear Systems
Bayesian Filters	Kalman filter (optimal estimates)	Extended Kalman filter, Unscented Kalman filter, Ensemble Kalman filter, Particle filter, etc.
State Observers	Luenberger observer	Observer error linearization, High-gain observer, etc.
Optimization-based Methods	Moving horizon estimation, etc.	

Table 1.1: Some commonly used model-based state estimation methods.

Dating back to the 1960's, the classic Kalman filter [53, 54] and Luenberger observer [55–58] were developed as effective methods for on-line state estimation, as long as the process dynamics is approximately linear. The Kalman filter is a stochastic and recursive estimator[2] for linear systems

[2] A recursive filtering approach means that received data can be processed sequentially rather than as a batch so that it is not necessary to store the complete dataset nor to reprocess existing data if a new measurement becomes available [59].

where additive Gaussian noises are considered in process model and measurement model. Hence, the word "filter" is used here to represent the process of finding the best estimates from noisy data which amounts to "filtering out" the noise. The Kalman filter consists of two steps, i.e., prediction and update. The prediction step uses the process model to predict forward the probability density function of the state so that the *a priori* estimate for the next time step can be obtained. The update step incorporates the most-recent measurement into the *a priori* estimate to obtain an improved *a posteriori* estimate, which is achieved by using Bayes' theorem. Such a filter provides the estimate that tries to minimize the *a posteriori* error covariance in the least squares sense by choosing a gain matrix carefully, which weighs the relative uncertainty in the process and the measurement. In this respect, the Kalman filter is an optimal estimator [60, 61]. It is worthwhile to mention that the first publicly known application of Kalman filter was made during the feasibility studies for the Apollo space program (see [62] for more details).

The Luenberger observer was first proposed in [55] and further developed in [56] for continuous-time linear time-invariant (LTI) systems. The observer itself is an LTI system driven by the inputs and outputs of the system it estimates. It is used to reconstruct the system state or a constant linear transformation of the state in a deterministic setting, which is distinguished from the Kalman filter. There is a great deal of freedom in the observer design such as convergence rate and dimensionality. A full-order observer, which reconstructs the entire state vector of the observed system, possesses a certain degree of redundancy, because part of the state vector is available by direct measurement. This redundancy can be eliminated and an observer of lower dimension can be constructed. Notice that even though most of the results in this dissertation were developed in a reduced-order observer formulation, the methodology can be applied to full-order observer formulation under appropriate modifications. Now it is important to consider the effect of an observer on the closed-loop stability properties of the system once the actual state in the control law is replaced by the estimate. It was shown in [55] that an observer has no effect on the poles of the original state feedback other than adding the poles of the observer. Hence, the design of state feedback and the design of state estimator can be carried out independently, which is known as the separation property. In practice, the

eigenvalues of the observer are selected to be negative (usually more negative than the eigenvalues of the observed system), so that the observer state will converge to the state of the observed system [57]. However, there is a trade-off between the convergence rate of the observer and the estimation accuracy affected by measurement noise. The optimal pole placement of observer is not a simple problem, which should be based on the criteria such as noise level, parameter variation, reliability, and ease of synthesis [56]. A rigorous approach for observer design by optimizing an appropriate performance index will also be discussed in this dissertation.

It is well-known that linear state estimators can be inadequate in the presence of process nonlinearities. For this reason, there have been many research efforts over the past decades to develop nonlinear estimators for chemical processes, which take the nonlinear process model and account for the nonlinear dynamic behavior [4,5,63–70]. Along the lines of the Kalman filter, one approach that has been tried by many researchers and industrial practitioners in an attempt to handle process nonlinearities is the EKF [71–88]. The EKF adopts the formulae of the classic Kalman filter with the Jacobian of the nonlinear system in place of the linear matrix at each step. The state distribution is approximated by a Gaussian random variable, which is then propagated analytically through the first-order linearization of the nonlinear system. Even though the EKF has successfully applied to many industrial applications and provides reliable estimates for the system which is almost linear on the time scale of update intervals, there have been many studies that established its serious difficulties in the presence of strong process nonlinearities and poor initial guess [42–44]. The method fails to account for the fully nonlinear dynamics in propagating the covariance matrix, which introduces large errors in the true posterior mean and covariance of the transformed Gaussian random variable. This could lead to suboptimal estimation performance and sometimes even divergence of the filter [89].

To overcome this limitation, the unscented Kalman filter (UKF) was developed based on the so-called unscented transformation to propagate mean and covariance information through nonlinear dynamics [90–92]. The state distribution is again approximated by a Gaussian random variable, but is now represented using a minimal set of carefully chosen sample points. By using a deterministic

sampling approach, the sample points completely capture the true mean and covariance accurately to the third order for any nonlinearities [91]. This approach is more accurate, easier to implement, and the computational cost is the same order of magnitude as the EKF implementation [92]. A few UKF applications to chemical processes can be found in [93–100]. However, divergence could still occur in some nonlinear systems despite the aforementioned improvements [101].

Since their introduction in 1993 [102], particle filters have become a popular class of numerical methods to solve optimal estimation problems in nonlinear non-Gaussian processes, where analytic solutions do not typically exist. The particle filter is an implementation of recursive Bayesian filter using the sequential importance sampling algorithm, which is a Monte Carlo method that serves as the basis for most sequential Monte Carlo filters developed over the past decades [103–105]. The probability density function in the particle filter is represented by a group of random samples with associated weights, as opposed to describing it using a functional form. As the number of samples becomes very large, this Monte Carlo characterization becomes an equivalent representation to the usual functional description, and the particle filter approaches the optimal Bayesian estimate [59]. The prediction step uses the process model to propagate each of the samples and generates a set of prior particles at the next step. Then these prior particles are resampled and replaced according to their associated weights so that a new set of particles will be produced. Notice that this weight is the measurement likelihood evaluated at each prior sample. A high likelihood function value indicates that the state is well supported by the measurement. Therefore, the resampling operation is biased towards the more plausible prior particles which are likely to be chosen repeatedly. In addition, the resampling operation avoids wasting majority of the computational efforts in propagating particles with very low weights, which reduces the effects of the degeneracy problem. It is also worthwhile to mention that the particle filtering can identify multiple modes and track multiple optima in the *a posteriori* distribution.

The ensemble Kalman filter (EnKF) is a special case of the particle filter, where the Bayesian update step is approximated with a linear update step using the first two moments of the predicted probability density function [106]. Unlike the EKF, it avoids the computational cost of evaluating

the Jacobian matrices of the nonlinear systems, because the filter gain can be approximated using the covariance of the ensemble. Unlike the particle filter, the EnKF does not resample the ensemble from the posterior probability density function, because each prior model realization is individually updated to generate the correct posterior ensemble [107]. The EnKF is used extensively in weather forecasting [108] and oil reservoir simulations [109], where the models are of extremely high order and nonlinear, and the initial conditions are highly uncertain, and a large number of measurements are available [106].

Other Bayesian filters have also been developed recently, such as the Gaussian filter [110] and the cubature Kalman filter [111]. Those who are interested in this topic are encouraged to study the comprehensive tutorial of nonlinear Bayesian filters [112] as well as their performance comparison [113], and references therein.

As seen in Table 1.1, another important class of the state estimation methods is based on optimization formulation, where it is allowed to incorporate prior knowledge in the form of inequality constraints on state variables as well as process disturbances. Several applications to the chemical processes can be found in [114–120]. However, one drawback of the optimization-based approach is that the computational burden increases as measurements become available. A possible solution that fixes the computational cost is to use a finite, fixed-size estimation window, which is known as moving horizon estimation (MHE) [121–124]. The stability property of the MHE has been studied for constrained linear and nonlinear systems in [125, 126], respectively. Comparative performance analysis of various Kalman filters and the MHE can be found in [42, 127–129].

Apart from the probabilistic setting, an alternative direction for handling process nonlinearities, originating from the nonlinear systems theory, is the design of nonlinear observers. A conceptually straightforward extension of observers to nonlinear systems is the extended Luenberger observer, but it is based upon local linearization around the reconstructed states [130]. High-gain observers have attracted lots of attention in the mathematical systems theory literature in the last thirty years. There have been two lines of thinking in high-gain observers. One, led by Gauthier and co-workers, focuses on deriving global results under global Lipschitz conditions [131–136]. The main technical

assumption says that the class of nonlinear systems should be observable for every input (i.e., uniformly observable systems), which is satisfied in many physical systems, at least in some operating domain. For this class of nonlinear systems, the high-gain observer can be designed according to a canonical form where the observer gain does not depend on the system inputs. However, due to the nonlinearity of the system, the choice of observer gain which gives the best compromise between fast convergence, noise rejection, and attenuation of the peak phenomenon is a difficult task [135]. The other, led by Khalil and co-workers, focuses on dealing with the peaking phenomenon when high-gain observer is used in feedback control (see the survey paper [137] and references therein). Several papers have studied a wide range of nonlinear control problems using high-gain observers, including stabilization, regulation, tracking, and adaptive control [138–143]. The main limitation of the high-gain observer is the significant loss of accuracy in the presence of measurement noise. Recent theoretical work [144] has derived precise estimation error bounds in the presence of noise. Besides it has been proved in [145] that the high-gain observer approximates a differentiator in the limit as the observer gain approaches to infinity.

One more approach, which is capable of directly dealing with process nonlinearities, involves using state-dependent gain in the observer. This approach enjoys the benefits of (i) computational simplicity in on-line implementation and (ii) rigorous mathematical foundation, without suffering from the inherent sensitivity to measurement noise of the high-gain observers. The observer contains a copy of the dynamics and a copy of the output map, but the observer gain is not necessarily constant, and this opens up many possibilities. Actually, under certain conditions, it is possible to select the gain function to "shape" the resulting error dynamics. In this direction, there has been a rich systems theory literature, involving a variety of mathematical approaches, including observer error Lyapunov function methods [146, 147], and exact linearization methods [148–159]. Notice that the nonlinear continuous-time observer design in this dissertation employs the exact linearization with eigenvalue assignment method [148], which will be discussed in more details in Chapter 2. In addition, overviews of sampled-data observer design and observer design with measurement delay will be provided in Chapters 3 to 6.

Other observer design methods, which address the estimation problem in a particular class of systems or applications, have also been developed, such as the unknown input observer [160–164] and the sliding mode observer [165].

As pointed out in [57], the following facts make the observer an attractive area of research: (i) it is computationally simple regarding design and on-line implementation; (ii) it provides a possible solution for process monitoring and feedback control; (iii) the associated theory is closely related to the fundamental linear/nonlinear system concepts of controllability, observability, stability, and dynamic response, and provides a simple setting where all of these concepts interact. Thus, it will be the focus of this dissertation.

1.2.2 Data-Driven Soft Sensors

In contrast to the model-based soft sensors reviewed in the last section, data-driven soft sensor does not require the knowledge of the process and is based on empirical observations of the process, which becomes a valuable alternative to the traditional monitoring algorithms. It has been receiving considerably increasing attention, in particular for industrial process monitoring, because the plants are usually heavily instrumented with a lot of sensors that collect a large amount of data on a daily basis, and a first-principle model is not always available or is too complicated for the model-based methods to be employed sometimes [166]. Based on the historical data, the data-driven soft sensor applies multivariate statistics and machine learning methods to predict the multivariate features or the process state variables, which can be used to make decisions towards a more efficient and safe process operation.

In this section, a very brief overview of the data-driven soft sensors will be provided, covering data characteristics in the process industry, typical procedures for the soft sensor development, and some popular data-driven approaches for soft sensing as well as their applications. It is encouraged to read some survey papers (e.g., [166–169]) and a comparison study of basic data-driven methods on the benchmark Tennessee Eastman process in [170] for a more detailed, comprehensive review on this topic.

The applications of data-driven soft sensors can be found in many areas of the process industry.

The most common application is the on-line prediction of variables of interest and product quality which cannot be measured in real time. It is commonly used in fermentation and refinery processes where rigorous models are usually not available owing to their complex dynamics. The data-driven methods collect the past input and output information, and then train a model based on the historical data to predict the difficult-to-measure variables in the process. A few applications to the chemical processes can be found in [171–174]. Another popular application area of data-driven soft sensors is the process monitoring and fault detection. Very often, a normal-case process model can be built based on the normal process data using data-driven methods, which is used to detect possible faults that deviate from the normal case. This methodology requires less modeling efforts as opposed to the other one where a data-driven model needs to be built for each interested fault case. Commonly, statistical process monitoring techniques based on principal component analysis (PCA) and partial least squares (PLS), or more precisely on Hotelling's T^2 indices [175] and Q-Statistics [176], offer a practical approach for fault detection [177–181]. Originally developed in [182], kernel PCA and PLS methods are similar to the linear counterparts in that a nonlinear transformation of the original variables into a feature space then PCA and PLS models are built in the feature space [183–187]. After a fault is detected, it is desirable to diagnose and identify the source of the fault, and apply necessary actions to correct the abnormal conditions. The procedure to identify a fault and estimate normal values in the faulty data is referred to as fault identification and reconstruction [188]. Some representative pieces of work from the literature can be found in [189–191].

Despite the above applications and a large number of publications on the data-driven soft sensors, there are still many challenging issues, in particular, caused by the common effects present in the industry data. For example, the failure of a hardware sensor or the failure of data transmission between the sensors and the database could cause missing data, where one or more variables have a value that does not reflect the actual state of the measured quantity. Data outliers could also occur where the sensor output deviates from the typical range of the measured values. Another issue for data-driven methods is data co-linearity, which is usually caused by redundant sensor arrangement in the process. For instance, two neighboring temperature sensors would deliver strongly correlated

measurements [167]. PCA and PLS methods are often used to transform the input variables into a new reduced space with less co-linearity, as mentioned in [192–194]. Another approach to handle co-linearity is called variable selection, where a subset of the input variables that are less co-linear will be selected.

From the above discussions, although data-driven methods are much simpler than the model-based methods, it is still meaningless to directly apply an arbitrarily selected data-driven model on the large amount of process data. It is important to first inspect the characteristics of each dataset and pre-process the dataset in such a way that it can be more effectively processed by the actual model. After that, model selection is a critical step for the performance of final soft sensor. So far, there is no unified theoretical approach for this task and thus the model type and its parameters are often selected in an *ad hoc* manner, subject to researcher's past experience and domain knowledge. Afterwards, model training and validation need to be performed on the training dataset.

Apart from the model-based and data-driven soft sensors, the so-called hybrid approach, which is a combination of the two methods, has been developed recently [195]. The intuition here is that the limitations of the model-based and data-driven methods can be overcome by combining them. In this way, the modeling efforts should be reduced compared to the model-based approaches, and the monitoring results should be improved compared to the data-driven approaches that do not use a first-principle model at all.

1.3 Polymerization Reactors

This section will provide a brief overview of the production processes of polyethylene terephthalate (PET) and polyethylene, respectively. The specific applications have been selected not only because of their major industrial significance, but also because they incorporate all the challenges that the proposed theory will try to address: presence of severe process nonlinearities, presence of both continuous and slow-sampled discrete measurements, presence of both delayed and delay-free measurements.

1.3.1 Polycondensation of Polyethylene Terephthalate

Although a lot of work has been done in monitoring and control of free radical polymerization reactors, very few state estimation studies are available for polycondensation processes. One of the most common polycondensation products is PET, which is the primary raw material for synthetic fibers, dielectric films, and beverage bottles. Figure 1.1(a) illustrates that polyester, which is commonly referred to as PET, dominates synthetic fibers industry over the years, accounting for nearly half of the global consumption. Figure 1.1(b) shows that the global demand for PET is predicted to be growing in the next few years. Therefore, producing PET with required properties is of major industrial importance.

There are several side reactions taking place along with the main polycondensation reaction. The amount of side products determines the quality and properties of the final product. To ensure PET product quality, the amount of byproducts needs to be well controlled within certain limits. A comprehensive understanding of PET synthesis is essential for effective quality control and process optimization. Generally speaking, there are three stages involved in the PET production. In the first stage, bis(2-hydroxyethyl) terephthalate (BHET) is produced through either melt transesterification or direct esterification. Methanol or water is removed continuously and in the meantime, ethylene glycol (EG) is completely refluxed back to the reactor. This stage often operates in a stirred vessel under atmospheric pressure [196–198]. In the second stage, BHET and oligomers from the first stage are transferred to a pre-polymerization reactor at an increased temperature (i.e., 250–280°C) and reduced pressure (i.e., 2–3 kPa), where the degree of polymerization (DP) can reach up to 30. The viscosity of reaction mixture is still low compared to the later stages, and diffusional limitation does not play an important role in this stage [199, 200]. The product is further polymerized in the third stage until the DP reaches 100 at 280–290°C. Because the main reaction is reversible, EG, as a byproduct, has to be vaporized continuously by applying vacuum to increase the yield. Meanwhile, viscosity of the reaction mixture also increases rapidly which makes mass transfer a limiting factor. Therefore, a special film forming device is used in the third stage to provide large surface area for desorption of EG [201, 202]. In injection or blow molding applications, solid state polymerization

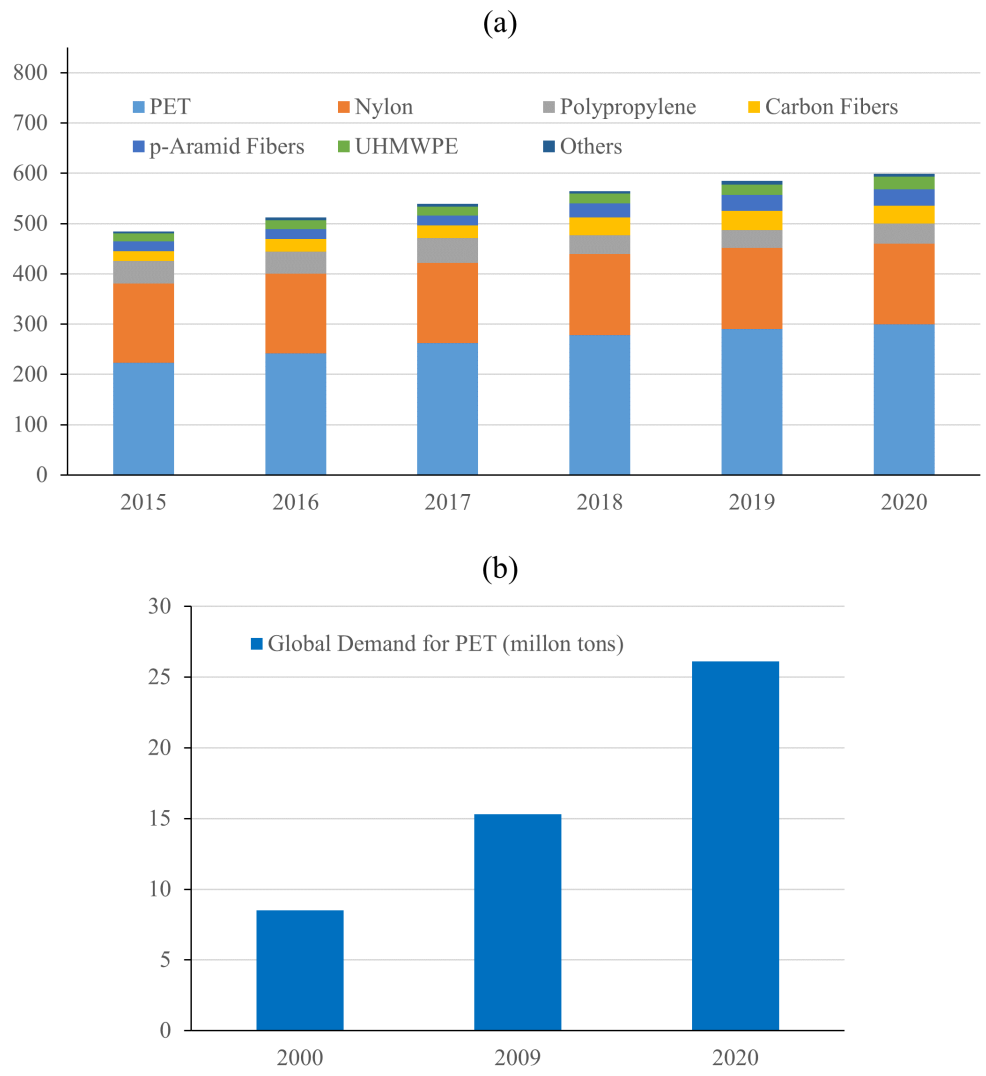

Figure 1.1: (a) Global webbing market volume by product (kilotons) [1]. (b) Demand forecast of the global PET market [2].

needs to be carried out to obtain products with DP over 150 [203]. These aforementioned modeling studies are very useful for process control and optimization purposes. For certain special-purpose applications, simplified models were also developed, which agreed well with experimental results [204–206].

Monitoring and control of polycondensation reactor is challenging owing to lack of fast on-line measurements and significant nonlinearities of the process. State estimation provides an alternative approach to track the change of molecular weight by integrating on-line sensing, reactor modeling,

and simulation. The objective in Chapter 2 is to estimate state variables and the degree of polymerization in the PET finishing stage using a nonlinear observer, where measurements with different sampling rates and output delays will be considered.

1.3.2 Industrial Gas-Phase Polyethylene Production

Polyethylene is the most used synthetic polymer worldwide with the largest annual production. Over the last seventy years, there has been a continued manufacturing growth from a few hundred tons in 1940 to more than 160 billion pounds in 2012 [207]. In the next few years, the demand is forecast to grow on a global basis. Polyethylene products are used as pipes, containers, agricultural mulch films, and many other applications. In the literature, polyethylene is generally classified into three groups: low-density polyethylene, linear low-density polyethylene at 0.910–0.930 g/cm^3, and high-density at 0.931–0.970 g/cm^3. Experimental results showed that these products are different in polymer microstructure, such as length of side chain branching, molecular weight and its distribution, degree of crystallinity, and as a result, it leads to different performance characteristics (e.g., thermal, physical properties, and rheological behaviors) [208–213].

Polyethylene technology has experienced revolutionary improvements in the last century. Prior to the 1950's, polyethylene was produced exclusively using conventional high-pressure polymerization processes operating at temperature above 200°C and at pressure above 1000 atm. This process only produces low-density polyethylene with long-chain branching because of its free radical mechanism. In order to achieve high molecular weight for practical applications, the high pressure is required in providing a high ethylene propagation rate. Later, the development of Ziegler-Natta catalyst made it possible to synthesize linear polyethylene at a more moderate condition via coordination polymerization mechanism.

Currently, there are three commercialized low pressure polyethylene processes: slurry, solution and gas phase. Among them, the gas-phase process, which does not involve any liquid phase, is the most versatile and can produce polyethylene covering a complete range of density and melt index because it is not limited by solubility and viscosity [214]. In a gas-phase reactor, the polymerization takes place at the interface between the solid catalyst and the polymer matrix. The feed to the

reactor, which comprises ethylene, comonomers, hydrogen, and inerts, provides the fluidization by using a high rate of gas recycle. A heterogeneous Ziegler-Natta catalyst is fed continuously to the reactor. Since the conversion per pass through the bed is very low (i.e., 2–5%), the unreacted gas is recycled with fresh feed to the base of the reactor and as a result, the overall monomer conversion could be as high as 98% [215]. At the same time, the heat generated from the exothermic polymerization is removed through a heat exchanger. Polymerization occurs at a pressure of 30–35 atm and a temperature of 80–100°C. The product, polyethylene, discharges near the base of the reactor as solid powder. Other advantages of gas-phase process over liquid-phase process include production of copolymer with high α-olefin content, which gives better mechanical properties [216]. Furthermore, the gas-phase process significantly reduces the capital cost up to 30% and the operating cost up to 35% compared with the conventional liquid-phase processes.

Researchers have made a lot of efforts to study this complex reaction system at different levels where physical and chemical phenomena take place simultaneously [217–221]. For reactor design, quality control, and grade changeover, it is essential to understand the dynamic behavior that incorporate kinetics of polymerization, heat and mass transfer, and reactor characteristics [222–232]. In general, the gas-phase polyethylene fluidized-bed reactor has been modeled as single-phase well-mixed continuous stirred-tank reactor (CSTR) [215], two-phase [217] and three-phase plug flow reactor [220]. It is assumed in the well-mixed CSTR model that there is little or no resistance in the monomer and heat transfer between the bubble and emulsion phases. In the operating range of industrial interest, the differences between the detailed model and the simplified model are less than 3 K in temperature and less than 2 mol% in monomer concentration [215]. Hence, the well-mixed assumption is valid for modeling the gas-phase polyethylene reactor.

In industrial settings, polyethylene grade is specified in terms of melt index and density [233]. Although reactor temperature, pressure, and gas concentrations are regularly measured on line, the product quality variables can only be obtained from off-line lab analysis. The sampled and delayed measurements are essential in the feedback control. A combination of the information from on-line and off-line measurements can achieve improved state estimation and quality control performance

between samples. Model-based and data-driven methods for product quality monitoring have been successfully applied in some polyolefin processes, including the development of on-line parameter estimation that captures the actual reactor operation conditions [116, 234–240]. However, very few model-based estimation methods have been reported for the gas-phase polyethylene reactor, where different nature of the measurements need to be considered. As for the off-line manual operations, perturbations in the sampling schedule will affect the convergence property of the error dynamics. A multi-rate multi-delay observer can benefit feedback control, quality monitoring, and therefore, reduction of off-specification products.

1.4 Dissertation Outline and Contributions

The dissertation is constructed in the following manner to illustrate the developments of multi-rate observer design for process monitoring, with application to polymerization reactors.

In Chapter 2, a nonlinear observer combined with an inter-sample output predictor is designed and applied to estimate the degree of polymerization in a series of polycondensation reactors. One continuous measurement and one sampled measurement with delay are considered. The observer performance is tested in the presence of sensor noise through simulation.

In Chapter 3, focus will shift towards theoretical developments in the area of multi-rate observer design in linear systems with asynchronous sampling. Sufficient and explicit conditions are derived to guarantee exponential stability of the multi-rate observer. An industrial gas-phase polyethylene reactor example is used to demonstrate the applicability of the proposed approach.

In Chapter 4, possible measurement delay is considered in the observer design. The multi-rate multi-delay observer adopts an available multi-rate observer design proposed in Chapter 3. A dead time compensation approach is developed to compensate for the delay. It is shown that stability of the multi-rate observer is preserved under nonconstant, arbitrarily large delays.

Chapter 5 develops a rigorous approach for observer gain selection to reach a compromise between the effect of modeling error on the accuracy of state estimate and the effect of measurement error on the accuracy of state estimate. The optimal multi-rate observer design is formulated as an optimization problem of minimizing a performance index. The approach is demonstrated on linear

systems with single-rate measurement and with fast and slow measurements, respectively.

Chapter 6 studies the problem of multi-rate sampled-data observer design in nonlinear systems under asynchronous sampling. Similar to the multi-rate observer in linear systems, it is based on a continuous-time design coupled with inter-sample predictors. It is shown that the error dynamics is input-to-output stable with respect to measurement errors by applying the Karafyllis-Jiang vector small-gain theorem.

Chapter 7 proposes a design method for multi-rate multi-delay observer in nonlinear systems. It is based on an available multi-rate observer design coupled with dead time compensation, in the same spirit as the multi-rate multi-delay observer in Chapter 4. The gas-phase polyethylene reactor example is reconsidered in the presence of measurement delays.

Finally, Chapter 8 summarizes the main conclusions of the dissertation and provides directions for future work.

2. STATE OBSERVER DESIGN IN A SERIES OF POLYCONDENSATION REACTORS *

As mentioned in Chapter 1, the presence of severe nonlinearities, the presence of both continuous and slowly sampled discrete measurements, and the presence of both delayed and delay-free measurements make it a challenging problem to monitor the progress of polymerization reactions in real time. In this chapter, a nonlinear reduced-order observer is applied to estimate the degree of polymerization in a series of polycondensation reactors [241]. The finishing stage of polyethylene terephthalate synthesis is considered as the case study. The process has a special structure of lower block triangular form, which is properly utilized to facilitate the calculation of the state-dependent gain in the observer design. There are two possible on-line measurements in each reactor. One is continuous, and the other is slow-sampled with dead time. For the slow-sampled titration measurement, inter-sample behavior is estimated from an inter-sample output predictor, which is essential in providing continuous corrections on the observer. Dead time compensation is carried out in the same spirit as the Smith predictor to compensate for the effect of sensor delay. By integrating the continuous-time reduced-order observer, the inter-sample predictor and the dead time compensator together, the degree of polymerization is accurately estimated in all three reactors. In addition, a pre-filtering technique is used in the presence of sensor noise. The observer performance is demonstrated by numerical simulations.

Despite the fact that both continuous, delay-free measurement and slow-sampled, delayed measurement are involved in this example, the reduced-order observer only takes the continuous measurement to estimate the unmeasured state but does not depend on the sampled measurement. This is achieved by taking advantage of the special system structure where a continuous-time observer with an inter-sample output predictor in the "downstream" is sufficient to handle the state estimation problem in this particular multi-rate polycondensation process.

This chapter is organized as follows: in Section 2.2, an overview of the reduced-order observer

*Reprinted with permission from "State Observer Design for Monitoring the Degree of Polymerization in a Series of Melt Polycondensation Reactors" by C. Ling and C. Kravaris, 2016. *Processes*, 4(1), 4. Copyright is retained by the authors for all articles published in MDPI journals.

and sampled-data observer design methods are presented. In particular, a block triangular observer form is derived from the serial subsystem structure (e.g., multiple CSTRs connected in series). In Section 2.3, the finishing stage of PET polycondensation, as well as its mathematical model is described. In Section 2.4, the performance of the state observer is evaluated in two different cases: (i) only continuous measurement is available; (ii) both continuous and slow-sampled measurements are available. Furthermore, sensor noise is considered, and the results show that there is a tradeoff between the convergence rate and noise sensitivity. Finally, in Section 2.5, conclusions are drawn from the results of the previous sections.

2.1 Introduction

Polymers are continuously substituting traditional materials, such as glass, woods, and metals, along with their low cost and good processability. Polyethylene terephthalate is the most common thermoplastic polymer resin, which is the primary raw material for synthetic fibers, dielectric films, and beverage bottles. PET has dominated the synthetic fibers industry over the years accounting for nearly half of the global consumption (see Figure 1.1(a)). Moreover, the global demand for PET is predicted to grow in the next few years. Therefore, producing PET with the required properties is of major industrial importance.

It is well known that the end-use properties of PET, such as drawing behavior, melting point, tensile strength and thermal stability, strongly depend on its molecular weight and byproduct concentrations [9,15]. There are several side reactions taking place along with the main polycondensation reaction. The amount of side products (i.e., diethylene glycol (DEG), acetaldehyde, carboxyl end groups, vinyl end groups, and water) determines the quality and properties of the final PET product. For example, every one percent of DEG in the polyester chain could cause a lower melting point by 5°C [242]. In addition, even a small amount of DEG leads to reduced heat resistance, decreased crystallinity and ultraviolet light stability. Vinyl end groups could be polymerized with other polyester chains to form polyvinyl ester, of which the pyrolysis products have been shown to be responsible for the coloration of PET [243]. A high initial concentration of carboxyl groups could induce a decrease in the degree of polymerization due to hydrolytic degradation [244]. In or-

der to ensure product quality, the amount of byproducts needs to be well controlled within certain limits.

However, the monitoring and control of polymerization reactors is not an easy task, owing to a lack of fast on-line measurements and the significant nonlinearity of the processes. Very often, critical quantities related to safety, product quality and/or economic performance of a polymerization process cannot be measured on line. Thus, state estimation plays an important role in providing frequent and reliable information of the process, which can be integrated into model-based control, as well. Since the early 1980's, there have been significant efforts in the design and application of state estimators to polymerization reactions, especially in free radical polymerization. The extended Kalman filter, as an industrially-popular estimator, has been widely used and achieved fairly good performance in many studies [20, 29–32, 34, 36, 245]. In this approach, the design is based on an approximate local linearization of the system along a reference trajectory. Even though the EKF has found industrial applications, there have been studies that established its serious difficulties in the presence of strong process nonlinearities [42–44]. An alternative approach for estimation in polymerization processes is state observer design [46–51, 70, 246]. It utilizes the dynamic process model, which captures the evolution of physical and chemical phenomena, and then generates a soft sensor that is able to reconstruct the missing state variables with additional appropriate feedback terms from all of the on-line measurements. For example, Van Dootingh *et al.* [50] developed a nonlinear high-gain observer with adjustable speed of convergence in a styrene polymerization reactor. Compared to the EKF, this observer does not only have a theoretical proof of convergence, but also greatly reduces computation time. Tatiraju and Soroush [49, 70] implemented a nonlinear reduced-order observer to a homopolymerization reactor. Together with an open-loop observer for the unobservable states, accurate estimates for all states were achieved. Astorga *et al.* [48] used a continuous-discrete observer to estimate monomer composition in an emulsion copolymerization reactor. The proposed observer was validated by comparing the observer outputs with the off-line gas chromatography results.

Although a significant amount of work has been done in monitoring and control of free radical

polymerization reactors, very few state estimation studies can be found for polycondensation reactors. Choi and Khan [247] implemented the EKF to estimate nine state variables in the transesterification stage of the PET synthesis. When supplemented by five additional off-line measurements, the overall performance of the state estimator was greatly improved. Appelhaus and Engell [248] designed an extended observer to estimate the concentrations of ethylene glycol and hydroxyl end groups along with a mass transfer parameter in the batch reactor. In their study, only the reversible polycondensation reaction was considered.

A comprehensive understanding of PET synthesis is essential for effective quality control and optimization of the process. Generally, there are three stages (i.e., transesterification/esterification, pre-polymerization, and polycondensation) involved in PET production. In each reactor, side reactions occur simultaneously and directly affect product quality. On-line measurements for byproduct concentrations are usually not available or at relatively low sampling rates [249]. Hence, based on the fact that available on-line measurements are not always of the same nature, it is necessary to develop estimation/monitoring algorithms that can utilize all of these different kinds of on-line measurements in a synergistic way to provide valuable information of the process.

In this study, the nonlinear observer design method of exact linearization with eigenvalue assignment [4, 148] is applied to a series of three continuous polycondensation reactors. A modified reaction-mass transfer model [206] is considered in our work. The objective is to estimate unmeasured concentrations, as well as the degree of polymerization in the PET finishing stage from continuous hydroxyl measurement and sampled acidimetric titration, where different sampling rates and time delays are considered. The basis of the observer design methodology is a continuous-time nonlinear observer design. Subsequently, an inter-sample output predictor [250] is used to account for the slow-sampled measurements and to provide continuous estimates during the time period in between two consecutive measurements. At the same time, an estimate of the current output from the delayed measurement is obtained in the same spirit as the Smith predictor, by initializing the process model with the most recent delayed output and integrating it up to the present time. In the presence of sensor noise, a pre-filtering technique is used to cut out the noise to avoid the break-

down of the observer. The performance of the observer with inter-sample prediction and dead time compensation is evaluated by numerical simulation.

2.2 Nonlinear Observer Design Method

This section briefly outlines the main results on nonlinear observer design [4, 148], block triangular observer design, and sampled-data observer design [250]. All of the observer synthesis and simulations in later sections are realized on the basis of reduced-order observer. Therefore, a brief necessary review is presented below.

2.2.1 Reduced-Order Observer

In chemical processes, on-line measurements typically involve a part of the state vector. While the full-order observer estimates the entire state vector, the reduced-order observer estimates only the unmeasured states. In this sense, the reduced-order observer is free of redundancy and is more computationally efficient than the full-order observer.

Consider a multi-output autonomous system whose outputs are a part of the state vector

$$\begin{aligned} \dot{x}_R &= f_R(x_R, x_M) \\ \dot{x}_M &= f_M(x_R, x_M) \\ y &= x_M \end{aligned} \tag{2.1}$$

where $x_R \in \mathbb{R}^{n-m}$ is the state vector that needs to be estimated, $x_M \in \mathbb{R}^m$ is the remaining state vector that is directly measured, and $y \in \mathbb{R}^m$ is the measurement vector; $f_R : \mathbb{R}^n \to \mathbb{R}^{n-m}$ and $f_M : \mathbb{R}^n \to \mathbb{R}^m$ are real analytic functions with $f_R(0,0) = 0$, $f_M(0,0) = 0$.

In the exact linearization method, the objective is to build an observer so that the resulting error dynamics is linear in curvilinear coordinates and with the pre-specified rate of decay of the error. A locally-analytic mapping $z = T(x_R, x_M)$ from $\mathbb{R}^n \to \mathbb{R}^{n-m}$ is sought that maps the system (2.1) to

$$\dot{z} = Az + By$$

where A is a $(n-m)\times(n-m)$ matrix and B is a $(n-m)\times m$ matrix. The reduced-order observer in the original coordinates can be expressed as

$$\dot{\hat{x}}_R = f_R(\hat{x}_R, y) + L(\hat{x}_R, y)\left(\frac{dy}{dt} - f_M(\hat{x}_R, y)\right) \tag{2.2}$$

This leads to the following selection of the state-dependent observer gain [4]:

$$L(\hat{x}_R, y) = -\left[\frac{\partial T}{\partial x_R}(\hat{x}_R, y)\right]^{-1} \frac{\partial T}{\partial x_M}(\hat{x}_R, y)$$

where $T(x)$ is a solution of the following system of partial differential equations (PDEs):

$$\frac{\partial T}{\partial x_R} f_R(x) + \frac{\partial T}{\partial x_M} f_M(x) = AT + Bx_M \tag{2.3}$$

Under the above choice of observer gain, the error dynamics in transformed coordinates becomes linear and is governed by the arbitrarily-selected A matrix

$$\frac{d}{dt}(T(x_R, y) - T(\hat{x}_R, y)) = A(T(x_R, y) - T(\hat{x}_R, y))$$

Thus, the matrix A is a design parameter that directly adjusts the speed of convergence of the error.

Remark 1. *In order to implement the above nonlinear observer design methodology, an approximate solution needs to be calculated for the system of PDEs of Equation (2.3). As discussed in [4, 148], it is possible to approximate $T(x_R, x_M)$ by using a truncated multivariable Taylor series around the origin. This requires each state expressed in deviation variable form. After expanding f_R, f_M and T in Taylor series up to a finite truncation order, the approximate solution can be obtained by equating the coefficient of each side of the PDEs. This calculation can be executed by using symbolic computation software (e.g., Maple) [4, 251].*

2.2.2 Reduced-Order Observer in Lower Block Triangular Form

The serial CSTR reactor configuration is used in many types of chemical processes [252, 253], leading to higher product yield and higher concentration. The serial CSTR reactor configuration usually possesses a special structure in lower block triangular (LBT) form. This special structure can be utilized properly in state observer design to reduce the complexity of the state dependence of observer gains. Consider a system in LBT form containing three subsystems

$$\dot{x}_{R\mathrm{I}} = f_R^{\mathrm{I}}(x_{R\mathrm{I}}, x_{M\mathrm{I}}) \qquad \dot{x}_{M\mathrm{I}} = f_M^{\mathrm{I}}(x_{R\mathrm{I}}, x_{M\mathrm{I}})$$

$$\dot{x}_{R\mathrm{II}} = f_R^{\mathrm{II}}(x_{R\mathrm{I}}, x_{R\mathrm{II}}, x_{M\mathrm{I}}, x_{M\mathrm{II}}) \qquad \dot{x}_{M\mathrm{II}} = f_M^{\mathrm{II}}(x_{R\mathrm{I}}, x_{R\mathrm{II}}, x_{M\mathrm{I}}, x_{M\mathrm{II}})$$

$$\dot{x}_{R\mathrm{III}} = f_R^{\mathrm{III}}(x_{R\mathrm{I}}, x_{R\mathrm{II}}, x_{R\mathrm{III}}, x_{M\mathrm{I}}, x_{M\mathrm{II}}, x_{M\mathrm{III}}) \quad \dot{x}_{M\mathrm{III}} = f_M^{\mathrm{III}}(x_{R\mathrm{I}}, x_{R\mathrm{II}}, x_{R\mathrm{III}}, x_{M\mathrm{I}}, x_{M\mathrm{II}}, x_{M\mathrm{III}})$$

$$y_{\mathrm{I}} = x_{M\mathrm{I}}$$

$$y_{\mathrm{II}} = x_{M\mathrm{II}}$$

$$y_{\mathrm{III}} = x_{M\mathrm{III}}$$

where I, II, III denote each subsystem, respectively. The objective of observer design is to reconstruct the missing state variables $x_{R\mathrm{I}}$, $x_{R\mathrm{II}}$ and $x_{R\mathrm{III}}$. Figure 2.1 depicts a general structure of the system in LBT form, with three subsystems.

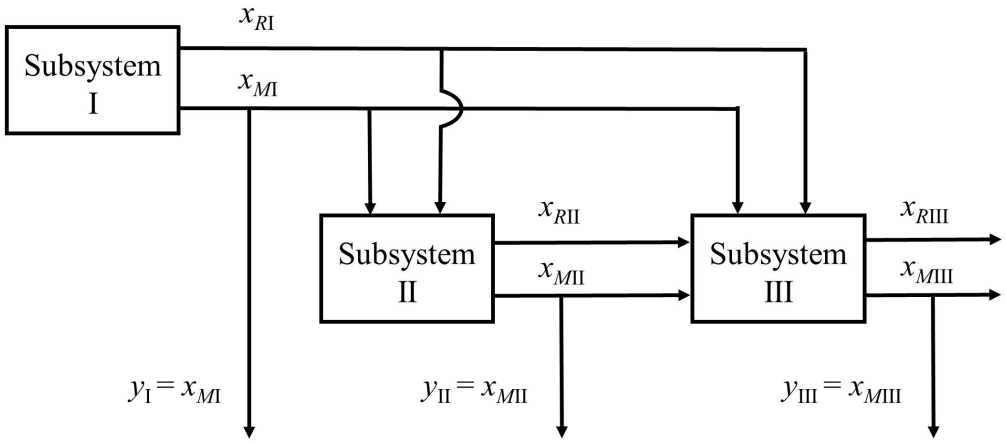

Figure 2.1: General structure of a system in lower block triangular form with three subsystems.

It is intuitive to design sequential observers by taking advantage of the particular LBT structure. For example, the observer for Subsystem I is designed based on its unmeasured state dynamics and its own measurements y_{I}, but is independent of the subsequent subsystems and their measurements. The observer for Subsystem II does not only utilize its own dynamics and measurements, but also depends on the measurements and state estimates from Subsystem I. Moreover, its state-dependent gain also depends on the gain of the first observer. Each observer needs to use the information from all of the previous stages and its own dynamics and measurements. In this way, the computational effort of calculating the state-dependent gain symbolically is significantly reduced.

After coordinate transformation, the observer in z-coordinates has linear dynamics

$$\begin{bmatrix} \dot{z}_{\mathrm{I}} \\ \dot{z}_{\mathrm{II}} \\ \dot{z}_{\mathrm{III}} \end{bmatrix} = \begin{bmatrix} A_{11} & 0 & 0 \\ A_{21} & A_{22} & 0 \\ A_{31} & A_{32} & A_{33} \end{bmatrix} \begin{bmatrix} z_{\mathrm{I}} \\ z_{\mathrm{II}} \\ z_{\mathrm{III}} \end{bmatrix} + \begin{bmatrix} B_{11} & 0 & 0 \\ B_{21} & B_{22} & 0 \\ B_{31} & B_{32} & B_{33} \end{bmatrix} \begin{bmatrix} y_{\mathrm{I}} \\ y_{\mathrm{II}} \\ y_{\mathrm{III}} \end{bmatrix}$$

where both A and B matrices have a special LBT structure. Eigenvalues of the diagonal submatrices can be assigned arbitrarily. As each subsystem's observer needs the estimates from the previous subsystems, it would make intuitive sense to tune the observer for Subsystem I faster than the one for Subsystem II, etc. Accordingly, the nonlinear reduced-order observer in original coordinates is of the form

$$\begin{aligned} \begin{bmatrix} \dot{\hat{x}}_{R\mathrm{I}} \\ \dot{\hat{x}}_{R\mathrm{II}} \\ \dot{\hat{x}}_{R\mathrm{III}} \end{bmatrix} &= \begin{bmatrix} f_R^{\mathrm{I}}(\hat{x}_{R\mathrm{I}}, y_{\mathrm{I}}) \\ f_R^{\mathrm{II}}(\hat{x}_{R\mathrm{I}}, \hat{x}_{R\mathrm{II}}, y_{\mathrm{I}}, y_{\mathrm{II}}) \\ f_R^{\mathrm{III}}(\hat{x}_{R\mathrm{I}}, \hat{x}_{R\mathrm{II}}, \hat{x}_{R\mathrm{III}}, y_{\mathrm{I}}, y_{\mathrm{II}}, y_{\mathrm{III}}) \end{bmatrix} \\ &\quad + \begin{bmatrix} L_{11} & 0 & 0 \\ L_{21} & L_{22} & 0 \\ L_{31} & L_{32} & L_{33} \end{bmatrix} \begin{bmatrix} \dfrac{dy_{\mathrm{I}}}{dt} - f_M^{\mathrm{I}}(\hat{x}_{R\mathrm{I}}, y_{\mathrm{I}}) \\ \dfrac{dy_{\mathrm{II}}}{dt} - f_M^{\mathrm{II}}(\hat{x}_{R\mathrm{I}}, \hat{x}_{R\mathrm{II}}, y_{\mathrm{I}}, y_{\mathrm{II}}) \\ \dfrac{dy_{\mathrm{III}}}{dt} - f_M^{\mathrm{III}}(\hat{x}_{R\mathrm{I}}, \hat{x}_{R\mathrm{II}}, \hat{x}_{R\mathrm{III}}, y_{\mathrm{I}}, y_{\mathrm{II}}, y_{\mathrm{III}}) \end{bmatrix} \end{aligned} \tag{2.4}$$

where the LBT state-dependent gain matrix $L(\hat{x}_R, y)$ can be designed according to

$$
\begin{aligned}
L_{11} &= -\left[\frac{\partial T_1}{\partial x_{R\mathrm{I}}}\right]^{-1} \frac{\partial T_1}{\partial x_{M\mathrm{I}}}, \\
L_{21} &= -\left[\frac{\partial T_2}{\partial x_{R\mathrm{II}}}\right]^{-1} \left[\frac{\partial T_2}{\partial x_{R\mathrm{I}}} L_{11} + \frac{\partial T_2}{\partial x_{M\mathrm{I}}}\right], & L_{22} &= -\left[\frac{\partial T_2}{\partial x_{R\mathrm{II}}}\right]^{-1} \frac{\partial T_2}{\partial x_{M\mathrm{II}}}, \\
L_{31} &= -\left[\frac{\partial T_3}{\partial x_{R\mathrm{III}}}\right]^{-1} \left[\frac{\partial T_3}{\partial x_{R\mathrm{I}}} L_{11} + \frac{\partial T_3}{\partial x_{R\mathrm{II}}} L_{21} + \frac{\partial T_3}{\partial x_{M\mathrm{I}}}\right], \\
L_{32} &= -\left[\frac{\partial T_3}{\partial x_{R\mathrm{III}}}\right]^{-1} \left[\frac{\partial T_3}{\partial x_{R\mathrm{II}}} L_{22} + \frac{\partial T_3}{\partial x_{M\mathrm{II}}}\right], & L_{33} &= -\left[\frac{\partial T_3}{\partial x_{R\mathrm{III}}}\right]^{-1} \frac{\partial T_3}{\partial x_{M\mathrm{III}}}
\end{aligned}
\tag{2.5}
$$

where $T(x) = \begin{bmatrix} T_1(x_{R\mathrm{I}}, x_{M\mathrm{I}}) \\ T_2(x_{R\mathrm{I}}, x_{R\mathrm{II}}, x_{M\mathrm{I}}, x_{M\mathrm{II}}) \\ T_3(x_{R\mathrm{I}}, x_{R\mathrm{II}}, x_{R\mathrm{III}}, x_{M\mathrm{I}}, x_{M\mathrm{II}}, x_{M\mathrm{III}}) \end{bmatrix}$ is a solution of the following system of PDEs:

$$
\begin{aligned}
&\frac{\partial T_1}{\partial x_{R\mathrm{I}}} f_R^{\mathrm{I}} + \frac{\partial T_1}{\partial x_{M\mathrm{I}}} f_M^{\mathrm{I}} = A_{11} T_1 + B_{11} x_{M\mathrm{I}} \\
&\frac{\partial T_2}{\partial x_{R\mathrm{I}}} f_R^{\mathrm{I}} + \frac{\partial T_2}{\partial x_{R\mathrm{II}}} f_R^{\mathrm{II}} + \frac{\partial T_2}{\partial x_{M\mathrm{I}}} f_M^{\mathrm{I}} + \frac{\partial T_2}{\partial x_{M\mathrm{II}}} f_M^{\mathrm{II}} = A_{21} T_1 + A_{22} T_2 + B_{21} x_{M\mathrm{I}} + B_{22} x_{M\mathrm{II}} \\
&\frac{\partial T_3}{\partial x_{R\mathrm{I}}} f_R^{\mathrm{I}} + \frac{\partial T_3}{\partial x_{R\mathrm{II}}} f_R^{\mathrm{II}} + \frac{\partial T_3}{\partial x_{R\mathrm{III}}} f_R^{\mathrm{III}} + \frac{\partial T_3}{\partial x_{M\mathrm{I}}} f_M^{\mathrm{I}} + \frac{\partial T_3}{\partial x_{M\mathrm{II}}} f_M^{\mathrm{II}} + \frac{\partial T_3}{\partial x_{M\mathrm{III}}} f_M^{\mathrm{III}} \\
&= A_{31} T_1 + A_{32} T_2 + A_{33} T_3 + B_{31} x_{M\mathrm{I}} + B_{32} x_{M\mathrm{II}} + B_{33} x_{M\mathrm{III}}
\end{aligned}
\tag{2.6}
$$

Under the above observer construction, the estimation error follows linear dynamics in z-coordinates, which is governed by the A matrix. It is selected to be Hurwitz to guarantee asymptotic stability.

2.2.3 Sampled-Data Observer

When sampling is performed at a slow rate, inter-sample behavior becomes very important and needs to be accurately estimated by the observer. For this purpose, the process model could be used to predict the evolution of output during the time period in between two consecutive measurements. The predictor is able to continuously apply a correction on the most recent sampled measurement during the sampling interval.

The inter-sample output predictor can be combined with the reduced-order observer. The orig-

inal system can be appropriately expressed in partitioned form as

$$\begin{aligned}
\dot{x}_R &= f_R(x_R, x_{Mc}, x_{Ms}) \\
\dot{x}_{Mc} &= f_{Mc}(x_R, x_{Mc}, x_{Ms}) \\
\dot{x}_{Ms} &= f_{Ms}(x_R, x_{Mc}, x_{Ms}) \\
y_c &= x_{Mc} \\
y_s &= x_{Ms}
\end{aligned}$$

where $x_{Mc} \in \mathbb{R}^{m-1}$ is the state vector that can be continuously measured, $x_{Ms} \in \mathbb{R}$ is the sampled state, y_c and y_s are the corresponding outputs. Here, the output vector is split into two parts: $(m-1)$ continuous measurements and one sampled measurement.

It is possible to estimate the rate of change of the output $\dfrac{dy_s}{dt}$ by utilizing the dynamic model of slow-sampled state variable. This leads to the following inter-sample output predictor:

$$\begin{aligned}
&\frac{d\psi}{dt} = f_{Ms}(\hat{x}_R, y_c, \psi), \quad t \in [t_k, t_{k+1}) \\
&\psi(t_k) = y_s(t_k)
\end{aligned} \tag{2.7}$$

with ψ representing the output prediction, and t_k, t_{k+1} denote two consecutive sampling instants. The predictor is reinitialized at the most recent measurement $y_s(t_k)$ and runs until the new measurement is obtained. When the continuous-time observer of Equation (2.2) is driven by the output predictor of Equation (2.7), this generates a sampled-data observer. Figure 2.2 illustrates the construction of a continuous-time reduced-order observer with an inter-sample output predictor.

In the earlier work [250], it was shown that, as long as the sampling period does not exceed a certain limit, the stability of the error dynamics and robustness with respect to measurement error for the continuous-time observer of Equation (2.2) implies the stability of the error dynamics and robustness with respect to measurement error for the sampled-data observer. In other words, the sampled-data implementation inherits the key properties of the continuous-time design, and in fact, these properties hold at all times, not just at the sampling instants.

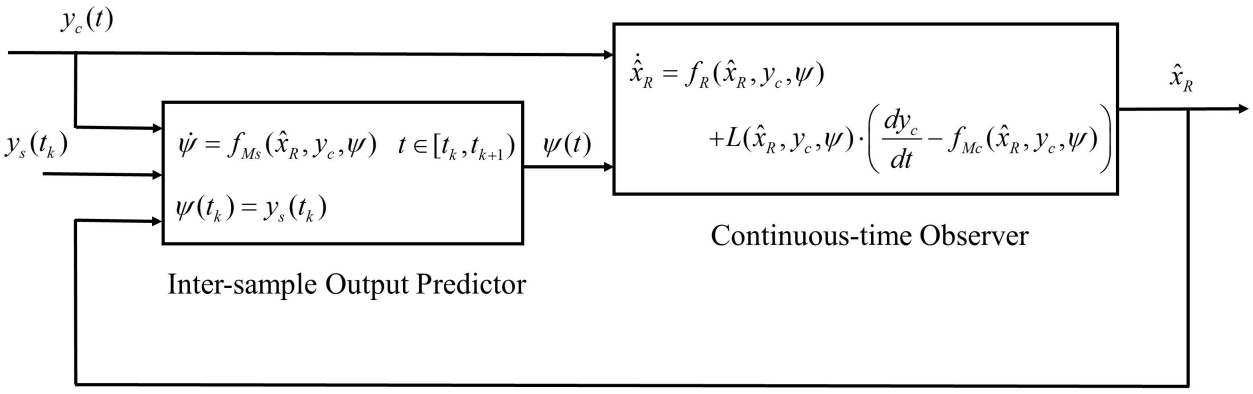

Figure 2.2: Structure of the reduced-order sampled-data observer.

2.3 A Series of Three Polycondensation Reactors

Modeling the finishing stage of PET synthesis is quite challenging owing to the complexity of reaction kinetics, coupled with mass transfer effects. For the finishing stage, plug flow reactors are commonly used because of their uniform residence time distribution, leading to a relatively narrow molecular weight distribution. In some continuous processes, a series of CSTRs are used [254]. The dynamics of plug flow polycondensation reactors can also be accurately modeled as multiple CSTRs in series [255].

For simplicity, a model of three CSTR in series, which is derived from Rafler's reaction-mass transfer model [206], will be used throughout this study. Figure 2.3 shows a three-CSTR in series configuration. In each reactor, the main polycondensation reaction and the thermal decomposition of ester groups are considered. Since the main reaction is reversible, EG, as a byproduct, has to be vaporized continuously by applying a vacuum to increase the yield of the product. The viscosity of the reaction mass also increases rapidly, which makes mass transfer a limiting factor. The dynamic process model has the following form

Dynamics in CSTR I:

$$\frac{dx_1}{dt} = \frac{1}{\tau_1}(x_{1,in} - x_1) - (\beta a)_1(x_1 - {x_1}^*) + \frac{1}{2}k_1({x_2}^2 - 8x_1x_4)$$
$$\frac{dx_2}{dt} = \frac{1}{\tau_1}(x_{2,in} - x_2) - k_1({x_2}^2 - 8x_1x_4)$$
$$\frac{dx_3}{dt} = \frac{1}{\tau_1}(x_{3,in} - x_3) + k_2x_4$$
$$\frac{dx_4}{dt} = \frac{1}{\tau_1}(x_{4,in} - x_4) + \frac{1}{2}k_1({x_2}^2 - 8x_1x_4) - k_2x_4$$

Dynamics in CSTR II:

$$\frac{dx_5}{dt} = \frac{1}{\tau_2}(x_1 - x_5) - (\beta a)_2(x_5 - {x_5}^*) + \frac{1}{2}k_1({x_6}^2 - 8x_5x_8)$$
$$\frac{dx_6}{dt} = \frac{1}{\tau_2}(x_2 - x_6) - k_1({x_6}^2 - 8x_5x_8)$$
$$\frac{dx_7}{dt} = \frac{1}{\tau_2}(x_3 - x_7) + k_2x_8$$
$$\frac{dx_8}{dt} = \frac{1}{\tau_2}(x_4 - x_8) + \frac{1}{2}k_1({x_6}^2 - 8x_5x_8) - k_2x_8$$

Dynamics in CSTR III:

$$\frac{dx_9}{dt} = \frac{1}{\tau_3}(x_5 - x_9) - (\beta a)_3(x_9 - {x_9}^*) + \frac{1}{2}k_1({x_{10}}^2 - 8x_9x_{12})$$
$$\frac{dx_{10}}{dt} = \frac{1}{\tau_3}(x_6 - x_{10}) - k_1({x_{10}}^2 - 8x_9x_{12})$$
$$\frac{dx_{11}}{dt} = \frac{1}{\tau_3}(x_7 - x_{11}) + k_2x_{12}$$
$$\frac{dx_{12}}{dt} = \frac{1}{\tau_3}(x_8 - x_{12}) + \frac{1}{2}k_1({x_{10}}^2 - 8x_9x_{12}) - k_2x_{12}$$

All three reactors are operated at constant temperature and pressure. There are four states in each reactor: the concentration of EG (x_1, x_5 and x_9), hydroxyl end groups (x_2, x_6 and x_{10}), carboxyl end groups (x_3, x_7 and x_{11}) and ester groups (x_4, x_8 and x_{12}). The concentration of EG on the melt surface is denoted by the superscript *.

A two-film model is applied to describe mass transfer of volatiles in the finishing stage of melt polycondensation under high conversion. It is postulated that there is a concentration gradient of

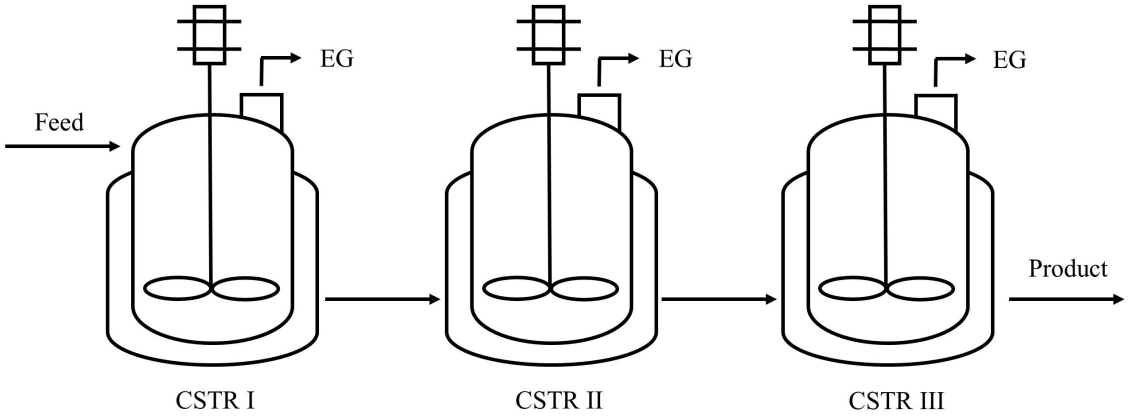

Figure 2.3: Schematic of three CSTRs in series in the polycondensation stage.

the volatile species throughout a liquid film near the gas-liquid interface, which is based on the existence of mass transfer resistance at the interface due to the high viscosity of the reaction mixture. Kim [256] verified the two-phase mass transfer model from experimental data in a polycondensation system and showed that the mass transfer resistance model provided accurate prediction of molecular weight and product composition over the entire stages. The interfacial equilibrium concentration of EG is calculated by using the Flory-Huggins equation (see [256] for equations; see [257, 258] for physical property parameters). The system parameters used in the simulations are given in Table 2.1.

Parameter	Description	Value
T	reactor temperature	553.15 K
P	reactor pressure	130 Pa
R	gas constant	1.987 cal/(mol·K)
$\tau_{1,2,3}$	residence time of each CSTR	60 min
k_1	rate constant of polycondensation reaction[2]	1.36×10^6 exp(−18,500/(RT)) L/(mol·min)
k_2	rate constant of thermal decomposition	7.20×10^9 exp(−37800/(RT)) min^{-1}
$(\beta a)_1$	mass transfer parameter in CSTR I[3]	2.70 min^{-1}
$(\beta a)_2$	mass transfer parameter in CSTR II[4]	2.03 min^{-1}
$(\beta a)_3$	mass transfer parameter in CSTR III	1.35 min^{-1}

Table 2.1: System parameters.

In the reactor simulation, the following assumptions are made: (i) only EG exists in the vapor phase; (ii) the mass transfer resistance on the gas side is negligible; (iii) the concentration of vinyl end groups in the feed is equal to the concentration of carboxyl end groups; (iv) the mass transfer parameter does not change over time in each reactor. The operating conditions of the three reactors are given in Table 2.2, where [OH], [COOH] stand for the hydroxyl and carboxyl end groups, and [Z] is the concentration of ester groups.

Concentration[5]	CSTR#	[EG]	[OH]	[COOH]	[Z]
Feed[6]	CSTR I	6.5×10^{-3}	0.40	2.57×10^{-3}	11.2
Initial Condition	CSTR I	2.0×10^{-3}	0.40	2.57×10^{-3}	8.0
	CSTR II	1.0×10^{-3}	0.30	5.10×10^{-3}	8.0
	CSTR III	6.0×10^{-4}	0.24	6.31×10^{-3}	8.1
Steady State	CSTR I	5.645×10^{-4}	0.283	8.203×10^{-3}	11.25
	CSTR II	4.046×10^{-4}	0.226	1.385×10^{-2}	11.28
	CSTR III	3.470×10^{-4}	0.197	1.950×10^{-2}	11.28

Table 2.2: Operating conditions and steady states.

[2]The rate constants of polycondensation reaction k_1 and thermal decomposition k_2 are obtained from [258].

[3]The mass transfer parameter $(\beta a)_1$ is obtained from [259].

[4]The mass transfer parameters in the last two reactors $(\beta a)_2$, $(\beta a)_3$ are assigned as follows: $(\beta a)_2 = 75\% \times (\beta a)_1$, $(\beta a)_3 = 50\% \times (\beta a)_1$.

[5]All of the concentrations are in units of mol/L.

[6]The feed condition is obtained from [260], which is the reactor outflow from the pre-polymerization stage.

As pointed out in Section 2.1, the number of on-line measurements in the polycondensation reactors is limited. In particular, measurements of various functional end groups are usually off-line, infrequent and delayed. In this study, two possible measurements are involved: one is continuous and the other is slow-sampled with dead time. The concentration of hydroxyl end groups can be obtained from a correlation using continuously-measured torque, temperature, and stirrer speed, which needs to be calibrated for the specific reactor [248]. This can be considered as a continuous measurement without time delay. The carboxyl concentration can be obtained by using acidimetric titration [261], which has a lower sampling rate and an approximately twenty-minute delay. DP is calculated from the state estimates using the following formula:

$$\text{DP} = 1 + \frac{2[\text{Z}]}{[\text{OH}] + [\text{COOH}] + [\text{E}_v]}$$

where $[\text{E}_v]$ denotes the concentration of vinyl end groups.

2.4 State Estimation via Reduced-Order Observer

Linear observability analysis was performed in two cases: (i) only hydroxyl end groups (x_2, x_6 and x_{10}) are continuously measured; (ii) in addition to hydroxyl end groups, carboxyl end groups (x_3, x_7 and x_{11}) are also measured by using on-line acidimetric titration. In Case (i), the conclusion is that the system is not observable, because carboxyl end groups are "downstream" relative to the hydroxyl end groups. It should be noticed that the interfacial concentration of EG does not depend on the state variables in the reactor. In Case (ii), the system of CSTRs is observable. The results of observability analysis suggest that the carboxyl measurement is necessary for accurate estimation of the states and therefore, of DP, and it should be utilized in the observer despite its low sampling rate.

From a physical point of view, the system of three CSTRs clearly possesses a serial structure: the outflow of the preceding reactor is the feed for the next reactor. Hence, it is straightforward to design sequential observers by taking advantage of the particular LBT structure, which is described in Section 2.2.2. The interconnection of these subsystems is shown in Figure 2.4, from which the

unobservability in the absence of carboxyl measurements is clearly visible.

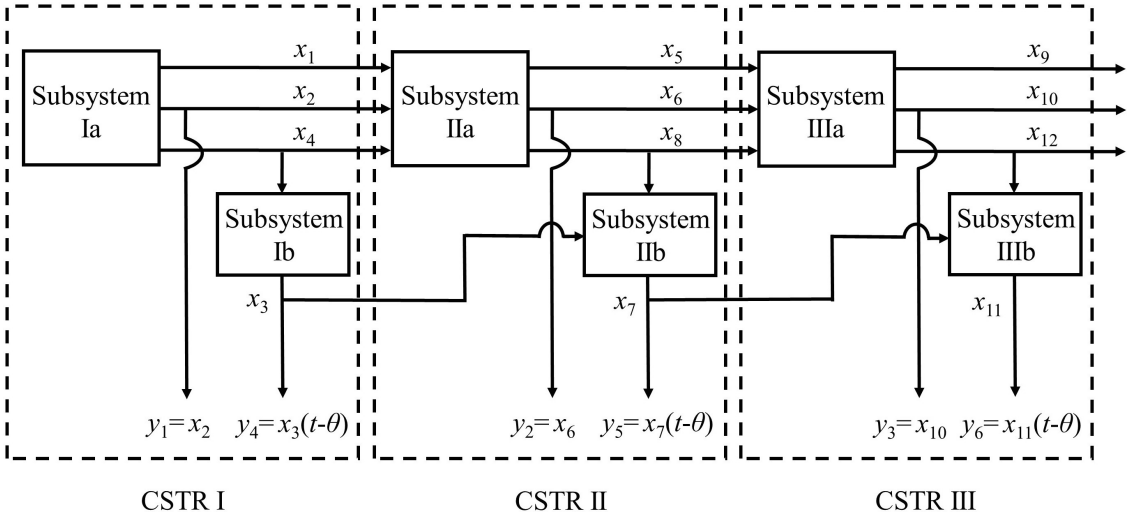

Figure 2.4: Subsystems representation of three CSTRs in series.

2.4.1 State Estimation with Continuous Measurement Exclusively

In Case (i), the output vector $y = \begin{bmatrix} x_2 & x_6 & x_{10} \end{bmatrix}^T$ represents the concentrations of hydroxyl end groups in three polycondensation reactors, which are continuously measured. Despite the fact that the entire system is unobservable in the absence of carboxyl measurement, if only Subsystems Ia, IIa and IIIa are taken into account, the new system becomes observable. In other words, the concentrations of EG and ester groups can be estimated by using only hydroxyl measurement. For the specific system (i.e., Ia, IIa and IIIa), we have implemented observer Equation (2.4) with state-dependent gain computed from Equation (2.5), where the mapping function $T(x)$ is a solution of the system of PDEs of Equation (2.6) with design parameters A and B. Two different choices of the A matrix, with different sets of eigenvalues, are considered in the simulations: "fast" (-2.0, -1.8, -1.6, -1.4, -1.2, -1.0) and "slow" (-0.2, -0.18, -0.16, -0.14, -0.12, -0.1). Truncation order N = 3 is used considering the balance between the accuracy of the approximate PDE solutions and computation time. The initial guess of the estimates is given in Table 2.3.

CSTR#	[EG] (mol/L)	[COOH] (mol/L)	[Z] (mol/L)
CSTR I	1.0×10^{-3}	7.57×10^{-3}	10.0
CSTR II	0	1.01×10^{-2}	10.0
CSTR III	1.6×10^{-3}	1.13×10^{-2}	10.1

Table 2.3: Initial estimated values for the observer.

As a result of being the "downstream" states, carboxyl dynamics are detached from Subsystems Ia, IIa and IIIa. An open-loop observer is designed to estimate the concentrations of carboxyl end groups, because their dynamics are open-loop stable. The open-loop observer equations are given as follows

$$\begin{aligned}
\frac{d\hat{x}_3}{dt} &= \frac{1}{\tau_1}(x_{3,in} - \hat{x}_3) + k_2\hat{x}_4 \\
\frac{d\hat{x}_7}{dt} &= \frac{1}{\tau_2}(\hat{x}_3 - \hat{x}_7) + k_2\hat{x}_8 \\
\frac{d\hat{x}_{11}}{dt} &= \frac{1}{\tau_3}(\hat{x}_7 - \hat{x}_{11}) + k_2\hat{x}_{12}
\end{aligned}$$

with $\hat{x}_4$, $\hat{x}_8$ and $\hat{x}_{12}$ obtained from the observer equations driven by the continuous measurements y_1, y_2 and y_3.

Figure 2.5 shows the performance of the reduced-order observer with the "fast" eigenvalues by comparing the actual and estimated states, as well as the DP in all three CSTRs. Consequently, the concentrations of EG and ester groups converge to the actual states very fast. Since the unobservable states (i.e., concentrations of carboxyl end groups) are estimated from an open-loop observer, the speed of convergence depends on the dynamics itself, and this is not adjustable. Therefore, it takes much longer to converge, which also explains the offset in the DP estimates in the beginning. However, the offset will be eliminated eventually as $\hat{x}_3$, $\hat{x}_7$ and $\hat{x}_{11}$ converge.

2.4.2 State Estimation with Both Measurements

In Case (ii), both the continuous and slow-sampled measurements are utilized in the observer design. Instead of using an open-loop observer, an inter-sample output predictor is used to estimate the evolution of the slow-sampled output between two consecutive sampling instants. At the same

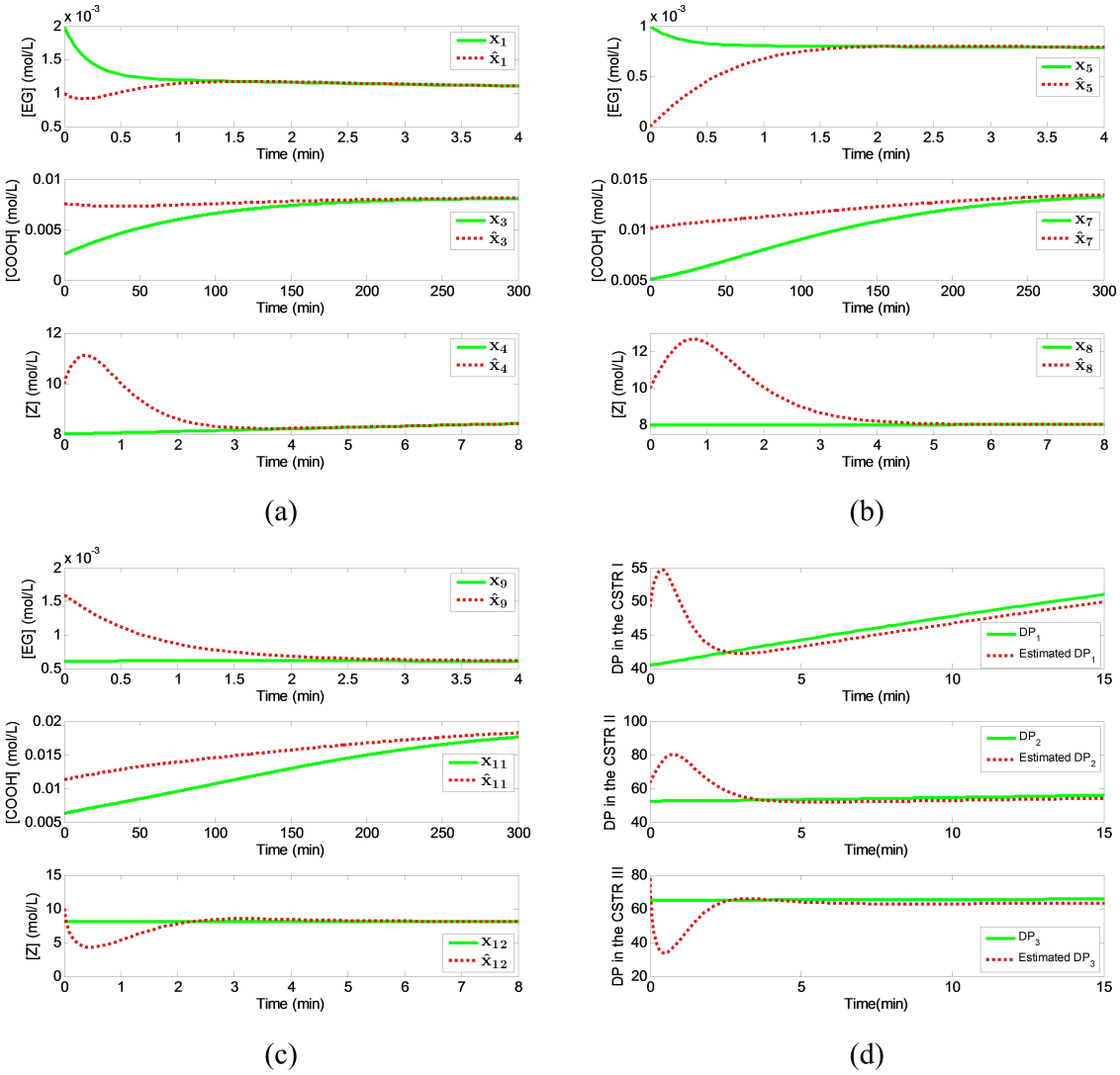

Figure 2.5: Performance of the reduced-order observer with the "fast" eigenvalues: (a) actual and estimated states in CSTR I; (b) actual and estimated states in CSTR II; (c) actual and estimated states in CSTR III; (d) actual and estimated degree of polymerization in all three CSTRs.

time, dead time compensation is carried out to account for the time delay between the present time and sensor dead time. For acidimetric titration, it is assumed that there is a ten-minute sampling interval, and the dead time of the sensor is twenty minutes. It should be noticed that the output of the predictor does not feed into the reduced-order observer because carboxyl concentrations do not affect the other states and are not used in the estimation of concentrations of EG and ester groups. However, they will affect the estimation of DP. In this case, the dead time compensator is actually

combined with the inter-sample output predictor, demonstrated as follows

$$\begin{aligned}
\frac{d\hat{y}_4}{dt} &= \frac{1}{\tau_1}(x_{3,in} - \hat{y}_4) + k_2\hat{x}_4, \quad t \in [t_k - \theta, t_k + \eta) \\
\frac{d\hat{y}_5}{dt} &= \frac{1}{\tau_2}(\hat{y}_4 - \hat{y}_5) + k_2\hat{x}_8, \qquad t \in [t_k - \theta, t_k + \eta) \\
\frac{d\hat{y}_6}{dt} &= \frac{1}{\tau_3}(\hat{y}_5 - \hat{y}_6) + k_2\hat{x}_{12}, \qquad t \in [t_k - \theta, t_k + \eta) \\
\hat{y}_4 &= y_4(t_k) \\
\hat{y}_5 &= y_5(t_k) \\
\hat{y}_6 &= y_6(t_k)
\end{aligned}$$

where the state estimates $\hat{x}_4$, $\hat{x}_8$ and $\hat{x}_{12}$ are obtained from the continuous-time observer. y_4, y_5 and y_6 are the delayed outputs with dead time θ, while $\hat{y}_4$, $\hat{y}_5$ and $\hat{y}_6$ are the estimates at the present time, respectively. The three equations are reinitialized at the most recent measurement at t_k and run from $t_k - \theta$ to $t_k + \eta$, where η is the length of the sampling interval. It serves as a dead time compensator between $t_k - \theta$ and t_k and also serves as an inter-sample output predictor between t_k and $t_k + \eta$. In the first θ time units of each simulation, an open-loop observer is used for estimating the carboxyl end groups, because there is no measurement information available.

In Figure 2.6, the convergence speed of EG and ester groups is slow because the "slow" eigenvalues are chosen in this case. In the estimates of carboxyl concentrations, a few steps are observed, because the slow-sampled measurement makes a correction on the predictor output when the most recent measurement becomes available each time. In addition, the observer together with the inter-sample output predictor and the dead time compensator can estimate the DP accurately in all three CSTRs.

2.4.3 Observer Performance under Sensor Noise

While the reduced-order observer is computationally more efficient by reconstructing only unmeasured state variables, it suffers from sensitivity to sensor noise. Therefore, the performance of the reduced-order observer needs to be tested under sensor noise. Pre-filtering of the measurement

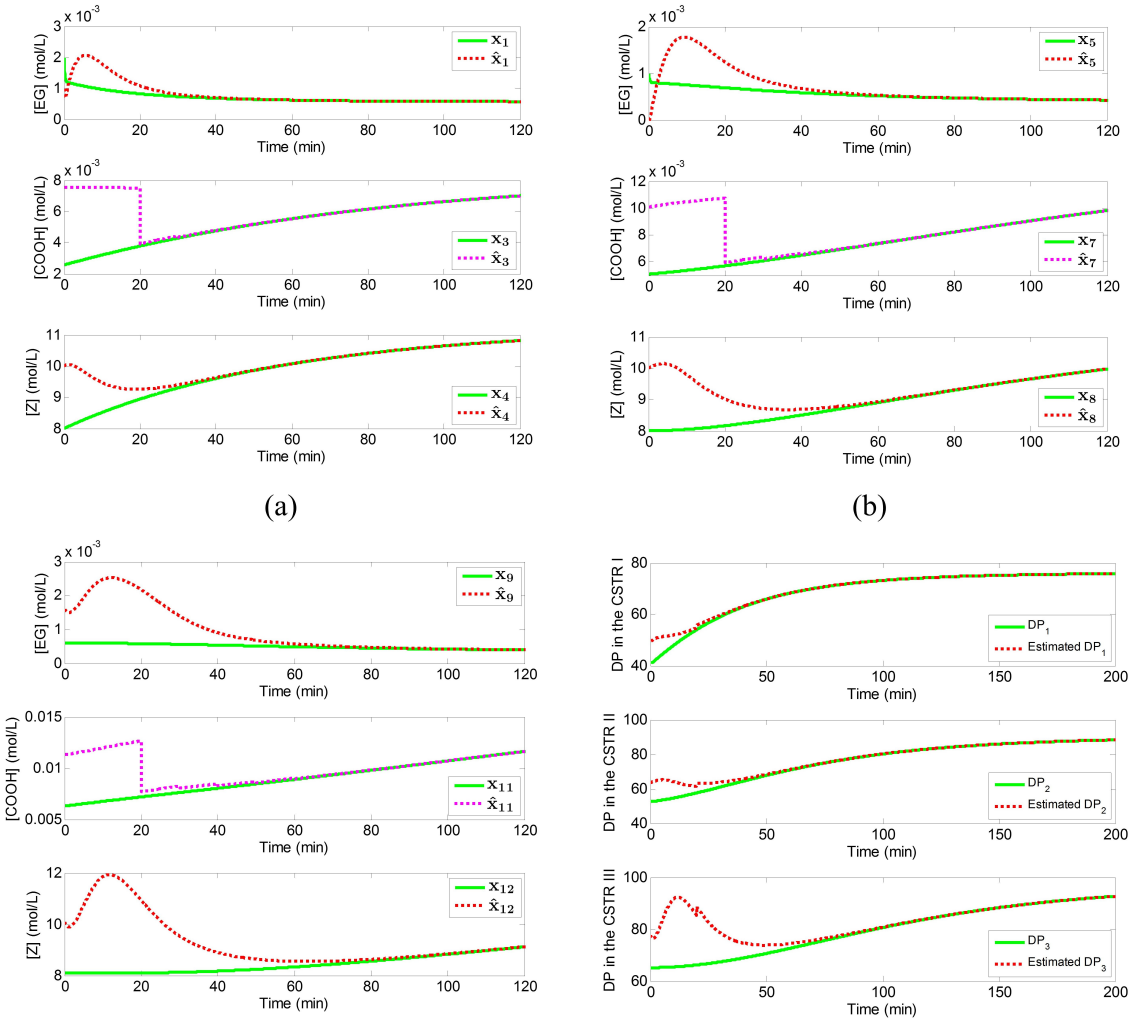

Figure 2.6: Performance of the reduced-order observer with "slow" eigenvalues when using both measurements: (a) actual and estimated states in CSTR I; (b) actual and estimated states in CSTR II; (c) actual and estimated states in CSTR III; (d) actual and estimated degree of polymerization in all three CSTRs.

signal may be necessary to cut out the noise, which inevitably introduces some lag.

Figure 2.7 shows that the same level of white noise is added to all three hydroxyl measurements with a standard deviation equal to 0.01. A first-order filter is employed to cut out the high frequency noise. The following filter factors, 0.005, 0.005, and 0.007, are selected respectively, according to the level of filtering needed. As expected, we can see lags in the filtered signal by comparing it with the actual state. Meanwhile, white noise with a standard deviation of 3×10^{-4} is also considered

for the on-line sampled titration measurements. Figure 2.7(d) shows the evolution of estimated and actual DP when the sensor noise is introduced. Despite the fact that the estimates deviate from the actual state quite significantly in the beginning, fairly accurate estimation is achieved after 70 min. The "slow" eigenvalues are used here because the "fast" eigenvalues will lead to a more aggressive response which may adversely affect observer performance.

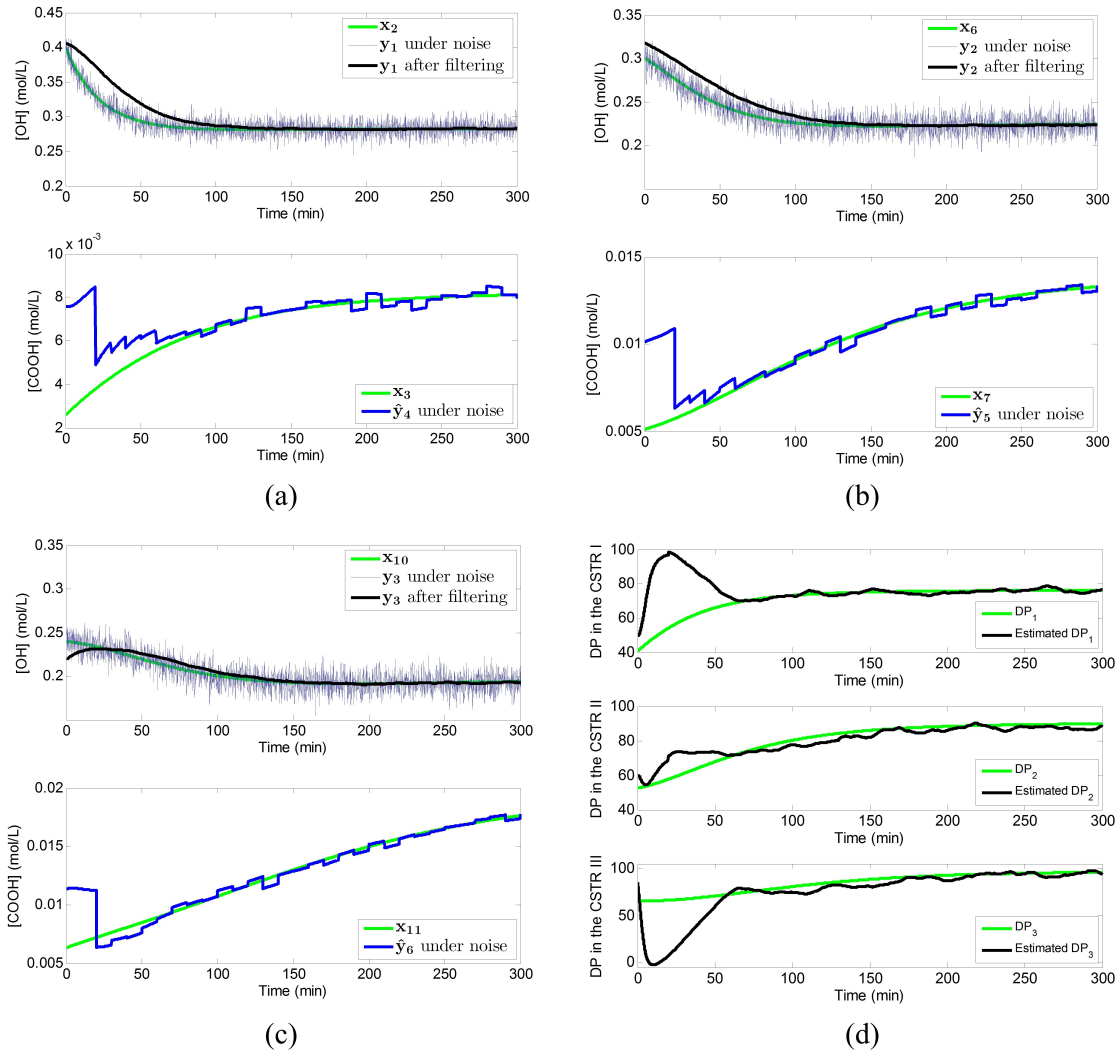

Figure 2.7: Measurement signals before (blue) and after (black) pre-filtering: (a) in CSTR I; (b) in CSTR II; (c) in CSTR III. Observer performance: (d) actual and estimated degree of polymerization in all three CSTRs.

2.5 Conclusions

This chapter presents an application of a nonlinear state observer for monitoring DP in a series of PET polycondensation reactors. By exploiting the special LBT structure of the system, sequential observers are designed, and as a result, the complexity of the state dependence of the observer gains is reduced. The unmeasurable states of EG and ester groups' concentrations are accurately estimated by using a reduced-order observer when only the continuous measurement is considered. The rate of convergence is adjustable by tuning the eigenvalues of the design parameter A. When the slow-sampled measurement of carboxyl end groups is also available, an inter-sample output predictor is used to estimate the evolution of the sampled output between two consecutive sampling instants. Furthermore, dead time compensation is used to compensate for the effect of delay in the output. Simulation results show that the degree of polymerization of PET is accurately estimated in all three reactors when both continuous and sampled measurements are considered. Even in the presence of sensor noise, the observer is still able to provide good estimates after applying pre-filtering.

3. MULTI-RATE OBSERVER DESIGN IN LINEAR SYSTEMS *

The necessity of developing a general observer design method that accounts for different sampling rates and measurement delays was explained in Chapter 1. Chapter 2 presented the observer design in a series of three polycondensation reactors where one continuous, delay-free measurement and one sampled, delayed measurement were considered. However, the problem of multi-rate observer design was bypassed because the sampled discrete measurement was not an input for the continuous-time observer, as a consequence of its special system structure.

In this chapter, the problem of state observer design in linear multi-output systems with asynchronous sampling is addressed. The proposed multi-rate observer is based on a continuous-time Luenberger observer design coupled with an inter-sample predictor for each sampled measurement, which generates an estimate of the output in between consecutive measurements. The sampling times are not necessarily uniformly spaced, but there exists a maximum sampling period among all the sensors. Sufficient and explicit conditions are derived to guarantee exponential stability of the multi-rate observer. The proposed framework of multi-rate observer design is examined through a mathematical example and a gas-phase polyethylene reactor. In the latter case, the amount of active catalyst sites is estimated, with a convergence rate that is comparable to the case of continuous measurements [52].

This chapter is organized as follows. In Section 3.2, the continuous-time reduced-order Luenberger observer design will be reviewed, which will serve as the basis for the multi-rate observer to be proposed in Section 3.3. An analytic proof of exponential stability of the multi-rate observer will be the provided in Section 3.3, including a special case where only continuous and single-rate measurements are involved. The effectiveness and applicability of the proposed multi-rate observer will be illustrated through two case studies in Section 3.4. In Section 3.5, conclusions are drawn from the results of the previous sections.

*Reprinted with permission from "Multi-Rate Observer Design for Process Monitoring Using Asynchronous Inter-Sample Output Predictions" by C. Ling and C. Kravaris, 2017. *AIChE Journal*, 63(8), 3384–3394, Copyright 2017 by John Wiley and Sons.

3.1 Introduction

Effective control and monitoring of chemical processes require frequent and reliable information acquisition on the essential state variables. Very often, the quantities related to safety, product quality, and/or economic performance of a chemical process cannot be measured on line. A state estimator, as a soft sensor, provides an alternative approach to reconstruct the states by utilizing the available measurements and a dynamic process model (see [5, 262, 263] and references therein). The problem of state estimator design has been widely studied for the systems under fast sampling [54,55,130,132,148,155,264]. However, a key issue in the operation of chemical processes is that the measurements are not available at the same rate. For example, temperature or liquid level can be continuously measured, while molecular weight or melt index is only available at infrequent and irregular times. Despite their slow sampling rate, the measurements that provide important quality information on the products, should be incorporated in an intelligent manner together with the continuous measurements, to make the entire system observable as well as improve the estimation accuracy.

The need for multi-rate estimation has been well recognized in polymer and biochemical industries since late 1980's [29, 241, 246, 265–269]. The problem of multi-rate estimation has been mainly studied in the extended Kalman filter framework [5]. A two-time-scale EKF was developed to accommodate both frequent and infrequent, delayed measurements in [29,265,266]. A fixed-lag smoothing based EKF algorithm was proposed for systems with multi-rate measurements in [267]. The performance was evaluated via an emulsion copolymerization batch process, which is shown to be superior to the standard EKF. Other multi-rate estimation methods, including state observer design [241, 246, 268], and moving horizon estimation [269–272], have also been investigated. In the multi-rate observer design, the method of least squares was used on the most-recent, infrequent measurements to predict the inter-sample behavior in [246, 268]. Under moderate nonlinearity and sampling period, this multi-rate observer was able to calculate reliable, continuous estimates in the presence of disturbances and model mismatch.

EKF and MHE-based approaches are primarily implemented by using an exact or approximate

discrete-time process model. Although it is a reasonable approach in the presence of sampled measurements, the inter-sample dynamic behavior is completely lost and the continuous measurements are not utilized in an efficient way. Furthermore, mismatch between the time step of the discrete-time model and the actual sampling schedule also induces estimation error. Despite the fact that fairly good estimation results have been achieved in the aforementioned studies, stability analysis of a multi-rate estimator remained open due to the asynchronous nature of measurements.

Motivated by the Luenberger observer developed in [55], the problem of designing single-rate sampled-data observers in a continuous-time manner has attracted lots of attention in the literature. One proposed approach is based on the continuous-discrete observer design method for a certain class of nonlinear systems, where a continuous-time observer runs in open-loop, with a reset map acting at the sampling instants [273–276]. Another approach is based on the design of observer matrices via linear matrix inequality (LMI), where an inter-sample injection term is introduced in between consecutive samples based on a continuous processing of the most-recent measurements [277, 278]. Sufficient conditions subject to the solvability of LMIs were established to guarantee global exponential stability of the error dynamics. Recently, a single-rate sampled-data observer was proposed using a continuous-time design coupled with an inter-sample output predictor, which utilizes the dynamic model to estimate the evolution of the output in between samples [250]. This idea was further exploited in the sampled-data observer design for nonlinear systems with delayed measurements in [279].

As mentioned before, the asynchronous nature of different sensors and uncertainty in the sampling schedule pose great challenges in the multi-rate observer design, even for linear systems. An approach that was recently proposed in [280] involves modeling each sensor as a sample-and-hold device and deriving sufficient Krasovskii-based conditions in terms of LMIs for the observer design in linear multi-rate sampled-data systems, given some maximum allowable sampling period for each sensor.

In this chapter, a new method for multi-rate observer design in linear systems will be proposed, where, for each slow-sampled measurement, an output predictor will be used in the same spirit as

in [250]. Differently from the aforementioned work (i.e., [280]), presence of possible continuous measurements is also considered in this framework. Therefore, the output map is of hybrid nature as opposed to just sampled-data outputs. In addition, the proposed approach offers a more meaningful way to approximate the inter-sample behavior by using model-based prediction instead of sample-and-hold strategy. The focus of Chapter 3 will be on the design of multi-rate reduced-order observers, however, the design of multi-rate full-order observer can be formulated in the same fashion as will be mentioned later. An analytic proof of exponential stability of the error dynamics will be provided, in the same spirit as the stability analysis of a networked control system with general multiple-packet transmission in [281]. As a special case, the stability condition of the multi-rate observer for a class of systems with continuous outputs and single-rate sampled outputs is also derived but in a different way, which gives a less conservative stability bound. The effectiveness and applicability of the proposed design is demonstrated through numerical examples of a third-order system and an industrial gas-phase polyethylene reactor.

3.2 Preliminaries

3.2.1 Notations

Throughout this chapter, the zero matrix and identity matrix of appropriate size are denoted by 0 and I, respectively. The operator $\|\cdot\|$ denotes the Euclidean norm of a vector or a matrix. For a matrix A, A' denotes its transpose matrix. If A is square, A^{-1} denotes the inverse matrix, $\rho(A)$ denotes the spectral radius, and $\lambda_{\min}(A)$ and $\lambda_{\max}(A)$ denote the smallest and largest eigenvalues of A, respectively. t_k represents the k-th sampling time in a system with sampled outputs. For any function $x : \mathbb{R} \to \mathbb{R}^n$, we define $x(t_k^+) = \lim_{h\to 0} x(t_k + h)$.

3.2.2 Reduced-Order Luenberger Observer Design

In the presence of multiple measurements, it makes more sense to use a reduced-order observer so that a significantly lower dimensionality can ease implementation of the observer. Therefore, a reduced-order observer formulation will be the focus in the chapter. However, as will be discussed in this chapter, a very similar approach can be applied to the multi-rate full-order observer design

as well.

Let us consider a continuous-time linear system, where without loss of generality, the output is assumed to be a part of the state vector

$$\begin{aligned} \dot{x}_R(t) &= F_{11}x_R(t) + F_{12}x_M(t) + G_1u(t) \\ \dot{x}_M(t) &= F_{21}x_R(t) + F_{22}x_M(t) + G_2u(t) \\ y(t) &= x_M(t) \end{aligned} \tag{3.1}$$

where $x_R \in \mathbb{R}^{n-m}$ denotes the unmeasured state vector, $x_M \in \mathbb{R}^m$ denotes the remaining state vector that is directly measured, y is the output vector, $u \in \mathbb{R}^q$ is the control input. F_{11}, F_{12}, F_{21}, F_{22}, G_1 and G_2 are matrices of appropriate dimensions. Suppose that the system of Equation (3.1) is observable and a continuous-time reduced-order observer design is available

$$\begin{aligned} \dot{z}(t) &= Az(t) + By(t) + Wu(t) \\ \hat{x}_R(t) &= {T_R}^{-1}(z(t) - T_M y(t)) \end{aligned} \tag{3.2}$$

where $z \in \mathbb{R}^{n-m}$ is the observer state, A is a Hurwitz matrix with desired eigenvalues, B is a matrix which forms a controllable pair with A, the matrix $W = T_R G_1 + T_M G_2$, and transformation matrices T_R, T_M satisfy the following Sylvester equation:

$$\begin{bmatrix} T_R & T_M \end{bmatrix} \begin{bmatrix} F_{11} & F_{12} \\ F_{21} & F_{22} \end{bmatrix} = A \begin{bmatrix} T_R & T_M \end{bmatrix} + B \begin{bmatrix} 0 & I \end{bmatrix} \tag{3.3}$$

Remark 2. *According to a well-known result [55], the stated assumptions: observability of the pair (F_{11}, F_{21}), controllability of the pair (A, B), and the matrices A and $\begin{bmatrix} F_{11} & F_{12} \\ F_{21} & F_{22} \end{bmatrix}$ not having common eigenvalues, should be satisfied to guarantee uniqueness of T_R and T_M, and the invertibility of T_R.*

3.3 Main Results

3.3.1 Proposed Multi-Rate Observer Design

Now consider a linear system of Equation (3.1) with $x_M(t)$ partitioned as $x_M = \begin{bmatrix} x_c' & x_d' \end{bmatrix}'$ to distinguish between continuous and sampled outputs

$$\begin{aligned} \begin{bmatrix} \dot{x}_R(t) \\ \dot{x}_c(t) \\ \dot{x}_d(t) \end{bmatrix} &= \begin{bmatrix} F_{11} & F_{12} & F_{13} \\ F_{21} & F_{22} & F_{23} \\ F_{31} & F_{32} & F_{33} \end{bmatrix} \begin{bmatrix} x_R(t) \\ x_c(t) \\ x_d(t) \end{bmatrix} + \begin{bmatrix} G_1 \\ G_2 \\ G_3 \end{bmatrix} u(t) \\ y_c(t) &= x_c(t) \\ y_d^i(t_k) &= x_d^i(t_j^i), \qquad k, j \in \mathbb{Z}^+, i = 1, 2, \ldots, m_d \end{aligned} \tag{3.4}$$

where $x_R \in \mathbb{R}^{n-m_c-m_d}$ is the unmeasured state vector, $x_c \in \mathbb{R}^{m_c}$ is the continuously measured state vector, $x_d \in \mathbb{R}^{m_d}$ is the remaining state vector that is slow-sampled, y_c denotes the continuous outputs, and y_d denotes the sampled outputs with different rates. t_j^i denotes the j-th sampling time for the i-th component in x_d, at some countable set of time instants. At a specific time, there may be measurements of more than one output. The sampling times for each sensor are not necessarily uniformly spaced, but there exists a maximum sampling period, τ_m, among all the sensors.

Motivated by [250], the question we consider here is whether the continuous-time observer of Equation (3.2) could still be the basis in the presence of "medium-size" sampling periods, when coupled with inter-sample predictors to estimate the output behavior between measurements. For the multi-rate system of Equation (3.4), the inter-sample output predictor will be utilized for each sampled output in y_d. These predictors will operate continuously at different time horizons, whose values need to feed the continuous-time observer. For $t \in [t_k^+, t_{k+1}]$ (notice that t_k, t_{k+1} are not necessarily the sampling times from the same sensor), we propose the following design of multi-

rate reduced-order observer

$$\begin{aligned}
\dot{z}(t) &= Az(t) + B_c y_c(t) + B_d w(t) + Wu(t) \\
\dot{w}(t) &= F_{31}\hat{x}_R(t) + F_{32}y_c(t) + F_{33}w(t) + G_3 u(t) \\
w^i(t_k^+) &= y_d^i(t_k) \\
\hat{x}_R(t) &= T_R^{-1}(z(t) - T_{Mc}y_c(t) - T_{Md}w(t))
\end{aligned} \tag{3.5}$$

with $w \in \mathbb{R}^{m_d}$ being the vector of predicted outputs during each sampling interval, and w^i being the i-th predicted state which is reinitialized once a measurement becomes available at t_k. Notice that only the associated component in w vector will get reinitialized and the others do not change until their measurements become available. Since the system contains continuous and sampled outputs, the matrices T_M and B in Equation (3.2) are partitioned into T_{Mc}, T_{Md} and B_c, B_d respectively, with appropriate dimensions from the continuous-time design. The multi-rate observer of Equation (3.5) possesses hybrid nature and demonstrates impulsive behavior at sampling times.

We label the estimation error in x-coordinates $e_R(t) = x_R(t) - \hat{x}_R(t)$, output prediction error $e_w(t) = x_d(t) - w(t)$, and observer error $e_z(t) = T_R e_R(t) + T_{Md}e_w(t)$. The estimation error $e_R(t)$ can also be written as $T_R^{-1}e_z(t) - T_R^{-1}T_{Md}e_w(t)$. Notice that $e_R(t)$ and $e_z(t)$ are estimation errors in different coordinates, so they are virtually the same after coordinates transformation. Consider the error dynamics of $e_z(t)$ and $e_w(t)$ in the sampling interval $[t_k^+, t_{k+1}]$

$$\begin{bmatrix} \dot{e}_z(t) \\ \dot{e}_w(t) \end{bmatrix} = \begin{bmatrix} A & B_d \\ F_{31}T_R^{-1} & F_{33} - F_{31}T_R^{-1}T_{Md} \end{bmatrix} \begin{bmatrix} e_z(t) \\ e_w(t) \end{bmatrix} \tag{3.6}$$

For simplicity, we denote

$$M = \begin{bmatrix} A & B_d \\ F_{31}T_R^{-1} & F_{33} - F_{31}T_R^{-1}T_{Md} \end{bmatrix} \tag{3.7}$$

Remark 3. *The multi-rate observer of Equation (3.5) can be applied to estimate the state of multi-*

rate sampled-data systems in [280], if there are exclusively sampled outputs, i.e., for systems in the form

$$\begin{bmatrix} \dot{x}_R(t) \\ \dot{x}_d(t) \end{bmatrix} = \begin{bmatrix} F_{11} & F_{12} \\ F_{21} & F_{22} \end{bmatrix} \begin{bmatrix} x_R(t) \\ x_d(t) \end{bmatrix} + \begin{bmatrix} G_1 \\ G_2 \end{bmatrix} u(t)$$
$$y_d^i(t_k) = x_d^i(t_j^i), \quad k, j \in \mathbb{Z}^+, i = 1, 2, \ldots, m_d$$

Inter-sample predictors, which are operating at different time horizons, are used for each sampled measurement to estimate the evolution of the output in between consecutive samples. This provides a more meaningful approach to predict the inter-sample behavior as opposed to a simple sample-and-hold policy.

Remark 4. *Since the design parameter A is Hurwitz, there exists a unique symmetric positive definite matrix P, satisfying the Lyapunov equation:*

$$A'P + PA = -I \tag{3.8}$$

We define $\sigma_1 = \lambda_{\min}(P)$ and $\sigma_2 = \lambda_{\max}(P)$. The following stability analysis is derived based on Lyapunov's second method and the prediction error is treated as a vanishing perturbation on the system. So choosing the right-hand side of Equation (3.8) equal to $-I$ is desirable for maximizing the tolerable perturbation bound [282].

Remark 5. *The continuous-time observer design coupled with inter-sample output predictors can be applied to build multi-rate full-order observers, under appropriate modifications. Consider a system in the form*

$$\dot{x}(t) = Fx(t) + Gu(t)$$
$$y_c(t) = H_c x(t)$$
$$y_d^i(t_k) = H_d^i x(t_k), \quad k \in \mathbb{Z}^+, i = 1, 2, \ldots, m_d$$

where H_c is the continuous-time output matrix, and H_d^i is the i-th row of the discrete-time output matrix. Likewise, we show the multi-rate full-order observer design for $t \in [t_k^+, t_{k+1}]$

$$\begin{aligned}
\dot{z}(t) &= Az(t) + B_c y_c(t) + B_d w(t) + Wu(t) \\
\dot{w}(t) &= H_d F\hat{x}(t) + H_d Gu(t) \\
w^i(t_k^+) &= y_d^i(t_k) \\
\hat{x}(t) &= T^{-1}z(t)
\end{aligned} \tag{3.9}$$

where $W = TG$ and the transformation matrix T satisfies the following Sylvester equation:

$$TF = AT + B_c H_c + B_d H_d$$

For $t \in [t_k^+, t_{k+1}]$, the error dynamics of the augmented state vector satisfies

$$\begin{bmatrix} \dot{e}_z(t) \\ \dot{e}_w(t) \end{bmatrix} = \begin{bmatrix} A & B_d \\ H_d F T^{-1} & 0 \end{bmatrix} \begin{bmatrix} e_z(t) \\ e_w(t) \end{bmatrix} \tag{3.10}$$

Only the associated component in $e_w(t)$ will be reinitialized to 0 at t_k. The state updates in the inter-sample predictors can be easily realized if the multi-rate observer is implemented on a microcontroller, and the states can be set to any value at any time [283].

Remark 6. *There are two major differences between the multi-rate full-order and reduced-order observers: (i) the dimension of the multi-rate full-order observer of Equation (3.9) is $(n + m_d)$, whereas it reduces to $(n - m_c)$ for the multi-rate reduced-order observer of Equation (3.5); (ii) different from the multi-rate reduced-order observer, the estimated states $\hat{x}$ in the multi-rate full-order observer do not show impulsive behavior.*

3.3.2 Stability Analysis

Using the same idea as in [281], the estimation error of Equation (3.6) is proved to exponentially converge to the origin. The Bellman-Gronwall Lemma is first introduced which provides an

explicit bound to the unknown function.

Lemma 1 (see [284, 285]). *Let $f(t)$ and $u(t)$ be nonnegative continuous functions on $I = [a, \infty)$, for which the inequality*

$$u(t) \leqslant c + \int_a^t f(s)u(s)\, ds, \quad t \in I$$

holds, where c is a nonnegative constant. Then

$$u(t) \leqslant c \cdot \exp\left(\int_a^t f(s)\, ds\right), \quad t \in I$$

The following theorem gives sufficient conditions with explicit stability bound of the multi-rate observer of Equation (3.5), in terms of the maximum sampling period.

Theorem 1. *Consider the linear system defined in Equation (3.4) and a multi-rate reduced-order observer of Equation (3.5) with error dynamics of Equation (3.6). If the maximum sampling period, τ_m, is less than the minimum of*

$$\frac{\ln 2}{\|M\|}, \quad \frac{1}{4m_d\left(\sqrt{\frac{\sigma_2}{\sigma_1}} + \frac{1}{4}\right)\|M\|}, \quad \frac{1}{16m_d\sigma_2\left(\frac{\sigma_2}{\sigma_1} + \frac{1}{4}\sqrt{\frac{\sigma_2}{\sigma_1}}\right)\|B_d\|\,\|M\|}$$

where M is given by Equation (3.7), and σ_1 and σ_2 are the smallest and largest eigenvalues of the solution of Equation (3.8), then the error dynamics of the multi-rate reduced-order observer is exponentially stable.

Proof. Denote by $\{t_k\}_{k=1}^{\infty}$ the entire set of sampling instants in ascending order. At every t_k, one or more components in $e_w(t)$ will be reinitialized to 0. According to the definition of τ_m, each state in x_d will be measured at least once in the period of length of τ_m. In other words, each component in $e_w(t)$ will get reinitialized at least once during any period of length of τ_m.

Let us consider any initial time t_0, with the initial condition $e(t_0) = \begin{bmatrix} e_z'(t_0) & e_w'(t_0) \end{bmatrix}'$. It is assumed that $\|e(t_0)\| > 0$. Applying Lemma 1 to Equation (3.6), we have

$$\|e(t)\| \leqslant \|e(t_0)\| \exp(\|M\|\,\tau_m)$$

for all $t \in [t_0, t_0 + \tau_m]$. Since $\tau_m < \dfrac{\ln 2}{\|M\|}$ is chosen, we obtain

$$\|e(t)\| < 2\|e(t_0)\|, \quad \forall t \in [t_0, t_0 + \tau_m] \tag{3.11}$$

Using Equation (3.11), in the interval of $[t_0, t_0 + \tau_m]$, the absolute value of the i-th component in $\dot{e}_w(t)$ satisfies

$$\begin{aligned} |\dot{e}_w^i(t)| &\leqslant \|\dot{e}(t)\| \\ &\leqslant \|M\| \, \|e(t)\| \\ &< 2\|M\| \, \|e(t_0)\| \end{aligned} \tag{3.12}$$

Since each component in $e_w(t)$ will get reinitialized to 0 at least once in any interval of length of τ_m, it is assumed that t_j^i is the last sampling time for $e_w^i(t)$ in $[t_0, t_0 + \tau_m]$ so that $e_w^i(t_j^{i+}) = 0$. Using Equation (3.12), $|e_w^i(t)|$ can be bounded in the interval of $[t_j^{i+}, t_0 + \tau_m]$

$$e_w^i(t) = e_w^i(t_j^{i+}) + \int_{t_j^i}^{t} \dot{e}_w^i(s)\, ds = \int_{t_j^i}^{t} \dot{e}_w^i(s)\, ds \tag{3.13}$$

$$|e_w^i(t)| \leqslant \int_{t_j^i}^{t} |\dot{e}_w^i(s)|\, ds < 2\|M\| \, \|e(t_0)\| \, \tau_m \tag{3.14}$$

Using Equation (3.14), $\|e_w(t)\|$ is bounded at $t = t_0 + \tau_m$

$$\begin{aligned} \|e_w(t_0 + \tau_m)\| &= \sqrt{\sum_{i=1}^{m_d} |e_w^i(t_0 + \tau_m)|^2} \\ &\leqslant \sum_{i=1}^{m_d} |e_w^i(t_0 + \tau_m)| \\ &< 2m_d \|M\| \, \|e(t_0)\| \, \tau_m \end{aligned} \tag{3.15}$$

Based on Equation (3.8), we define a Lyapunov function $V(e_z(t)) = e_z'(t) P e_z(t)$, which satis-

fies the following inequalities

$$\sigma_1 \|e_z(t)\|^2 \leqslant V(e_z(t)) \leqslant \sigma_2 \|e_z(t)\|^2, \quad \forall t \geqslant t_0 \tag{3.16}$$

Using Equations (3.11) and (3.16), we obtain for all $t \in [t_0, t_0 + \tau_m]$

$$V(e_z(t)) \leqslant \sigma_2 \|e_z(t)\|^2 < 4\sigma_2 \|e(t_0)\|^2 \tag{3.17}$$

Next, we would like to show that for all $t \geqslant t_0 + \tau_m$

$$\|e_w(t)\| < \gamma_1 \|e(t_0)\| \tag{3.18}$$

$$V(e_z(t)) < 4\sigma_2 \|e(t_0)\|^2 \tag{3.19}$$

where $\gamma_1 = 2m_d \left(\sqrt{\frac{\sigma_2}{\sigma_1}} + \frac{1}{4} \right) \|M\| \tau_m$. From Equations (3.15) and (3.17), it is obvious that both inequalities hold at $t = t_0 + \tau_m$ (Notice that $\frac{\sigma_2}{\sigma_1} \geqslant 1$). For those $t > t_0 + \tau_m$, we will prove that the two inequalities hold by contradiction. Let us now consider the following two disjoint events which cover all possibilities.

1. Suppose there exists $\hat{t} > t_0 + \tau_m$ such that Equation (3.18) is violated first. In other words, we have $\left\|e_w(\hat{t})\right\| = \gamma_1 \|e(t_0)\|$ and $V(e_z(\hat{t})) < 4\sigma_2 \|e(t_0)\|^2$. From the inequality and Equation (3.16), we obtain $\left\|e_z(\hat{t})\right\| < 2\sqrt{\frac{\sigma_2}{\sigma_1}} \|e(t_0)\|$. Because of this bound, we have that for all $t \in [\hat{t} - \tau_m, \hat{t}]$

$$\begin{aligned} \|\dot{e}_w(t)\| &\leqslant \|M\| \sqrt{\|e_z(t)\|^2 + \|e_w(t)\|^2} \\ &\leqslant \|M\| \left(\|e_z(t)\| + \|e_w(t)\| \right) \\ &< \left(2\sqrt{\frac{\sigma_2}{\sigma_1}} + \gamma_1 \right) \|M\| \|e(t_0)\| \end{aligned} \tag{3.20}$$

Using Equation (3.20) and the fact that there exists at least one sampling instant $t_j^i \in [\hat{t} - \tau_m, \hat{t}]$, at

which the associated $e_w^i(t)$ will be reinitialized to 0, we obtain

$$\begin{aligned}
|e_w^i(\hat{t})| &\leqslant \int_{t_j^i}^{\hat{t}} |\dot{e}_w^i(s)|\, ds \\
&\leqslant \int_{t_j^i}^{\hat{t}} \|\dot{e}_w(s)\|\, ds \\
&< 2\left(\sqrt{\frac{\sigma_2}{\sigma_1}} + \frac{\gamma_1}{2}\right) \|M\| \, \|e(t_0)\| \, (\hat{t} - t_j^i) \\
&< 2\left(\sqrt{\frac{\sigma_2}{\sigma_1}} + \frac{\gamma_1}{2}\right) \|M\| \, \|e(t_0)\| \, \tau_m
\end{aligned}$$

Since we have selected τ_m such that γ_1 is smaller than 0.5, $|e_w^i(\hat{t})| < 2\left(\sqrt{\frac{\sigma_2}{\sigma_1}} + \frac{1}{4}\right) \|M\| \, \|e(t_0)\| \, \tau_m$ always holds. As a result, we have that at $t = \hat{t}$

$$\begin{aligned}
\left\|e_w(\hat{t})\right\| &= \sqrt{\sum_{i=1}^{m_d} |e_w^i(\hat{t})|^2} \\
&\leqslant \sum_{i=1}^{m_d} |e_w^i(\hat{t})| \\
&< 2m_d\left(\sqrt{\frac{\sigma_2}{\sigma_1}} + \frac{1}{4}\right) \|M\| \, \|e(t_0)\| \, \tau_m \\
&= \gamma_1 \|e(t_0)\|
\end{aligned} \tag{3.21}$$

Equation (3.21) leads to a contradiction. Therefore, we prove that $\|e_w(t)\| < \gamma_1 \|e(t_0)\|$ holds for all $t > t_0 + \tau_m$.

2. Suppose there exists $\hat{t} > t_0 + \tau_m$ such that Equation (3.19) is violated first or both inequalities are violated at time $\hat{t}$. In other words, we have $\left\|e_w(\hat{t})\right\| \leqslant \gamma_1 \|e(t_0)\|$ and $V(e_z(\hat{t})) = 4\sigma_2 \|e(t_0)\|^2$. Using this equality and Equation (3.16), we obtain $\left\|e_z(\hat{t})\right\| \geq 2\|e(t_0)\|$. Thus, $\dot{V}(t)$ satisfies

$$\begin{aligned}
\dot{V}(t) &= -\|e_z(t)\|^2 + 2e_z'(t)PB_d e_w(t) \\
&\leqslant -\|e_z(t)\|^2 + 2\|e_z'(t)\| \, \|P\| \, \|B_d e_w(t)\| \\
&\leqslant -\|e_z(t)\| \left(\|e_z(t)\| - 2\sigma_2 \|B_d\| \, \|e_w(t)\|\right)
\end{aligned} \tag{3.22}$$

Since τ_m has been chosen such that γ_1 is smaller than $\dfrac{1}{\sigma_2 \|B_d\|}$, we obtain that at $t = \hat{t}$

$$\dot{V}(\hat{t}) \leqslant - \left\|e_z(\hat{t})\right\| \left(\left\|e_z(\hat{t})\right\| - 2\sigma_2 \|B_d\| \left\|e_w(\hat{t})\right\|\right)$$

which is strictly negative. It implies that $V(e_z(\hat{t}))$ will never reach $4\sigma_2 \|e(t_0)\|^2$, which leads to a contradiction.

Therefore, it is concluded that both $\|e_w(t)\| < \gamma_1 \|e(t_0)\|$ and $V(e_z(t)) < 4\sigma_2 \|e(t_0)\|^2$ hold for all $t \geqslant t_0 + \tau_m$.

Next, we would like to prove that for all time $t \geqslant t_0$, we have $V(e_z(t)) < 4\sigma_2^3 \|B_d\|^2 \gamma_1^2 \|e(t_0)\|^2$. If it reached equality, we obtain $\|e_z(t)\| \geqslant 2\sigma_2 \|B_d\| \gamma_1 \|e(t_0)\|$, which makes $\dot{V}(e_z(t)) < 0$. This leads to a contradiction. Using Equation (3.16) and the above inequality, we have

$$\begin{aligned} V(e_z(t)) &< 4\sigma_2^3 \|B_d\|^2 \gamma_1^2 \|e(t_0)\|^2, \quad t \geqslant t_0 \\ \|e_z(t)\| &< 2\sigma_2 \sqrt{\frac{\sigma_2}{\sigma_1}} \|B_d\| \gamma_1 \|e(t_0)\|, \quad t \geqslant t_0 \end{aligned}$$

Since we have chosen τ_m such that $\gamma_1 < \dfrac{1}{8\sigma_2 \sqrt{\dfrac{\sigma_2}{\sigma_1}} \|B_d\|}$, $\|e_z(t)\| < \dfrac{1}{4} \|e(t_0)\|$ holds for all $t \geqslant t_0$. Using the fact that $\gamma_1 < 0.5$, we have

$$\|e(t)\| \leqslant \|e_z(t)\| + \|e_w(t)\| < \frac{3}{4} \|e(t_0)\|, \quad t \geqslant t_0 + \tau_m$$

After a period of length of τ_m, $\|e(t + \tau_m)\| < \dfrac{3}{4} \|e(t)\|$. Hence, for any positive integer k, we have

$$\|e(t_0 + k\tau_m)\| < \left(\frac{3}{4}\right)^k \|e(t_0)\|$$

The error dynamics of Equation (3.6) of the multi-rate reduced-order observer is exponentially stable. □

Remark 7. *Following the above steps, the error dynamics of the multi-rate full-order observer of*

Equation (3.10) can be shown to converge to the origin exponentially, given the same upper bound formula of τ_m as stated in Theorem 1.

Next consider a special case where the multi-rate observer design is applied to a class of systems with continuous outputs and single-rate sampled outputs. The set of sampling instants $\{t_k\}_{k=1}^{\infty}$ is not necessarily uniformly spaced, but satisfies $0 < t_{k+1} - t_k < \tau_m$ for all $k \in \mathbb{Z}^+$, for some $\tau_m > 0$. Technically, it is still a multi-rate observer design problem taking the different nature of two measurements into account. The difference with the more general multi-rate observer design of Equation (3.5) is that the entire e_w will be reinitialized to 0 at t_k. As a special case, the stability condition is derived in a different way, which gives a less conservative stability bound.

Lemma 2 (see [281])**.** *Given $\lambda(t)$ and $k(t)$ nonnegative piecewise continuous functions of time t with $\lambda(t)$ differentiable. If the function $y(t)$ satisfies $y(t) \leqslant \lambda(t) + \int_t^{t_f} k(s)y(s)\, ds$, $\forall t_f \geqslant t \geqslant 0$, then $y(t) \leqslant \lambda(t_f)\exp(\int_t^{t_f} k(s)\, ds) - \int_t^{t_f} \dot{\lambda}(s)\exp(\int_t^{s} k(\tau)\, d\tau)\, ds$, $\forall t_f \geqslant t \geqslant 0$.*

Theorem 2. *Consider a class of linear systems defined in Equation (3.4) with continuous outputs and nonuniformly-spaced single-rate sampled outputs, and a multi-rate reduced-order observer of Equation (3.5) with error dynamics of Equation (3.6). If the maximum sampling period τ_m satisfies*

$$\tau_m < \frac{\ln 2}{\|M\|} \tag{3.23a}$$

$$\exp(\|A\|\,\tau_m)(\|A\|^{-1} + 2\sigma_2\,\|M\|\,\tau_m) < \frac{1 + 2\,\|B_d\|\,\|A\|^{-1}}{2\,\|B_d\|} \tag{3.23b}$$

where M is given by Equation (3.7) and σ_2 is the largest eigenvalue of the solution of Equation (3.8), then the error dynamics of the multi-rate reduced-order observer is exponentially stable.

Proof. Applying Lemma 1 to Equation (3.6), we can obtain $\|e(t)\| \leqslant 2\left\|e(t_k^+)\right\|$ since $\tau_m < \frac{\ln 2}{\|M\|}$

is chosen. Therefore, in each sampling interval $[t_k^+, t_{k+1}]$, we have

$$\begin{aligned} \|\dot{e}_w(t)\| &\leqslant \|\dot{e}(t)\| \\ &\leqslant \|M\| \, \|e(t)\| \\ &\leqslant 2 \, \|M\| \, \left\|e(t_k^+)\right\| \end{aligned} \tag{3.24}$$

Using Equation (3.24), $\|e_w(t)\|$ is bounded for all $t \in [t_k^+, t_{k+1}]$

$$\begin{aligned} \|e_w(t)\| &\leqslant \left\|e_w(t_k^+)\right\| + \int_{t_k}^{t} \|\dot{e}_w(s)\| \; ds \\ &\leqslant 2 \, \|M\| \, \left\|e(t_k^+)\right\| \tau_m \end{aligned} \tag{3.25}$$

Select two times in the sampling interval $[t_k^+, t_{k+1}]$, t and t' (i.e., $t_k^+ \leqslant t \leqslant t' < t_{k+1}$), where t' is fixed here. Consequently, it yields

$$e_z(t) = e_z(t') - \int_t^{t'} \left(A e_z(s) + B_d e_w(s)\right) ds \tag{3.26}$$

$$\begin{aligned} \|e_z(t)\| &\leqslant \|e_z(t')\| + \int_t^{t'} \left(\|A\| \, \|e_z(s)\| + \|B_d\| \, \|e_w(s)\|\right) ds \\ &\leqslant \|e_z(t')\| + 2 \, \|B_d\| \, \left\|e(t_k^+)\right\| (t' - t) + \int_t^{t'} \|A\| \, \|e_z(s)\| \; ds \end{aligned} \tag{3.27}$$

Applying Lemma 2 to Equation (3.27), we have

$$\|e_z(t)\| \leqslant \|e_z(t')\| \exp(\|A\| \, (t' - t)) + 2 \, \|B_d\| \, \left\|e(t_k^+)\right\| \, \|A\|^{-1} \left(\exp(\|A\| \, (t' - t)) - 1\right) \tag{3.28}$$

Let $t' = t$, $t = t_k^+$ in Equation (3.28) and it yields

$$\left\|e_z(t_k^+)\right\| \leqslant \|e_z(t)\| \exp(\|A\| \, (t - t_k^+)) + 2 \, \|B_d\| \, \left\|e(t_k^+)\right\| \, \|A\|^{-1} \left(\exp(\|A\| \, (t - t_k^+)) - 1\right) \tag{3.29}$$

Since $\left\|e_z(t_k^+)\right\| = \left\|e(t_k^+)\right\|$, the left-hand side in Equation (3.29) is replaced by $\left\|e(t_k^+)\right\|$ and it

yields

$$\|e_z(t)\| \geqslant \frac{\left\|e(t_k^+)\right\| \left(1 - 2\left\|B_d\right\| \|A\|^{-1} \left(\exp(\|A\|\,\tau_m) - 1\right)\right)}{\exp(\|A\|\,\tau_m)} \tag{3.30}$$

Since τ_m is chosen such that

$$\exp(\|A\|\,\tau_m)(\|A\|^{-1} + 2\sigma_2\,\|M\|\,\tau_m) < \frac{1 + 2\,\|B_d\|\,\|A\|^{-1}}{2\,\|B_d\|}$$

using Equations (3.22), (3.25), and (3.30), we conclude that $\dot{V}(t)$ is strictly negative in each sampling interval $[t_k^+, t_{k+1}]$. As a result, the error dynamics of the multi-rate observer is exponentially stable. □

Notice that for Equation (3.23b) in Theorem 2, the left-hand side is a monotonically increasing function of τ_m once the observer parameters are assigned, whereas the right-hand side is a constant. Based on the facts that Equation (3.23b) holds true at $\tau_m = 0$ and the left-hand side is monotonically increasing and unbounded, it indicates that this inequality will be violated at some $\tau_m > 0$. Therefore, conditions of Theorem 2 will be satisfied for all positive τ_ms that do not exceed a certain bound. The error dynamics of the multi-rate observer will be stable as long as the sampling period is small enough, under the assumption that a continuous-time Luenberger observer design is available.

3.4 Case Studies

3.4.1 A Mathematical Example

A third-order system with one continuous measurement and one sampled measurement is presented here to illustrate the relationship between the sampling period and the feasible range of the eigenvalues of the design parameter A, which will be scalar in this case. The state-space model of

the system is

$$\begin{bmatrix} \dot{x}_1(t) \\ \dot{x}_2(t) \\ \dot{x}_3(t) \end{bmatrix} = \begin{bmatrix} 3 & 1 & -3 \\ 0 & 1 & 2 \\ 5 & 1 & -4 \end{bmatrix} \begin{bmatrix} x_1(t) \\ x_2(t) \\ x_3(t) \end{bmatrix} \tag{3.31}$$

$$y_c(t) = x_2(t)$$

$$y_d(t_k) = x_3(t_k), \qquad k \in \mathbb{Z}^+$$

where x_2 is continuously measured and x_3 is sampled. The eigenvalues of the system of Equation (3.31) are 1.91 and $-0.96 \pm 1.66i$, respectively. It will be assumed that the sampling period τ is uniform. Using Equation (3.6), the error vectors $e(t)$ at two consecutive sampling instants t_k^+, t_{k+1}^+ follow

$$\begin{bmatrix} e_z(t_{k+1}^+) \\ e_w(t_{k+1}^+) \end{bmatrix} = \begin{bmatrix} 1 & 0 \\ 0 & 0 \end{bmatrix} \exp(M\tau) \begin{bmatrix} e_z(t_k^+) \\ e_w(t_k^+) \end{bmatrix}$$

with $e_w(t_k^+) = 0$, once the predictor is reinitialized after sampling. We will choose $B = \begin{bmatrix} 1 & 2 \end{bmatrix}$ throughout this example. Then, $M = \begin{bmatrix} A & 2 \\ \frac{7-A^3}{2A} & -1-A \end{bmatrix}$ and for simplicity, we will denote

$$G = \begin{bmatrix} 1 & 0 \\ 0 & 0 \end{bmatrix} \exp(M\tau)$$

$e_z(t)$ will converge to 0 if $\rho(G) < 1$.

At first, the design parameter of the multi-rate reduced-order observer for the system of Equation (3.31) is fixed as $A = -10$. Figure 3.1(a) shows how the uniform sampling period τ affects the spectral radius of G. It is observed that the error dynamics becomes unstable once $\tau > 0.215$ s. At $\tau = 0.101$ s, the spectral radius of G becomes 0, and the observer becomes deadbeat.

Second, the feasible range of A that guarantees stability of the error dynamics as a function of

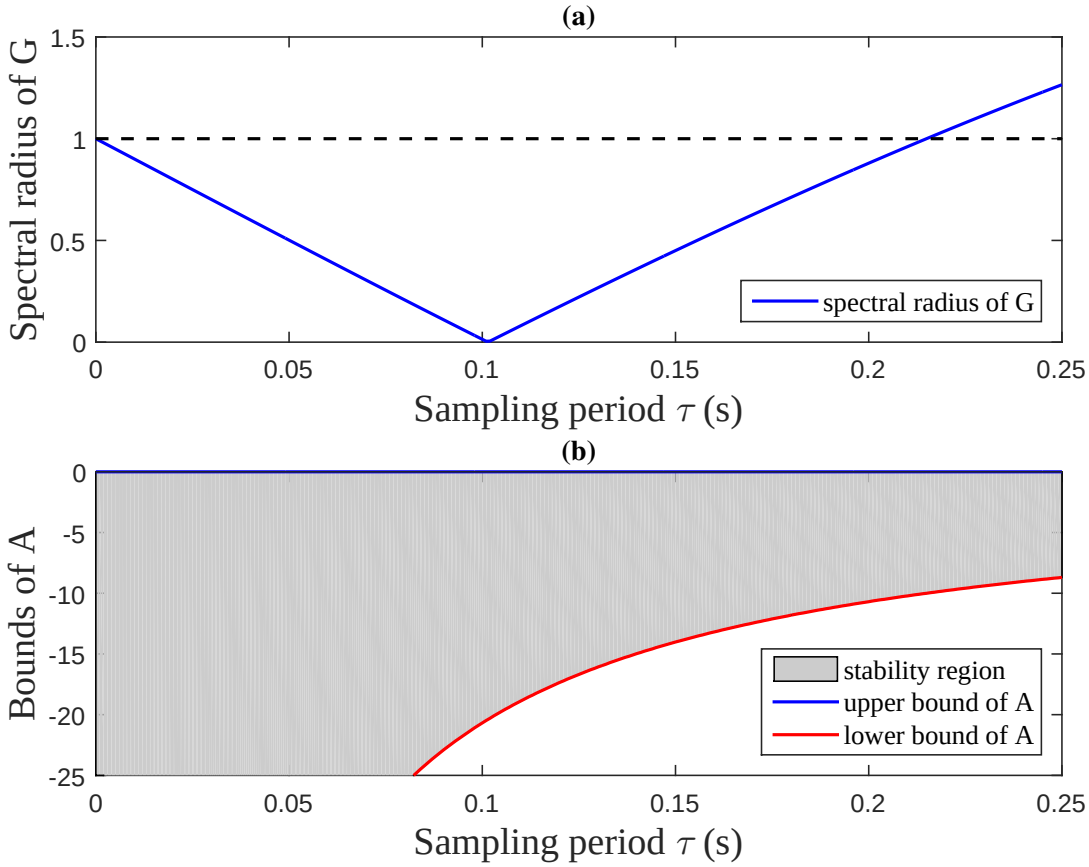

Figure 3.1: (a) Spectral radius of G as a function of the sampling period τ (uniform) when $A = -10$, $B_c = 1$ and $B_d = 2$; (b) feasible range of A as a function of the sampling period τ (uniform) when $B_c = 1$ and $B_d = 2$.

the sampling period τ is shown in Figure 3.1(b). The upper stability limit for A is zero. The lower stability limit for A was calculated numerically by solving the equation $\rho(G) = 1$ where

$$G = \begin{bmatrix} 1 & 0 \\ 0 & 0 \end{bmatrix} \exp\left(\begin{bmatrix} A & 2 \\ \frac{7-A^3}{2A} & -1-A \end{bmatrix} \tau \right)$$

using interval halving.

We see from Figure 3.1(b) that as the sampling period goes to zero, an arbitrarily fast eigenvalue is allowed for A. However, this might deteriorate the observer performance (e.g., large overshoot) during the transient period, and the multi-rate observer will be sensitive to noise. Conversely, as

the sampling period becomes larger and larger, it is necessary to use slower and slower eigenvalue for A, leading to poor observer performance. Figure 3.1 also indicates that basically there are two ways to guarantee stability of the multi-rate observer. One is to assign a slower eigenvalue for the design parameter A. The other is to increase the sampling frequency. When designing a multi-rate observer, the eigenvalues of A are often assigned an order of magnitude larger than the smallest eigenvalue of the system. If the error dynamics becomes unstable and the sampling period cannot be reduced any more, then slower eigenvalues need to be selected.

Next, we compare the maximum sampling period that satisfies the conditions of the two Theorems in the previous section. We choose $A = -10$ and have $\tau_m = 3.835 \times 10^{-3}$ s from Theorem 1, $\tau_m = 0.0133$ s from Theorem 2, respectively. It shows that Theorem 2 provides a less conservative bound on the maximum sampling period to guarantee stability for a certain class of multi-rate systems.

Figure 3.2 shows the multi-rate reduced-order observer performance for system (3.31), with the following design parameters and initial conditions: $A = -10$, $B = \begin{bmatrix} 1 & 2 \end{bmatrix}$, $x(0) = \begin{bmatrix} 80 & -30 & 0 \end{bmatrix}'$, and $\hat{x}_1(0) = 40$. Sampling normally takes place every 0.14 s. However, perturbations in the sampling schedule is considered here and the actual sampling times are 0, 0.11, 0.28, 0.40, 0.56, 0.66, 0.78, and 0.95 s. In Figure 3.2, the estimates from multi-rate observer converge to the actual state after approximately 0.4 s. In addition, the performance of the multi-rate observer is compared with that of using sample-and-hold approach and discrete-time observer in Figure 3.2(a). Note that the discrete-time observer is designed based on the discrete-time model of the system (3.31) with a sampling period of 0.14 s. The eigenvalue is placed at 0.2466 in order to match the continuous-time observer design. The sample-and-hold approach has very poor performance because of the large sampling period. In general, the discrete-time observer design performs better than the sample-and-hold approach. However, the presence of perturbation in the sampling schedule causes inaccuracy in the estimation. Besides, the inter-sample behavior is completely lost and the continuous measurement is not efficiently used. We see from Figure 3.2(a) that the estimation error does not converge to zero in either sample-and-hold approach or discrete-time observer design. Therefore,

the proposed multi-rate observer provides a more meaningful way for state estimation in multi-rate systems.

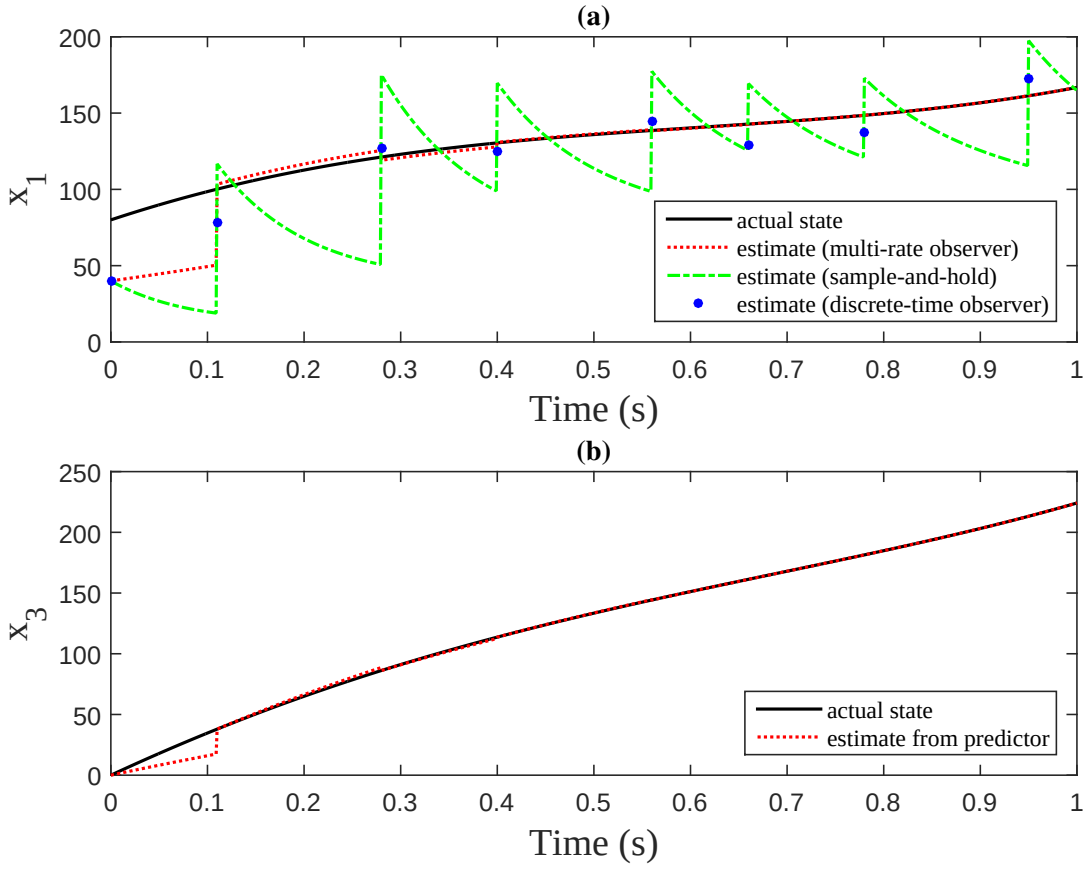

Figure 3.2: Performance of the multi-rate reduced-order observer with an inter-sample predictor for the system of Equation (3.31): (a) actual and estimated state of x_1 (comparison with sample-and-hold approach and discrete-time observer design); (b) actual and estimated state of x_3.

Remark 8. *In the multi-rate observer design, a continuous-time observer will be the basis where A and B are two free parameters to be selected. In particular, A plays a significant role in shaping the error dynamics of the continuous-time design and its eigenvalues are often selected an order of magnitude larger than the smallest eigenvalue of the system. If the error dynamics of the multi-rate observer is not stable, then either faster sampling or slower eigenvalues of A are required to*

guarantee stability. In most cases, the sampling rate of a sensor is limited by its capability. Hence, iteration is required to find a good choice of A with satisfactory multi-rate observer performance.

3.4.2 A Gas-Phase Polyethylene Reactor

The application of multi-rate reduced-order observer is also explored in an industrial gas-phase polyethylene reactor (see Figure 3.3). In the reactor, the polymerization takes place at the interface between the solid catalyst and the polymer matrix. The feed to the reactor, which contains ethylene, comonomers, hydrogen, and inerts, provides the fluidization by using a high rate of gas recycle. Ziegler-Natta catalysts are fed continuously to the reactor. The heat generated from the exothermic reaction is removed through a heat exchanger. The product, polyethylene, discharges near the base of the reactor as solid powder.

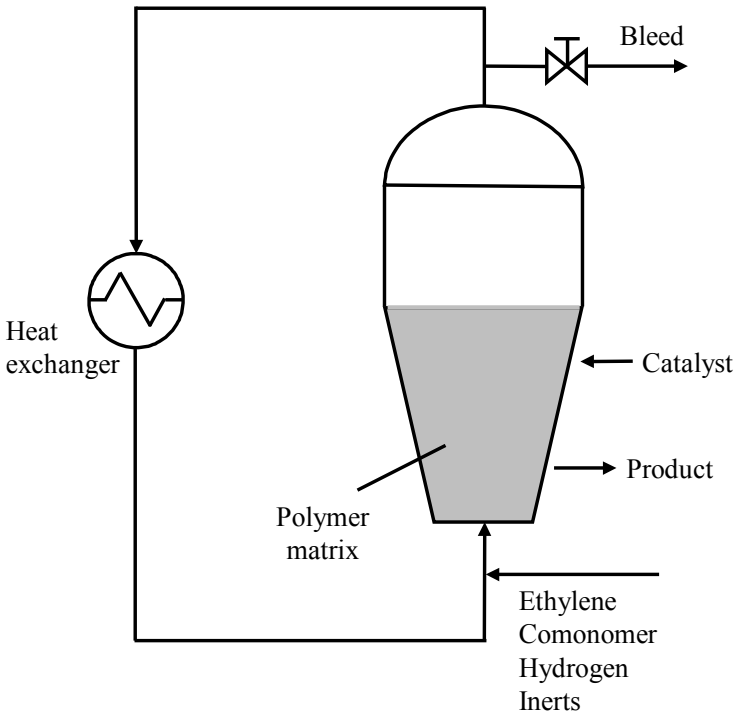

Figure 3.3: Schematic of an industrial gas-phase polyethylene reactor.

As previously mentioned in Section 1.3.2, the fluidized-bed reactor in Figure 3.3 can be mod-

eled as a single-phase, well-mixed continuous stirred-tank reactor in the operating range of industrial interest [215]. A property kinetic model was developed for the gas-phase polyethylene process accounting for the evolution of melt index and density of the product, the amount of catalytic sites, and gas concentrations in the reactor. In the reactor modeling, the following assumptions are made and justified [286]

1. The time-delay associated with the recycle gas flow through the heat exchanger and recycle lines is neglected.

2. The rate of catalyst deactivation is independent of reactor temperature and is not influenced by the terminal monomer nor chain length.

3. The vertical concentration and temperature gradient are uniform through the bed.

4. The fludized-bed reactor can be modeled as a CSTR that contains a well-mixed solid phase interacting with a well-mixed gas phase because of a high ratio of the recycle gas to the fresh feed.

5. The ethylene and comonomer propagation reactions have similar activation energies.

6. The temperature of the heat exchanger is constant.

Apart from the above assumptions, it is assumed that there is only one type of active catalyst sites

for simplicity [227]. A mathematical model for this reactor has the form [226]

$$
\begin{aligned}
\frac{dY}{dt} &= F_c a_c - k_d Y - \frac{(R_{M_1} M_{W_1} + R_{M_2} M_{W_2})Y}{B_w} \\
\frac{dT}{dt} &= \frac{H_f + H_g - H_{top} - H_r - H_{pol}}{M_r C_{pr} + B_w C_{ppol}} \\
\frac{d[In]}{dt} &= \frac{F_{In} - x_{In} b_t}{V_g} \\
\frac{d[M_1]}{dt} &= \frac{F_{M_1} - x_{M_1} b_t - R_{M_1}}{V_g} \\
\frac{d[M_2]}{dt} &= \frac{F_{M_2} - x_{M_2} b_t - R_{M_2}}{V_g} \\
\frac{d[H]}{dt} &= \frac{F_H - x_H b_t}{V_g} \\
\frac{dMI_c^{-\frac{1}{3.5}}}{dt} &= \frac{1}{\tau_r} MI_i^{-\frac{1}{3.5}} - \frac{1}{\tau_r} MI_c^{-\frac{1}{3.5}} \\
\frac{dD_c^{-1}}{dt} &= \frac{1}{\tau_r} D_i^{-1} - \frac{1}{\tau_r} D_c^{-1}
\end{aligned}
\tag{3.32}
$$

where

$$
\begin{aligned}
R_{M_1} &= k_{p1} \exp\left[-\frac{E_a}{R}\left(\frac{1}{T}-\frac{1}{T_{ref}}\right)\right]\cdot Y\cdot[M_1]\\
R_{M_2} &= k_{p2} \exp\left[-\frac{E_a}{R}\left(\frac{1}{T}-\frac{1}{T_{ref}}\right)\right]\cdot Y\cdot[M_2]\\
H_f &= (F_{M_1}C_{p1}+F_{M_2}C_{p2}+F_{In}C_{pIn}+F_HC_{pH})(T_f-T_{ref})\\
H_g &= F_gC_{pg}(T_g-T_{ref})\\
C_{pg} &= x_{M_1}C_{p1}+x_{M_2}C_{p2}+x_{In}C_{pIn}+x_HC_{pH}\\
H_{top} &= (F_g+b_t)(T-T_f)C_{pg}\\
b_t &= V_pC_v\sqrt{([In]+[M_1]+[M_2]+[H])RR\cdot T-P_v}\\
H_r &= \Delta H_{reac}M_{W_1}R_{M_1}\\
H_{pol} &= C_{ppol}(R_{M_1}M_{W_1}+R_{M_2}M_{W_2})(T-T_{ref})\\
MI_i &= \exp\left[k_7\left(\frac{1}{T}-\frac{1}{T_{ref}}\right)\right]\left(k_0+k_1\frac{[M_2]}{[M_1]}+k_3\frac{[H]}{[M_1]}\right)^{3.5}\\
D_i &= p_0+p_1\cdot\ln(MI_i)-\left(p_2\frac{[M_2]}{[M_1]}\right)^{p_4}\\
\tau_r &= \frac{B_w}{R_{M_1}M_{W_1}+R_{M_2}M_{W_2}}
\end{aligned}
\tag{3.33}
$$

The definitions of all the variables in Equations (3.32) and (3.33) are listed in Table 3.1. The values of the process parameters are listed in Table 3.2 [222, 227, 228]. Notice that the parameters used in calculating the melt index and density have been scaled for proprietary reasons [222].

The process model of Equation (3.32) is linearized at the design steady state given in Table 3.3. A linear state-space model with eight deviation variables can be obtained, where x_1 denotes moles of active catalyst sites, x_2 denotes reactor temperature, x_3, x_4, x_5 and x_6 represent gas concentrations of inerts, ethylene, comonomer, and hydrogen respectively, and x_7, x_8 denote the cumulative melt index and density of the product. As for the outputs, $y_c(t) = x_2(t)$ is continuously measured on line. $y_{d,1} = \begin{bmatrix} x_3 & x_4 & x_5 & x_6 \end{bmatrix}'$ is obtained every 20 min by using on-line gas chromatography. In addition, the off-line lab analysis of melt index and density, $y_{d,2} = \begin{bmatrix} x_7 & x_8 \end{bmatrix}'$, is sampled every

Parameter	Description
Y	Moles of active catalyst site
F_c, F_g	Flow rate of catalyst and recycle gas
a_c	Active site concentration of catalyst
k_d	Deactivation rate constant for the catalyst site
B_w	Mass of polymer in the fluidized bed
R_{M1}, R_{M2}	Ethylene and comonomer consumption rate due to reaction
M_{W_1}, M_{W_2}	Molecular weight of ethylene and comonomer
k_{p1}, k_{p2}	Pre-exponential factor for polymer propagation rate
E_a	Activation energy
R, RR	Ideal gas constant, unit of J/(mol·K) and m^3atm/(mol·K)
T, T_{ref}, T_f, T_g	Reactor, reference, feed and recycle gas temperature
$[In]$, $[M_1]$, $[M_2]$, $[H]$	Molar concentration of inerts, ethylene, comonomer, hydrogen in the gas phase
C_{pIn}, C_{p1}, C_{p2}, C_{pH}	Specific heat capacity of inerts, ethylene, comonomer and hydrogen
F_{In}, F_{M_1}, F_{M_2}, F_H	Flow rate of inerts, ethylene, comonomer and hydrogen
x_{In}, x_{M_1}, x_{M_2}, x_H	Mole fraction of inerts, ethylene, comonomer, hydrogen in the gas
H_f, H_g	Enthalpy of fresh feed stream, cooled recycle gas stream to reactor
H_{top}, H_{pol}	Enthalpy of total gas outflow stream from reactor and polymer
H_r	Heat generated by polymerization reaction
b_t	Overhead gas bleed
V_p	Bleed stream valve position
C_v	Vent flow coefficient
P_v	Pressure downstream of bleed vent
ΔH_{reac}	Heat of reaction
C_{pg}, C_{ppol}	Specific heat capacity of the recycle gas and polymer
$M_r C_{pr}$	Product of mass and heat capacity of reactor walls
V_g	Volume of gas phase in the reactor
MI_i, MI_c	Instantaneous and cumulative melt index of polymer
D_i, D_c	Instantaneous and cumulative density of polymer
τ_r	Solid phase residence time
k_0, k_1, k_3, k_7	Parameters in the inference model for instantaneous melt index of polymer
p_0, p_1, p_2, p_4	Parameters in the inference model for instantaneous density of polymer

Table 3.1: Process variables.

30 min, which provides quality information of the polyethylene. In the reaction, the active catalyst site may become inactive due to spontaneous decay and adsorption of impurities, which forms dead site and dead polymer chains. Because of the difficulty in measuring the amount of active catalyst sites, it is necessary to monitor this quantity from a reliable on-line soft sensor. Besides, providing continuous and reliable estimates for the inter-sample dynamic behavior of these sampled outputs is also significant for quality control and monitoring.

a_c = 0.548 mol/kg	k_d = 0.0001 s^{-1}
B_w = 7×10^4 kg	F_c = 1.611×10^{-3} kg/s
M_{W_1} = 0.02805 kg/mol	M_{W_2} = 0.0562 kg/mol
k_{p1} = 0.085 m^3/(mol·s)	k_{p1} = 0.003 m^3/(mol·s)
E_a = 37681.2 J/mol	T_{ref} = 360 K
R = 8.314 J/(mol·K)	RR = 8.2058×10^{-5} m^3 atm/(mol·K)
C_{pIn} = 28.889 J/(mol·K)	C_{pH} = 32.238 J/(mol·K)
C_{p1} = 46.055 J/(mol·K)	C_{p2} = 100.48 J/(mol·K)
F_{In} = 2.52 mol/s	F_H = 1.6 mol/s
F_{M_1} = 131.13 mol/s	F_{M_2} = 3.51 mol/s
T_f = 293 K	F_g = 8500 mol/s
T_g = 324.7 K	V_p = 0.5
C_v = 7.5 $atm^{-0.5}$ mol/s	P_v = 17 atm
ΔH_{reac} = -3.7430×10^6 J/kg	C_{ppol} = 3558.8 J/(kg·K)
M_rC_{pr} = 5.8615×10^7 J/K	V_g = 500 m^3
k_0 = 0.41	k_1 = 0.0726
k_3 = 0.3298	k_7 = 2.2627×10^4
p_0 = 28.35	p_1 = 1.227
p_2 = 85.29	p_4 = 0.5292

Table 3.2: Process values and units.

Y = 5.778 mol	T = 356.68 K
$[In]$ = 217.59 mol/m^3	$[M_1]$ = 292.40 mol/m^3
$[M_2]$ = 130.00 mol/m^3	$[H]$ = 138.16 mol/m^3
$MI_c^{-\frac{1}{3.5}}$ = 1.4148	D_c^{-1} = 0.0500

Table 3.3: Steady-state operating conditions of system (3.32).

Consider the following multi-rate reduced-order observer design based on Equation (3.5)

$$A = -0.00068, \quad B_c = 0.01,$$

$$B_d = \begin{bmatrix} 0.01 & 0.01 & 0.01 & 0.01 & 0.01 & 0.01 \end{bmatrix},$$

$$T_R = -562.7, \quad T_{Mc} = 72.6,$$

$$T_{Md} = \begin{bmatrix} 13.3 & 6.03 & 23.3 & 13.7 & 15.9 & 15.9 \end{bmatrix}$$

It is assumed that the first available outputs $y_{d,1}$, $y_{d,2}$ are obtained at $t = 10$ min. The initial condi-

tions of the process and the observer are given in Table 3.4. The multi-rate observer performance is tested via MATLAB simulation shown in Figure 3.4.

Initial Condition of the Process		Initial Guess of the Observer	
Y = 4.6 mol	T = 360 K	Y = 2.44 mol	$[In]$ = 380.28 mol/m^3
$[In]$ = 450 mol/m^3	$[M_1]$ = 340 mol/m^3	$[M_1]$ = 325.72 mol/m^3	$[M_2]$ = 144.00 mol/m^3
$[M_2]$ = 150 mol/m^3	$[H]$ = 200 mol/m^3	$[H]$ = 181.45 mol/m^3	$MI_c^{-\frac{1}{3.5}}$ = 1.5250
$MI_c^{-\frac{1}{3.5}}$ = 1.5723	D_c^{-1} = 0.0511	D_c^{-1} = 0.0507	

Table 3.4: Initial conditions of the process (3.32) and the observer.

In Figure 3.4, the response of inter-sample output predictors (i.e., dotted lines in (b)-(f)) demonstrates impulsive behavior at sampling times, caused by reinitialization, which brings the predicted output back to the actual state. As a consequence, it creates discontinuity in the estimates $\hat{x}_1$ as the observer state z does not change at sampling instants. Figure 3.4(a) shows that the estimates from the multi-rate observer (i.e., dotted line) has approximately the same convergence rate as that from the continuous-time design (i.e., dash-dot line). The multi-rate observer design of Equation (3.5) provides reliable estimation results.

3.5 Conclusions

This chapter proposes a design method for multi-rate observers in linear multi-output systems, considering both continuous and discrete measurements with asynchronous sampling. It is based on an available continuous-time Luenberger observer design coupled with multiple, asynchronous inter-sample predictors for the sampled outputs. This new observer is of hybrid nature, and it is able to make use of all possible measurements in the system. The stability analysis was carried out based on Lyapunov's second method and it is concluded that the error dynamics of the proposed multi-rate observer will be exponentially stable as long as the sampling period is sufficiently small. It provides sufficient and explicit conditions, in terms of maximum sampling period, to guarantee exponential stability, irrespective of perturbations in the sampling schedule. Iteration on the design

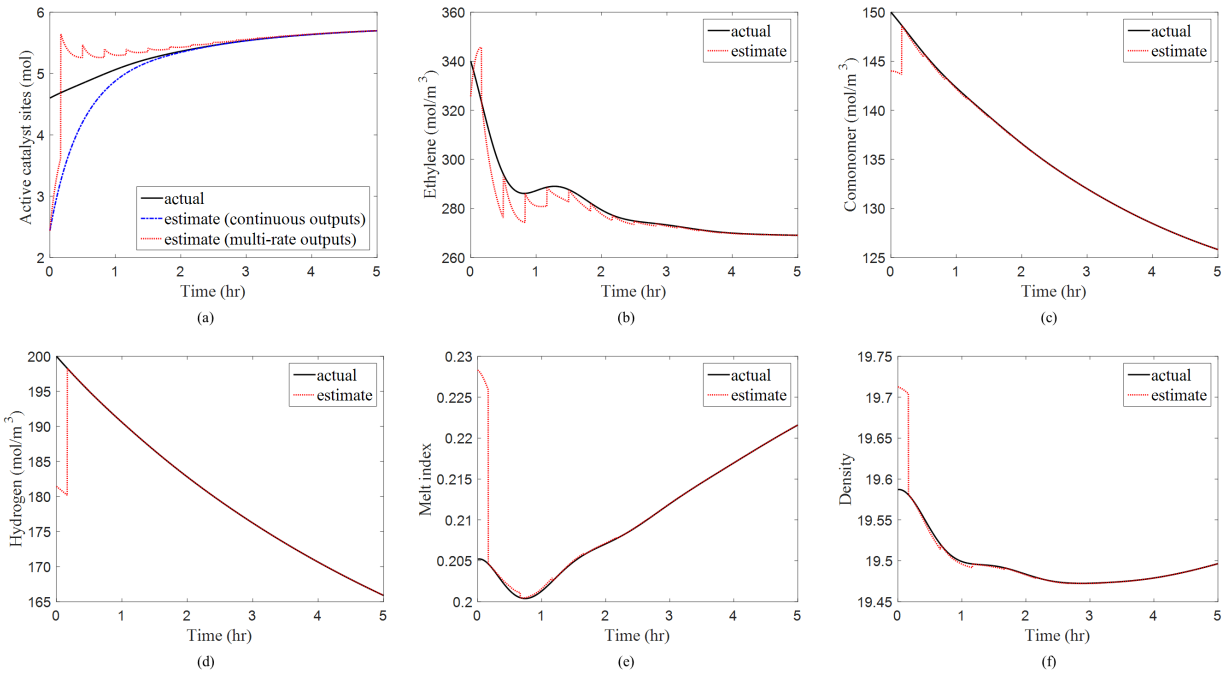

Figure 3.4: Performance of the multi-rate reduced-order observer with inter-sample output predictors: (a) x_1 (solid), $\hat{x}_1$ (dash-dot) assuming continuous outputs for all the sensors, and $\hat{x}_1$ (dotted) with multi-rate outputs; (b) x_4 (solid) and $\hat{x}_4$ (dotted) from predictor; (c) x_5 (solid) and $\hat{x}_5$ (dotted) from predictor; (d) x_6 (solid) and $\hat{x}_6$ (dotted) from predictor; (e) x_7 (solid) and $\hat{x}_7$ (dotted) from predictor; (f) x_8 (solid) and $\hat{x}_8$ (dotted) from predictor.

parameter A is required to achieve satisfactory observer performance, which is limited by the sensor hardware. From the simple third-order example considered, we see that the multi-rate observer performs much better than the sample-and-hold approach and discrete-time observer design.

The upper bound of the maximum sampling period given by Theorems 1 and 2 is found to be very conservative from the simulation. Finding a tighter bound would help to select appropriate sensors for particular systems. This open question will be the subject of future research.

Another important characteristic of the process output, which is time delay, will be taken into account in the linear observer design in Chapter 4.

4. MULTI-RATE OBSERVER DESIGN IN LINEAR SYSTEMS WITH MEASUREMENT DELAY *

In Chapter 3, we developed a multi-rate observer design method in linear systems with asynchronous sampling based on a Luenberger observer design coupled with inter-sample predictors. In this chapter, the problem of multi-rate multi-delay observer design are addressed where both asynchronous sampling and possible measurement delays are accounted for [287]. The proposed observer adopts an available multi-rate observer design in the time interval between two consecutive delayed measurements. A dead time compensation approach is developed to compensate for the effect of delay and update the past estimates when a delayed measurement arrives. The stability and robustness properties of the multi-rate observer will be preserved under nonconstant, arbitrarily large measurement delays. A mathematical example and a gas-phase polyethylene reactor example demonstrate good performance of the proposed observer in the presence of nonuniform sampling and nonconstant measurement delays.

The chapter is organized as follows. In Section 4.1, the necessity of incorporating measurement delay in the observer design is given. In Section 4.2, the multi-rate observer design in the absence of measurement delays are reviewed, which will serve as the basis for the multi-rate multi-delay observer to be proposed in Section 4.3. Stability analysis of the observer is quite straightforward based on the stability analysis of a delay-free multi-rate observer and will be discussed in Section 4.3. The applicability of the proposed observer will be illustrated via two case studies in Section 4.4. In Section 4.5, conclusions are drawn from the results of the previous sections.

4.1 Introduction

Motivated by many engineering applications, state estimation of continuous-time dynamic systems in the presence of sampled and delayed measurements has received lots of attention recently.

*Reprinted with permission from "A Dead Time Compensation Approach for Multirate Observer Design with Large Measurement Delays" by C. Ling and C. Kravaris, 2019. *AIChE Journal*, 65(2), 562–570, Copyright 2018 by John Wiley and Sons.

In networked control systems, for example, output data is transmitted over a digital communication channel in discrete packets, and the network-induced delay becomes non-negligible if the system to be controlled or monitored is located far away from the computing unit. In chemical processes, product quality measurements are sampled infrequently and require off-line lab analysis which inevitably introduces delay as a consequence of sample preparation, analysis and calculation. Since the aforementioned systems are usually equipped with multiple sensors of different sampling rates and different measurement delays, continuous-time and/or single-rate sampled-data observer design methods from the literature are not directly applicable any more. Hence, the objective of this work is to develop a state observer which is able to handle multi-rate multi-delay measurements in linear systems.

Most of the observer design methods using delayed output are based on a chain of state observation algorithms, where various types of output delay (e.g., constant, time-varying, piecewise) have been considered. A chain structure algorithm was proposed in [288] for globally drift-observable systems where the measurement became available after a constant delay. The chain observer consisted of a number of cascaded subsystems where each subsystem reconstructed the system states at different delayed time instants. It was shown that there exists an observer of suitable dimension which achieves exponential error decay for any size of delay. A similar methodology was applied to single-output systems with constant delay where the observer design followed a different path by using the error linearization with eigenvalue assignment method [148], and consequently enhanced design flexibility was achieved [289]. A set of cascade high-gain observers with the same structure was proposed to estimate the states of triangular nonlinear systems when the delay was arbitrarily long and constant [290]. To reduce the number of subsystems and avoid a long oscillatory transient behavior, an alternative cascade structure was developed where the first subsystem was an observer for the delayed state whereas each one of the remaining subsystems was replaced by a state predictor [291]. This design approach can be appropriately adapted to deal with time-varying delay. The assumption on constant output delay has been relaxed in recent studies. Motivated by the chain-like structure, a cascade of two observers was proposed for linear systems where the output delay

was assumed to be a piecewise constant function of time [292]. A simple observer was derived for nonlinear systems with time-varying measurement delay and asymptotic stability of the estimation error was proved by using Lyapunov-Razumikhin tools [293]. In this design, the observer had the same size as the original system and no particular hypothesis on the delay function was required.

The delayed output considered in all the above contributions is assumed to be continuous. As most of the product quality measurements in chemical processes are sampled infrequently and are obtained with a delay, sampling and delay effects need to be simultaneously considered and compensated for in the observer design. A chain observer, composed of several elementary observers and output predictors in series, was designed to compensate for sampling and large measurement delay in a class of triangular nonlinear systems in [294]. A robust global exponential observer was proposed for certain classes of nonlinear systems under sampled measurement with a constant delay, where a state predictor was used to estimate the current state [279]. Two classes of observers were presented for multi-input multi-output state affine systems based on the continuous-discrete observer design [273], and the sampled-data observer design coupled with an inter-sample output predictor [250], respectively. The unknown output delay had an upper bound and it was assumed that the sampled measurements will become available before the next sampling [295]. Multi-rate observer design in the presence of multiple measurement delays was proposed and implemented in a polymerization reactor in [246, 296] where the evolution of the slow measurements was predicted by using the method of least squares. In spite of the fact that fairly good estimation results have been achieved, stability analysis of a multi-rate multi-delay observer remained open. Other multi-rate estimation methods considering measurement delays, such as the extended Kalman filter [266, 297, 298], and the moving horizon estimation [269–271], have also been investigated. In addition, a number of results are available in the literature regarding controller design for nonlinear systems with delays in states, actuators and measurements [299–303].

The problem of multi-rate observer design in the absence of measurement delays was studied in Chapter 3 for linear systems and will be studied in Chapter 6 for nonlinear systems. Motivated by the single-rate sampled-data observer design in [250], a multi-rate observer was developed

based on an available continuous-time design coupled with multiple, asynchronous inter-sample predictors for the sampled measurements. Each predictor generated an estimate of a sampled output in between two consecutive measurements using a model-based method. The predictor was reinitialized once the associated, most-recent measurement became available. Sufficient conditions were derived to guarantee stability of the error dynamics using Lyapunov's second method [281], and the vector small-gain theorem [304], respectively. Furthermore, the multi-rate design provided robustness with respect to perturbations in the sampling schedule.

In this chapter, we will address the problem of observer design in a linear multi-output system where measurements are available at different sampling rates and with different delays. Notice that input delay and state delay are not in the scope of this study. In the case of linear systems, the problem of controller design that is capable of handling dead time was solved by the well-known Smith predictor in [305]. It simulates the difference between the delay-free part of the process model and the process model with dead time. Motivated by dead time compensation algorithms in [305, 306], we approach the multi-rate multi-delay observer design in a two-step manner. First, a multi-rate observer design [52] is adopted as a starting point and estimates of the current state are obtained in the time interval between consecutive delayed measurements. Second, we propose a model-based dead time compensation approach to handle possible measurement delays and show that the stability property of the multi-rate observer will be preserved under arbitrarily large measurement delays. Differently from the Smith predictor, the assumption that the process is open-loop stable is not required. Two attractive features of the approach are that it inherits the stability and robustness properties from a delay-free multi-rate observer and convergence is not affected by nonconstant measurement delays. The mathematical example and the industrial gas-phase polyethylene reactor example of [52] will be reconsidered in the presence of delays to illustrate the applicability of the proposed method.

4.2 Preliminaries

4.2.1 Notations

The zero matrix and identity matrix of appropriate size are denoted by 0 and I, respectively. The operator $\|\cdot\|$ denotes the Euclidean norm of a vector or a matrix. For a matrix A, A' denotes its transpose matrix. If A is square, A^{-1} denotes the inverse matrix. The set of nonnegative integers is denoted by $\mathbb{Z}^+$. For any function $x : \mathbb{R} \to \mathbb{R}^n$, we define $x(t^+) = \lim_{h\to 0} x(t+h)$.

4.2.2 Multi-Rate Observer Design in the Absence of Output Delays

This section contains a brief summary of the theoretical results presented in Chapter 3 on linear multi-rate observer design in the absence of measurement delays, which will serve as the basis of the multi-rate multi-delay observer design to be proposed in Section 4.3. A reduced-order observer formulation will be the focus in this chapter because lower dimensionality can ease implementation of the observer.

Consider a linear system with continuous and sampled outputs in the absence of delays, where without loss of generality, the outputs are assumed to be a part of the state

$$\begin{aligned}
\begin{bmatrix} \dot{x}_R(t) \\ \dot{x}_c(t) \\ \dot{x}_d(t) \end{bmatrix} &= \begin{bmatrix} F_{11} & F_{12} & F_{13} \\ F_{21} & F_{22} & F_{23} \\ F_{31} & F_{32} & F_{33} \end{bmatrix} \begin{bmatrix} x_R(t) \\ x_c(t) \\ x_d(t) \end{bmatrix} + \begin{bmatrix} G_1 \\ G_2 \\ G_3 \end{bmatrix} u(t) \\
y_c(t) &= x_c(t) \\
y_d^i(t_k) &= x_d^i(t_j^i), \qquad k, j \in \mathbb{Z}^+, i = 1, 2, \ldots, m_d
\end{aligned} \tag{4.1}$$

where $x_R \in \mathbb{R}^{n-m_c-m_d}$ is the unmeasurable state, $x_c \in \mathbb{R}^{m_c}$ is the continuously measured state, $x_d \in \mathbb{R}^{m_d}$ is the remaining state that is slow-sampled, y_c denotes the continuous outputs, y_d denotes the sampled outputs at different rates, and $u \in \mathbb{R}^q$ denotes the control inputs. F_{ij} and $G_i, \forall i, j = 1, 2, 3$, are matrices of appropriate dimensions. t_j^i is the j-th sampling time for the i-th component in x_d, at some sequence of time instants $S = \{t_k\}_{k=0}^{\infty}$. Notice that S is the sequence of all sampling times in ascending order. The sampling times of each sensor are not necessarily uniformly spaced,

but satisfying $0 < t^i_{j+1} - t^i_j \leqslant \tau_m, \forall j \in \mathbb{Z}^+$, where τ_m is the maximum sampling period among all the sensors.

The multi-rate observer design is based on a continuous-time Luenberger observer design coupled with multiple asynchronous inter-sample predictors. The system of Equation (4.1) can be used to predict the evolution of the sampled outputs in between two consecutive measurements. The predicted outputs will then replace the continuous outputs in the implementation of a continuous-time observer. It was seen in [52] that the model-based prediction provides a more meaningful approach to approximate the inter-sample behavior as opposed to a sample-and-hold strategy, especially under large sampling period. For $t \in [t^+_k, t_{k+1}]$, suppose a multi-rate observer design of the following form is available for the multi-rate system of Equation (4.1)

$$\begin{aligned}
\dot{z}(t) &= Az(t) + B_c y_c(t) + B_d w(t) + Wu(t) \\
\dot{w}(t) &= F_{31}\hat{x}_R(t) + F_{32} y_c(t) + F_{33} w(t) + G_3 u(t) \\
w^i(t^+_k) &= y^i_d(t_k) \\
\hat{x}_R(t) &= T_R^{-1}(z(t) - T_{Mc} y_c(t) - T_{Md} w(t))
\end{aligned} \tag{4.2}$$

where $z \in \mathbb{R}^{n-m_c-m_d}$ is the observer state, $\hat{x}_R \in \mathbb{R}^{n-m_c-m_d}$ is the state estimates, and $w \in \mathbb{R}^{m_d}$ is the predicted outputs in the sampling interval. The i-th component in $w(t)$ will be reinitialized once a new measurement $y^i_d(t_k)$ becomes available at t_k, while the rest of the predictor states do not change until their measurements are obtained. At a specific time t_k, there may be measurement of more than one output or the sampling of one sensor may coincide with another. Therefore, some sampling instants may be present more than once in the sequence S, where the reinitialization step will occur repeatedly but on different elements in $w(t)$.

All the matrices in the multi-rate observer of Equation (4.2) are inherited from a continuous-time Luenberger observer design under appropriate partitions, where A is a Hurwitz matrix with desired eigenvalues, $\begin{bmatrix} B_c & B_d \end{bmatrix}$ is a matrix that forms a controllable pair with A, the matrix $W = T_R G_1 + T_{Mc} G_2 + T_{Md} G_3$, and the transformation matrices T_R, T_{Mc}, T_{Md} satisfy the following

Sylvester equation

$$\begin{bmatrix} T_R & T_{Mc} & T_{Md} \end{bmatrix} \begin{bmatrix} F_{11} & F_{12} & F_{13} \\ F_{21} & F_{22} & F_{23} \\ F_{31} & F_{32} & F_{33} \end{bmatrix} = A \begin{bmatrix} T_R & T_{Mc} & T_{Md} \end{bmatrix} + \begin{bmatrix} B_c & B_d \end{bmatrix} \begin{bmatrix} 0 & I & 0 \\ 0 & 0 & I \end{bmatrix} \tag{4.3}$$

Notice that observability of the pair $\left(F_{11}, \begin{bmatrix} F_{21} \\ F_{31} \end{bmatrix} \right)$, controllability of the pair $\left(A, \begin{bmatrix} B_c & B_d \end{bmatrix} \right)$, and the Hurwitz matrix A and the transition matrix F not having common eigenvalues, should be satisfied to guarantee uniqueness of T_R, T_{Mc}, T_{Md}, and invertibility of T_R.

We denote the estimation error in x-coordinates $e_R(t) = x_R(t) - \hat{x}_R(t)$, output prediction error $e_w(t) = x_d(t) - w(t)$, and observer error $e_z(t) = T_R e_R(t) + T_{Md} e_w(t)$. Under the above choice of the observer matrices, the multi-rate observer (4.2) induces the following error dynamics of $e_z(t)$ and $e_w(t)$ in the sampling interval $[t_k^+, t_{k+1}]$

$$\begin{aligned} \begin{bmatrix} \dot{e}_z(t) \\ \dot{e}_w(t) \end{bmatrix} &= \begin{bmatrix} A & B_d \\ F_{31} T_R^{-1} & F_{33} - F_{31} T_R^{-1} T_{Md} \end{bmatrix} \begin{bmatrix} e_z(t) \\ e_w(t) \end{bmatrix} \\ e_w^i(t_k^+) &= 0 \end{aligned} \tag{4.4}$$

Notice that $e_R(t)$ and $e_z(t)$ represent estimation errors in different coordinates. For simplicity, we denote

$$M = \begin{bmatrix} A & B_d \\ F_{31} T_R^{-1} & F_{33} - F_{31} T_R^{-1} T_{Md} \end{bmatrix} \tag{4.5}$$

To ensure exponential stability of the error dynamics of Equation (4.4), the maximum sampling period τ_m should be less than the minimum of

$$\frac{\ln 2}{\|M\|}, \quad \frac{1}{4m_d \left(\sqrt{\frac{\sigma_2}{\sigma_1}} + \frac{1}{4} \right) \|M\|}, \quad \frac{1}{16 m_d \sigma_2 \left(\frac{\sigma_2}{\sigma_1} + \frac{1}{4} \sqrt{\frac{\sigma_2}{\sigma_1}} \right) \|B_d\| \, \|M\|} \tag{4.6}$$

where σ_1 and σ_2 are the smallest and largest eigenvalues of a unique symmetric positive definite matrix P respectively, satisfying the Lyapunov equation

$$A'P + PA = -I \tag{4.7}$$

This is a sufficient and explicit condition derived from Lyapunov's second method and it is concluded that the error dynamics of the multi-rate observer will be exponentially stable as long as the sampling period is sufficiently small, irrespective of perturbations in the sampling schedule (see [52] for more details).

Remark 9. *The multi-rate observer design contains a continuous-time Luenberger observer and multiple inter-sample output predictors. Consequently, the error dynamics is governed by the matrix M instead of the Hurwitz matrix A exclusively. A, B_c and B_d are the three design parameters to be selected which play a significant role in "shaping" the error dynamics of the multi-rate observer. If the error dynamics is not stable, then either faster sampling or slower eigenvalues of A are required to guarantee stability. In most cases, the sampling rate of a sensor is limited by its capability. Hence, iteration is required to find a good choice of A with satisfactory multi-rate observer performance.*

4.3 Main Results

4.3.1 Proposed Multi-Rate Multi-Delay Observer Design

Now consider a linear multi-rate system of Equation (4.1) with possible delays in the sampled measurements $y_d(t)$

$$\begin{aligned}
\begin{bmatrix} \dot{x}_R(t) \\ \dot{x}_c(t) \\ \dot{x}_d(t) \end{bmatrix} &= \begin{bmatrix} F_{11} & F_{12} & F_{13} \\ F_{21} & F_{22} & F_{23} \\ F_{31} & F_{32} & F_{33} \end{bmatrix} \begin{bmatrix} x_R(t) \\ x_c(t) \\ x_d(t) \end{bmatrix} + \begin{bmatrix} G_1 \\ G_2 \\ G_3 \end{bmatrix} u(t), \quad t \geqslant -\Delta \\
y_c(t) &= x_c(t) \\
y_d^i(t_j^i) &= x_d^i(t_j^i - \delta_j^i), \qquad j \in \mathbb{Z}^+, i = 1, 2, \ldots, m_d
\end{aligned} \tag{4.8}$$

where t_j^i denotes the time when the j-th measurement of x_d^i becomes available after some possible delay $\delta_j^i \geqslant 0$. In other words, the measured output $y_d^i(t_j^i)$ is a function of the state x_d^i at time $t_j^i - \delta_j^i$. The measurement delay δ_j^i is not constant but is assumed bounded by a positive real number Δ. Notice that $\delta_j^i = 0$ if there is no delay in the output y_d^i. Similar to the multi-rate system of Equation (4.1), the sampling times of each measurement are not necessarily uniformly spaced, but satisfying $0 < \left|(t_{j'}^i - \delta_{j'}^i) - (t_j^i - \delta_j^i)\right| \leqslant \tau_m$ for any consecutive sampling instants.

The proposed observer for the system (4.8) with multiple measurement delays is based on the multi-rate observer design (4.2) combined with dead time compensation. As depicted in Figure 4.1 (notice that the continuous outputs are not shown), the estimation process is composed of two steps. First, dead time compensation will be triggered once a delayed measurement is obtained at t_j^i. Past estimates are recalculated by integrating the observer and compensator equations from $t_j^i - \delta_j^i$ to t_j^i. Any available measurement can be used as a delay-free output to reinitialize the corresponding compensator at its sampling time. The estimates of the current state at t_j^i are consequently updated at the end of the compensation. This step ensures that these available measurements are used in the observer without delay, in the same order as they are sampled. Second, the updated estimates are used as the initial condition of the observer and the inter-sample output predictors at t_j^i. The multi-rate multi-delay observer operates like a delay-free multi-rate observer when there is no delayed measurement.

When a sampled and delayed measurement becomes available at t_j^i, dead time compensation is executed to update the past estimates. For all $t \in [t_j^i - \delta_j^i, t_j^i)$ where $\delta_j^i \neq 0$, the following design

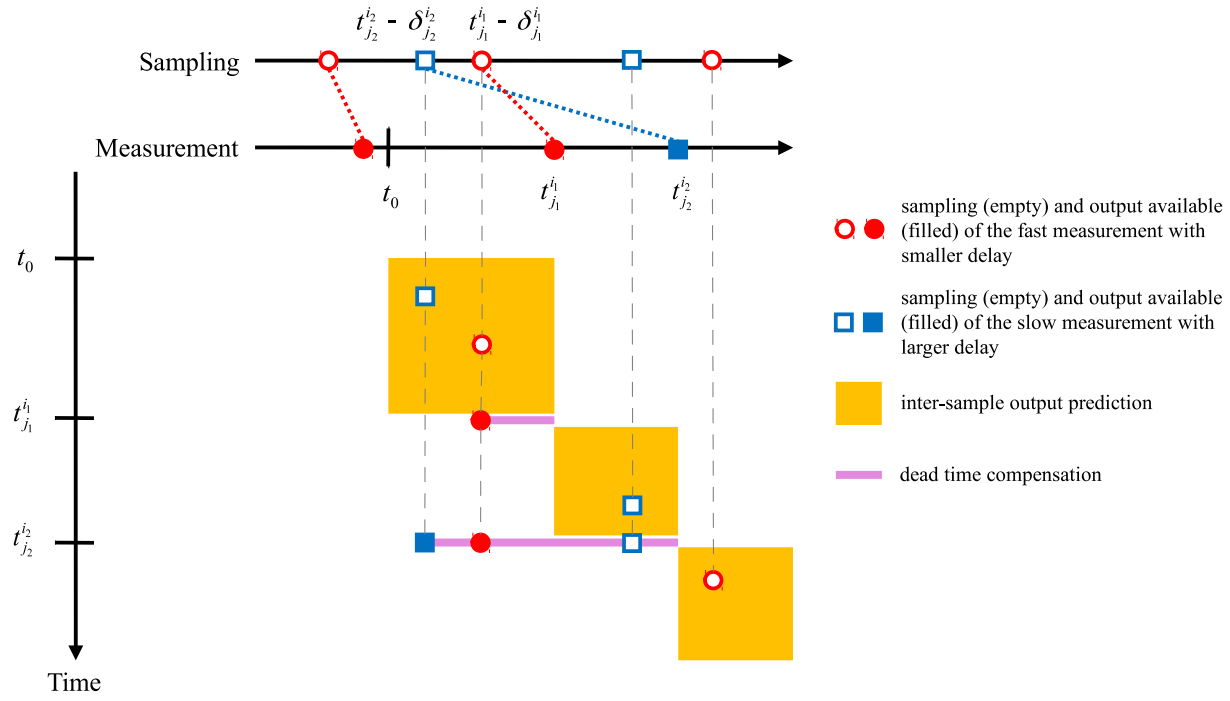

Figure 4.1: An illustration of the proposed two-step estimation process of a multi-rate multi-delay observer in the presence of two sampled and delayed measurements starting from t_0.

of a multi-rate observer with dead time compensation is proposed

$$\dot{z}(t) = Az(t) + B_c y_c(t) + B_d w(t) + Wu(t) \tag{4.9a}$$

$$\dot{w}(t) = F_{31}\hat{x}_R(t) + F_{32}y_c(t) + F_{33}w(t) + G_3 u(t) \tag{4.9b}$$

$$w^i((t_j^i - \delta_j^i)^+) = y_d^i(t_j^i) \tag{4.9c}$$

$$w^{i'}((t_{j'}^{i'} - \delta_{j'}^{i'})^+) = y_d^{i'}(t_{j'}^{i'}), \qquad \forall t_{j'}^{i'}, (t_{j'}^{i'} - \delta_{j'}^{i'}) \in [t_j^i - \delta_j^i, t_j^i) \tag{4.9d}$$

$$\hat{x}_R(t) = T_R^{-1}(z(t) - T_{Mc}y_c(t) - T_{Md}w(t)) \tag{4.9e}$$

where $w \in \mathbb{R}^{m_d}$ is the compensator state representing the past estimates for $x_d(t)$. Equation (4.9c) shows the reinitialization of the i-th dead time compensator using the delayed measurement $y_d^i(t_j^i)$ at its sampling time $t_j^i - \delta_j^i$. The outputs that are sampled and measured between $t_j^i - \delta_j^i$ and t_j^i can be used to reset the compensators at their respective sampling times as seen in Equation (4.9d), where $t_{j'}^{i'} - \delta_{j'}^{i'}$ is the sampling time of the j'-th measurement of $x_d^{i'}$ at $t_{j'}^{i'}$ for all $j' \in \mathbb{Z}^+, i' = 1, 2, \ldots, m_d$.

Remark 10. *If the delayed measurement at t_j^i has more than one output, reinitialization should be performed on multiple dead time compensators in Equation (4.9c).*

Remark 11. *In Equation (4.9), the observer state $z(t)$, compensator state $w(t)$, control input $u(t)$, continuous outputs $y_c(t)$, and sampled outputs $y_d(t)$ all represent the past information in the system throughout the dead time compensation, which need to be stored in a buffer. Notice that the past estimates are generated for the purpose of correcting the state estimates at t_j^i based on the delayed measurement $y_d^i(t_j^i)$ and therefore improving the estimation accuracy afterwards. The memory size of the buffer will be finite as long as the upper bound of the measurement delay Δ is finite, as will be discussed later.*

Once the estimates at t_j^i are obtained after the dead time compensation, inter-sample prediction comes into play in the time interval between two consecutive measurements at t_j^i and $t_{j'}^{i'}$. For all $t \in [t_j^i, t_{j'}^{i'})$, the multi-rate multi-delay observer follows

$$\begin{aligned} \dot{z}(t) &= Az(t) + B_c y_c(t) + B_d w(t) + Wu(t) \\ \dot{w}(t) &= F_{31}\hat{x}_R(t) + F_{32} y_c(t) + F_{33} w(t) + G_3 u(t) \\ \hat{x}_R(t) &= T_R^{-1}(z(t) - T_{Mc} y_c(t) - T_{Md} w(t)) \end{aligned} \tag{4.10}$$

where $w \in \mathbb{R}^{m_d}$ is the predicted outputs for the sampled measurements $y_d(t)$ in the sampling interval. The inter-sample predictors run simultaneously with the observer, and estimate the evolution of the sampled outputs, in the same spirit as in a delay-free multi-rate observer. The estimates in Equation (4.10) can be used for real-time monitoring or control purposes. If a sampled, undelayed measurement becomes available at t_j^i, the inter-sample prediction will run immediately after reinitialization and no dead time compensation will be needed. Algorithm 1 summarizes the estimation process of the proposed multi-rate multi-delay observer.

Remark 12. *Unlike the chain observer where a high dimensionality may be required to reconstruct the state in the case of large measurement delays [288–291], the proposed multi-rate multi-delay observer does not require a chain-like structure and the dimension of the observer (4.9) and (4.10)*

Algorithm 1 Algorithm for Linear Multi-rate Multi-delay Observer

STEP 0: Initialize $z(t_0)$, $w(t_0)$, and solve Equation (4.10) for $[t_0, t_j^i)$.
STEP 1: Calculate $z(t)$ and $w(t)$ when a sampled measurement becomes available at t_j^i.
if $\delta_j^i > 0$ **then**
  Solve Equation (4.9) for $[t_j^i - \delta_j^i, t_j^i)$ and update $z(t_j^i)$, $w(t_j^i)$. ▷ Dead time compensation
end if
Reinitialize Equation (4.10) with $z(t_j^i)$, $w(t_j^i)$, and solve it for $[t_j^i, t_{j'}^{i'})$. ▷ Inter-sample prediction
STEP 2: Set $t_j^i = t_{j'}^{i'}$ and go to Step 1.

is significantly reduced to $(n - m_c)$*. Moreover, it can handle multiple nonconstant measurement delays.*

Remark 13. *Notice that the continuous measurement considered in the system (4.8) was assumed delay-free. In case it is delayed, one method is to sample the output at a certain sampling frequency so that it can be treated as a sampled measurement with delay in the same manner as* $y_d(t)$*, at the expense of losing some information from the measurement signals. The sampling period should be less than* τ_m *to guarantee stability.*

4.3.2 Stability Analysis

Past estimates are recalculated in the dead time compensation once a sampled, delayed measurement becomes available. Estimates at certain times may be calculated more than once, if the measurement order differs from the sampling order. We name the last updated estimates obtained from the multi-rate multi-delay observer "final estimates". We denote $\tilde{t}$ the most-recent sampling time where the measurements of all the samples taken before $\tilde{t}$ (including $\tilde{t}$) are available. It implies that the final estimates are obtained for all $t \leqslant \tilde{t}$. Because the measurements are used in the same order as the way they are sampled when calculating the final estimates, the final estimates $z(t)$, $w(t)$ and $\hat{x}_R(t)$ for all $t \leqslant \tilde{t}$ in the multi-rate multi-delay observer are identical to those in a delay-free multi-rate observer, under the same design parameters. Once the final estimates at $\tilde{t}$ are obtained, all the stored measurements that are sampled before $\tilde{t}$, control inputs, etc. can be cleared from the buffer.

Because of the previous assumption that the measurement delay in the system (4.8) has a finite upper bound Δ, $\tilde{t}$ will approach infinity as t goes to infinity. We label the estimation error $e_R(t) = x_R(t) - \hat{x}_R(t)$, compensation error (or output prediction error) $e_w(t) = x_d(t) - w(t)$, and observer error $e_z(t) = T_R e_R(t) + T_{Md} e_w(t)$. According to the two-step estimation process, we would like to show convergence of the error dynamics in the dead time compensation as well as the inter-sample prediction, respectively.

We denote t_j^i the time where the most-recent, delayed measurement becomes available. The dead time compensation will be performed and for all $t \in [t_j^i - \delta_j^i, t_j^i)$ the error dynamics follows

$$\begin{aligned}
&\dot{e}_z(t) = A e_z(t) + B_d e_w(t) \\
&\dot{e}_w(t) = F_{31} T_R^{-1} e_z(t) + (F_{33} - F_{31} T_R^{-1} T_{Md}) e_w(t) \\
&e_w^i((t_j^i - \delta_j^i)^+) = 0 \\
&e_w^{i'}((t_{j'}^{i'} - \delta_{j'}^{i'})^+) = 0, \qquad \forall t_{j'}^{i'}, (t_{j'}^{i'} - \delta_{j'}^{i'}) \in [t_j^i - \delta_j^i, t_j^i)
\end{aligned} \tag{4.11}$$

Notice that the transition matrix in the above error dynamics is identical to the matrix M given by Equation (4.5) in the multi-rate observer formulation. We denote $e(t) = \begin{bmatrix} e_z'(t) & e_w'(t) \end{bmatrix}'$. From Equation (4.11), we have $e(t) = \exp(M(t - t_{j'}^{i'} + \delta_{j'}^{i'})) e(t_{j'}^{i'} - \delta_{j'}^{i'})$ where some elements in $e_w(t_{j'}^{i'} - \delta_{j'}^{i'})$ are reinitialized to 0. If the maximum sampling period τ_m in the multi-rate multi-delay system of Equation (4.8) is guaranteed to be less than the minimum of the expressions in Equation (4.6), the final estimates $e(\tilde{t})$ will exponentially converge to 0, in the same manner as a multi-rate observer in the absence of delay. As the estimates in the dead time compensation are generated by forward predicting the process model from $\tilde{t}$ with reinitialization at some sampling instants, as a result, $e(t)$ will converge to zero exponentially in the compensation.

In the inter-sample prediction that follows up, we have that for all $t \in [t_j^i, t_{j'}^{i'})$

$$\begin{aligned}
&\dot{e}_z(t) = A e_z(t) + B_d e_w(t) \\
&\dot{e}_w(t) = F_{31} T_R^{-1} e_z(t) + (F_{33} - F_{31} T_R^{-1} T_{Md}) e_w(t)
\end{aligned} \tag{4.12}$$

Likewise, we have $e(t) = \exp(M(t - t_j^i))e(t_j^i)$ for all $t \in [t_j^i, t_{j'}^{i'})$. Since $\lim_{t \to +\infty} e(t_j^i) = 0$ holds at the end of the dead time compensation, it is obvious that $e(t)$ will exponentially converge to zero in the inter-sample prediction. When a sampled, undelayed measurement becomes available at t_j^i, the i-th predictor will get reinitialized immediately, and this does not affect stability of the observer.

It can be seen that stability of the proposed multi-rate multi-delay observer completely depends on the maximum sampling period as in a delay-free multi-rate observer. Thus, the assumption on an open-loop stable process is not required. In addition, stability of the multi-rate observer will be preserved under nonconstant and arbitrarily large delays. Another attractive feature of the proposed approach is that it can handle the situation where the delayed measurement sequence is not in the same order as the sampling sequence.

Remark 14. *The above multi-rate multi-delay observer design can be adapted to a full-order observer formulation, under appropriate modifications. Consider a multi-rate system in the presence of output delays in the form*

$$\begin{aligned} \dot{x}(t) &= Fx(t) + Gu(t), \quad t \geqslant -\Delta \\ y_c(t) &= H_c x(t) \\ y_d^i(t_j^i) &= H_d^i x(t_j^i - \delta_j^i), \quad j \in \mathbb{Z}^+, i = 1, 2, \ldots, m_d \end{aligned} \tag{4.13}$$

where H_c is a $m_c \times n$ matrix for continuous outputs, and H_d^i is the i-th row of the matrix H_d for sampled and delayed outputs.

Likewise, we first propose the following design of multi-rate full-order observer with dead time

compensation for all $t \in [t_j^i - \delta_j^i, t_j^i)$

$$\begin{aligned}
&\dot{z}(t) = Az(t) + B_c y_c(t) + B_d w(t) + Wu(t) \\
&\dot{w}(t) = H_d F\hat{x}(t) + H_d Gu(t) \\
&w^i((t_j^i - \delta_j^i)^+) = y_d^i(t_j^i) \\
&w^{i'}((t_{j'}^{i'} - \delta_{j'}^{i'})^+) = y_d^{i'}(t_{j'}^{i'}), \qquad \forall t_{j'}^{i'}, (t_{j'}^{i'} - \delta_{j'}^{i'}) \in [t_j^i - \delta_j^i, t_j^i) \\
&\hat{x}(t) = T^{-1} z(t)
\end{aligned} \tag{4.14}$$

where $W = TG$*, and the transformation matrix* T *satisfies the following Sylvester equation*

$$TF = AT + B_c H_c + B_d H_d$$

After the dead time compensation, inter-sample prediction is used to estimate the evolution of the sampled outputs in the time interval between two consecutive measurements at t_j^i *and* $t_{j'}^{i'}$*. For all* $t \in [t_j^i, t_{j'}^{i'})$*, the multi-rate multi-delay observer follows*

$$\begin{aligned}
&\dot{z}(t) = Az(t) + B_c y_c(t) + B_d w(t) + Wu(t) \\
&\dot{w}(t) = H_d F\hat{x}(t) + H_d Gu(t) \\
&\hat{x}(t) = T^{-1} z(t)
\end{aligned} \tag{4.15}$$

The multi-rate full-order observer with output delays has a dimension of $(n + m_d)$*. Stability is inherited from stability of a multi-rate observer in the absence of measurement delays.*

4.4 Case Studies

In this section, the third-order system and the industrial gas-phase polyethylene reactor examples of Chapter 3 are utilized to test the performance of the proposed observer. Perturbations in the sampling schedule and nonconstant measurement delays will be considered for sampled outputs in the simulations.

4.4.1 A Mathematical Example

Consider a third-order system in the presence of one continuous output without delay and one sampled, delayed output

$$\begin{aligned}
\begin{bmatrix} \dot{x}_1(t) \\ \dot{x}_2(t) \\ \dot{x}_3(t) \end{bmatrix} &= \begin{bmatrix} 3 & 1 & -3 \\ 0 & 1 & 2 \\ 5 & 1 & -4 \end{bmatrix} \begin{bmatrix} x_1(t) \\ x_2(t) \\ x_3(t) \end{bmatrix} \\
y_c(t) &= x_2(t) \\
y_d(t_j) &= x_3(t_j - \delta_j), \qquad j \in \mathbb{Z}^+
\end{aligned} \tag{4.16}$$

where t_j is the j-th measurement time of $x_3(t)$ with output delay $\delta_j > 0$, which is not constant.

The system (4.16) was studied in the absence of measurement delay in Chapter 3. It was found that the convergence rate of a multi-rate observer depends on the sampling period and this should be accounted for in the selection of parameters in the multi-rate observer design. As the sampling period goes to zero, an arbitrarily fast eigenvalue is allowed for A. However, this might deteriorate observer performance (e.g., large overshoot) in the transient period and the multi-rate observer will be sensitive to noise. Conversely, as the sampling period becomes larger and larger, it is necessary to use a slower and slower eigenvalue for A, leading to lower observer performance. Thus, iteration is required to find a good choice of A with satisfactory performance.

A multi-rate reduced-order observer design [52], which serves as the basis of a multi-rate multi-delay observer, is used with the following design parameters: $A = -10$, $B_c = 1$, and $B_d = 2$. Sampling normally takes place every 0.14 s. However, perturbations in the sampling schedule and nonconstant measurement delays are considered here. The actual sampling times and their corresponding measurement delays are listed in Table 4.1. As can be seen, the measurement delay could be either smaller or larger than the following sampling period. It has been illustrated in Section 3.4 that the estimates from the multi-rate observer converge to the actual state after approximately 0.4 s. Next, we would like to show that stability of the multi-rate observer will be preserved in the pres-

ence of measurement delays. Figure 4.2 shows the performance of multi-rate multi-delay observer for the system (4.16), with the following initial conditions: $x(0) = \begin{bmatrix} 80 & -30 & 0 \end{bmatrix}'$, $\hat{x}_1(0) = 92$, and $w(0) = 20$. We see from Figure 4.2(a) that the estimate from multi-rate multi-delay observer converges to the actual state after 0.53 s, which is about 0.13 s slower than the multi-rate observer in the absence of delay. In Figure 4.2(b), the inter-sample predictor can estimate the inter-sample behavior with high accuracy after a few samplings. Inevitably, the presence of measurement delay induces slower convergence of the observer compared with the delay-free multi-rate observer.

Sampling (s)	0	0.11	0.28	0.40	0.56	0.66	0.78	0.95
Delay (s)	0.12	0.13	0.14	0.13	0.12	0.14	0.13	0.15

Table 4.1: Actual sampling schedule and measurement delays in system (4.16).

4.4.2 A Gas-Phase Polyethylene Reactor

The application of a multi-rate multi-delay observer is then explored in an industrial gas-phase polyethylene reactor (see Figure 3.3), where the measurement delays of on-line gas chromatography and off-line lab analysis will be accounted for. In this reactor, the polymerization takes place at the interface between the solid catalyst and the polymer matrix. The feed to the reactor, which consists of ethylene, comonomers, hydrogen, and inerts, provides the fluidization by using a high rate of gas recycle. Ziegler-Natta catalysts are fed continuously to the reactor. The heat generated from the exothermic reaction is removed through a heat exchanger. The product, polyethylene, discharges near the base of the reactor as solid powder.

In the operating range of industrial interest, the fluidized-bed reactor in Figure 3.3 can often be modeled as a single-phase, well-mixed CSTR [215]. For simplicity, it is assumed that there is only one type of active catalyst sites [227]. A mathematical model for this reactor has the form [226]

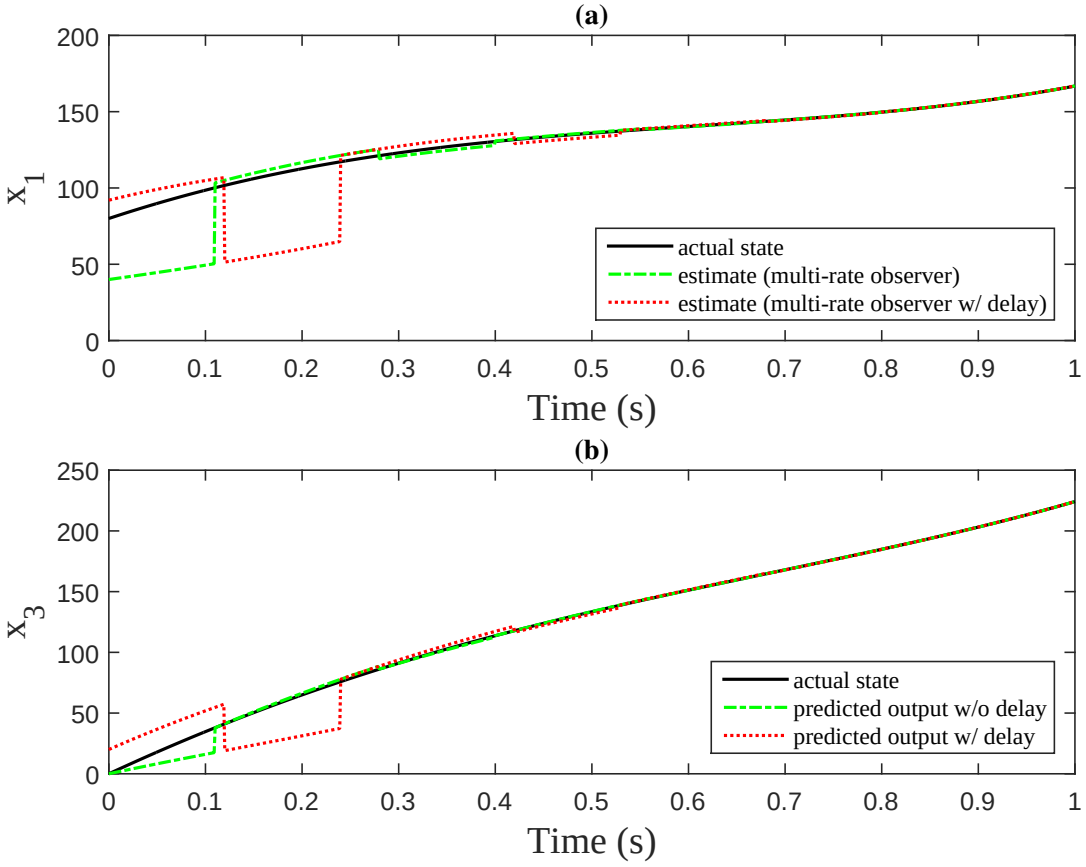

Figure 4.2: Comparison of the multi-rate multi-delay observer (red) for the system (4.16) and the multi-rate observer in the absence of measurement delay (green): (a) actual and estimated state of x_1, (b) actual and estimated state of x_3 from an inter-sample predictor.

$$
\begin{aligned}
\frac{dY}{dt} &= F_c a_c - k_d Y - \frac{(R_{M_1} M_{W_1} + R_{M_2} M_{W_2}) Y}{B_w} \\
\frac{dT}{dt} &= \frac{H_f + H_g - H_{top} - H_r - H_{pol}}{M_r C_{pr} + B_w C_{ppol}} \\
\frac{d[In]}{dt} &= \frac{F_{In} - x_{In} b_t}{V_g} \\
\frac{d[M_1]}{dt} &= \frac{F_{M_1} - x_{M_1} b_t - R_{M_1}}{V_g} \\
\frac{d[M_2]}{dt} &= \frac{F_{M_2} - x_{M_2} b_t - R_{M_2}}{V_g} \\
\frac{d[H]}{dt} &= \frac{F_H - x_H b_t}{V_g} \\
\frac{dMI_c^{-\frac{1}{3.5}}}{dt} &= \frac{1}{\tau_r} MI_i^{-\frac{1}{3.5}} - \frac{1}{\tau_r} MI_c^{-\frac{1}{3.5}} \\
\frac{dD_c^{-1}}{dt} &= \frac{1}{\tau_r} D_i^{-1} - \frac{1}{\tau_r} D_c^{-1}
\end{aligned}
\tag{4.17}
$$

where

$$
\begin{aligned}
R_{M_1} &= k_{p1} \exp\left[-\frac{E_a}{R}\left(\frac{1}{T}-\frac{1}{T_{ref}}\right)\right]\cdot Y\cdot[M_1]\\
R_{M_2} &= k_{p2} \exp\left[-\frac{E_a}{R}\left(\frac{1}{T}-\frac{1}{T_{ref}}\right)\right]\cdot Y\cdot[M_2]\\
H_f &= (F_{M_1}C_{p1}+F_{M_2}C_{p2}+F_{In}C_{pIn}+F_HC_{pH})(T_f-T_{ref})\\
H_g &= F_gC_{pg}(T_g-T_{ref})\\
C_{pg} &= x_{M_1}C_{p1}+x_{M_2}C_{p2}+x_{In}C_{pIn}+x_HC_{pH}\\
H_{top} &= (F_g+b_t)(T-T_f)C_{pg}\\
b_t &= V_pC_v\sqrt{([In]+[M_1]+[M_2]+[H])RR\cdot T-P_v}\\
H_r &= \Delta H_{reac}M_{W_1}R_{M_1}\\
H_{pol} &= C_{ppol}(R_{M_1}M_{W_1}+R_{M_2}M_{W_2})(T-T_{ref})\\
MI_i &= \exp\left[k_7\left(\frac{1}{T}-\frac{1}{T_{ref}}\right)\right]\left(k_0+k_1\frac{[M_2]}{[M_1]}+k_3\frac{[H]}{[M_1]}\right)^{3.5}\\
D_i &= p_0+p_1\cdot\ln(MI_i)-\left(p_2\frac{[M_2]}{[M_1]}\right)^{p_4}\\
\tau_r &= \frac{B_w}{R_{M_1}M_{W_1}+R_{M_2}M_{W_2}}
\end{aligned}
\tag{4.18}
$$

The definitions of all the variables in Equations (4.17), (4.18) and the values of the process parameters are listed in Tables 3.1 and 3.2 in Section 3.4.

As for outputs, the reactor temperature is continuously measured on line without delay. The gas concentrations of inerts, ethylene, comonomer and hydrogen are normally sampled every 20 min and measured by using on-line gas chromatography, which induces about 8 min delay caused by sample preparation (2.5 min), analysis (4 min), and computer calculation (1.5 min) [307]. In addition, the off-line lab analysis of melt index and density is normally sampled every 40 min with 60 min delay, which provides quality information of the polyethylene [222]. During the reaction, the active catalyst site may become inactive due to spontaneous decay and adsorption of impurities, which forms dead site and dead polymer chains. Because of the difficulty in measuring the amount

of active catalyst sites in the reactor, it is necessary to monitor this quantity from a reliable on-line soft sensor. Providing continuous and reliable estimates for the inter-sample dynamic behavior of these sampled outputs is also significant for quality control and monitoring.

The process model (4.17) is linearized at the design steady state given in Table 4.2 and a linear state-space model can be obtained. System output to be used in an observer will be generated from the linearized model. The multi-rate multi-delay observer is based on a multi-rate observer design in the absence of delay with the following design parameters

$$
\begin{aligned}
&A = -0.00068, \quad B_c = 0.01, \\
&B_d = \begin{bmatrix} 0.01 & 0.01 & 0.01 & 0.01 & 0.01 & 0.01 \end{bmatrix}, \\
&T_R = -562.7, \quad T_{Mc} = 72.6, \\
&T_{Md} = \begin{bmatrix} 13.3 & 6.03 & 23.3 & 13.7 & 15.9 & 15.9 \end{bmatrix}
\end{aligned}
$$

It is assumed that the first sample of gas chromatography is taken at $t = 5$ min and the first sample of lab analysis is taken at $t = 10$ min. Perturbations in the sampling schedule and nonconstant measurement delays are considered in the simulation, whereas it was assumed uniform sampling without delay in Section 3.4. The actual sampling schedule and their corresponding measurement delays are given in Table 4.3. Notice that the measurement delay of gas chromatography is smaller than its sampling period whereas the delay of off-line lab analysis is relatively larger. The initial conditions of the process and the observer are given in Table 4.4.

Y = 5.778 mol	T = 356.68 K
$[In]$ = 217.59 mol/m^3	$[M_1]$ = 292.40 mol/m^3
$[M_2]$ = 130.00 mol/m^3	$[H]$ = 138.16 mol/m^3
$MI_c^{-\frac{1}{3.5}}$ = 1.4148	D_c^{-1} = 0.0500

Table 4.2: Steady-state operating conditions of system (4.17).

Gas chromatography	Sampling (min)	5	23	43	62.5	81.5	102	122	140
	Delay (min)	8.0	8.7	8.5	7.5	8.0	8.0	8.2	7.8
	Sampling (min)	161.5	179.5	199.5	219	238	258.5	278.5	300.5
	Delay (min)	8.5	8.3	8.0	8.2	7.7	8.0	8.0	8.3
Lab analysis	Sampling (min)	10	48	93	134	170	210	248	288
	Delay (min)	60	56	62.8	66.3	54.5	60	60.5	66.7

Table 4.3: Actual sampling schedule and measurement delays in system (4.17).

Initial Condition of the Process		Initial Guess of the Observer	
Y = 4.6 mol	T = 360 K	Y = 2.44 mol	$[In]$ = 380.28 mol/m^3
$[In]$ = 450 mol/m^3	$[M_1]$ = 340 mol/m^3	$[M_1]$ = 325.72 mol/m^3	$[M_2]$ = 144.00 mol/m^3
$[M_2]$ = 150 mol/m^3	$[H]$ = 200 mol/m^3	$[H]$ = 181.45 mol/m^3	$MI_c^{-\frac{1}{3.5}}$ = 1.5250
$MI_c^{-\frac{1}{3.5}}$ = 1.5723	D_c^{-1} = 0.0511	D_c^{-1} = 0.0507	

Table 4.4: Initial conditions of the process (4.17) and the observer.

The performance of multi-rate multi-delay observer is shown in Figure 4.3, where it is compared with a multi-rate observer in the absence of measurement delays with the same design parameters. Figure 4.3(a) shows that the estimate from the multi-rate multi-delay observer has approximately the same convergence rate as that from the multi-rate design. Figures 4.3(b)-(f) show the evolution of estimated outputs obtained from inter-sample predictors and in this way, the inter-sample behavior can be reconstructed under nonuniform sampling schedule. When a sampled and delayed measurement arrives, dead time compensation is performed by integrating Equation (4.9) from sampling time to current time and therefore the estimates will get updated, which explains the impulsive behavior. The multi-rate multi-delay observer design (4.9)&(4.10) provides reliable estimation results. In the presence of multiple measurements, the reduced-order observer formulation is preferred because the dimension would be significantly lower than the full-order formulation.

Remark 15. *In Figure 4.3, the estimates of the linear multi-rate multi-delay observer is evaluated against the states of the linearized process model around the designed steady state. However, it is well-known that linear observers can be inadequate in the presence of strong process nonlinearities. To broaden the applicability of the proposed method, a nonlinear observer with constant*

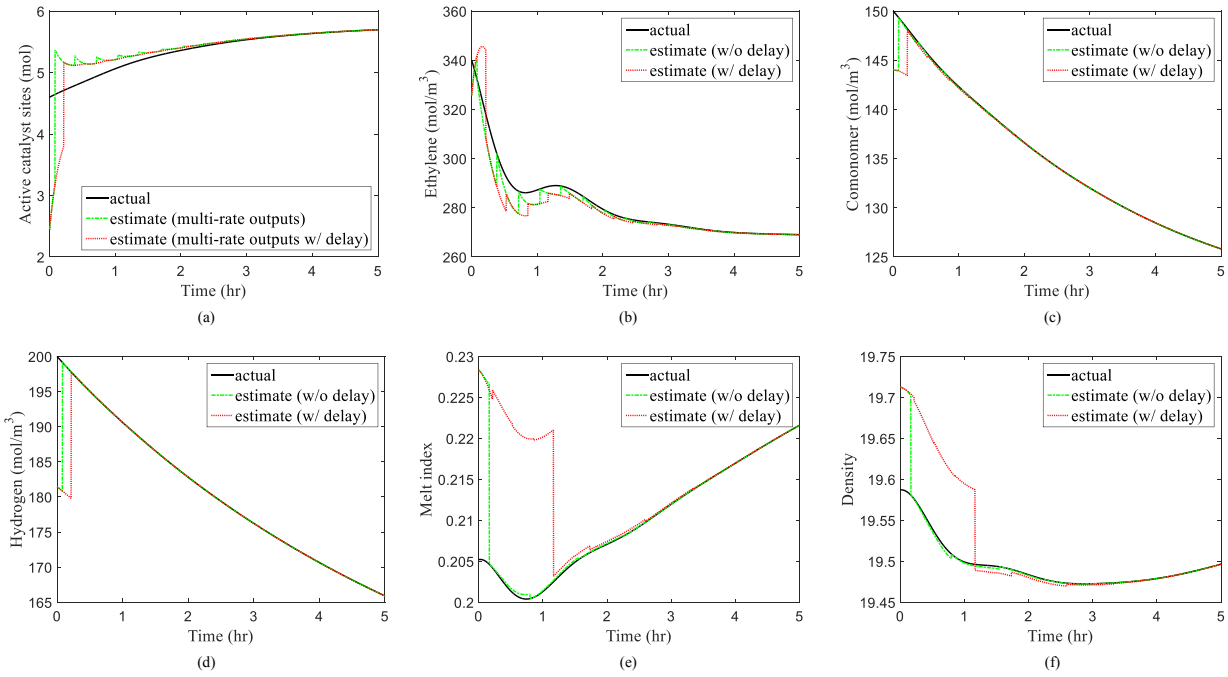

Figure 4.3: Comparison of the multi-rate multi-delay observer (red) and the multi-rate observer in the absence of measurement delay (green) in the linearized gas-phase polyethylene reactor example.

gain computed from linearization can be constructed to estimate the states in a nonlinear system, where the nonlinear model will be used in the dead time compensation and inter-sample prediction to cope with the nonlinearities.

4.5 Conclusions

The chapter proposes a design method for multi-rate multi-delay observers in linear systems. It is based on an available multi-rate observer design (see Chapter 3) combined with dead time compensation, where continuous and sampled measurements, in the presence of possible measurement delays, are accounted for. The estimation process has two steps: (i) dead time compensation when a delayed measurement becomes available and then current estimates are updated, (ii) inter-sample prediction in the time interval between two consecutive delayed measurements. Two attractive features of the proposed observer are that it inherits the stability and robustness properties from a delay-free multi-rate observer and it can handle nonconstant and arbitrarily large measurement de-

lays. Unlike the chain observers in the literature where a high dimension may be required in the case of large delays, the proposed observer has the same dimension as a multi-rate observer for a delay-free system. From the two case studies, we see that the multi-rate multi-delay observer can provide reliable estimation results. The presence of delays in the measurements inevitably slows down convergence of the observer.

5. OPTIMAL MULTI-RATE OBSERVER DESIGN IN LINEAR SYSTEMS

The previous Chapters 3 and 4 have focused on the problem of incorporating different types of measurements in a unified observer framework in linear multi-rate systems, for prescribed eigenvalues of the error dynamics. There is still one piece of information missing regarding the selection of observer design parameters. In many practical problems, it is possible to use empirical rules for the selection of the eigenvalues of the error dynamics, in conjunction with trial and error (i.e., simulation and evaluation of the observer response in the presence of modeling error and measurement error), and obtain an observer with satisfactory performance.

In this chapter, the desirable eigenvalues of the error dynamics are adjustable parameters in the observer design procedure. Because the observer is dual to the state feedback controller, a rigorous approach for observer design by optimizing an appropriate performance index will be developed in the same spirit as gain selection in optimal state feedback control. As mentioned in Chapter 1, there is a trade-off between the convergence rate of the observer and the estimation accuracy affected by measurement noise. The optimal pole placement of observer is not a simple problem, which should be based on the criteria such as noise level, parameter variation, reliability, and ease of synthesis. In general, as the eigenvalues of the error dynamics get faster, the decay of the initial error will get faster. But at the same time, state estimates lose accuracy because the effect of measurement noise gets magnified. Conversely, as the eigenvalues of the error dynamics get slower, state estimates get less affected by measurement noise, but the decay of the initial error will get slower and the effect of modeling error of the the process dynamics will get more pronounced.

Because of this qualitative behavior and the fact that measurement error is usually independent of modeling error of state dynamics, it makes sense to use a performance index which is a weighted sum of measure of the effect of dynamic model error on the accuracy of state estimates and measure of the effect of measurement error on the accuracy of state estimates. The weight coefficient may be selected in accordance with the relative magnitude between modeling error and measurement error in the dynamic system.

The use of a performance index of the above form is in alignment with the intuitive formulation of linear multi-rate observer design of Equation (3.5), as trying to reach a compromise between the dynamic model and the measurement model, which are not perfectly consistent due to the presence of errors. Optimization of the performance index will give the optimal compromise.

The rest of the chapter is organized as follows. We start from the problem of optimal single-rate observer design in Section 5.1, where the selection of observer gain is formulated as an optimization problem. A few important properties of a single-rate observer will be discussed. Second-order systems and a numerical example are used to study the relationship between sampling period and feasible range of the eigenvalues of observer design parameter, and an analytical bound can be obtained. The optimal single-rate observer design method is then illustrated via studying the observer response to single unit impulse in the modeling and measurement error. In Section 5.2, the optimal multi-rate observer design is demonstrated on a class of linear systems in the presence of two types of measurements, i.e., one fast-sampled and the other slow-sampled. A numerical example is used to illustrate the applicability of the method. In Section 5.3, conclusions are drawn from the results of the previous sections.

5.1 Optimal Single-Rate Observer Design

The study in this section is developed based on the multi-rate observer design in Chapter 3 with focus on the reduced-order observer formulation. Single-rate measurements are considered here as a special case and it is assumed that no continuous measurements are involved. In other words, all the measurements are discrete and synchronized in this class of sampled-data systems.

5.1.1 Problem Formulation

Consider a linear single-rate sampled-data system where the output is assumed to be available at discrete time instants t_k

$$\begin{aligned} \dot{x}_R(t) &= F_{11}x_R(t) + F_{12}x_M(t) + \gamma_1 v(t) \\ \dot{x}_M(t) &= F_{21}x_R(t) + F_{22}x_M(t) + \gamma_2 v(t) \\ y(t_k) &= x_M(t_k) + \beta u(t_k), \qquad k = 0, 1, 2, \dots \end{aligned} \tag{5.1}$$

where $x_R \in \mathbb{R}^{n-m}$ is the unmeasured state vector, $x_M \in \mathbb{R}^m$ is the remaining state vector which is directly measured, y is the output vector, v and u are two unknown scalar functions of time that represent uncertainty in the dynamic model and in the measurement model respectively. γ_1, γ_2 and β are constant column vectors that account for the relative accuracy of the model and measurement equations. The sampling times of all the measurements are synchronized and it is assumed that the sampling period τ is uniform. The system input is omitted here for brevity.

Suppose the system (5.1) is observable if the outputs were assumed to be continuous and hence, a continuous-time Luenberger observer design is available. From the proposed multi-rate observer design (3.5), for $t \in [t_k^+, t_{k+1}]$, we have the following single-rate reduced-order observer design

$$\begin{aligned} \dot{z}(t) &= Az(t) + Bw(t) \\ \dot{w}(t) &= F_{21}\hat{x}_R(t) + F_{22}w(t) \\ w(t_k^+) &= y(t_k) \\ \hat{x}_R(t) &= {T_R}^{-1}(z(t) - T_M w(t)) \end{aligned} \tag{5.2}$$

where $z = T_R\hat{x}_R + T_M w$ is the observer state, $w \in \mathbb{R}^m$ is the predicted output, and T_R, T_M satisfy the following Sylvester equation:

$$\begin{bmatrix} T_R & T_M \end{bmatrix} \begin{bmatrix} F_{11} & F_{12} \\ F_{21} & F_{22} \end{bmatrix} = A \begin{bmatrix} T_R & T_M \end{bmatrix} + B \begin{bmatrix} 0 & I \end{bmatrix} \tag{5.3}$$

We denote the estimation error in x-coordinates $e_R(t) = x_R(t) - \hat{x}_R(t)$, output prediction error $e_w(t) = x_M(t) - w(t)$, and observer error $e_z(t) = T_R e_R(t) + T_M e_w(t)$. The difference between the single-rate observer (5.2) and the multi-rate observer (3.5) is that the entire vector of prediction error $e_w(t)$ will be reinitialized to 0 at t_k, as shown in the following error dynamics of the observer for $t \in [t_k^+, t_{k+1}]$ in the absence of modeling and measurement error

$$\begin{aligned} \dot{e}_z(t) &= A e_z(t) + B e_w(t) \\ \dot{e}_w(t) &= F_{21} T_R^{-1} e_z(t) + (F_{22} - F_{21} T_R^{-1} T_M) e_w(t) \\ e_w(t_k^+) &= 0 \end{aligned} \tag{5.4}$$

In Equation (5.2), the observer state $z(t)$ does not change at the sampling instants. For simplicity, we denote

$$F = \begin{bmatrix} F_{11} & F_{12} \\ F_{21} & F_{22} \end{bmatrix}$$

$$M = \begin{bmatrix} A & B \\ F_{21} T_R^{-1} & F_{22} - F_{21} T_R^{-1} T_M \end{bmatrix}$$

It can be shown that the matrix M shares the same eigenvalues as the transition matrix F

$$\begin{bmatrix} T_R^{-1} & -T_R^{-1} T_M \\ 0 & I \end{bmatrix} \begin{bmatrix} A & B \\ F_{21} T_R^{-1} & F_{22} - F_{21} T_R^{-1} T_M \end{bmatrix} \begin{bmatrix} T_R & T_M \\ 0 & I \end{bmatrix} = \begin{bmatrix} F_{11} & F_{12} \\ F_{21} & F_{22} \end{bmatrix}$$

Thus, the error dynamics of the observer in the sampling interval has the same stability property as the original system dynamics. Using Equation (5.4), the error vectors at two consecutive sampling instants t_k^+, t_{k+1}^+ satisfy

$$\begin{bmatrix} e_z(t_{k+1}^+) \\ e_w(t_{k+1}^+) \end{bmatrix} = \begin{bmatrix} I & 0 \\ 0 & 0 \end{bmatrix} \exp(M\tau) \begin{bmatrix} e_z(t_k^+) \\ e_w(t_k^+) \end{bmatrix} \tag{5.5}$$

We will denote $e(t) = \begin{bmatrix} e_z'(t) & e_w'(t) \end{bmatrix}'$ and $G = \begin{bmatrix} I & 0 \\ 0 & 0 \end{bmatrix} \exp(M\tau)$ for simplicity. As mentioned in the mathematical example of Chapter 3, the estimation error will converge to 0 if $\rho(G) < 1$, where $\rho(G)$ is the spectral radius of G.

Remark 16. *As the sampling period τ approaches 0, we calculate the change of estimation error at two consecutive sampling instants t_k^+ and t_{k+1}^+*

$$\dot{e}(t) = \lim_{\tau \to 0} \frac{e(t_{k+1}^+) - e(t_k^+)}{\tau} = \lim_{\tau \to 0} \frac{(G - I)e(t_k^+)}{\tau}$$

Because of the fact that $\lim_{\tau \to 0} G = \begin{bmatrix} I & 0 \\ 0 & 0 \end{bmatrix}$, we have $\lim_{\tau \to 0}(G - I)e(t_k^+) = 0$. Using L'Hôpital's rule, the above equation can be simplified

$$\begin{aligned} \dot{e}(t) &= \lim_{\tau \to 0} \begin{bmatrix} I & 0 \\ 0 & 0 \end{bmatrix} M \exp(M\tau) e(t_k^+) \\ &= \lim_{\tau \to 0} \begin{bmatrix} A & B \\ 0 & 0 \end{bmatrix} \exp(M\tau) e(t_k^+) \\ &= \begin{bmatrix} A & B \\ 0 & 0 \end{bmatrix} \begin{bmatrix} e_z(t_k^+) \\ 0 \end{bmatrix} \end{aligned}$$

where $e_w(t_k^+)$ will be reinitialized to 0 at each sampling instant.

As the sampling period τ approaches 0, the adjacent sampling instants become infinitely close so that we will remove the index k and consider the sampling is performed in a continuous manner. Therefore, the error dynamics of $z(t)$ follows

$$\dot{e}_z(t) = A e_z(t)$$

which is governed by the arbitrarily selected A matrix. Thus, the error dynamics in z-coordinates

will behave exactly the same as in a continuous-time Luenberger observer.

The single-rate observer (5.2) is designed in z-coordinates and state estimates in the original x-coordinates can be reconstructed after linear transformation. Equivalently, there exists an observer in x-coordinates, and it can be derived using Equations (5.2) and (5.3)

$$\begin{aligned}
\dot{\hat{x}}_R &= T_R^{-1}(\dot{z} - T_M\dot{w}) \\
&= T_R^{-1}Az + T_R^{-1}Bw - T_R^{-1}T_M F_{21}\hat{x}_R - T_R^{-1}T_M F_{22}w - T_R^{-1}T_M(y(t_k) - w(t_k^-))\delta(t - t_k) \\
&= F_{11}\hat{x}_R + F_{12}w + l \cdot (y(t_k) - w(t_k^-))\delta(t - t_k) \\
\dot{w} &= F_{21}\hat{x}_R + F_{22}w + (y(t_k) - w(t_k^-))\delta(t - t_k)
\end{aligned}$$

where $l = -T_R^{-1}T_M$ is the observer gain in a reduced-order Luenberger observer design, $\delta(t)$ is a unit impulse function that has the effect of reinitializing the state estimates $\hat{x}_R(t)$ and the predictor state $w(t)$ at each sampling time t_k. We denote $w(t_k^-) = \lim_{h\to 0} w(t_k - h)$. For $t \in [t_k^+, t_{k+1}]$, we have the following single-rate observer coupled with inter-sample predictors

$$\begin{aligned}
\dot{\hat{x}}_R(t) &= F_{11}\hat{x}_R(t) + F_{12}w(t) \\
\dot{w}(t) &= F_{21}\hat{x}_R(t) + F_{22}w(t) \\
\hat{x}_R(t_k^+) &= \hat{x}_R(t_k^-) + l \cdot (y(t_k) - w(t_k^-)) \\
w(t_k^+) &= y(t_k)
\end{aligned} \tag{5.6}$$

where the reinitialization step is shown explicitly on the state $\hat{x}_R$ and w at t_k. For $t \in [t_k^+, t_{k+1}]$, the error dynamics of the observer (5.6), in the absence of modeling and measurement error, follows

$$\begin{aligned}
\dot{e}_R(t) &= F_{11}e_R(t) + F_{12}e_w(t) \\
\dot{e}_w(t) &= F_{21}e_R(t) + F_{22}e_w(t) \\
e_R(t_k^+) &= e_R(t_k^-) - l \cdot (y(t_k) - w(t_k^-)) \\
e_w(t_k^+) &= 0
\end{aligned} \tag{5.7}$$

Using Equation (5.7), the error vectors at two consecutive sampling instants t_k^+, t_{k+1}^+ satisfy

$$\begin{bmatrix} e_R(t_{k+1}^+) \\ e_w(t_{k+1}^+) \end{bmatrix} = \begin{bmatrix} I & -l \\ 0 & 0 \end{bmatrix} \exp(F\tau) \begin{bmatrix} e_R(t_k^+) \\ e_w(t_k^+) \end{bmatrix}$$

We denote $\Gamma = \begin{bmatrix} I & -l \\ 0 & 0 \end{bmatrix} \exp(F\tau)$ for simplicity. It can be shown that the matrix G shares the same eigenvalues as the matrix Γ

$$\begin{aligned} &\begin{bmatrix} T_R^{-1} & -T_R^{-1}T_M \\ 0 & I \end{bmatrix} \begin{bmatrix} I & 0 \\ 0 & 0 \end{bmatrix} \exp(M\tau) \begin{bmatrix} T_R & T_M \\ 0 & I \end{bmatrix} \\ &= \begin{bmatrix} T_R^{-1} & 0 \\ 0 & 0 \end{bmatrix} \begin{bmatrix} T_R & T_M \\ 0 & I \end{bmatrix} \exp(F\tau) \begin{bmatrix} T_R^{-1} & -T_R^{-1}T_M \\ 0 & I \end{bmatrix} \begin{bmatrix} T_R & T_M \\ 0 & I \end{bmatrix} \\ &= \begin{bmatrix} I & -l \\ 0 & 0 \end{bmatrix} \exp(F\tau) \end{aligned}$$

Thus, it is concluded that the estimation error will converge to zero if $\rho(\Gamma) < 1$.

Note that the discussions above do not consider the modeling error $v(t)$ and measurement error $u(t)$ in the derived error dynamics of the observer. Next, the problem of optimal gain selection will be discussed. It makes more sense to adopt the single-rate observer in x-coordinates as the gain l would be the only parameter to be optimized, as opposed to optimize two design parameters A and B if the observer in z-coordinates is adopted.

Now we denote $\hat{x} = \begin{bmatrix} \hat{x}_R \\ w \end{bmatrix}, L = \begin{bmatrix} l \\ I \end{bmatrix}, \gamma = \begin{bmatrix} \gamma_1 \\ \gamma_2 \end{bmatrix}, \varepsilon = \begin{bmatrix} x_R \\ x_M \end{bmatrix} - \begin{bmatrix} \hat{x}_R \\ w \end{bmatrix}$, and we can write the observer (5.6) in a compact form

$$\begin{aligned} \dot{\hat{x}}(t) &= F\hat{x}(t) \\ \hat{x}(t_k^+) &= \hat{x}(t_k^-) + L \cdot (y(t_k) - w(t_k^-)) \end{aligned}$$

The dynamics of the estimation error $\varepsilon(t)$, in the presence of modeling error and measurement error, is described by

$$\begin{aligned} \dot{\varepsilon}(t) &= F\varepsilon(t) + \gamma v(t) \\ \varepsilon(t_k^+) &= \varepsilon(t_k^-) - L \cdot (y(t_k) - w(t_k^-)) \end{aligned} \tag{5.8}$$

We see that the uncertainties $v(t)$ and $u(t)$, in the model and the measurement respectively, are inputs to the dynamics of the state estimation error $\varepsilon(t)$ so that it is possible to evaluate their effect by studying the response of $\varepsilon(t)$ to standard changes, e.g., unit impulse. Since measurement error is often independent of modeling error of state dynamics, it is possible to calculate the corresponding estimation error caused by the modeling error $v(t)$ and the measurement error $u(t)$ separately. So we denote $\varepsilon_v(t)$ the corresponding state estimation error if the modeling error is a continuous-time unit impulse function (i.e., $v(t) = \delta(t)$), in the absence of measurement error and initial condition error. Likewise, we denote $\varepsilon_u(t)$ the corresponding state estimation error if the measurement error is a discrete-time unit impulse function (i.e., $u(t) = \delta[t]$), in the absence of initial condition error and modeling error.

In case $v(t)$ and $u(t)$ are superpositions of impulses of random magnitude occurring at random time instants (also known as noise), i.e.,

$$\begin{aligned} v(t) &= \sum_i M_{v_i} \delta(t - t_i) \\ u(t) &= \sum_k M_{u_k} \delta[t - t_k] \end{aligned}$$

where M_{v_i} is the magnitude of the impulse occurring at t_i and M_{u_k} is the magnitude of the impulse occurring at discrete time instants t_k. The effect of each impulse on the state estimation error will be additive

$$\varepsilon_{\text{due to noise}}(t) = \sum_i M_{v_i} \varepsilon_v(t - t_i) + \sum_k M_{u_k} \varepsilon_u(t - t_k)$$

It should be emphasized at this point that a rigorous analysis of the error due to the presence of noise should be based on a stochastic formulation of the problem, to calculate and minimize the covariance of the state estimation error (see the discussions on Kalman filter in Chapter 1), which is beyond the scope of this dissertation.

A simpler approach to the problem of finding the optimal compromise between modeling error and measurement error is to consider a single continuous-time unit impulse for $v(t)$ and a single discrete-time unit impulse for $u(t)$, and seek for the minimum of the performance index

$$J = \int_0^\infty \|\varepsilon_v(t)\|^2 \, dt + \rho \int_0^\infty \|\varepsilon_u(t)\|^2 \, dt \tag{5.9}$$

where $\|\cdot\|$ is the Euclidean norm in $\mathbb{R}^n$ (i.e., $\|x\|^2 = x'x$), $\varepsilon_v(t)$ and $\varepsilon_u(t)$ are the responses of the estimation error to unit impulse changes in $v(t)$ and $u(t)$ respectively. $\rho > 0$ is a weight coefficient. The first integral is a measure of the effect of modeling error on the accuracy of the state observer, whereas the second integral is a measure of the effect of measurement error on the accuracy of the observer.

Because $\varepsilon_v(t)$ and $\varepsilon_u(t)$ are responses to unit-magnitude impulses in $v(t)$ and $u(t)$, and because they are squared inside the integrals, it is reasonable to choose the weight coefficient as the ratio of the mean value of $[u(t)]^2$ divided by the mean value of $[v(t)]^2$, so that the performance index J is proportional to the overall measure of the squared error. In particular, given statistical information on $v(t)$ and $u(t)$, the weight coefficient ρ may be chosen as

$$\rho = \frac{(\text{Standard deviation of noise } u)^2}{(\text{Standard deviation of noise } v)^2}$$

First, the response of the estimation error to a unit impulse change in $v(t)$ will be investigated, in the absence of measurement error and initial condition error. $\varepsilon_v(t)$ can be calculated in the first

few sampling periods using Equation (5.8) as follows

$$
\begin{aligned}
t \in [0,\tau): \quad & \varepsilon_v(0^+) = \gamma, && \varepsilon_v(t) = \exp(Ft)\varepsilon_v(0^+),\\
& \varepsilon_v(\tau^-) = \exp(F\tau)\varepsilon_v(0^+) &&\\
t \in [\tau,2\tau): \quad & \varepsilon_v(\tau^+) = (I-LH)\varepsilon_v(\tau^-), && \varepsilon_v(t) = \exp(F(t-\tau))\varepsilon_v(\tau^+),\\
& \varepsilon_v(2\tau^-) = \exp(F\tau)\varepsilon_v(\tau^+) &&\\
t \in [2\tau,3\tau): \quad & \varepsilon_v(2\tau^+) = (I-LH)\varepsilon_v(2\tau^-), && \varepsilon_v(t) = \exp(F(t-2\tau))\varepsilon_v(2\tau^+),\\
& \varepsilon_v(3\tau^-) = \exp(F\tau)\varepsilon_v(2\tau^+) &&\\
\cdots \quad & \cdots &&
\end{aligned}
$$

where $H = \begin{bmatrix} 0 & I \end{bmatrix}$ and the previously mentioned matrix $\Gamma = (I - LH)\exp(F\tau)$.

Consider the first integral in the performance index (5.9) corresponding to $\varepsilon_v(t)$, which will be integrated piecewise

$$
\begin{aligned}
J_v = & \int_0^\infty \|\varepsilon_v(t)\|^2 \, dt\\
= & \operatorname{Tr}\Bigg(\int_0^\tau \exp(Ft)\varepsilon_v(0^+)\varepsilon_v'(0^+)\exp(F't)\, dt\\
& + \int_\tau^{2\tau} \exp(F(t-\tau))\varepsilon_v(\tau^+)\varepsilon_v'(\tau^+)\exp(F'(t-\tau))\, dt\\
& + \int_{2\tau}^{3\tau} \exp(F(t-2\tau))\varepsilon_v(2\tau^+)\varepsilon_v'(2\tau^+)\exp(F'(t-2\tau))\, dt + \cdots \Bigg)
\end{aligned}
$$

where $\operatorname{Tr}(\cdot)$ denotes the trace of a square matrix. Setting $J_v = \operatorname{Tr}(P_v)$, we observe that

$$
\begin{aligned}
FP_v + P_vF' = & \int_0^\tau \left[\frac{d}{dt}\left(\exp(Ft)\varepsilon_v(0^+)\varepsilon_v'(0^+)\exp(F't)\right)\right] dt\\
& + \int_\tau^{2\tau} \left[\frac{d}{dt}\left(\exp(F(t-\tau))\varepsilon_v(\tau^+)\varepsilon_v'(\tau^+)\exp(F'(t-\tau))\right)\right] dt\\
& + \int_{2\tau}^{3\tau} \left[\frac{d}{dt}\left(\exp(F(t-2\tau))\varepsilon_v(2\tau^+)\varepsilon_v'(2\tau^+)\exp(F'(t-2\tau))\right)\right] dt + \cdots
\end{aligned}
$$

Simplify the above equation and we have

$$\begin{aligned} FP_v + P_vF' = \quad & \exp(F\tau)\varepsilon_v(0^+)\varepsilon_v'(0^+)\exp(F'\tau) - \varepsilon_v(0^+)\varepsilon_v'(0^+) \\ & + \exp(F\tau)\varepsilon_v(\tau^+)\varepsilon_v'(\tau^+)\exp(F'\tau) - \varepsilon_v(\tau^+)\varepsilon_v'(\tau^+) \\ & + \exp(F\tau)\varepsilon_v(2\tau^+)\varepsilon_v'(2\tau^+)\exp(F'\tau) - \varepsilon_v(2\tau^+)\varepsilon_v'(2\tau^+) + \cdots \end{aligned} \tag{5.10}$$

For simplicity, we denote $S_v = \sum_{i=0}^{\infty} \varepsilon_v(i\tau^+)\varepsilon_v'(i\tau^+) = \sum_{i=0}^{\infty} \Gamma^i\gamma\gamma'(\Gamma')^i$ and we have

$$\Gamma S_v\Gamma' = \Gamma\gamma\gamma'\Gamma' + \Gamma^2\gamma\gamma'(\Gamma')^2 + \cdots \tag{5.11}$$

$$S_v - \Gamma S_v\Gamma' = \gamma\gamma' \tag{5.12}$$

where $\lim_{n\to\infty}\Gamma^n = 0$ as long as the error dynamics is stable.

Second, the response of the estimation error to a unit impulse change in $u(t)$ will be discussed, in the absence of modeling error and initial condition error. $\varepsilon_u(t)$ can be calculated in the first few sampling periods using Equation (5.8) as follows

$$\begin{aligned} t \in [0,\tau): \quad & \varepsilon_u(0^+) = -L\beta, && \varepsilon_u(t) = \exp(Ft)\varepsilon_u(0^+), \\ & \varepsilon_u(\tau^-) = \exp(F\tau)\varepsilon_u(0^+) \\ t \in [\tau,2\tau): \quad & \varepsilon_u(\tau^+) = (I-LH)\varepsilon_u(\tau^-), && \varepsilon_u(t) = \exp(F(t-\tau))\varepsilon_u(\tau^+), \\ & \varepsilon_u(2\tau^-) = \exp(F\tau)\varepsilon_u(\tau^+) \\ t \in [2\tau,3\tau): \quad & \varepsilon_u(2\tau^+) = (I-LH)\varepsilon_u(2\tau^-), && \varepsilon_u(t) = \exp(F(t-2\tau))\varepsilon_u(2\tau^+), \\ & \varepsilon_u(3\tau^-) = \exp(F\tau)\varepsilon_u(2\tau^+) \\ \cdots \quad & \cdots \end{aligned} \tag{5.13}$$

We denote $J_u = \int_0^{\infty} \|\varepsilon_u(t)\|^2\, dt = \mathrm{Tr}(P_u)$ and $S_u = \sum_{i=0}^{\infty} \varepsilon_u(i\tau^+)\varepsilon_u'(i\tau^+) = \sum_{i=0}^{\infty} \Gamma^i L\beta\beta' L'(\Gamma')^i$. By

following the similar steps above, we obtain

$$FP_u + P_uF' = \exp(F\tau)S_u\exp(F'\tau) - S_u \tag{5.14}$$

$$S_u - \Gamma S_u\Gamma' = L\beta\beta'L' \tag{5.15}$$

as long as the error dynamics of the observer is stable.

Now we combine the two integrals J_v, J_u, and seek for the minimum of the performance index (5.9). Using Equations (5.10), (5.12), (5.14) and (5.15), the problem of single-rate observer design can be formulated as an optimization problem

$$\begin{aligned} \min_{l} \quad & \mathrm{Tr}(P) \\ s.t. \quad & FP + PF' = \exp(F\tau)S\exp(F'\tau) - S \\ & S - \Gamma S\Gamma' = \gamma\gamma' + \rho L\beta\beta'L' \end{aligned} \tag{5.16}$$

where $P = P_v + \rho P_u$ and $S = S_v + \rho S_u$.

5.1.2 Case Studies

In Section 3.4, the proposed multi-rate observer was first applied to a third-order system with one continuous measurement and one sampled measurement. The feasible range of observer design parameter A (that guarantees stability of the error dynamics) as a function of the sampling period τ was calculated numerically using interval halving and was illustrated in Figure 3.1. In this section, second-order systems will be used to study the relationship between sampling period and feasible range of the eigenvalue of design parameter and a closed-form bound can be derived in the absence of modeling error and measurement error. The optimal single-rate observer design method will be illustrated through a second-order numerical example.

Consider a general second-order system in the presence of one sampled output

$$\begin{aligned} \dot{x}_R(t) &= F_{11}x_R(t) + F_{12}x_M(t) \\ \dot{x}_M(t) &= F_{21}x_R(t) + F_{22}x_M(t) \\ y(t_k) &= x_M(t_k), \qquad k = 0, 1, 2, \ldots \end{aligned} \tag{5.17}$$

where $y \in \mathbb{R}$ is the sampled output. It will be assumed that the sampling period τ is uniform. F_{11}, F_{12}, F_{21} and F_{22} are scalars in this case. The single-rate observer will be designed in z-coordinates and using Equation (5.5), the estimation error vectors $e(t)$ at two consecutive sampling instants t_k^+, t_{k+1}^+ satisfy

$$\begin{bmatrix} e_z(t_{k+1}^+) \\ e_w(t_{k+1}^+) \end{bmatrix} = \begin{bmatrix} 1 & 0 \\ 0 & 0 \end{bmatrix} \exp(M\tau) \begin{bmatrix} e_z(t_k^+) \\ e_w(t_k^+) \end{bmatrix}$$

with $e_w(t_k^+) = 0$, once the predictor state is reinitialized after sampling.

Next we would like to study the feasible range of A as a function of the sampling period τ. In [308], an explicit formula was derived for the exponential of a general 2×2 complex matrix, given in terms of the eigenvalues of the matrix. It is assumed that M has two distinct eigenvalues λ and μ satisfying $\mu > \lambda$. Then an explicit formula of G, which involves the calculation of an exponential matrix (i.e., $\exp(M\tau)$), can be obtained

$$\begin{aligned} G &= \begin{bmatrix} 1 & 0 \\ 0 & 0 \end{bmatrix} \exp\left(\begin{bmatrix} A & B \\ F_{21}T_R^{-1} & F_{22} - F_{21}T_R^{-1}T_M \end{bmatrix} \tau \right) \\ &= \begin{bmatrix} 1 & 0 \\ 0 & 0 \end{bmatrix} \left(\frac{\mu\exp(\lambda\tau) - \lambda\exp(\mu\tau)}{\mu - \lambda} \begin{bmatrix} 1 & 0 \\ 0 & 1 \end{bmatrix} + \frac{\exp(\mu\tau) - \exp(\lambda\tau)}{\mu - \lambda} M \right) \\ &= \begin{bmatrix} \dfrac{\mu\exp(\lambda\tau) - \lambda\exp(\mu\tau) + A\exp(\mu\tau) - A\exp(\lambda\tau)}{\mu - \lambda} & \dfrac{B\exp(\mu\tau) - B\exp(\lambda\tau)}{\mu - \lambda} \\ 0 & 0 \end{bmatrix} \end{aligned}$$

The estimation error $e(t)$ will converge to zero if $\rho(G) < 1$. Hence, the following inequalities

need to be solved

$$\frac{\mu\exp(\lambda\tau)-\lambda\exp(\mu\tau)+A\exp(\mu\tau)-A\exp(\lambda\tau)}{\mu-\lambda}>-1$$
$$\frac{\mu\exp(\lambda\tau)-\lambda\exp(\mu\tau)+A\exp(\mu\tau)-A\exp(\lambda\tau)}{\mu-\lambda}<1$$

As a result, the feasible range of the design parameter A satisfies

$$\frac{\lambda-\mu+\lambda\exp(\mu\tau)-\mu\exp(\lambda\tau)}{\exp(\mu\tau)-\exp(\lambda\tau)}<A<\frac{\mu-\lambda+\lambda\exp(\mu\tau)-\mu\exp(\lambda\tau)}{\exp(\mu\tau)-\exp(\lambda\tau)} \tag{5.18}$$

A numerical example will be used to study the relationship between the sampling period τ and the feasible range of the eigenvalues of the design parameter A. Consider the following state-space model of a second-order system

$$\begin{bmatrix}\dot{x}_1(t)\\ \dot{x}_2(t)\end{bmatrix}=\begin{bmatrix}-0.007 & 0.005\\ 0.002 & -0.003\end{bmatrix}\begin{bmatrix}x_1(t)\\ x_2(t)\end{bmatrix}+\begin{bmatrix}1\\ 1\end{bmatrix}v(t)$$
$$y(t_k)=x_2(t_k)+u(t_k),\qquad k=0,1,2,\ldots$$

where $x_1\in\mathbb{R}$ is the unmeasured state and $x_2\in\mathbb{R}$ is the sampled state. In the absence of modeling error and measurement error (i.e., $v(t)=u(t)\equiv 0$), the design parameters of single-rate observer are fixed as $A=-0.05$ and $B=1$. Figure 5.1(a) shows how the uniform sampling period τ affects the spectral radius of G. It is observed that the error dynamics become unstable once $\tau>51$ s. At $\tau=22.3$ s, the spectral radius of G becomes 0 and the observer becomes deadbeat. Figure 5.1(b) depicts the feasible range of A as a function of the sampling period τ, which is obtained using the closed-form expression in Equation (5.18).

In the presence of modeling error and measurement error, an optimal single-rate observer will be designed in the case that a single continuous-time unit impulse for $v(t)$ and a single discrete-time unit impulse for $u(t)$ are considered and a performance index of Equation (5.9) is minimized. The sampling period $\tau=10$ and the weight coefficient $\rho=1$ are chosen. Solving the optimization

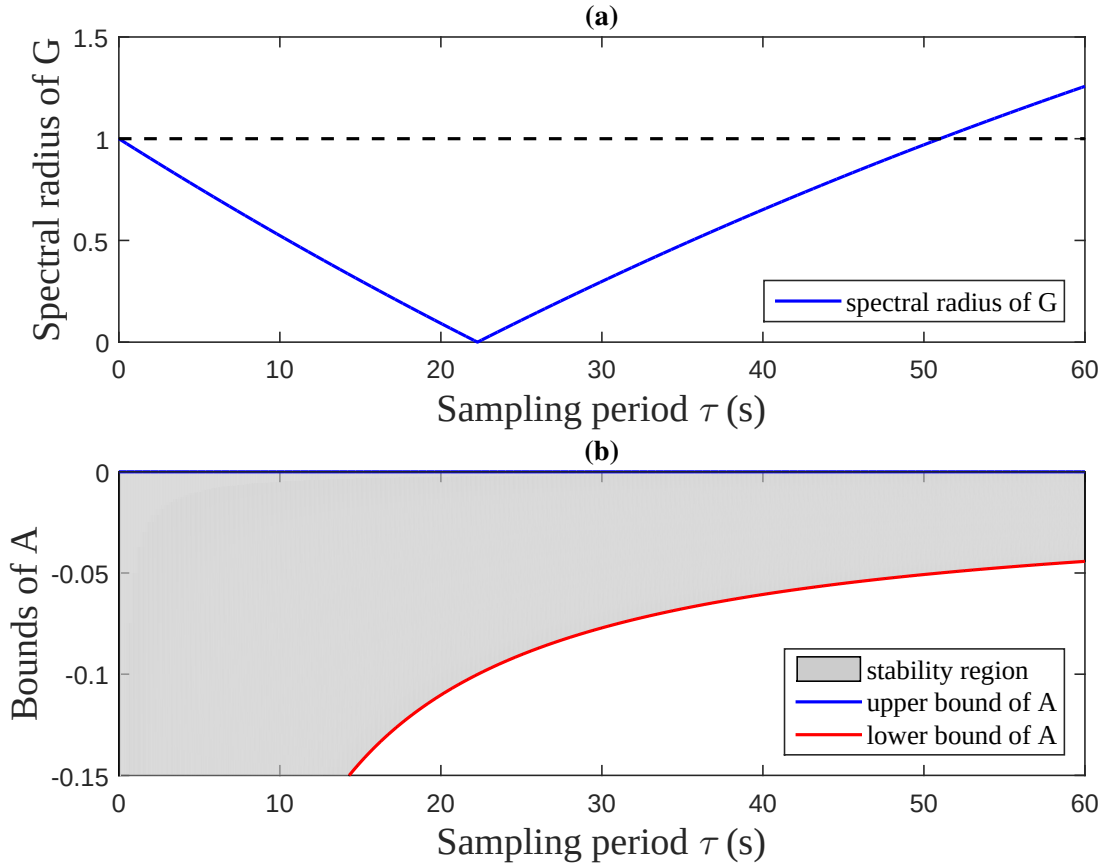

Figure 5.1: (a) Spectral radius of G as a function of the sampling period τ (uniform) when $A = -0.05$ and $B = 1$; (b) feasible range of A as a function of the sampling period τ (uniform) when $B = 1$.

of Equation (5.16), the optimal observer design has the following parameters

$$l = 0.8488, \quad P = \begin{bmatrix} 18.0782 & 18.2493 \\ 18.2493 & 19.7712 \end{bmatrix}, \quad S = \begin{bmatrix} 1.8436 & 1.8488 \\ 1.8488 & 2.0000 \end{bmatrix}$$

5.2 Optimal Multi-Rate Observer Design with Fast and Slow Measurements

In this section, optimal multi-rate observer design is demonstrated on a class of systems in the presence of two sampling rates. Besides, it will be assumed that the high sampling rate is an integer multiple of the low sampling rate, which implies that the two types of sampling are synchronized

at the sampling time instants of the slow measurement.

5.2.1 Problem Formulation

Consider a linear multi-rate sampled-data system with fast- and slow-sampled measurements, where without loss of generality, the output is assumed to be a part of the state vector

$$\begin{aligned}
\dot{x}_R(t) &= F_{11}x_R(t) + F_{12}x_{Mf}(t) + F_{13}x_{Ms}(t) + \gamma_1 v(t) \\
\dot{x}_{Mf}(t) &= F_{21}x_R(t) + F_{22}x_{Mf}(t) + F_{23}x_{Ms}(t) + \gamma_2 v(t) \\
\dot{x}_{Ms}(t) &= F_{31}x_R(t) + F_{32}x_{Mf}(t) + F_{33}x_{Ms}(t) + \gamma_3 v(t) \\
y_f(t_{f,i}) &= x_{Mf}(t_{f,i}) + \beta_f u_f(t_{f,i}), \qquad i = 0, 1, 2, \dots \\
y_s(t_{s,j}) &= x_{Ms}(t_{s,j}) + \beta_s u_s(t_{s,j}), \qquad j = 0, 1, 2, \dots
\end{aligned} \tag{5.19}$$

where $x_R \in \mathbb{R}^{n-m_f-m_s}$ is the unmeasured state vector, $x_{Mf} \in \mathbb{R}^{m_f}$ is the fast-sampled state vector, $x_{Ms} \in \mathbb{R}^{m_s}$ is the slow-sampled state vector, $t_{f,i}$ is the i-th sampling time for the fast measurement y_f, and $t_{s,j}$ is the j-th sampling time for the slow measurement y_s. v, u_f and u_s are the unknown scalar functions of time that represent uncertainty in the dynamic model, fast measurement model, and slow measurement model respectively. γ_1, γ_2 and γ_3 are constant column vectors that account for the relative accuracy of the model equations. β_f and β_s are constant column vectors that account for the relative accuracy of the measurement equations. It will be assumed that the sampling period of the fast measurement is uniform (i.e., $\tau_f = \tau$), and the sampling period of the slow measurement is uniform and is an integer multiple of τ_f (i.e., $\tau_s = a\tau$ where a is a positive integer).

Suppose the system (5.19) is observable if the outputs were assumed to be continuous and thus, a continuous-time Luenberger observer design is available. From the proposed multi-rate observer

design (3.5), for $t \in [t_{f,i}^+, t_{f,i+1}]$, we have the following multi-rate reduced-order observer design

$$\begin{aligned}
\dot{z}(t) &= Az(t) + B_f w_f(t) + B_s w_s(t) \\
\dot{w}_f(t) &= F_{21}\hat{x}_R(t) + F_{22} w_f(t) + F_{23} w_s(t) \\
\dot{w}_s(t) &= F_{31}\hat{x}_R(t) + F_{32} w_f(t) + F_{33} w_s(t) \\
w_f(t_{f,i}^+) &= y_f(t_{f,i}) \\
w_s(t_{s,j}^+) &= y_s(t_{s,j}), \qquad \text{if } t_{f,i} = t_{s,j} \\
\hat{x}_R(t) &= {T_R}^{-1}(z(t) - T_{Mf} w_f(t) - T_{Ms} w_s(t))
\end{aligned} \tag{5.20}$$

where $z = T_R \hat{x}_R + T_{Mf} w_f + T_{Ms} w_s$ is the observer state, $w_f \in \mathbb{R}^{m_f}$, $w_s \in \mathbb{R}^{m_s}$ are the predicted outputs for the fast and slow measurements, respectively. If the sampling of the slow measurement coincides with the sampling of the fast measurement, all the predictor states, including w_s, will get reinitialized when $t_{f,i} = t_{s,j}$. T_R, T_{Mf}, T_{Ms} satisfy the following Sylvester equation:

$$\begin{bmatrix} T_R & T_{Mf} & T_{Ms} \end{bmatrix} \begin{bmatrix} F_{11} & F_{12} & F_{13} \\ F_{21} & F_{22} & F_{23} \\ F_{31} & F_{32} & F_{33} \end{bmatrix} = A \begin{bmatrix} T_R & T_{Mf} & T_{Ms} \end{bmatrix} + \begin{bmatrix} B_f & B_s \end{bmatrix} \begin{bmatrix} 0 & I & 0 \\ 0 & 0 & I \end{bmatrix} \tag{5.21}$$

The multi-rate observer (5.20) is designed in z-coordinates and state estimates in the original x-coordinates can be reconstructed after linear transformation. Equivalently, there exists an observer in x-coordinates, and it can be derived using Equations (5.20) and (5.21)

$$\begin{aligned}
\dot{\hat{x}}_R = \;& T_R^{-1}(\dot{z} - T_{Mf}\dot{w}_f - T_{Ms}\dot{w}_s) \\
= \;& F_{11}\hat{x}_R + F_{12} w_f + F_{13} w_s + l_f \cdot (y_f(t_{f,i}) - w_f(t_{f,i}^-))\delta(t - t_{f,i}) \\
& + l_s \cdot (y_s(t_{s,j}) - w_s(t_{s,j}^-))\delta(t - t_{s,j}) \\
\dot{w}_f = \;& F_{21}\hat{x}_R + F_{22} w_f + F_{23} w_s + (y_f(t_{f,i}) - w_f(t_{f,i}^-))\delta(t - t_{f,i}) \\
\dot{w}_s = \;& F_{31}\hat{x}_R + F_{32} w_f + F_{33} w_s + (y_s(t_{s,j}) - w_s(t_{s,j}^-))\delta(t - t_{s,j})
\end{aligned}$$

where $l_f = -T_R^{-1}T_{Mf}$ and $l_s = -T_R^{-1}T_{Ms}$ are the observer gains in a reduced-order Luenberger observer design, $\delta(t)$ is a unit impulse function that has the effect of reinitializing the state estimates $\hat{x}_R(t)$ and the predictor states $w_f(t)$, $w_s(t)$ at corresponding sampling instants. For $t \in [t_{f,i}^+, t_{f,i+1}]$, we have the following multi-rate observer coupled with inter-sample predictors

$$\dot{\hat{x}}_R(t) = F_{11}\hat{x}_R(t) + F_{12}w_f(t) + F_{13}w_s(t) \tag{5.22a}$$

$$\dot{w}_f(t) = F_{21}\hat{x}_R(t) + F_{22}w_f(t) + F_{23}w_s(t) \tag{5.22b}$$

$$\dot{w}_s(t) = F_{31}\hat{x}_R(t) + F_{32}w_f(t) + F_{33}w_s(t) \tag{5.22c}$$

$$\dot{\hat{x}}_R(t_{f,i}^+) = \hat{x}_R(t_{f,i}^-) + l_f \cdot (y_f(t_{f,i}) - w_f(t_{f,i}^-)) \tag{5.22d}$$

$$\dot{\hat{x}}_R(t_{s,j}^+) = \hat{x}_R(t_{s,j}^-) + l_s \cdot (y_s(t_{s,j}) - w_s(t_{s,j}^-)), \qquad \text{if } t_{f,i} = t_{s,j} \tag{5.22e}$$

$$w_f(t_{f,i}^+) = y_f(t_{f,i}) \tag{5.22f}$$

$$w_s(t_{s,j}^+) = y_s(t_{s,j}), \qquad \text{if } t_{f,i} = t_{s,j} \tag{5.22g}$$

where the reinitialization step is shown explicitly on $\hat{x}_R$, w_f, w_s at corresponding sampling instants. At $t_{f,i} = t_{s,j}$, both fast and slow measurements become available and thus, Equations (5.22e) and (5.22g) will be executed to reset the states using the most-recent slow measurement.

Denote $\hat{x} = \begin{bmatrix} \hat{x}_R \\ w_f \\ w_s \end{bmatrix}, L_f = \begin{bmatrix} l_f \\ I \\ 0 \end{bmatrix}, L_s = \begin{bmatrix} l_s \\ 0 \\ I \end{bmatrix}, L = \begin{bmatrix} L_f & L_s \end{bmatrix} = \begin{bmatrix} l_f & l_s \\ I & 0 \\ 0 & I \end{bmatrix}, \gamma = \begin{bmatrix} \gamma_1 \\ \gamma_2 \\ \gamma_3 \end{bmatrix}, \varepsilon =$

$\begin{bmatrix} x_R \\ x_{Mf} \\ x_{Ms} \end{bmatrix} - \begin{bmatrix} \hat{x}_R \\ w_f \\ w_s \end{bmatrix}, F = \begin{bmatrix} F_{11} & F_{12} & F_{13} \\ F_{21} & F_{22} & F_{23} \\ F_{31} & F_{32} & F_{33} \end{bmatrix}$, and we can write the observer (5.22) in a compact form

$$\begin{aligned} \dot{\hat{x}} &= F\hat{x} \\ \hat{x}(t_{f,i}^+) &= \hat{x}(t_{f,i}^-) + L_f \cdot (y_f(t_{f,i}) - w_f(t_{f,i}^-)), \quad \text{if } t_{f,i} \neq t_{s,j} \\ \hat{x}(t_{s,j}^+) &= \hat{x}(t_{s,j}^-) + L \cdot \begin{bmatrix} y_f(t_{f,i}) - w_f(t_{f,i}^-) \\ y_s(t_{s,j}) - w_s(t_{s,j}^-) \end{bmatrix}, \quad \text{if } t_{f,i} = t_{s,j} \end{aligned}$$

The dynamics of the estimation error $\varepsilon(t)$, in the presence of modeling error and measurement error, is described by

$$\begin{aligned} \dot{\varepsilon}(t) &= F\varepsilon(t) + \gamma v(t) \\ \varepsilon(t_{f,i}^+) &= \varepsilon(t_{f,i}^-) - L_f \cdot (y_f(t_{f,i}) - w_f(t_{f,i}^-)), \quad \text{if } t_{f,i} \neq t_{s,j} \\ \varepsilon(t_{s,j}^+) &= \varepsilon(t_{s,j}^-) - L \cdot \begin{bmatrix} y_f(t_{f,i}) - w_f(t_{f,i}^-) \\ y_s(t_{s,j}) - w_s(t_{s,j}^-) \end{bmatrix}, \quad \text{if } t_{f,i} = t_{s,j} \end{aligned} \tag{5.23}$$

Similar to the optimal single-rate observer design, it is possible to evaluate the effects of modeling error $v(t)$ and measurement errors $u_f(t)$, $u_s(t)$ separately by studying the response of $\varepsilon(t)$ to standard changes, e.g., unit impulse. We will denote $\varepsilon_v(t)$ the corresponding state estimation error if the modeling error is a continuous-time unit impulse function (i.e., $v(t) = \delta(t)$), in the absence of measurement error and initial condition error. We denote $\varepsilon_f(t)$ the corresponding state estimation error if the error of the fast measurement is a discrete-time unit impulse function (i.e., $u_f(t) = \delta[t]$), in the absence of modeling error, initial condition error and error of the slow measurement. Last, we denote $\varepsilon_s(t)$ the corresponding state estimation error if the error of the slow measurement is a discrete-time unit impulse function (i.e., $u_s(t) = \delta[t]$), in the absence of modeling error, initial condition error and fast measurement error.

The optimal observer gain will be selected by finding the optimal compromise among modeling

error, error of the fast measurement and error of the slow measurement. We consider a single unit impulse for $v(t)$, $u_f(t)$ and $u_s(t)$ separately, and seek for the minimum of the performance index

$$J = \int_0^\infty \|\varepsilon_v(t)\|^2 \ dt + \rho_f \int_0^\infty \|\varepsilon_f(t)\|^2 \ dt + \rho_s \int_0^\infty \|\varepsilon_s(t)\|^2 \ dt \tag{5.24}$$

where $\varepsilon_v(t)$ is the response of the estimation error to a unit impulse change in $v(t)$, $\varepsilon_f(t)$ and $\varepsilon_s(t)$ are the responses of the estimation error to a unit impulse change in $u_f(t)$ and $u_s(t)$, respectively. $\rho_f, \rho_s > 0$ are the weight coefficients of estimation error caused by the fast measurement error and the slow measurement error, respectively.

First, the response of the estimation error to a unit impulse change in $v(t)$ will be discussed, in the absence of measurement error and initial condition error. $\varepsilon_v(t)$ can be calculated for $t \in [0, a\tau)$ using Equation (5.23) as follows

$$\begin{aligned}
&t \in [0,\tau): && \varepsilon_v(0^+) = \gamma, && \varepsilon_v(t) = \exp(Ft)\varepsilon_v(0^+),\\
& && \varepsilon_v(\tau^-) = \exp(F\tau)\varepsilon_v(0^+)\\
&t \in [\tau,2\tau): && \varepsilon_v(\tau^+) = (I - L_f H_f)\varepsilon_v(\tau^-),\\
& && \varepsilon_v(t) = \exp(F(t-\tau))\varepsilon_v(\tau^+),\\
& && \varepsilon_v(2\tau^-) = \exp(F\tau)\varepsilon_v(\tau^+)\\
&\cdots && \cdots\\
&t \in [(a-1)\tau, a\tau): && \varepsilon_v((a-1)\tau^+) = (I - L_f H_f)\varepsilon_v((a-1)\tau^-),\\
& && \varepsilon_v(t) = \exp(F(t-(a-1)\tau))\varepsilon_v((a-1)\tau^+),\\
& && \varepsilon_v(a\tau^-) = \exp(F\tau)\varepsilon_v((a-1)\tau^+)\\
&t \in [a\tau, (a+1)\tau): && \varepsilon_v(a\tau^+) = (I - LH)\varepsilon_v(a\tau^-),\\
& && \varepsilon_v(t) = \exp(F(t-a\tau))\varepsilon_v(a\tau^+),\\
& && \varepsilon_v((a+1)\tau^-) = \exp(F\tau)\varepsilon_v(a\tau^+)\\
&\cdots && \cdots
\end{aligned}$$

where $H_f = \begin{bmatrix} 0 & I & 0 \end{bmatrix}$, $H_s = \begin{bmatrix} 0 & 0 & I \end{bmatrix}$, $H = \begin{bmatrix} H_f \\ H_s \end{bmatrix} = \begin{bmatrix} 0 & I & 0 \\ 0 & 0 & I \end{bmatrix}$, $\Gamma_f = (I - L_f H_f)\exp(F\tau)$, and $\Gamma = (I - LH)\exp(F\tau)$.

Consider the first integral in the performance index (5.24) corresponding to $\varepsilon_v(t)$, which will be integrated piecewise

$$\begin{aligned} J_v = & \int_0^\infty \|\varepsilon_v(t)\|^2 \, dt \\ = & \operatorname{Tr}\Bigg(\int_0^\tau \exp(Ft)\varepsilon_v(0^+)\varepsilon_v'(0^+)\exp(F't)\, dt \\ & + \int_\tau^{2\tau} \exp(F(t-\tau))\varepsilon_v(\tau^+)\varepsilon_v'(\tau^+)\exp(F'(t-\tau))\, dt + \cdots \\ & + \int_{a\tau}^{(a+1)\tau} \exp(F(t-a\tau))\varepsilon_v(a\tau^+)\varepsilon_v'(a\tau^+)\exp(F'(t-a\tau))\, dt + \cdots \Bigg) \end{aligned}$$

where $\operatorname{Tr}(\cdot)$ denotes the trace of a square matrix. Setting $J_v = \operatorname{Tr}(P_v)$, we have

$$\begin{aligned} FP_v + P_vF' = & \exp(F\tau)\varepsilon_v(0^+)\varepsilon_v'(0^+)\exp(F'\tau) - \varepsilon_v(0^+)\varepsilon_v'(0^+) \\ & + \exp(F\tau)\varepsilon_v(\tau^+)\varepsilon_v'(\tau^+)\exp(F'\tau) - \varepsilon_v(\tau^+)\varepsilon_v'(\tau^+) + \cdots \\ & + \exp(F\tau)\varepsilon_v(a\tau^+)\varepsilon_v'(a\tau^+)\exp(F'\tau) - \varepsilon_v(a\tau^+)\varepsilon_v'(a\tau^+) + \cdots \end{aligned} \tag{5.25}$$

For simplicity, we denote $S_v = \sum_{k=0}^{\infty} \varepsilon_v(k\tau^+)\varepsilon_v'(k\tau^+)$ and we have

$$\begin{aligned} \Gamma_f S_v \Gamma_f' - S_v = & (\Gamma_f^a \gamma\gamma'(\Gamma_f')^a - \gamma\gamma') \\ & + (\Gamma_f^a \Gamma \Gamma_f^{a-1}\gamma\gamma'(\Gamma_f')^{a-1}\Gamma'(\Gamma_f')^a - \Gamma\Gamma_f^{a-1}\gamma\gamma'(\Gamma_f')^{a-1}\Gamma') \\ & + (\Gamma_f^a \Gamma \Gamma_f^{a-1}\Gamma\Gamma_f^{a-1}\gamma\gamma'(\Gamma_f')^{a-1}\Gamma'(\Gamma_f')^{a-1}\Gamma'(\Gamma_f')^a \\ & - \Gamma\Gamma_f^{a-1}\Gamma\Gamma_f^{a-1}\gamma\gamma'(\Gamma_f')^{a-1}\Gamma'(\Gamma_f')^{a-1}\Gamma') + \cdots \\ = & \sum_{k=0}^{\infty} (\Gamma_f^a \Gamma_c^k \gamma\gamma'(\Gamma_c')^k(\Gamma_f')^a - \Gamma_c^k\gamma\gamma'(\Gamma_c')^k) \end{aligned} \tag{5.26}$$

where $\Gamma_c = \Gamma\Gamma_f^{a-1}$. For simplicity, we denote $Q_v = \sum_{k=0}^{\infty} \Gamma_c^k \gamma\gamma'(\Gamma_c')^k$. From Equation (5.26), it can

be derived that

$$\Gamma_f S_v \Gamma_f' - S_v = \Gamma_f^a Q_v (\Gamma_f')^a - Q_v \tag{5.27}$$

$$Q_v - \Gamma_c Q_v \Gamma_c' = \gamma\gamma' \tag{5.28}$$

where $\lim_{n\to\infty} \Gamma_c^n = 0$ as long as the error dynamics is stable.

Second, the response of the estimation error to a unit impulse change in $u_f(t)$ will be discussed, in the absence of modeling error, initial condition error and error of the slow measurement. $\varepsilon_f(t)$ can be calculated for $t \in [0, a\tau)$ using Equation (5.23) as follows

$$\begin{aligned}
&t \in [0,\tau): && \varepsilon_f(0^+) = -L_f\beta_f, && \varepsilon_f(t) = \exp(Ft)\varepsilon_f(0^+),\\
& && \varepsilon_f(\tau^-) = \exp(F\tau)\varepsilon_f(0^+) &&\\
&t \in [\tau,2\tau): && \varepsilon_f(\tau^+) = (I - L_f H_f)\varepsilon_f(\tau^-), &&\\
& && \varepsilon_f(t) = \exp(F(t-\tau))\varepsilon_f(\tau^+), &&\\
& && \varepsilon_f(2\tau^-) = \exp(F\tau)\varepsilon_f(\tau^+) &&\\
&\cdots && \cdots &&\\
&t \in [(a-1)\tau, a\tau): && \varepsilon_f((a-1)\tau^+) = (I - L_f H_f)\varepsilon_f((a-1)\tau^-), &&\\
& && \varepsilon_f(t) = \exp(F(t-(a-1)\tau))\varepsilon_f((a-1)\tau^+), &&\\
& && \varepsilon_f(a\tau^-) = \exp(F\tau)\varepsilon_f((a-1)\tau^+) &&\\
&t \in [a\tau, (a+1)\tau): && \varepsilon_f(a\tau^+) = (I - LH)\varepsilon_f(a\tau^-), &&\\
& && \varepsilon_f(t) = \exp(F(t-a\tau))\varepsilon_f(a\tau^+), &&\\
& && \varepsilon_f((a+1)\tau^-) = \exp(F\tau)\varepsilon_f(a\tau^+) &&\\
&\cdots && \cdots &&
\end{aligned}$$

For simplicity, we denote $J_f = \int_0^\infty \|\varepsilon_f(t)\|^2 \, dt = \mathrm{Tr}(P_f)$, $S_f = \sum_{k=0}^{\infty} \varepsilon_f(k\tau^+)\varepsilon_f'(k\tau^+)$ and

$Q_f = \sum_{k=0}^{\infty} \Gamma_c^k L_f \beta_f \beta_f' L_f' (\Gamma_c')^k$. By following the similar steps above, we obtain

$$FP_f + P_f F' = \exp(F\tau) S_f \exp(F'\tau) - S_f \tag{5.29}$$

$$\Gamma_f S_f \Gamma_f' - S_f = \Gamma_f^a Q_f (\Gamma_f')^a - Q_f \tag{5.30}$$

$$Q_f - \Gamma_c Q_f \Gamma_c' = L_f \beta_f \beta_f' L_f' \tag{5.31}$$

as long as the error dynamics of the observer is stable.

Third, the response of the estimation error to a unit impulse change in $u_s(t)$ will be discussed, in the absence of modeling error, initial condition error and error of the fast measurement. Notice that the detailed derivation of $\varepsilon_s(t)$ in each sampling period is omitted here which can be obtained in the same spirit as the analysis of $\varepsilon_f(t)$.

For simplicity, we denote $J_s = \int_0^\infty \|\varepsilon_s(t)\|^2 \, dt = \mathrm{Tr}(P_s)$, $S_s = \sum_{k=0}^{\infty} \varepsilon_s(k\tau^+)\varepsilon_s'(k\tau^+)$ and $Q_s = \sum_{k=0}^{\infty} \Gamma_c^k L_s \beta_s \beta_s' L_s' (\Gamma_c')^k$. By following the similar steps above, we obtain

$$FP_s + P_s F' = \exp(F\tau) S_s \exp(F'\tau) - S_s \tag{5.32}$$

$$\Gamma_f S_s \Gamma_f' - S_s = \Gamma_f^a Q_s (\Gamma_f')^a - Q_s \tag{5.33}$$

$$Q_s - \Gamma_c Q_s \Gamma_c' = L_s \beta_s \beta_s' L_s' \tag{5.34}$$

as long as the error dynamics of the observer is stable.

We combine the three integrals J_u, J_f, J_s, and seek for the minimum of the performance index (5.24). The optimal multi-rate observer design can be formulated as an optimization problem

$$\begin{aligned} \min_{l_f, l_s} \quad & \mathrm{Tr}(P) \\ s.t. \quad & FP + PF' = \exp(F\tau) S \exp(F'\tau) - S \\ & \Gamma_f S \Gamma_f' - S = \Gamma_f^a Q (\Gamma_f')^a - Q \\ & Q - \Gamma_c Q \Gamma_c' = \gamma\gamma' + \rho_f L_f \beta_f \beta_f' L_f' + \rho_s L_s \beta_s \beta_s' L_s' \end{aligned} \tag{5.35}$$

where $P = P_v + \rho_f P_f + \rho_s P_s$, $S = S_v + \rho_f S_f + \rho_s S_s$, and $Q = Q_v + \rho_f Q_f + \rho_s Q_s$.

5.2.2 A Numerical Example

In this section, the optimal multi-rate observer design will be illustrated via a third-order mathematical example. Consider a multi-rate system of the following state-space model

$$\begin{bmatrix} \dot{x}_1(t) \\ \dot{x}_2(t) \\ \dot{x}_3(t) \end{bmatrix} = \begin{bmatrix} 3 & 1 & -3 \\ 0 & 1 & 2 \\ 5 & 1 & -4 \end{bmatrix} \begin{bmatrix} x_1(t) \\ x_2(t) \\ x_3(t) \end{bmatrix} + \begin{bmatrix} 1 \\ 1 \\ 1 \end{bmatrix} v(t)$$

$$y_f(t_{f,i}) = x_2(t_{f,i}) + u_f(t_{f,i}), \qquad i = 0, 1, 2, \ldots$$

$$y_s(t_{s,j}) = x_3(t_{s,j}) + u_s(t_{s,j}), \qquad j = 0, 1, 2, \ldots$$

where x_1 is the unmeasured state, x_2 is the fast-sampled state with uniform sampling period $\tau_f = 0.04$ s, and x_3 is the slow-sampled state with uniform sampling period $\tau_s = 0.08$ s. So it is obvious that $a = 2$. Besides, $\rho_f = \rho_s = 1$ are selected as the weight coefficients in the performance index (5.24), which will be minimized. Solving the optimization of Equation (5.35), the optimal observer design has the following parameters

$$\begin{aligned} L &= \begin{bmatrix} 0.2742 & 0.6376 \\ 1 & 0 \\ 0 & 1 \end{bmatrix}, \qquad P = \begin{bmatrix} 0.1047 & 0.0592 & 0.1208 \\ 0.0592 & 0.0872 & 0.0511 \\ 0.1208 & 0.0511 & 0.1644 \end{bmatrix}, \\ S &= \begin{bmatrix} 2.6091 & 1.2742 & 3.0132 \\ 1.2742 & 2.0000 & 1.0000 \\ 3.0132 & 1.0000 & 4.1161 \end{bmatrix}, \quad Q = \begin{bmatrix} 1.5980 & 1.2742 & 1.6376 \\ 1.2742 & 2.0000 & 1.0000 \\ 1.6376 & 1.0000 & 2.0000 \end{bmatrix} \end{aligned} \tag{5.36}$$

5.3 Conclusions

This chapter develops an optimal multi-rate observer design method based on the linear multi-rate observer design in Chapter 3. A rigorous approach for observer gain selection is proposed to

reach a compromise between the effect of dynamic model error on the accuracy of state estimates and the effect of measurement error on the accuracy of state estimates. The effects of measurement error and modeling error are evaluated by studying the response of the observer error dynamics to a unit impulse function. The optimal observer design is formulated as an optimization problem of minimizing a performance index, and is demonstrated through two classes of linear systems, i.e., systems with single-rate measurements and systems with fast and slow measurements. The optimal observer design is obtained in the case that a single unit impulse is considered for modeling error and measurement error respectively.

It is possible to generalize the optimal observer design approach to systems with measurements of more than two sampling rates, but at the cost of more constraints in the optimization formulation. The derivations can be carried over to more complex linear multi-rate systems.

6. MULTI-RATE OBSERVER DESIGN IN NONLINEAR SYSTEMS *

The previous Chapters 3 to 5 have focused on the multi-rate observer design in linear systems. However, it is well-known that linear observers can be inadequate in the presence of strong process nonlinearities. In this chapter, the problem of multi-rate sampled-data observer design in nonlinear systems under asynchronous sampling will be investigated [309]. The proposed multi-rate observer is based on a continuous-time design coupled with inter-sample output predictors for the sampled measurements. The multi-rate system together with the multi-rate observer forms a hybrid system and it is shown that the error dynamics of the overall system is input-to-output stable with respect to measurement errors, by applying the Karafyllis-Jiang vector small-gain theorem. The multi-rate design also offers robustness with respect to perturbations in the sampling schedule. The proposed method is evaluated on linear detectable systems and two nonlinear examples.

The rest of this chapter is organized as follows. In Section 6.2, we formulate the representation of a multi-rate sampled-data observer and propose the definitions of robust observers with respect to measurement errors for forward complete systems. In Section 6.3, we derive the sufficient conditions that guarantee stability of the error dynamics of the multi-rate observer and robustness with respect to measurement errors as well as perturbations in the sampling schedule. The effectiveness and applicability of the proposed multi-rate sampled-data observer is illustrated through linear detectable systems and two nonlinear examples in Section 6.4. In Section 6.5, conclusions are drawn from the results of the previous sections.

6.1 Introduction

The objective of this chapter is to develop an observer in multi-rate sampled-data systems under asynchronous sampling. The problem of nonlinear observer design has been intensively studied for systems under fast sampling [130, 132, 148, 155, 264], which can be potentially applied to estima-

*Parts of this chapter are reproduced with permission from "Multi-Rate Sampled-Data Observers Based on a Continuous-Time Design" by C. Ling and C. Kravaris, 2017. in *Proceedings of the 56th IEEE Conference on Decision and Control*, Melbourne, Australia, 3664–3669, Copyright 2017 by IEEE.

tion, process control, and fault detection and identification. Motivated by practical implementation needs, however, one of the biggest challenges is to design a state observer for general multi-rate systems (e.g., chemical processes, biological systems, networked control systems), where different sampling rates of sensors need to be accommodated in the observer design framework.

The observer design for linear multi-rate systems was investigated in [52] and [280]. The approach in [280] involves modeling each sensor as a sample-and-hold device and deriving sufficient Krasovskii-based conditions for exponential stability in terms of linear matrix inequalities, given some maximum allowable sampling period for each sensor. In [52], we reported a continuous-time Luenberger observer design coupled with asynchronous inter-sample predictors. Each predictor, in the same spirit as in [250, 279], generates an estimate of a sampled output in between consecutive measurements, and will get reinitialized once the associated, most-recent measurement becomes available. Sufficient and explicit conditions were established in terms of maximum sampling period in [52] to guarantee exponential stability of the error dynamics. Both approaches adopted an available continuous-time observer design but employed different methods (i.e., sample-and-hold strategy and model-based prediction, respectively) to approximate the inter-sample behavior. The two approaches also provide robustness with respect to perturbations in the sampling schedule.

In nonlinear systems, the focus has been primarily on single-rate sampled-data observer design based on a mixed continuous and discrete strategy. Inspired by [72], the continuous-discrete time Kalman filter has been adapted to the framework of observer design for continuous-time systems with sampled measurements. In [273], an observer for continuous-discrete state affine systems was designed, similar to the structure of the Kalman filter, when the inputs are regularly persistent. The results in [273] were extended to observer design for state affine systems up to output injection in [274] and adaptive observer design in [310]. The continuous-discrete approach has been applied to high-gain observers in [131, 275, 276, 311–313]. In general, the continuous-discrete observer consists of two steps: (i) open-loop prediction when no measurements are available, and (ii) impulsive correction once a new measurement becomes available. A similar idea was used in [277, 314], and sufficient conditions with guaranteed global convergence of estimation error were derived in terms

of LMIs.

The problem of nonlinear multi-rate observer design has received very little attention, considering the challenge in stability analysis that arises from the asynchronous nature of different sensors and uncertainty in the sampling schedule. A nonlinear multi-rate observer design was developed in [315] based on an approximate discrete-time model, with guaranteed semiglobal practical input-to-state stability (ISS) from exogenous disturbance to estimation error. An artificial fast-rate sampler and a hold device were introduced to reconstruct the missing outputs as well as the inputs between sampling times, which were then fed to a single-rate observer working at a base sampling period of the plant. The results were extended to one-sided Lipschitz systems in [316]. A hybrid observer was reported for a class of nonlinear systems with multi-rate sampled and delayed measurements, with global exponential stability of the error dynamics [317]. However, it assumes a certain special structure of the nonlinear system for the method to be applicable.

In this work, the proposed multi-rate sampled-data observer design adopts the idea in [250,279] of using a state predictor to approximate the inter-sample behavior, but in a more general context, where multiple inter-sample predictors are utilized for the multi-rate system. These predictors will be running asynchronously at the same time and each predictor generates an estimate of the evolution of a sampled output between consecutive measurements, in the same spirit as [52] for linear systems. The existence of a continuous-time observer is a prerequisite for a multi-rate observer design. This is a common assumption in the continuous-discrete observer design for sampled-data systems [311]. Taking the measurement errors as inputs and the estimation errors as outputs, the notion of input-to-output stability (IOS), originated from [318] for systems described by ordinary differential equations, is adopted for stability analysis of the sampled-data system and the multi-rate observer. Since the overall system is a hybrid system in the sense that the classical semigroup property does not hold, the notion of weak semigroup property introduced in [319, 320] will be utilized, as it is more relaxed than the semigroup property and allows to study a very general class of systems (e.g., sampled-data systems, networked control systems, and hybrid systems). A direct product from this system theoretic framework is a small-gain theorem for two interconnected feed-

back systems [321], which played an important role in the stability analysis of the single-output sampled-data observer in [250]. The result was further generalized to a vector small-gain theorem in [304], which allows to study the IOS and ISS properties for large-scale systems that consist of multiple interacting subsystems, such as the proposed multi-rate sampled-data observer in Section 6.2.

The multi-rate observer design philosophy in this chapter is different from a multi-rate Kalman filter. This paragraph gives a brief overview of the multi-rate Kalman filtering from the literature. Wavelet transform-based algorithms for dynamical multi-resolutional distributed filtering were introduced in [322–324]. However, these algorithms were limited to the systems where the ratio of any two sampling rates was a power of two. The results were extended in [325] such that the ratio of any two sampling rates was allowed to be any positive integer. Some of the local estimators can even handle non-uniform sampling rates. However, it is required in the algorithm that the measurement with the highest sampling rate samples uniformly and the number of samples per block of the other measurements needs to be fixed [325, 326], which limits applications of the algorithm. The results in [327, 328] on asynchronous estimation problem are relatively computational expensive, since the state transition matrices need to be computed at every estimation time. The measurement augmentation at every estimation time also results in high dimensionality and expensive computational cost. Multi-sensor fusion estimation with non-uniform estimation rates was studied in [329] where the estimation rate switches between a fast mode and a slow mode according to its power situation, requirements of estimation performance, and dynamic change of the process. However, the synchronization assumption on two or more local estimates at some time instants was imposed in the algorithm. Lin and Sun [330] presented a distributed estimation algorithm for multi-sensor multi-rate systems where the state update rate is positive integer multiples of the measurement sampling rates and all the sensors have uniform sampling schedule. Notice that all the aforementioned multi-rate Kalman filter design [322–330] did not account for control input, on the understanding that the multi-rate estimation can be used for process or condition monitoring, target tracking, and localization.

In summary, the proposed multi-rate observer is different from the existing multi-rate Kalman filters in the following aspects:

- This chapter addresses the multi-rate state estimation problem in general nonlinear systems and rigorous stability analysis is conducted. To the best of the author's knowledge, almost all the multi-rate Kalman filters in the literature [322–330] are limited to linear systems.

- The proposed multi-rate design can handle non-uniform and asynchronous sampling in nonlinear systems, whereas the multi-rate Kalman filters in [322–330] required that the sampling period of each measurement is uniform, the ratio of any two sampling periods is an integer, and the sampling of different measurements synchronize at some time instants periodically. Up to now, optimal multi-rate Kalman filter with arbitrary ratio of sampling periods is still an open problem [325]. However, these assumptions are removed from the multi-rate observer design to be proposed in this chapter.

- As long as the maximum sampling period does not exceed a certain limit, the error dynamics of the proposed multi-rate observer is input-to-output stable, irrespective of perturbations in the sampling schedule. The robustness property is important in practical implementation as non-uniform sampling could occur if the sample is taken manually by operators.

6.2 Formulation of the Sampled-Data Observer

6.2.1 Notations

Throughout the chapter, we adopt the following notations.

- $\mathcal{K}^+$ denotes the class of positive, continuous functions defined on $\mathbb{R}_+ := \{x \in \mathbb{R} : x \geqslant 0\}$. We say that a function $\rho : \mathbb{R}_+ \to \mathbb{R}_+$ is positive definite if $\rho(0) = 0$ and $\rho(s) > 0, \forall s > 0$. $\mathcal{K}$ denotes the set of positive definite, increasing and continuous functions. We say a positive definite, increasing and continuous function $\rho : \mathbb{R}_+ \to \mathbb{R}_+$ is of class $\mathcal{K}_\infty$ if $\lim_{s\to+\infty} \rho(s) = +\infty$. We denote by $\mathcal{KL}$ the set of all continuous functions $\sigma = \sigma(s,t) : \mathbb{R}_+ \times \mathbb{R}_+ \to \mathbb{R}_+$

with the two properties: (i) the mapping $\sigma(\cdot, t)$ is of class $\mathcal{K}$ for each $t \geqslant 0$; (ii) the mapping $\sigma(s, \cdot)$ is non-increasing with $\lim_{t\to+\infty} \sigma(s, t) = 0$ for each $s \geqslant 0$.

- The set of nonnegative integers is denoted by $\mathbb{Z}_+$.

- $\mathbb{R}^n_+ := \{[x_1, \ldots, x_n]' \in \mathbb{R}^n : x_1 \geqslant 0, \ldots, x_n \geqslant 0\}$. Let $x, y \in \mathbb{R}^n$. We say that $x \leqslant y$ if and only if $(y - x) \in \mathbb{R}^n_+$. We say that a function $\rho : \mathbb{R}^n_+ \to \mathbb{R}_+$ is of class $\mathcal{N}_n$ if ρ is continuous with $\rho(0) = 0$ and such that $\rho(x) \leqslant \rho(y)$ for all $x, y \in \mathbb{R}^n_+$ with $x \leqslant y$.

- For every positive integer l and an open, non-empty set $A \subseteq \mathbb{R}^n$, $C^l(A; \Omega)$ denotes the class of continuous functions on A with continuous derivatives of order l, which take values in $\Omega \subseteq \mathbb{R}^m$. $C^0(A; \Omega)$ denotes the class of continuous functions on A which take values in Ω.

- We denote by $\|\cdot\|_{\mathcal{X}}$ the norm of the normed linear space $\mathcal{X}$. By $|\cdot|$, we denote the ℓ_1-norm of $\mathbb{R}^n$. Let $I \subseteq \mathbb{R}_+$ be an interval and $D \subseteq \mathbb{R}^l$ be a non-empty set. By $\mathcal{L}^\infty_{loc}(I; D)$, we denote the class of all Lebesgue measurable and locally bounded functions $u : I \to D$. For $u \in \mathcal{L}^\infty_{loc}(\mathbb{R}_+; \mathbb{R}^n)$, we define the norm $\|u(t)\|_{\mathcal{U}} := \sum_{i=1}^n \sup_{\tau\in[0,t]} |u_i(\tau)|$. Notice that $\sup_{\tau\in[0,t]} |u_i(\tau)|$ denotes the actual supremum of $|u_i(t)|$ on $[0, t]$.

6.2.2 Problem Formulation

Consider a multi-output continuous-time autonomous system, where without loss of generality, the output is assumed to be a part of the state vector

$$\begin{aligned} \dot{x}_R(t) &= f_R(x_R(t), x_M(t)) \\ \dot{x}_M(t) &= f_M(x_R(t), x_M(t)) \\ y(t) &= x_M(t) \end{aligned} \tag{6.1}$$

with $x_R \in \mathbb{R}^{n-m}$ being the unmeasured state vector, $x_M \in \mathbb{R}^m$ being the remaining state vector that is directly measured, y denoting the output vector, and $f_R \in C^1(\mathbb{R}^{n-m} \times \mathbb{R}^m; \mathbb{R}^{n-m})$, $f_M \in C^1(\mathbb{R}^{n-m} \times \mathbb{R}^m; \mathbb{R}^m)$ with $f_R(0, 0) = 0$, $f_M(0, 0) = 0$.

Note that the above system does not have an input. The understanding here is that an observer will be built for the purpose of condition monitoring of system (6.1).

In the presence of multiple measurements, it makes more sense to use a reduced-order observer so that a significantly lower dimensionality can ease implementation of the observer. Therefore, a reduced-order observer formulation will be the focus of this work. Suppose that a continuous-time reduced-order observer design is available for system (6.1)

$$\begin{aligned} \dot{z}(t) &= F(z(t), y(t)) \\ \hat{x}_R(t) &= \Psi(z(t), y(t)) \end{aligned} \tag{6.2}$$

where $z \in \mathbb{R}^k$ is the observer state, $\hat{x}_R \in \mathbb{R}^{n-m}$ is the state estimates, and $F \in C^1(\mathbb{R}^k \times \mathbb{R}^m; \mathbb{R}^k)$, $\Psi \in C^1(\mathbb{R}^k \times \mathbb{R}^m; \mathbb{R}^{n-m})$ with $F(0,0) = 0$, $\Psi(0,0) = 0$.

The output equation of system (6.1) should be modified under slow-sampled measurements, which yields the following multi-rate sampled-data system

$$\begin{aligned} \dot{x}_R(t) &= f_R(x_R(t), x_M(t)) \\ \dot{x}_M(t) &= f_M(x_R(t), x_M(t)) \\ y^i(t_j^i) &= x_M^i(t_j^i), \qquad j \in \mathbb{Z}_+, i = 1, 2, \ldots, m \end{aligned} \tag{6.3}$$

where t_j^i denotes the j-th sampling time for the i-th component in x_M, at some sequence of time instants $S = \{t_k\}_{k=0}^{\infty}$. The sampling times of the i-th sensor form an infinite subsequence which tends to infinity. These sampling times are not necessarily uniformly spaced, but satisfying $0 < t_{j+1}^i - t_j^i \leqslant r$ for all $j \in \mathbb{Z}_+$, where r is the maximum sampling period among all the sensors. The sampling times from all the subsequences are considered as the sampling times of the multi-rate sampled-data system (6.3). Notice that S is the sequence of all sampling times in ascending order. There is a one-to-one mapping from $\{t_j^i : j \in \mathbb{Z}_+, i = 1, 2, \ldots, m\}$ to $\{t_k\}_{k=0}^{\infty}$. Finally, we assume there is no measurement available at the initial time t_0.

As mentioned in Section 6.1, a continuous-time design (6.2) will serve as the basis of a multi-

rate observer design in the presence of asynchronous sampled measurements, as long as the inter-sample behavior is taken care of. In this way, a continuous-time observer design from the literature can be reused in the context of a multi-rate observer so that we do not need to design from scratch. System (6.3) can be used to predict the evolution of the output between consecutive measurements. As depicted in Figure 6.1, we propose the multi-rate sampled-data observer design

$$\begin{aligned}
&\dot{z}(t) = F(z(t), w(t)), && t \in [t_k, t_{k+1}) \\
&\dot{w}(t) = f_M(\Psi(z(t), w(t)), w(t)), && t \in [t_k, t_{k+1}) \\
&w^i(t_{k+1}) = y^i(t_{k+1}) \\
&\hat{x}_R(t) = \Psi(z(t), w(t)), && \hat{x}_R \in \mathbb{R}^{n-m}
\end{aligned} \tag{6.4}$$

This observer has the same dynamics as the continuous-time observer (6.2). The predictors operate continuously at different time horizons, which generate additional signals $w(t)$ to approximate and replace the output $y(t)$ in the implementation of the continuous-time observer (6.2). $w^i(t)$ will be reinitialized once a new measurement $y^i(t_{k+1})$ becomes available, while the rest of the predictor states do not change until their measurements are obtained. By integrating the predictor equations, a model-based correction is applied on the most-recent measurement. Notice that t_k and t_{k+1} are not necessarily the sampling times from the same sensor. It was seen in [52] that the model-based prediction offers a more meaningful approach to approximate the inter-sample behavior instead of a simple sample-and-hold strategy, especially under large sampling period.

It is important to point out that the sampled-data system (6.3) together with the multi-rate observer (6.4) is a hybrid system, which does not satisfy the classical semigroup property. However, the weak semigroup property still holds (see [319, 320]). The recent results in [304, 319–321] for a wide class of systems will be used in the proof of the main theorem to be stated in the next section. From the main theorem, other important features of this multi-rate sampled-data observer include: (i) the missing inter-sample behavior can be reconstructed by using the inter-sample predictors, (ii) as long as the maximum sampling period is sufficiently small, if the continuous-time observer implementation guarantees stability of the error dynamics and robustness with respect to measure-

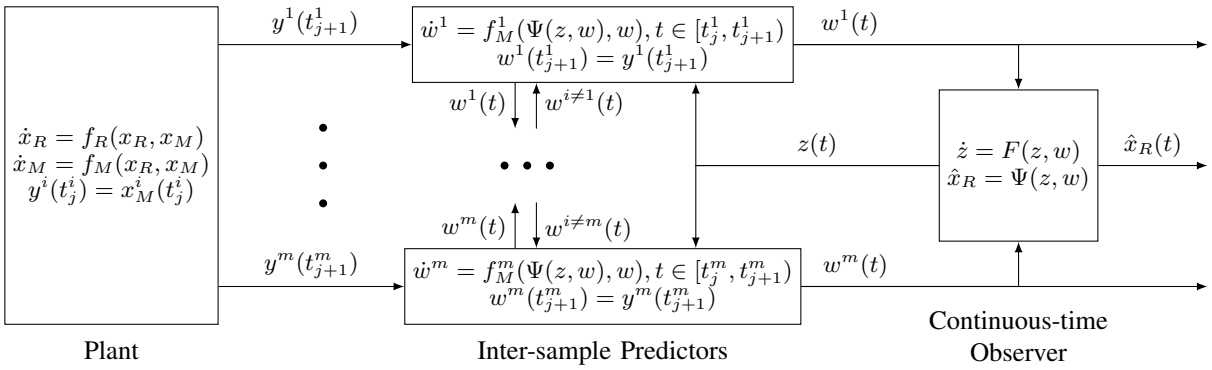

Figure 6.1: Schematic of the multi-rate sampled-data observer with the plant in the absence of measurement error.

ment errors, then the multi-rate observer will inherit these properties as well. These properties are unaffected by perturbations in the sampling schedule, which is a major advantage of the proposed hybrid implementation as opposed to an approximate discrete-time observer approach. Moreover, this continuous-discrete observer approach is able to use all possible measurements with different sampling rates, without making common assumptions when a discrete-time observer is used, such as that the sampling periods of the sensors are uniform and/or their ratios are rational numbers.

6.2.3 Basic Notions

We require that the following assumption holds.

Assumption 1. *System (6.1) is forward complete.*

Assumption 1, according to the main results in [331], implies the existence of functions $\mu \in \mathcal{K}^+$ and $a \in \mathcal{K}_\infty$ such that for every $(x_{R,0}, x_{M,0}) \in \mathbb{R}^{n-m} \times \mathbb{R}^m$, the solution $(x_R(t), x_M(t))$ of (6.1) with initial condition $(x_R(0), x_M(0)) = (x_{R,0}, x_{M,0})$ exists for all $t \geqslant 0$ and satisfies

$$|(x_R(t), x_M(t))| \leqslant \mu(t) a(|(x_{R,0}, x_{M,0})|), \quad \forall t \geqslant 0 \tag{6.5}$$

In other words, a finite dimensional system described by ordinary differential equations is forward

complete if and only if the corresponding solution exists for all $t \geqslant 0$ and for every initial condition [279].

Similarly to Definition 2.1 in [250] but in the context of a reduced-order observer, it is necessary to propose the following notion of robust observer for system (6.1) with respect to measurement errors, which is important for developing the main results of this work.

Definition 1. *The system*

$$\begin{aligned} \dot{z}(t) &= F(z(t), y(t)), \quad z \in \mathbb{R}^k \\ \hat{x}_R(t) &= \Psi(z(t), y(t)), \quad \hat{x}_R \in \mathbb{R}^{n-m} \end{aligned} \tag{6.6}$$

where $F \in C^1(\mathbb{R}^k \times \mathbb{R}^m; \mathbb{R}^k)$, $\Psi \in C^1(\mathbb{R}^k \times \mathbb{R}^m; \mathbb{R}^{n-m})$ with $F(0,0) = 0$, $\Psi(0,0) = 0$, is called a robust observer for system (6.1) with respect to measurement errors, if the following conditions are met:

(i) there exist functions $\sigma \in \mathcal{KL}$, $\gamma, p \in \mathcal{N}_1$, $\mu \in \mathcal{K}^+$ and $a \in \mathcal{K}_\infty$ such that for every $(x_{R,0}, x_{M,0}, z_0, v) \in \mathbb{R}^{n-m} \times \mathbb{R}^m \times \mathbb{R}^k \times \mathcal{L}^\infty_{loc}(\mathbb{R}_+; \mathbb{R}^m)$, the solution $(x_R(t), x_M(t), z(t))$ of

$$\begin{aligned} \dot{x}_R(t) &= f_R(x_R(t), x_M(t)) \\ \dot{x}_M(t) &= f_M(x_R(t), x_M(t)) \\ \dot{z}(t) &= F(z(t), x_M(t) + v(t)) \\ \hat{x}_R(t) &= \Psi(z(t), x_M(t) + v(t)) \end{aligned} \tag{6.7}$$

with initial condition $(x_R(0), x_M(0), z(0)) = (x_{R,0}, x_{M,0}, z_0)$ corresponding to $v \in \mathcal{L}^\infty_{loc}(\mathbb{R}_+; \mathbb{R}^m)$ exists for all $t \geqslant 0$ and satisfies the following estimates

$$|\hat{x}_R(t) - x_R(t)| \leqslant \sigma(|(x_{R,0}, x_{M,0}, z_0)|, t) + \gamma(\|v(t)\|_{\mathcal{U}}), \qquad \forall t \geqslant 0 \tag{6.8a}$$

$$|z(t)| \leqslant \mu(t)[a(|(x_{R,0}, x_{M,0}, z_0)|) + p(\|v(t)\|_{\mathcal{U}})], \qquad \forall t \geqslant 0 \tag{6.8b}$$

(ii) for every $(x_{R,0}, x_{M,0}) \in \mathbb{R}^{n-m} \times \mathbb{R}^m$, there exists $z_0 \in \mathbb{R}^k$ such that the solution $(x_R(t), x_M(t), z(t))$ of system (6.7) with initial condition $(x_R(0), x_M(0), z(0)) = (x_{R,0}, x_{M,0}, z_0)$

corresponding to $v \equiv 0$*, satisfies* $x_R(t) = \Psi(z(t), x_M(t))$ *for all* $t \geqslant 0$*.*

Remark 17. *If the system (6.6) is a robust observer for system (6.1) with respect to measurement errors, then system (6.7) with the output* $Y = \Psi(z, x_M + v) - x_R$ *satisfies the uniform input-to-output stability (UIOS) property from the input* $v \in \mathcal{L}^\infty_{loc}(\mathbb{R}_+; \mathbb{R}^m)$ *with gain* $\gamma \in \mathcal{N}_1$ *(see [321] for more details).*

Instead of using on-line, continuous outputs, a multi-rate sampled-data observer uses outputs at discrete sampling times in $S = \{t_k\}_{k=0}^{\infty}$. The sampling partition is not necessarily uniform, but there exists a maximum sampling period r acting as the upper bound on each sampling interval. Next, we propose the definition of a robust multi-rate sampled-data observer.

Definition 2. *The system*

$$\begin{aligned} \dot{\zeta}(t) &= g(\zeta(t), \zeta(t_k)), \qquad t \in [t_k, t_{k+1}) \\ \zeta(t_{k+1}) &= G\left(\lim_{t \to t_{k+1}^-} \zeta(t), y^i(t_{k+1})\right) \\ \hat{x}_R(t) &= \Psi(\zeta(t)) \end{aligned} \tag{6.9}$$

where $g \in C^1(\mathbb{R}^k \times \mathbb{R}^k; \mathbb{R}^k)$*,* $G \in C^0(\mathbb{R}^k \times \mathbb{R}; \mathbb{R}^k)$*,* $\Psi \in C^1(\mathbb{R}^k; \mathbb{R}^{n-m})$ *with* $g(0,0) = 0$*,* $G(0,0) = 0$*,* $\Psi(0) = 0$*, is called a robust multi-rate sampled-data observer for system (6.3) with respect to measurement errors, if the following conditions are met:*

(i) there exist functions $\sigma \in \mathcal{KL}$*,* $\gamma, p \in \mathcal{N}_1$*,* $\mu \in \mathcal{K}^+$ *and* $a \in \mathcal{K}_\infty$ *such that for every* $(x_{R,0}, x_{M,0}, \zeta_0, d, v) \in \mathbb{R}^{n-m} \times \mathbb{R}^m \times \mathbb{R}^k \times \mathcal{L}^\infty_{loc}(\mathbb{R}_+; [0,1]) \times \mathcal{L}^\infty_{loc}(\mathbb{R}_+; \mathbb{R}^m)$*, the solution*

$(x_R(t), x_M(t), \zeta(t))$ *of*

$$
\begin{aligned}
&\dot{x}_R(t) = f_R(x_R(t), x_M(t)) \\
&\dot{x}_M(t) = f_M(x_R(t), x_M(t)) \\
&\dot{\zeta}(t) = g(\zeta(t), \zeta(t_k)), \qquad t \in [t_k, t_{k+1}) \\
&\zeta(t_{k+1}) = G\left(\lim_{t \to t_{k+1}^-} \zeta(t), x_M^i(t_{k+1}) + v^i(t_{k+1})\right) \\
&t_{k+1} = t_k + rd(t_k) \\
&\hat{x}_R(t) = \Psi(\zeta(t))
\end{aligned}
\tag{6.10}
$$

with initial condition $(x_R(0), x_M(0), \zeta(0)) = (x_{R,0}, x_{M,0}, \zeta_0)$ *corresponding to* $d \in \mathcal{L}^\infty_{loc}(\mathbb{R}_+; [0,1])$ *and* $v \in \mathcal{L}^\infty_{loc}(\mathbb{R}_+; \mathbb{R}^m)$ *exists for all* $t \geqslant 0$ *and satisfies the following estimates*

$$
|\hat{x}_R(t) - x_R(t)| \leqslant \sigma(|(x_{R,0}, x_{M,0}, \zeta_0)|, t) + \gamma(\|v(t)\|_{\mathcal{U}}), \qquad \forall t \geqslant 0 \tag{6.11a}
$$

$$
|\zeta(t)| \leqslant \mu(t)[a(|(x_{R,0}, x_{M,0}, \zeta_0)|) + p(\|v(t)\|_{\mathcal{U}})], \qquad \forall t \geqslant 0 \tag{6.11b}
$$

(ii) for every $(x_{R,0}, x_{M,0}) \in \mathbb{R}^{n-m} \times \mathbb{R}^m$*, there exists* $\zeta_0 \in \mathbb{R}^k$ *such that for all* $d \in \mathcal{L}^\infty_{loc}(\mathbb{R}_+; [0,1])$*, the solution* $(x_R(t), x_M(t), \zeta(t))$ *of (6.10) with initial condition* $(x_R(0), x_M(0), \zeta(0)) = (x_{R,0}, x_{M,0}, \zeta_0)$ *corresponding to* $d \in \mathcal{L}^\infty_{loc}(\mathbb{R}_+; [0,1])$ *and* $v \equiv 0$*, satisfies* $x_R(t) = \Psi(\zeta(t))$ *for all* $t \geqslant 0$*.*

Remark 18. *If the system (6.9) is a robust multi-rate sampled-data observer for system (6.3) with respect to measurement errors, then the system (6.10) with the output* $Y = \Psi(\zeta) - x_R$ *satisfies the UIOS property from the input* $v \in \mathcal{L}^\infty_{loc}(\mathbb{R}_+; \mathbb{R}^m)$*, with gain* $\gamma \in \mathcal{N}_1$ *(see [321], where the notion of UIOS is defined for hybrid systems, e.g., (6.10), which does not satisfy the classical semigroup property).*

Remark 19. *The sampling period in each subsequence is allowed to be time-varying. The equation* $t_{k+1} = t_k + rd(t_k)$ *generates the sampling instants in* S *sequentially with* $0 \leqslant t_{k+1} - t_k \leqslant r$ *for all* $k \in \mathbb{Z}_+$*. The value that* $d(t_k)$ *takes introduces uncertainty to the end-point of each sampling*

interval. Proving stability for any disturbance $d \in \mathcal{L}^{\infty}_{loc}(\mathbb{R}_+; [0,1])$ *will guarantee stability for all sampling schedules of system (6.10).*

Remark 20. *At a specific instant* t_k*, there could be measurement of more than one output or the sampling of one sensor may coincide with another (i.e.,* $d(t_k) = 0$*). Hence, some sampling instants may appear more than once in the sequence* S*, where the reinitialization step will occur repeatedly but on different elements in* $w(t)$*.*

6.3 Main Results

Recently, the nonlinear small-gain theorem was generalized from two interconnected systems to large-scale complex systems consisting of multiple, interacting input-to-output stable (or input-to-state stable) subsystems in [332–334]. In [334], a more general cyclic small-gain criterion was developed for continuous-time, input-to-output stable systems. It can be described in general terms as follows: the composition of the gain functions along every simple cycle is less than the identity function, where a simple cycle is a closed path with no repeated subsystems other than the starting and ending ones [335]. In [304], a generalization of several previously developed nonlinear small-gain theorems was obtained. Uniform and non-uniform IOS and ISS properties were studied for a wide class of nonlinear feedback systems that do not satisfy the semigroup property, such as hybrid and switched systems.

In this section, we assume there exists a robust observer for system (6.1) in the sense of Definition 1, and would like to give conditions such that stability of the error dynamics and robustness with respect to measurement errors still hold for the multi-rate design.

Theorem 3. *Consider system (6.1) under Assumption 1 and suppose that (6.6) is a robust observer for system (6.1) with respect to measurement errors. Moreover, suppose that there exist constants* $C^i \geqslant 0$ *and functions* $\bar{\sigma}^i \in \mathcal{KL}$ *for all* $i = 1, 2, \ldots, m$*, such that for every* $(x_{R,0}, x_{M,0}, z_0, v) \in \mathbb{R}^{n-m} \times \mathbb{R}^m \times \mathbb{R}^k \times \mathcal{L}^{\infty}_{loc}(\mathbb{R}_+; \mathbb{R}^m)$*, the solution* $(x_R(t), x_M(t), z(t))$ *of (6.7) with initial condition* $(x_R(0), x_M(0), z(0)) = (x_{R,0}, x_{M,0}, z_0)$ *corresponding to* $v \in \mathcal{L}^{\infty}_{loc}(\mathbb{R}_+; \mathbb{R}^m)$ *exists for all* $t \geqslant 0$

and satisfies the following estimate

$$\begin{aligned}&|f_M^i(\Psi(z(t),x_M(t)+v(t)),x_M(t)+v(t))-f_M^i(x_R(t),x_M(t))|\\&\leqslant\bar{\sigma}^i(|(x_{R,0},x_{M,0},z_0)|,t)+C^i\left\|v(t)\right\|_{\mathcal{U}},\qquad\forall t\geqslant 0\end{aligned}\tag{6.12}$$

Additionally, suppose that (i) $3rC^im<1$ *for* $i=1,2,\ldots,m$*; (ii)* $3\gamma(ms)<s$ *for all* $s>0$*, where* $\gamma\in\mathcal{N}_1$ *is the gain function in the estimate (6.8a) of the robust observer. Then (6.4) is a robust multi-rate sampled-data observer for system (6.3) with respect to measurement errors.*

Proof. We focus on the following hybrid system, consisting of a sampled-data system and a multi-rate observer

$$\begin{aligned}&\dot{x}_R(t)=f_R(x_R(t),x_M(t))\\&\dot{x}_M(t)=f_M(x_R(t),x_M(t))\\&\dot{z}(t)=F(z(t),w(t)),&&t\in[t_k,t_{k+1})\\&\dot{w}(t)=f_M(\Psi(z(t),w(t)),w(t)),&&t\in[t_k,t_{k+1})\\&w^i(t_{k+1})=x_M^i(t_{k+1})+v^i(t_{k+1})\\&t_{k+1}=t_k+rd(t_k)\\&Y(t)=\Psi(z(t),w(t))-x_R(t)\end{aligned}\tag{6.13}$$

By virtue of Definition 2, it is necessary to show that system (6.13) with the output $Y=\Psi(z,w)-x_R$ satisfies the UIOS property from the input $v\in\mathcal{L}_{loc}^{\infty}(\mathbb{R}_+;\mathbb{R}^m)$.

Notice that the hybrid system (6.13) has a distributed structure, where each inter-sample predictor is a subsystem operating asynchronously. Each subsystem receives the corresponding system output and reinitializes its own inter-sample predictor. These subsystems also communicate with each other as well as the continuous-time observer by transmitting the predicted outputs. We focus on the i-th subsystem and treat $w^j(t)$ ($j\neq i$) and $v^i(t)$ as inputs to this subsystem. First, the boundedness of $\|w(t)-x_M(t)\|_{\mathcal{U}}$ will be established. Next, we will focus on the overall hybrid system (6.13) and study the UIOS property from the actual input $v\in\mathcal{L}_{loc}^{\infty}(\mathbb{R}_+;\mathbb{R}^m)$. A vector small-gain theorem (see [304]) will be used to complete the proof.

Now consider the i-th subsystem from the distributed structure, where $w^j(t)$ ($j \neq i$) and $v^i(t)$ is considered as inputs

$$\begin{aligned}
&\dot{x}_R(t) = f_R(x_R(t), x_M(t)) \\
&\dot{x}_M(t) = f_M(x_R(t), x_M(t)) \\
&\dot{z}(t) = F(z(t), w(t)), && t \in [t_j^i, t_{j+1}^i) \\
&\dot{w}^i(t) = f_M^i(\Psi(z(t), w(t)), w(t)), && t \in [t_j^i, t_{j+1}^i) \\
&w^i(t_{j+1}^i) = x_M^i(t_{j+1}^i) + v^i(t_{j+1}^i) \\
&t_{j+1}^i = t_j^i + rd(t_j^i) \\
&Y(t) = \Psi(z(t), w(t)) - x_R(t)
\end{aligned} \tag{6.14}$$

which satisfies the weak semigroup property. Because any two different samplings can never occur at the same time in a subsystem (i.e., $t_{j_1}^i \neq t_{j_2}^i$ if $j_1 \neq j_2$), disturbance $d \in \mathcal{L}_{loc}^{\infty}(\mathbb{R}_+; (0, 1])$ is used to introduce perturbations in the sampling schedule of the i-th subsystem, and this rules out the Zeno phenomenon. Because system (6.6) is a robust observer for system (6.1) with respect to measurement errors, it follows from (6.8a), (6.8b), and (6.12) that for every $(x_{R,0}, x_{M,0}, z_0, w_0^i, d) \in \mathbb{R}^{n-m} \times \mathbb{R}^m \times \mathbb{R}^k \times \mathbb{R} \times \mathcal{L}_{loc}^{\infty}(\mathbb{R}_+; (0, 1])$, the solution $(x_R(t), x_M(t), z(t), w^i(t))$ of (6.14) with initial condition $(x_R(0), x_M(0), z(0), w^i(0)) = (x_{R,0}, x_{M,0}, z_0, w_0^i)$ corresponding to the inputs $w^j(t)$ where $j \neq i$ (i.e., predicted outputs from other predictors) satisfies the following estimates for all $t \in [0, t_{\max})$

$$|Y(t)| \leqslant \hat{\sigma}(|(x_{R,0}, x_{M,0}, z_0)|, t) + \gamma(\|w(t) - x_M(t)\|_{\mathcal{U}}) \tag{6.15}$$

$$|z(t)| \leqslant \mu(t)[a(|(x_{R,0}, x_{M,0}, z_0)|) + p(\|w(t) - x_M(t)\|_{\mathcal{U}})] \tag{6.16}$$

$$|f_M^i(\Psi(z(t), w(t)), w(t)) - f_M^i(x_R(t), x_M(t))| \leqslant \bar{\sigma}^i(|(x_{R,0}, x_{M,0}, z_0)|, t) + C^i \|w(t) - x_M(t)\|_{\mathcal{U}} \tag{6.17}$$

Since Assumption 1 holds, we obtain from (6.5) and (6.16)

$$|(x_R(t), x_M(t), z(t))| \leqslant \bar{\mu}(t)[\bar{a}(|(x_{R,0}, x_{M,0}, z_0)|) + p(\|w(t) - x_M(t)\|_{\mathcal{U}})], \quad \forall t \in [0, t_{\max}) \tag{6.18}$$

for appropriate functions $\hat{\sigma}, \bar{\sigma}^i \in \mathcal{KL}$, $\gamma, p \in \mathcal{N}_1$, $\mu, \bar{\mu} \in \mathcal{K}^+$ and $a, \bar{a} \in \mathcal{K}_\infty$, where $t_{\max} \in (0, +\infty]$ is the maximal existence time of the solution.

Consider those time intervals where the reinitialization step occurs at the beginning. For all $t \in [t_j^i, t_{j+1}^i) \cap [0, t_{\max})$ with $j \geqslant 1$, we have

$$\begin{aligned} |w^i(t) - x_M^i(t)| &\leqslant \int_{t_j^i}^t \left| f_M^i(\Psi(z(s), w(s)), w(s)) - f_M^i(x_R(s), x_M(s)) \right| \, ds + |v^i(t_j^i)| \\ &\leqslant r\bar{\sigma}^i(|(x_{R,0}, x_{M,0}, z_0)|, t_j^i) + rC^i \|w(t) - x_M(t)\|_{\mathcal{U}} + |v^i(t_j^i)| \\ &\leqslant \sigma_1^i(|(x_{R,0}, x_{M,0}, z_0)|, t) + rC^i \|w(t) - x_M(t)\|_{\mathcal{U}} + \sup_{0 \leqslant \tau \leqslant t} |v^i(\tau)| \end{aligned} \tag{6.19}$$

where $\sigma_1^i(s,t) = r\bar{\sigma}^i(s, t-r)$ for $t \geqslant r$ and $\sigma_1^i(s,t) = \exp(r-t)r\bar{\sigma}^i(s,0)$ for $t < r$. Notice that $\sigma_1^i(s,t) \in \mathcal{KL}$. Because there is no measurement available at the initial time $t_0^i = 0$, we make an initial guess $w^i(t_0^i) = w^i(0) = w_0^i$ for the i-th state of the predictor. For all $t \in [0, t_1^i) \cap [0, t_{\max})$, we get

$$\begin{aligned} |w^i(t) - x_M^i(t)| &\leqslant |w_0^i - x_{M,0}^i| + r \sup_{0 \leqslant s \leqslant t} |f_M^i(\Psi(z(s), w(s)), w(s)) - f_M^i(x_R(s), x_M(s))| \\ &\leqslant |w_0^i| + |x_{M,0}^i| + r\bar{\sigma}^i(|(x_{R,0}, x_{M,0}, z_0)|, 0) + rC^i \|w(t) - x_M(t)\|_{\mathcal{U}} \\ &\leqslant \sigma_2^i(|(x_{R,0}, x_{M,0}, z_0, w_0^i)|, t) + rC^i \|w(t) - x_M(t)\|_{\mathcal{U}} \end{aligned} \tag{6.20}$$

where $\sigma_2^i(s,t) = [r\bar{\sigma}^i(s,0) + s]\exp(r-t)$ and $\sigma_2^i(s,t) \in \mathcal{KL}$. Combining (6.19) and (6.20), we conclude that the following estimate holds for all $t \in [0, t_{\max})$ and for $i = 1, 2, \ldots, m$

$$|w^i(t) - x_M^i(t)| \leqslant \sigma^i(|(x_{R,0}, x_{M,0}, z_0, w_0^i)|, t) + rC^i \|w(t) - x_M(t)\|_{\mathcal{U}} + \sup_{0 \leqslant \tau \leqslant t} |v^i(\tau)| \tag{6.21}$$

From Equation (6.21), the fact that $\sum_{i=1}^{m} rC^i < 1/3$, and the assumption that $t_{\max}$ is finite, it suffices to show the boundedness of $\|w(t) - x_M(t)\|_{\mathcal{U}}$ for all $t \in [0, t_{\max})$. In fact,

$$\|w(t) - x_M(t)\|_{\mathcal{U}} \leqslant \frac{\sum_{i=1}^{m} \sigma^i(|(x_{R,0}, x_{M,0}, z_0, w_0^i)|, 0) + \|v(t)\|_{\mathcal{U}}}{1 - \sum_{i=1}^{m} rC^i} \tag{6.22}$$

From (6.18), (6.21), (6.22), and the Boundedness-Implies-Continuation (BIC) property (see [319]) for system (6.14), we conclude that $t_{\max} = +\infty$. Consequently, all the above inequalities hold for all $t \geqslant 0$ and thus, $t \in [0, t_{\max})$ can be replaced by $t \geqslant 0$ in these inequalities. In addition, the BIC property of each subsystem implies that the BIC property holds true for the overall hybrid system (6.13) with $t_{\max} = +\infty$.

Now, we are in a position to study the UIOS property of the overall hybrid, multi-rate system (6.13) from the actual input $v \in \mathcal{L}^{\infty}_{loc}(\mathbb{R}_+; \mathbb{R}^m)$. A vector small-gain theorem will be used to check stability of the large-scale hybrid systems composed of multiple interconnected subsystems.

Without loss of generality, we may assume that $\bar{\mu}(t) \geqslant 1$ in (6.18). From (6.18), (6.22), and the triangle inequality $|w(t)| \leqslant |w(t) - x_M(t)| + |x_M(t)|$, we obtain for all $t \geqslant 0$

$$|(x_R(t), x_M(t), z(t), w(t))| \leqslant 2\bar{\mu}(t)[\hat{a}(|(x_{R,0}, x_{M,0}, z_0, w_0)|) + \hat{p}(\|v(t)\|_{\mathcal{U}})] \tag{6.23}$$

for appropriate functions $\hat{a}(s) = \bar{a}(s) + \dfrac{\sum_{i=1}^{m} \sigma^i(s, 0)}{1 - \sum_{i=1}^{m} rC^i} + p\left(\dfrac{2\sum_{i=1}^{m} \sigma^i(s, 0)}{1 - \sum_{i=1}^{m} rC^i}\right)$ (notice that $\hat{a} \in \mathcal{K}_{\infty}$) and $\hat{p}(s) = \dfrac{1}{1 - \sum_{i=1}^{m} rC^i} s + p\left(\dfrac{2s}{1 - \sum_{i=1}^{m} rC^i}\right)$ (notice that $\hat{p} \in \mathcal{N}_1$). Furthermore, (6.23) and the BIC property of the hybrid system (6.13) imply the following important properties:

- System (6.13) is robustly forward complete from the input $v \in \mathcal{L}^{\infty}_{loc}(\mathbb{R}_+; \mathbb{R}^m)$.
- $0 \in \mathbb{R}^{n-m} \times \mathbb{R}^m \times \mathbb{R}^k \times \mathbb{R}^m$ is a robust equilibrium point from the input $v \in \mathcal{L}^{\infty}_{loc}(\mathbb{R}_+; \mathbb{R}^m)$, with any output function $H(t, x_R, x_M, z, w, v)$ with $H(t, 0, 0, 0, 0, 0) = 0$ for all $t \geqslant 0$.

The inequality (6.23) also yields

$$\begin{aligned}|(x_R(t), x_M(t), z(t), w(t))| &\leqslant \bar{\mu}^2(t) + [\hat{a}(|(x_{R,0}, x_{M,0}, z_0, w_0)|) + \hat{p}(\|v(t)\|_{\mathcal{U}})]^2 \\ &\leqslant \bar{\mu}^2(t) + 2\hat{a}^2(|(x_{R,0}, x_{M,0}, z_0, w_0)|) + 2\hat{p}^2(\|v(t)\|_{\mathcal{U}}) \\ &\leqslant 3\max\left\{\bar{\mu}^2(t), 2\hat{a}^2(|(x_{R,0}, x_{M,0}, z_0, w_0)|), 2\hat{p}^2(\|v(t)\|_{\mathcal{U}})\right\}\end{aligned} \tag{6.24}$$

Consider system (6.13) with the output map that we have defined and apply the vector small-gain theorem with the following functions

$$\gamma_{i,j}(s) = \begin{bmatrix} 3rC^1ms & \dots & 3rC^1ms & 0 & \dots & 0 \\ \vdots & \ddots & \vdots & \vdots & \ddots & \vdots \\ 3rC^mms & \dots & 3rC^mms & 0 & \dots & 0 \\ 3\gamma(ms) & \dots & 3\gamma(ms) & 0 & \dots & 0 \\ \vdots & \ddots & \vdots & \vdots & \ddots & \vdots \\ 3\gamma(ms) & \dots & 3\gamma(ms) & 0 & \dots & 0 \end{bmatrix}, \quad \forall i, j = 1, 2, \dots, n$$

$$V(t, x_R, x_M, z, w, v) = \begin{bmatrix} |w^1(t) - x_M^1(t)| \\ \vdots \\ |w^m(t) - x_M^m(t)| \\ |Y(t)| \\ \vdots \\ |Y(t)| \end{bmatrix} \in \mathbb{R}^n,$$

$$\Gamma(x) = \begin{bmatrix} 3rC^1m\max_{i=1,2\dots,m}\{x_i\} \\ \vdots \\ 3rC^mm\max_{i=1,2\dots,m}\{x_i\} \\ 3\gamma(m\max_{i=1,2\dots,m}\{x_i\}) \\ \vdots \\ 3\gamma(m\max_{i=1,2\dots,m}\{x_i\}) \end{bmatrix} : \mathbb{R}^n_+ \to \mathbb{R}^n_+,$$

$$L(t, x_R, x_M, z, w) = |(x_R(t), x_M(t), z(t), w(t))|,$$
$$\sigma(s,t) = 3\left(\sum_{i=1}^{m} \sigma^i(s,t) + \hat{\sigma}(s,t)\right),$$
$$\nu(t) = 3\bar{\mu}^2(t), c \equiv 1, \zeta(s) = 3s,$$
$$a(s) = 6\hat{a}^2(s), p^u(s) = 6\hat{p}^2(s), p \equiv 0,$$
$$b(s) = s, g \equiv 0, \mu(t) = \beta(t) = \kappa(t) \equiv 1, q(x) = x_n (x \in \mathbb{R}^n_+)$$

where $\Gamma(x) : \mathbb{R}^n_+ \to \mathbb{R}^n_+$ is a MAX-preserving continuous map (see [304] for the definition) with $\Gamma(0) = 0$.

Now, Hypotheses (H1)-(H4) of the vector small-gain theorem are satisfied by virtue of the above definitions, and inequalities (6.15), (6.21), (6.22) and (6.23). We conclude that the hybrid system (6.13) satisfies the UIOS property from the input $v \in \mathcal{L}^\infty_{loc}(\mathbb{R}_+; \mathbb{R}^m)$. In other words, there exist functions $\tilde{\sigma} \in \mathcal{KL}$, $\tilde{\gamma}, \tilde{p} \in \mathcal{N}_1$, $\tilde{\mu} \in \mathcal{K}^+$ and $\tilde{a} \in \mathcal{K}_\infty$ such that for every $(x_{R,0}, x_{M,0}, z_0, w_0, d, v)$ $\in \mathbb{R}^{n-m} \times \mathbb{R}^m \times \mathbb{R}^k \times \mathbb{R}^m \times \mathcal{L}^\infty_{loc}(\mathbb{R}_+; [0,1]) \times \mathcal{L}^\infty_{loc}(\mathbb{R}_+; \mathbb{R}^m)$, the solution $(x_R(t), x_M(t), z(t), w(t))$ of (6.13) with initial condition $(x_R(0), x_M(0), z(0), w(0)) = (x_{R,0}, x_{M,0}, z_0, w_0)$ corresponding to $d \in \mathcal{L}^\infty_{loc}(\mathbb{R}_+; [0,1])$ and $v \in \mathcal{L}^\infty_{loc}(\mathbb{R}_+; \mathbb{R}^m)$ satisfies the following estimates for all $t \geqslant 0$

$$|Y(t)| \leqslant \tilde{\sigma}(|(x_{R,0}, x_{M,0}, z_0, w_0)|, t) + \tilde{\gamma}(\|v(t)\|_{\mathcal{U}}) \tag{6.25a}$$
$$|(z(t), w(t))| \leqslant \tilde{\mu}(t)[\tilde{a}(|(x_{R,0}, x_{M,0}, z_0, w_0)|) + \tilde{p}(\|v(t)\|_{\mathcal{U}})] \tag{6.25b}$$

Moreover, for every $(x_{R,0}, x_{M,0}) \in \mathbb{R}^{n-m} \times \mathbb{R}^m$, there exists $(z_0, w_0) \in \mathbb{R}^k \times \mathbb{R}^m$ with $w_0 = x_{M,0}$ such that for all $d \in \mathcal{L}^\infty_{loc}(\mathbb{R}_+; [0,1])$, the solution $(x_R(t), x_M(t), z(t), w(t))$ of (6.13) with initial condition $(x_R(0), x_M(0), z(0), w(0)) = (x_{R,0}, x_{M,0}, z_0, w_0)$ corresponding to $d \in \mathcal{L}^\infty_{loc}(\mathbb{R}_+; [0,1])$ and $v \equiv 0$, satisfies $x_R(t) = \Psi(z(t), w(t))$ for all $t \geqslant 0$. □

Remark 21. *If we consider system (6.13) with the prediction error as the output map, i.e., $Y'(t) = w(t) - x_M(t)$, by applying the vector small-gain theorem again, we conclude that with this output, the hybrid system (6.13) also satisfies the UIOS property from the input $v \in \mathcal{L}^\infty_{loc}(\mathbb{R}_+; \mathbb{R}^m)$. In other words, there exist functions $\tilde{\sigma} \in \mathcal{KL}$ and $\tilde{\gamma} \in \mathcal{N}_1$ such that for every $(x_{R,0}, x_{M,0}, z_0, w_0, d, v) \in$*

$\mathbb{R}^{n-m} \times \mathbb{R}^m \times \mathbb{R}^k \times \mathbb{R}^m \times \mathcal{L}^\infty_{loc}(\mathbb{R}_+; [0,1]) \times \mathcal{L}^\infty_{loc}(\mathbb{R}_+; \mathbb{R}^m)$*, the solution* $(x_R(t), x_M(t), z(t), w(t))$ *of (6.13) with initial condition* $(x_R(0), x_M(0), z(0), w(0)) = (x_{R,0}, x_{M,0}, z_0, w_0)$ *corresponding to* $d \in \mathcal{L}^\infty_{loc}(\mathbb{R}_+; [0,1])$ *and* $v \in \mathcal{L}^\infty_{loc}(\mathbb{R}_+; \mathbb{R}^m)$ *satisfies*

$$|w(t) - x_M(t)| \leqslant \tilde{\sigma}(|(x_{R,0}, x_{M,0}, z_0, w_0)|, t) + \tilde{\gamma}(\|v(t)\|_{\mathcal{U}}), \qquad \forall t \geqslant 0 \tag{6.26}$$

Without measurement errors, the error dynamics of the multi-rate sampled-data observer, including the inter-sample predictors, will converge to zero asymptotically.

Remark 22. *The continuous-time observer design coupled with inter-sample predictors can be applied to multi-rate full-order observer design, under appropriate modifications. The vector small-gain theorem is applicable to study the UIOS property of the overall system (i.e., the sampled-data system and the multi-rate observer) from measurement errors.*

6.4 Applications

In this section, the performance of the proposed multi-rate sampled-data observer is illustrated through linear systems and two nonlinear third-order examples. An explicit formula for estimating the maximum sampling period will be derived for the linear detectable systems with application to an oscillator example.

6.4.1 Linear Detectable Systems

Consider a linear detectable system, where without loss of generality, the output is assumed to be a part of the state vector

$$\begin{aligned} \dot{x}_R(t) &= A_{11}x_R(t) + A_{12}x_M(t), \quad x_R \in \mathbb{R}^{n-m} \\ \dot{x}_M(t) &= A_{21}x_R(t) + A_{22}x_M(t), \quad x_M \in \mathbb{R}^m \\ y(t) &= x_M(t) \end{aligned} \tag{6.27}$$

A reduced-order Luenberger observer design is available

$$\begin{aligned} \dot{z}(t) &= Fz(t) + Hy(t) \\ \hat{x}_R(t) &= T_R^{-1}(z(t) - T_M y(t)) \end{aligned} \tag{6.28}$$

where F is a Hurwitz matrix with desired eigenvalues and forms a controllable pair with H. The transformation matrices T_R, T_M satisfy the following Sylvester equation:

$$\begin{bmatrix} T_R & T_M \end{bmatrix} \begin{bmatrix} A_{11} & A_{12} \\ A_{21} & A_{22} \end{bmatrix} = F \begin{bmatrix} T_R & T_M \end{bmatrix} + H \begin{bmatrix} 0 & I \end{bmatrix} \tag{6.29}$$

Consequently, there exists a positive definite matrix P such that $F'P + PF$ is negative definite and there exist constants $\alpha, \delta > 0$ such that

$$x'(F'P + PF)x + 2x'PHv \leqslant -2\alpha x'Px + \delta|v|^2 \tag{6.30}$$

for all $(x, v) \in \mathbb{R}^{n-m} \times \mathbb{R}^m$. Inequality (6.30) implies for every $(x_{R,0}, x_{M,0}, z_0, v) \in \mathbb{R}^{n-m} \times \mathbb{R}^m \times \mathbb{R}^{n-m} \times \mathcal{L}^\infty_{loc}(\mathbb{R}_+; \mathbb{R}^m)$, the solution of (6.27) with

$$\dot{z}(t) = Fz(t) + H(y(t) + v(t))$$

with initial condition $(x_R(0), x_M(0), z(0)) = (x_{R,0}, x_{M,0}, z_0)$ corresponding to $v \in \mathcal{L}^\infty_{loc}(\mathbb{R}_+; \mathbb{R}^m)$ satisfies the estimates for $i = 1, 2, \ldots, m$

$$\begin{aligned}
|\hat{x}_R - x_R| \leqslant\ & |T_R^{-1}| \exp(-\alpha t)\sqrt{\frac{K_2}{K_1}}|z_0 - T_R x_{R,0} - T_M x_{M,0}| \\
& + \left(|T_R^{-1}|\sqrt{\frac{\delta}{2\alpha K_1}} + |T_R^{-1}T_M|\right) \sup_{0\leqslant\tau\leqslant t} |v(\tau)|, \\
& \forall t \geqslant 0 \\
|A^i_{21}(\hat{x}_R - x_R) + A^i_{22} v| \leqslant\ & |A^i_{21}||T_R^{-1}| \exp(-\alpha t)\sqrt{\frac{K_2}{K_1}}|z_0 - T_R x_{R,0} - T_M x_{M,0}| \\
& + \left(|A^i_{21}||T_R^{-1}|\sqrt{\frac{\delta}{2\alpha K_1}} + |A^i_{21}||T_R^{-1}T_M| + |A^i_{22}|\right) \sup_{0\leqslant\tau\leqslant t} |v(\tau)|, \\
& \forall t \geqslant 0
\end{aligned}$$

where $K_1, K_2 > 0$ are constants such that $K_1|x|^2 \leqslant x'Px \leqslant K_2|x|^2$ for all $x \in \mathbb{R}^{n-m}$, and A^i_{21}, A^i_{22} are the i-th row of the matrices A_{21}, A_{22} respectively. We conclude from Theorem 3 that the following system

$$\begin{aligned}
\dot{z}(t) &= Fz(t) + Hw(t), && t \in [t_k, t_{k+1}) \\
\dot{w}(t) &= A_{21}\hat{x}_R(t) + A_{22}w(t), && t \in [t_k, t_{k+1}) \\
w^i(t_{k+1}) &= x^i_M(t_{k+1}) + v^i(t_{k+1}) \\
\hat{x}_R(t) &= T_R^{-1}(z(t) - T_M w(t))
\end{aligned} \tag{6.31}$$

is a robust multi-rate sampled-data observer for system (6.27) with respect to measurement errors given that the maximum sampling period r satisfies the inequalities

$$3rm\left(|A^i_{21}||T_R^{-1}|\sqrt{\frac{\delta}{2\alpha K_1}} + |A^i_{21}||T_R^{-1}T_M| + |A^i_{22}|\right) < 1, \quad i = 1, 2, \ldots, m \tag{6.32}$$

and

$$3m\left(|T_R^{-1}|\sqrt{\frac{\delta}{2\alpha K_1}} + |T_R^{-1}T_M|\right) < 1 \tag{6.33}$$

Remark 23. *It seems that one of the conditions in Theorem 3, i.e.,* $3rC^i m < 1$*, becomes harder to*

satisfy as the number of outputs m increases. However, this is not always true. From the condition $3rC^i m < 1$, it can be seen that the maximum sampling period does not only depend on the number of outputs, but also depends on the constants C^i in the estimate (6.12) of a robust observer. As m increases, the dynamics of a continuous-time observer will become different from the one with less outputs. It is possible that the maximum sampling period increases as m increases.

A fourth-order linear system will be discussed where the maximum sampling period with three asynchronous discrete outputs is actually larger than the one with two outputs. Consider a linear system of the following state-space model

$$\begin{bmatrix} \dot{x}_1(t) \\ \dot{x}_2(t) \\ \dot{x}_3(t) \\ \dot{x}_4(t) \end{bmatrix} = \begin{bmatrix} -0.1 & 0 & 0 & 0 \\ 100 & -1 & 0 & 0 \\ 50 & 5 & -0.5 & 0 \\ 200 & 12 & 0 & -0.3 \end{bmatrix} \begin{bmatrix} x_1(t) \\ x_2(t) \\ x_3(t) \\ x_4(t) \end{bmatrix}$$

with two cases:

1. Case I ($m = 2$): There are two asynchronous measurements that measure x_3 and x_4 at discrete time instants. Inequality (6.30) holds with the following parameters

$$F = \begin{bmatrix} -1.2 & 0 \\ 0 & -1.03 \end{bmatrix}, \quad H = \begin{bmatrix} 1 & 2 \\ 1 & 1 \end{bmatrix}, \quad P = \begin{bmatrix} 1 & 0 \\ 0 & 1 \end{bmatrix},$$

$$K_1 = K_2 = 1, \qquad \delta = 8.34, \qquad \alpha = 0.6$$

Inequalities (6.32) and (6.33) are satisfied with the maximum sampling period $r < 0.005$.

2. Case II ($m = 3$): There are three asynchronous measurements that measure x_2, x_3 and x_4 at discrete time instants. Inequality (6.30) holds with the following parameters

$$F = -1.03, \quad H = \begin{bmatrix} 1 & 1 & 1 \end{bmatrix}, \quad P = K_1 = K_2 = 1,$$

$$\delta = 2.913, \qquad \alpha = 0.515$$

Inequalities (6.32) and (6.33) are satisfied with the maximum sampling period $r < 0.008$.

However, the relationship between r and C^i is very complicated even in linear systems as seen in (6.32) and (6.33). The maximum sampling period given by Theorem 3 is a sufficient condition which is very conservative. The stability and robustness properties of a multi-rate observer can be maintained under much larger sampling period.

Consider a third-order linear oscillator

$$\begin{aligned}
\begin{bmatrix} \dot{x}_1(t) \\ \dot{x}_2(t) \\ \dot{x}_3(t) \end{bmatrix} &= \begin{bmatrix} 0 & 0 & -0.1 \\ 20 & -1 & 0 \\ 20 & 0 & 0 \end{bmatrix} \begin{bmatrix} x_1(t) \\ x_2(t) \\ x_3(t) \end{bmatrix} \\
y^1(t_j^1) &= x_2(t_j^1), \qquad j \in \mathbb{Z}_+ \\
y^2(t_j^2) &= x_3(t_j^2), \qquad j \in \mathbb{Z}_+
\end{aligned} \tag{6.34}$$

where x_2 and x_3 are sampled with different sampling rates. A reduced-order Luenberger observer is designed with $F = -2$, $H = \begin{bmatrix} 1 & 2 \end{bmatrix}$. Inequality (6.30) holds true with $P = K_1 = K_2 = 3$, $\alpha = 1$, $\delta = 7.5$. It is concluded from (6.32), (6.33) that there exists a multi-rate sampled-data observer for system (6.34) given that the maximum sampling period $r < 0.039$. Notice that conditions (6.32), (6.33) are very conservative. Indeed, simulations show the stability and robustness of the multi-rate observer will be preserved under much larger sampling period. The actual sampling subsequences of y^1 and y^2 are as follows

$$\begin{aligned}
t_j^1 &= \{0.40, 2.15, 4.05, 5.88, 7.70\}, \\
t_j^2 &= \{0.20, 1.07, 2.17, 3.02, 4.07, 5.13, 6.20, 7.07\}
\end{aligned}$$

where perturbations in the sampling schedule are considered.

Figure 6.2 illustrates the performance of the multi-rate sampled-data observer with the initial conditions: $x(0) = \begin{bmatrix} 0 & 0.5 & 0.3 \end{bmatrix}'$, $\hat{x}_1(0) = -0.5$, $w^1(0) = 3$, $w^2(0) = -7.2$. It is clear that the multi-rate observer provides reliable estimation of the state.

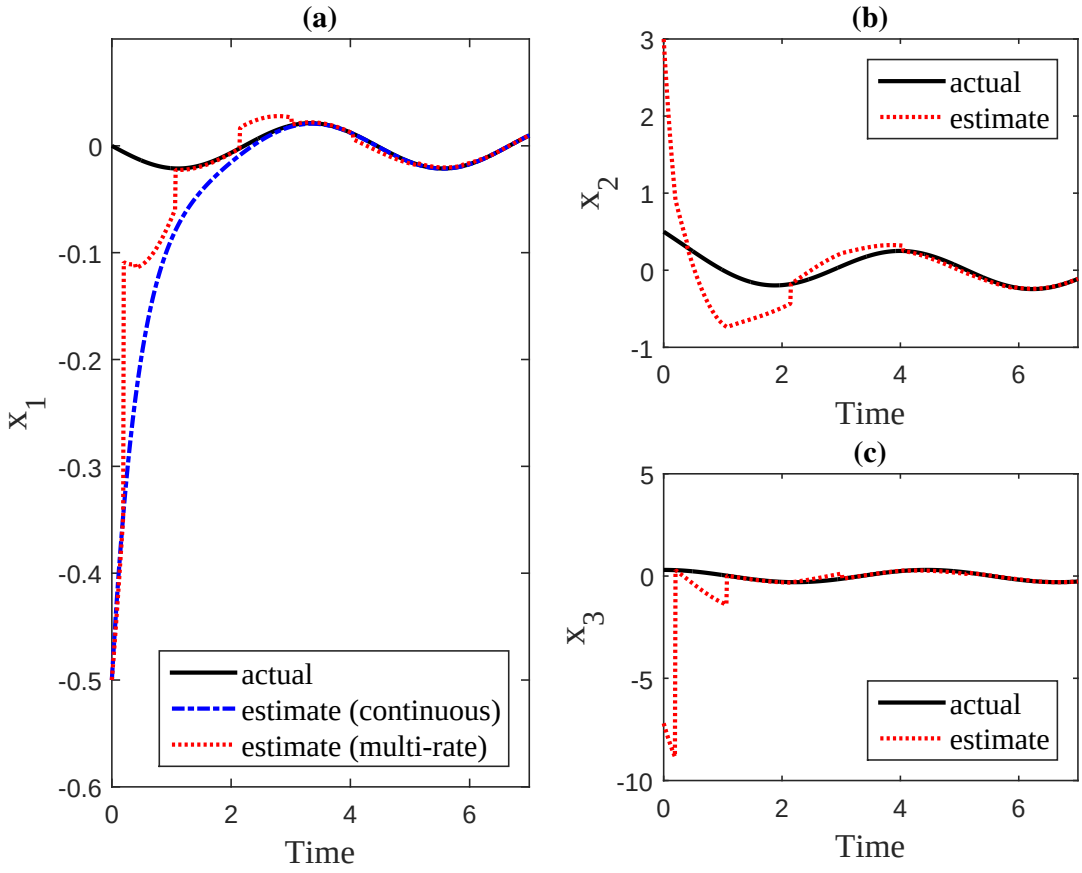

Figure 6.2: (a) Comparison of the multi-rate sampled-data observer with a continuous-time observer using continuous measurements for system (6.34); (b),(c) Performance of the inter-sample output predictors for the sampled measurements y^1 and y^2 respectively for system (6.34).

6.4.2 A Batch Chemical Reactor

Consider an isothermal batch reactor, where the following series reactions are taking place

$$M \to P$$

$$2P \to Q \to R$$

The reaction rates of M, P and Q are assumed to be

$$
\begin{aligned}
r_M &= -k_1 C_M \\
r_P &= k_1 C_M - k_2 {C_P}^2 \\
r_Q &= k_2 {C_P}^2 - k_3 C_Q
\end{aligned}
$$

where $k_1 = 0.4$ h^{-1}, $k_2 = 1$ L/(mol·h), and $k_3 = 0.5$ h^{-1}. The concentrations of P and Q can be measured by on-line analytical instruments, with different sampling rates. Let x_1, x_2, x_3 represent the concentrations of M, P and Q respectively. The state-space model is given by

$$
\begin{aligned}
\dot{x}_1(t) &= f_1(x_1, x_2, x_3) = -0.4x_1(t) \\
\dot{x}_2(t) &= f_2(x_1, x_2, x_3) = 0.4x_1(t) - x_2^2(t) \\
\dot{x}_3(t) &= f_3(x_1, x_2, x_3) = x_2^2(t) - 0.5x_3(t) \\
y^1(t_j^1) &= x_2(t_j^1), \qquad j \in \mathbb{Z}_+ \\
y^2(t_j^2) &= x_3(t_j^2), \qquad j \in \mathbb{Z}_+
\end{aligned}
\tag{6.35}
$$

There exists only one equilibrium point $x_e = (0, 0, 0)$. The eigenvalues of the linearized system around x_e are 0, -0.4 and -0.5, respectively, which indicate that the equilibrium point is locally asymptotically stable. Sampling normally occurs every 0.4 h for y^1 and every 0.5 h for y^2. However, perturbations in the sampling schedule are considered and the actual sampling subsequences of y^1 and y^2 are as follows

$$
\begin{aligned}
t_j^1 &= \{0.38, 0.79, 1.23, 1.60, 1.98, 2.41, 2.82, 3.20\}, \\
t_j^2 &= \{0.50, 0.99, 1.52, 2.01, 2.48, 3.01, 3.52, 4.01\}
\end{aligned}
$$

A continuous-time observer, which serves as the basis of the multi-rate sampled-data observer, will be designed by using the exact error linearization method (see [148] for the full-order observer

formulation, and [4] for the reduced-order observer formulation) as follows

$$\dot{z}(t) = Az(t) + B \begin{bmatrix} y^1(t) \\ y^2(t) \end{bmatrix}$$

with $A = -2$ and $B = \begin{bmatrix} 2 & 1.5 \end{bmatrix}$. The immersion map $z = T(x)$ satisfies

$$\frac{\partial T}{\partial x_1} f_1(x) + \frac{\partial T}{\partial x_2} f_2(x) + \frac{\partial T}{\partial x_3} f_3(x) = AT(x) + B \begin{bmatrix} x_2 \\ x_3 \end{bmatrix}$$

which admits a global solution

$$T(x) = -0.25x_1 + x_2 + x_3$$

which is solvable with respect to the unmeasured state x_1.

We design a multi-rate sampled-data observer based on (6.4) and the performance is illustrated in Figure 6.3 with the initial conditions: $x(0) = \begin{bmatrix} 1 & 0.7 & 0 \end{bmatrix}'$, $\hat{x}_1(0) = 1.5$, $w^1(0) = 0.6$, $w^2(0) = 0.1$. Figure 6.3(a) shows that the speed of convergence of the multi-rate sampled-data observer and the continuous-time observer is comparable under the selected design parameters. From Figures 6.3(b) and (c), the inter-sample output predictors are able to predict the inter-sample behavior with high accuracy after a few samplings by using model-based prediction.

6.4.3 A Numerical Example

In this section, the performance of the proposed multi-rate sampled-data observer is illustrated through a third-order example, in the presence of two asynchronous sampled measurements. Con-

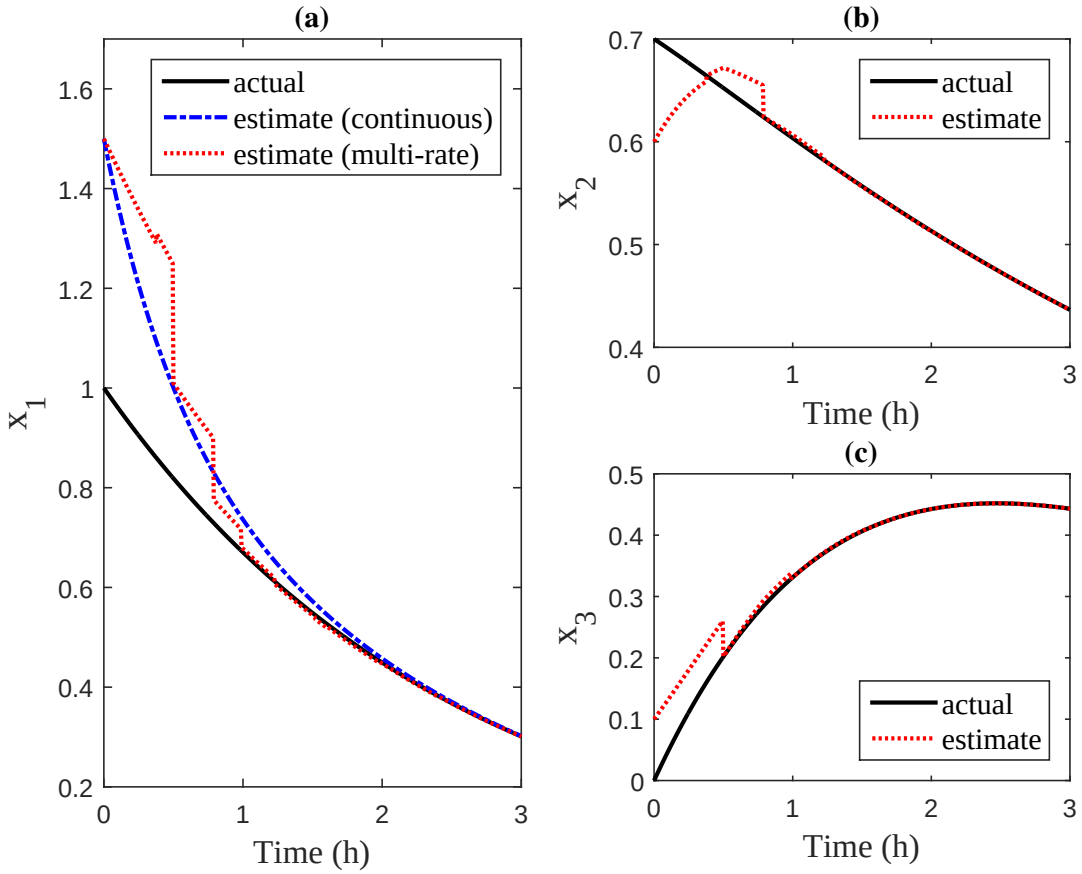

Figure 6.3: (a) Comparison of the multi-rate sampled-data observer with a continuous-time observer using continuous measurements for system (6.35); (b),(c) Performance of the inter-sample output predictors for the sampled measurements y^1 and y^2 respectively for system (6.35).

sider the following state-space model

$$\begin{aligned}
\dot{x}_1(t) &= f_1(x_1, x_2, x_3) = -x_1(t)x_2(t) - x_1(t)x_3(t) + x_2(t)x_3(t) + 9x_2(t) + 3x_3(t) \\
\dot{x}_2(t) &= f_2(x_1, x_2, x_3) = -x_1(t) - x_2(t) \\
\dot{x}_3(t) &= f_3(x_1, x_2, x_3) = -x_1(t) \\
y^1(t_j^1) &= x_2(t_j^1), \qquad j \in \mathbb{Z}_+ \\
y^2(t_j^2) &= x_3(t_j^2), \qquad j \in \mathbb{Z}_+
\end{aligned} \tag{6.36}$$

There exists only one equilibrium point $x_e = (0, 0, 0)$. The eigenvalues of the linearized system

around x_e are -0.254 and $-0.373 \pm 3.416i$, respectively, which indicate that the equilibrium point is locally asymptotically stable. Sampling normally takes place every 0.4 h for y^1 and every 0.5 h for y^2. Perturbations in the sampling schedule are considered and the actual sampling subsequences of y^1 and y^2 are as follows

$$t_j^1 = \{0.38, 0.79, 1.23, 1.60, 1.98, 2.41, 2.82, 3.20\},$$
$$t_j^2 = \{0.50, 0.99, 1.52, 2.01, 2.48, 3.01, 3.52, 4.01\}$$

A continuous-time observer, which serves as the basis of the multi-rate sampled-data observer, will be designed by using the exact error linearization method (see [148] for the full-order observer formulation, and [4] for the reduced-order observer formulation) as follows

$$\dot{z}(t) = Az(t) + B \begin{bmatrix} y^1(t) \\ y^2(t) \end{bmatrix}$$

with $A = -2$ and $B = \begin{bmatrix} -10 & -5 \end{bmatrix}$. The immersion map $z = T(x)$ satisfies

$$\frac{\partial T}{\partial x_1} f_1(x) + \frac{\partial T}{\partial x_2} f_2(x) + \frac{\partial T}{\partial x_3} f_3(x) = AT(x) + B \begin{bmatrix} x_2 \\ x_3 \end{bmatrix}$$

which admits a global solution

$$T(x_1, x_2, x_3) = x_2 x_3 - x_1 - x_2 - x_3$$

which is solvable with respect to the unmeasured state x_1.

We design a multi-rate sampled-data observer based on (6.4) and the performance is illustrated in Figure 6.4 with the initial conditions: $x(0) = \begin{bmatrix} -2 & -1 & 2 \end{bmatrix}'$, $\hat{x}_1(0) = -6$, $w^1(0) = 0$, $w^2(0) = 3$. Figure 6.4(a) shows that the speed of convergence of the multi-rate sampled-data observer and the continuous-time observer is comparable under the selected design parameters. From Figures

6.4(b) and (c), the inter-sample output predictors are able to predict the inter-sample behavior with high accuracy after a few samplings by using model-based prediction.

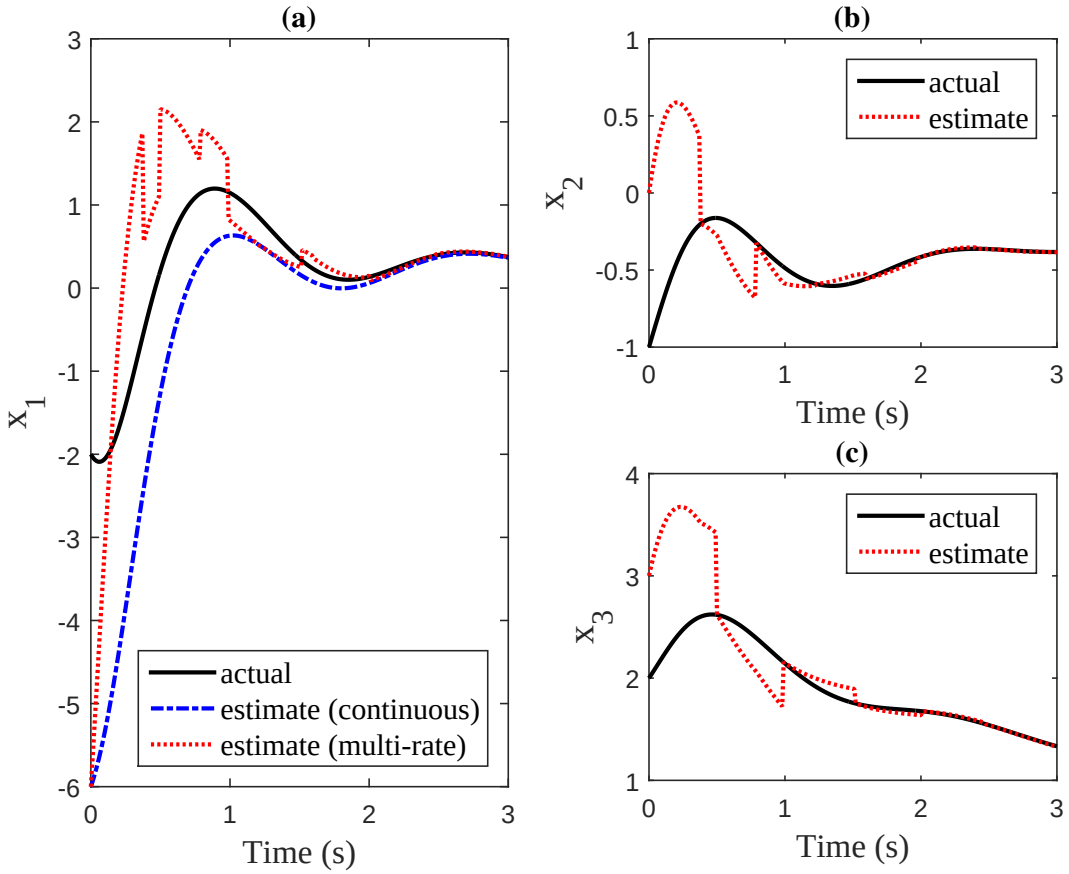

Figure 6.4: (a) Comparison of the multi-rate sampled-data observer with a continuous-time observer using continuous measurements for system (6.36); (b),(c) Performance of the inter-sample output predictors for the sampled measurements y^1 and y^2 respectively for system (6.36).

6.5 Conclusions

This chapter develops a design method for nonlinear multi-rate sampled-data observer based on an available continuous-time design, coupled with inter-sample predictors. The main contributions are: (i) the input-to-output stability property is established for the estimation errors and prediction errors with respect to measurement errors; (ii) the multi-rate design can handle non-uniform and

asynchronous sampling without any assumption on the ratio of sampling periods to be an integer, as seen in the oscillator and nonlinear examples; (iii) as long as the maximum sampling period does not exceed a certain limit, the error dynamics of the proposed multi-rate observer is input-to-output stable, irrespective of perturbations in the sampling schedule. (ii) and (iii) are the major advantages of the proposed hybrid observer over an approximate discrete-time observer. Checkable sufficient conditions for stability and robustness are derived for linear detectable systems.

The theoretical framework of this study refers to a global observer design. For general nonlinear systems, a local observer formulation is of great interest, subject to future research. In addition, measurement delay will be considered in nonlinear multi-rate observer design in Chapter 7.

7. MULTI-RATE OBSERVER DESIGN IN NONLINEAR SYSTEMS WITH MEASUREMENT DELAY

In Chapter 6, we developed a robust multi-rate observer design method for nonlinear systems in the presence of asynchronous sampling. In this chapter, measurement delays are accounted for in the observer design. Motivated by dead time compensation algorithms in [305, 306], the multi-rate multi-delay observer design is approached in a two-step manner, which is similar to the multi-rate multi-delay observer design for linear systems developed in Chapter 4. First, a multi-rate observer design of Chapter 6 is adopted as a starting point and estimates of the current state are obtained in the time interval between consecutive delayed measurements. Second, a dead time compensation approach is developed to compensate for the effect of delay and update the past estimates when a delayed measurement arrives. It is shown that stability of the multi-rate observer will be preserved under nonconstant, arbitrarily large delays, in the absence of measurement errors. A nonlinear gas-phase polyethylene reactor example demonstrates good performance of the multi-rate multi-delay observer under nonuniform sampling and nonconstant delays. There are two attractive features of the proposed approach: it inherits the stability property from a multi-rate observer in the absence of measurement errors and convergence is not affected by nonconstant delays. Notice that input delay and state delay are not in the scope of this study.

This chapter is organized as follows. In Section 7.1, a brief summary of the theoretical results presented in Chapter 6 on a nonlinear delay-free multi-rate observer is provided. In Section 7.2, a dead time compensation approach is proposed to handle measurement delays and stability analysis is conducted. The applicability and effectiveness of the observer is examined through a gas-phase polyethylene reactor example in Section 7.3 where we directly cope with the process nonlinearities and sampled, delayed measurements. In Section 7.4, conclusions are drawn from the results of the previous sections.

7.1 Preliminaries

The notations in Section 6.2 are adopted throughout this chapter. This section outlines the main results in [309] on multi-rate observer design for nonlinear systems under asynchronous sampling, in the absence of measurement delays. It is based on a continuous-time design coupled with inter-sample output predictors. The stability and robustness properties of the observer will be reviewed. The delay-free multi-rate observer design serves as a point of departure when measurement delays are considered in the next section.

7.1.1 Delay-Free Multi-Rate Observer Design

A reduced-order observer design is preferred for multi-output systems, as lower dimensionality can ease implementation of the observer. In addition, continuous estimates of the sampled outputs in each sampling interval can be reconstructed from the inter-sample predictors. Hence, a reduced-order observer formulation will be the focus of this work.

Consider a nonlinear forward complete system with continuous outputs, where without loss of generality, the outputs are assumed to be a part of the state

$$\begin{aligned} \dot{x}_R(t) &= f_R(x_R(t), x_M(t)) \\ \dot{x}_M(t) &= f_M(x_R(t), x_M(t)) \\ y(t) &= x_M(t) + v(t) \end{aligned} \tag{7.1}$$

where $x_R \in \mathbb{R}^{n-m}$ is the unmeasured state, $x_M \in \mathbb{R}^m$ is the remaining state that can be measured, y is the continuous outputs subject to measurement errors $v \in \mathcal{L}^\infty_{loc}(\mathbb{R}_+; \mathbb{R}^m)$, and $f_R \in C^1(\mathbb{R}^{n-m} \times \mathbb{R}^m; \mathbb{R}^{n-m})$, $f_M \in C^1(\mathbb{R}^{n-m} \times \mathbb{R}^m; \mathbb{R}^m)$ with $f_R(0,0) = 0$, $f_M(0,0) = 0$.

Suppose that there exists a robust observer for system (7.1) with respect to measurement errors, in the sense of Definition 1 of Section 6.2

$$\begin{aligned} \dot{z}(t) &= F(z(t), y(t)) \\ \hat{x}_R(t) &= \Psi(z(t), y(t)) \end{aligned} \tag{7.2}$$

where $z \in \mathbb{R}^k$ is the observer state, $\hat{x}_R \in \mathbb{R}^{n-m}$ is the state estimates, and $F \in C^1(\mathbb{R}^k \times \mathbb{R}^m; \mathbb{R}^k)$, $\Psi \in C^1(\mathbb{R}^k \times \mathbb{R}^m; \mathbb{R}^{n-m})$ with $F(0,0) = 0$, $\Psi(0,0) = 0$. In other words, there exist functions $\sigma \in \mathcal{KL}$, $\gamma, p \in \mathcal{N}_1$, $\mu \in \mathcal{K}^+$ and $a \in \mathcal{K}_\infty$ such that for every $(x_{R,0}, x_{M,0}, z_0, v) \in \mathbb{R}^{n-m} \times \mathbb{R}^m \times \mathbb{R}^k \times \mathcal{L}^\infty_{loc}(\mathbb{R}_+; \mathbb{R}^m)$, the solution $(x_R(t), x_M(t), z(t))$ of (7.1) and (7.2) with initial condition $(x_R(0), x_M(0), z(0)) = (x_{R,0}, x_{M,0}, z_0)$ corresponding to $v \in \mathcal{L}^\infty_{loc}(\mathbb{R}_+; \mathbb{R}^m)$ exists for all $t \geqslant 0$ and satisfies the following estimates

$$|\hat{x}_R(t) - x_R(t)| \leqslant \sigma(|(x_{R,0}, x_{M,0}, z_0)|, t) + \gamma(\|v(t)\|_{\mathcal{U}}), \qquad \forall t \geqslant 0 \tag{7.3a}$$

$$|z(t)| \leqslant \mu(t)[a(|(x_{R,0}, x_{M,0}, z_0)|) + p(\|v(t)\|_{\mathcal{U}})], \qquad \forall t \geqslant 0 \tag{7.3b}$$

Next we present a robust multi-rate sampled-data observer design with respect to measurement errors for a multi-rate system. Consider system (7.1) with asynchronous, sampled outputs

$$\begin{aligned} \dot{x}_R(t) &= f_R(x_R(t), x_M(t)) \\ \dot{x}_M(t) &= f_M(x_R(t), x_M(t)) \\ y^i(t^i_j) &= x^i_M(t^i_j) + v^i(t^i_j), \qquad j \in \mathbb{Z}_+, i = 1, 2, \ldots, m \end{aligned} \tag{7.4}$$

where t^i_j denotes the j-th sampling time for the state x^i_M, at some sequence of time instants $S = \{t_k\}_{k=0}^\infty$. The sampling times of each sensor are not necessarily uniformly spaced, but satisfying $0 < t^i_{j+1} - t^i_j \leqslant r$ for all $j \in \mathbb{Z}_+$, where r is the maximum sampling period among all the sensors. There is a one-to-one mapping from $\{t^i_j : j \in \mathbb{Z}_+, i = 1, 2, \ldots, m\}$ to $\{t_k\}_{k=0}^\infty$.

Consider a multi-rate sampled-data observer design of the following form

$$\begin{aligned} \dot{z}(t) &= F(z(t), w(t)), && t \in [t_k, t_{k+1}) \\ \dot{w}(t) &= f_M(\Psi(z(t), w(t)), w(t)), && t \in [t_k, t_{k+1}) \\ w^i(t_{k+1}) &= y^i(t_{k+1}) \\ t_{k+1} &= t_k + rd(t_k) \\ \hat{x}_R(t) &= \Psi(z(t), w(t)) \end{aligned} \tag{7.5}$$

where $w \in \mathbb{R}^m$ is the predicted outputs, $d \in \mathcal{L}^\infty_{loc}(\mathbb{R}_+; [0,1])$ generates the actual sampling schedule which is allowed to be time-varying. This multi-rate observer design consists of a continuous-time observer coupled with m inter-sample predictors. Therefore, the existence of a robust continuous-time observer (7.2) is a prerequisite for the observer design in a multi-rate system. The inter-sample predictors continuously generate estimates of the sampled outputs in each sampling interval. $w^i(t)$ will get reinitialized once a new measurement $y^i(t_{k+1})$ becomes available, whereas the rest of the predictor states do not change until their measurements are obtained.

The multi-rate design offers two attractive features: (i) a continuous-time observer design from the literature can be reused in the context of a multi-rate design by coupling with predictors; (ii) the unmeasured state is reconstructed from the observer, and continuous estimates of the sampled outputs are reconstructed from the inter-sample predictors. It was seen in [52] that the model-based prediction offers a more meaningful approach to approximate the inter-sample behavior compared with a sample-and-hold strategy, especially under large sampling period.

Suppose that there exists a robust continuous-time observer (7.2) for system (7.1) with respect to measurement errors. Moreover, suppose that there exist constants $C^i \geqslant 0$ and functions $\bar{\sigma}^i \in \mathcal{KL}$ for all $i = 1, 2, \ldots, m$, such that for every $(x_{R,0}, x_{M,0}, z_0, v) \in \mathbb{R}^{n-m} \times \mathbb{R}^m \times \mathbb{R}^k \times \mathcal{L}^\infty_{loc}(\mathbb{R}_+; \mathbb{R}^m)$, the solution $(x_R(t), x_M(t), z(t))$ of the overall system (i.e., the continuous-time system (7.1) and robust observer (7.2)) with initial condition $(x_R(0), x_M(0), z(0)) = (x_{R,0}, x_{M,0}, z_0)$ corresponding to $v \in \mathcal{L}^\infty_{loc}(\mathbb{R}_+; \mathbb{R}^m)$ exists for all $t \geqslant 0$ and satisfies the following estimate

$$\begin{aligned} &|f^i_M(\Psi(z(t), x_M(t) + v(t)), x_M(t) + v(t)) - f^i_M(x_R(t), x_M(t))| \\ &\leqslant \bar{\sigma}^i(|(x_{R,0}, x_{M,0}, z_0)|, t) + C^i \left\| v(t) \right\|_{\mathcal{U}}, \qquad \forall t \geqslant 0 \end{aligned} \tag{7.6}$$

In addition, suppose that (i) $3rC^i m < 1$ for $i = 1, 2, \ldots, m$; (ii) $3\gamma(ms) < s$ for all $s > 0$, where $\gamma \in \mathcal{N}_1$ is the gain function in the estimate (7.3a) of the robust observer.

If the above properties are satisfied in a continuous-time observer design, it can be proved that (7.5) is a robust multi-rate sampled-data observer for (7.4) with respect to measurement errors. In other words, there exist functions $\tilde{\sigma}_R, \tilde{\sigma}_M \in \mathcal{KL}$, $\tilde{\gamma}_R, \tilde{\gamma}_M, \tilde{p} \in \mathcal{N}_1$, $\tilde{\mu} \in \mathcal{K}^+$ and $\tilde{a} \in \mathcal{K}_\infty$ such that

for every $(x_{R,0}, x_{M,0}, z_0, w_0, d, v) \in \mathbb{R}^{n-m} \times \mathbb{R}^m \times \mathbb{R}^k \times \mathbb{R}^m \times \mathcal{L}^\infty_{loc}(\mathbb{R}_+; [0,1]) \times \mathcal{L}^\infty_{loc}(\mathbb{R}_+; \mathbb{R}^m)$, the solution $(x_R(t), x_M(t), z(t), w(t))$ of the overall system of (7.4) and (7.5) with initial condition $(x_R(0), x_M(0), z(0), w(0)) = (x_{R,0}, x_{M,0}, z_0, w_0)$ corresponding to $d \in \mathcal{L}^\infty_{loc}(\mathbb{R}_+; [0,1])$ and $v \in \mathcal{L}^\infty_{loc}(\mathbb{R}_+; \mathbb{R}^m)$ satisfies the following estimates

$$|\hat{x}_R(t) - x_R(t)| \leqslant \tilde{\sigma}_R(|(x_{R,0}, x_{M,0}, z_0, w_0)|, t) + \tilde{\gamma}_R(\|v(t)\|_{\mathcal{U}}), \qquad \forall t \geqslant 0 \tag{7.7a}$$

$$|w(t) - x_M(t)| \leqslant \tilde{\sigma}_M(|(x_{R,0}, x_{M,0}, z_0, w_0)|, t) + \tilde{\gamma}_M(\|v(t)\|_{\mathcal{U}}), \qquad \forall t \geqslant 0 \tag{7.7b}$$

$$|(z(t), w(t))| \leqslant \tilde{\mu}(t)[\tilde{a}(|(x_{R,0}, x_{M,0}, z_0, w_0)|) + \tilde{p}(\|v(t)\|_{\mathcal{U}})], \qquad \forall t \geqslant 0 \tag{7.7c}$$

The input-to-output stability property has been established for the observer and predictor errors of the overall system with respect to measurement noises, by applying the Karafyllis-Jiang vector small-gain theorem (see detailed proof in Section 6.3). In addition, the multi-rate design provides robustness with respect to perturbations in the sampling schedule.

7.2 Main Results

In this section, an available multi-rate observer design (7.5) is the starting point. Similar to the multi-rate multi-delay observer in linear systems, a dead time compensation algorithm is proposed to handle possible measurement delays. Measurement errors are not considered (i.e., $v \equiv 0$) in the system. It is shown that the multi-rate multi-delay observer is asymptotically stable in the presence of nonconstant and arbitrarily large delays.

7.2.1 Proposed Multi-Rate Multi-Delay Observer Design

Consider a multi-rate system (7.4) with possible delays in the outputs $y^i(t^i_j)$ for all $j \in \mathbb{Z}_+, i = 1, 2, \ldots, m$, in the absence of measurement errors

$$\begin{aligned} \dot{x}_R(t) &= f_R(x_R(t), x_M(t)) \\ \dot{x}_M(t) &= f_M(x_R(t), x_M(t)), \quad t \geqslant -\Delta \\ y^i(t^i_j) &= x^i_M(t^i_j - \delta^i_j) \end{aligned} \tag{7.8}$$

where t_j^i denotes the time when the j-th measurement of x_M^i becomes available after some possible delay $\delta_j^i \geqslant 0$. In other words, the measured output $y^i(t_j^i)$ is a function of the state x_M^i at time $t_j^i - \delta_j^i$. The measurement delay δ_j^i is not constant but is assumed bounded by a positive real number Δ. Notice that $\delta_j^i = 0$ if there is no delay in the output y^i. Similar to the multi-rate system of Equation (7.4), the sampling times of each measurement are not necessarily uniformly spaced, but satisfying $0 < \left|(t_{j'}^i - \delta_{j'}^i) - (t_j^i - \delta_j^i)\right| \leqslant r$ for any consecutive sampling instants.

The proposed observer for the system (7.4) with multiple measurement delays is based on the multi-rate observer design (7.5) combined with dead time compensation. As depicted in Figure 4.1 (notice the continuous outputs are not considered), the estimation process is composed of two steps. First, dead time compensation will be triggered once a delayed measurement is obtained at t_j^i. Past estimates are recalculated by integrating the observer and compensator equations from $t_j^i - \delta_j^i$ to t_j^i. Any available measurement can be used as a delay-free output to reinitialize the corresponding compensator at its sampling time. The estimates of the current state at t_j^i are consequently updated at the end of the compensation. This step ensures that these available measurements are used in the observer without delay, in the same order as they are sampled. Second, the updated estimates are used as the initial condition of the observer and the inter-sample output predictors at t_j^i. The multi-rate multi-delay observer operates like a delay-free multi-rate observer when there is no delayed measurement.

When a sampled and delayed measurement becomes available at t_j^i, dead time compensation is performed to update the past estimates. For all $t \in [t_j^i - \delta_j^i, t_j^i)$ where $\delta_j^i \neq 0$, the following design

of a multi-rate observer with dead time compensation is proposed

$$\dot{z}(t) = F(z(t), w(t)) \tag{7.9a}$$

$$\dot{w}(t) = f_M(\Psi(z(t), w(t)), w(t)) \tag{7.9b}$$

$$w^i(t_j^i - \delta_j^i) = y^i(t_j^i) \tag{7.9c}$$

$$w^{i'}(t_{j'}^{i'} - \delta_{j'}^{i'}) = y^{i'}(t_{j'}^{i'}), \qquad \forall t_{j'}^{i'}, (t_{j'}^{i'} - \delta_{j'}^{i'}) \in [t_j^i - \delta_j^i, t_j^i) \tag{7.9d}$$

$$\hat{x}_R(t) = \Psi(z(t), w(t)) \tag{7.9e}$$

where $w \in \mathbb{R}^m$ is the compensator state representing the past estimates for $x_M(t)$. From (7.9c), it shows the reinitialization step of the i-th dead time compensator by using the delayed measurement $y^i(t_j^i)$ at its sampling time $t_j^i - \delta_j^i$. The outputs that are sampled and measured between $t_j^i - \delta_j^i$ and t_j^i can be used to reset the compensators at their respective sampling times, as seen in (7.9d).

Remark 24. *The observer state $z(t)$, compensator state $w(t)$, and sampled outputs $y^{i'}$ in (7.9) all represent the past information in the system throughout the dead time compensation, which need to be stored in a buffer. Notice that the past estimates are generated for the purpose of correcting the state estimates at t_j^i and therefore improving the estimation accuracy afterwards. The memory size of the buffer will be finite as long as the upper bound of the measurement delay Δ is finite, as will be discussed later.*

Once the estimates at t_j^i are obtained after the dead time compensation, inter-sample prediction comes into play in the time interval between two consecutive measurements at t_j^i and $t_{j'}^{i'}$. For all $t \in [t_j^i, t_{j'}^{i'})$, the multi-rate multi-delay observer follows

$$\begin{aligned} \dot{z}(t) &= F(z(t), w(t)) \\ \dot{w}(t) &= f_M(\Psi(z(t), w(t)), w(t)) \\ \hat{x}_R(t) &= \Psi(z(t), w(t)) \end{aligned} \tag{7.10}$$

where $w \in \mathbb{R}^m$ is the predicted outputs for the sampled measurements y^i in the sampling interval.

These predictors estimate the evolution of the sampled outputs, in the same spirit as in a delay-free multi-rate observer. If an undelayed measurement is available at t_j^i, the inter-sample prediction will run immediately after reinitialization, and no dead time compensation will be needed. Algorithm 2 summarizes the estimation process of the proposed multi-rate multi-delay observer.

Algorithm 2 Algorithm for Nonlinear Multi-rate Multi-delay Observer

STEP 0: Initialize $z(t_0)$, $w(t_0)$, and solve Equation (7.10) for $[t_0, t_j^i)$.
STEP 1: Calculate $z(t)$ and $w(t)$ when a sampled measurement becomes available at t_j^i.
if $\delta_j^i > 0$ **then**
    Solve Equation (7.9) for $[t_j^i - \delta_j^i, t_j^i)$ and update $z(t_j^i)$, $w(t_j^i)$. ▷ Dead time compensation
end if
Reinitialize Equation (7.10) with $z(t_j^i)$, $w(t_j^i)$, and solve it for $[t_j^i, t_{j'}^{i'})$. ▷ Inter-sample prediction
STEP 2: Set $t_j^i = t_{j'}^{i'}$ and go to Step 1.

7.2.2 Stability Analysis

Past estimates are recalculated in the dead time compensation once a sampled, delayed measurement becomes available. Estimates at certain times may be calculated more than once, if the measurement order differs from the sampling order. We name the last updated estimates obtained from the multi-rate multi-delay observer "final estimates". We denote $\tilde{t}$ the most-recent sampling time where the measurements of all the samples taken before $\tilde{t}$ (including $\tilde{t}$) are available. It implies that the final estimates are obtained for all $t \leqslant \tilde{t}$. Because the measurements are used in the same order as the way they are sampled when calculating the final estimates, the final estimates $z(t)$, $w(t)$ and $\hat{x}_R(t)$ for all $t \leqslant \tilde{t}$ in the multi-rate multi-delay observer are identical to those in a delay-free multi-rate observer, under the same design parameters. Once the final estimates at $\tilde{t}$ are obtained, all the stored measurements that are sampled before $\tilde{t}$ can be cleared from the buffer.

Despite the fact that the estimation process depicted in Figure 4.1 involves two steps, stability of the multi-rate multi-delay observer will be presented in a unified manner, as the essence of both compensation and prediction is to predict the dynamic model forward.

It is straightforward to show that the estimates and predicted outputs are bounded for all $t \geqslant 0$. The fact that the system (7.1) is forward complete implies the existence of functions $\mu \in \mathcal{K}^+$ and $a \in \mathcal{K}_\infty$ such that for every $(x_{R,0}, x_{M,0}) \in \mathbb{R}^{n-m} \times \mathbb{R}^m$, the solution $(x_R(t), x_M(t))$ of (7.1) with initial condition $(x_R(0), x_M(0)) = (x_{R,0}, x_{M,0})$ exists for all $t \geqslant 0$ and satisfies

$$|(x_R(t), x_M(t))| \leqslant \mu(t) a(|(x_{R,0}, x_{M,0})|) \tag{7.11}$$

Obviously, $|(\hat{x}_R(t), w(t))|$ will be bounded before the first measurement becomes available as the initial condition of the observer is finite. After the first measurement, the estimates in the compensation (or prediction) will be generated by forward predicting the model from $\tilde{t}$ with reinitialization at some sampling times. The estimates at $\tilde{t}$ are identical to those in a delay-free multi-rate observer, which are bounded from (7.7a) and (7.7b). Therefore, $|(\hat{x}_R(t), w(t))|$ is bounded for all $t \geqslant \tilde{t}$.

Because of the previous assumption that the measurement delay in the system (7.8) has a finite upper bound, $\tilde{t}$ will approach infinity as t goes to infinity. From (7.7a) and (7.7b), we have

$$\lim_{\tilde{t} \to +\infty} \hat{x}_R(\tilde{t}) = x_R(\tilde{t}) \tag{7.12a}$$

$$\lim_{\tilde{t} \to +\infty} w(\tilde{t}) = x_M(\tilde{t}) \tag{7.12b}$$

Hence, the observer can accurately estimate the actual state in the compensation and prediction as t goes to infinity, in the absence of measurement errors. Reinitialization in the compensation does not affect the convergence property.

An attractive feature of the approach is that it can handle the situation where the delayed measurement sequence is not in the same order as the sampling sequence.

Remark 25. *The proposed dead time compensation approach can be applied to a multi-rate full-order observer formulation, under appropriate modifications.*

7.3 A Gas-Phase Polyethylene Reactor

The application of a multi-rate multi-delay observer is then explored in an industrial gas-phase polyethylene reactor (see Figure 3.3), where the measurement delays of on-line gas chromatography and off-line lab analysis will be accounted for. In this reactor, the polymerization takes place at the interface between the solid catalyst and the polymer matrix. The feed to the reactor, which consists of ethylene, comonomers, hydrogen, and inerts, provides the fluidization by using a high rate of gas recycle. Ziegler-Natta catalysts are fed continuously to the reactor. The heat generated from the exothermic reaction is removed through a heat exchanger. The product, polyethylene, discharges near the base of the reactor as solid powder.

In the operating range of industrial interest, the fluidized-bed reactor in Figure 3.3 can often be modeled as a single-phase, well-mixed CSTR [215]. For simplicity, it is assumed that there is only one type of active catalyst sites [227]. The mathematical model for this reactor can be found in Section 4.4. The definitions of all the variables in Equations (4.17), (4.18) and the values of the process parameters are listed in Tables 3.1 and 3.2 in Section 3.4.

As for outputs, the reactor temperature is continuously measured on line without delay. The gas concentrations of inerts, ethylene, comonomer and hydrogen are normally sampled every 20 min and measured by using on-line gas chromatography, which induces about 8 min delay caused by sample preparation (2.5 min), analysis (4 min), and computer calculation (1.5 min) [307]. In addition, the off-line lab analysis of melt index and density is normally sampled every 40 min with 60 min delay, which provides quality information of the polyethylene [222]. During the reaction, the active catalyst site may become inactive due to spontaneous decay and adsorption of impurities, which forms dead site and dead polymer chains. Because of the difficulty in measuring the amount of active catalyst sites in the reactor, it is necessary to monitor this quantity from a reliable on-line soft sensor. Providing continuous and reliable estimates for the inter-sample dynamic behavior of these sampled outputs is also significant for quality control and monitoring.

A continuous-time observer, which serves as the basis of the multi-rate multi-delay observer, will be designed by using the exact error linearization method (see [148] for the full-order observer

formulation, and [4] for the reduced-order observer formulation) as follows

$$\dot{z}(t) = Az(t) + By(t)$$

where

$$A = -0.00068,$$
$$B = \begin{bmatrix} 0.01 & 0.01 & 0.01 & 0.01 & 0.01 & 0.01 & 0.01 \end{bmatrix}$$

The immersion map $z = T(x)$ satisfies

$$\frac{\partial T}{\partial x_R} f_R(x) + \frac{\partial T}{\partial x_M} f_M(x) = AT(x) + Bx_M$$

It is possible to calculate the solution $T(x)$ in the form of a multivariate Taylor series around the steady state. The truncation order is set to $N = 4$ when solving the system of linear PDEs.

It is assumed that the first sample of gas chromatography is taken at $t = 5$ min and the first sample of lab analysis is taken at $t = 10$ min. Perturbations in the sampling schedule and nonconstant measurement delays are considered in the simulation. The actual sampling schedule and their corresponding measurement delays are given in Table 7.1. Note that the measurement delay of gas chromatography is smaller than its sampling period, whereas the delay of lab analysis is relatively larger. The initial conditions of the process and the observer are given in Table 4.4.

Gas chromatography	Sampling (min)	5	23	43	62.5	81.5	102	122	140
	Delay (min)	8.0	8.7	8.5	7.5	8.0	8.0	8.2	7.8
	Sampling (min)	161.5	179.5	199.5	219	238	258.5	278.5	300.5
	Delay (min)	8.5	8.3	8.0	8.2	7.7	8.0	8.0	8.3
Lab analysis	Sampling (min)	10	48	93	134	170	210	248	288
	Delay (min)	60	56	62.8	66.3	54.5	60	60.5	66.7

Table 7.1: Actual sampling schedule and measurement delays in the gas-phase polyethylene reactor example.

The performance of multi-rate multi-delay observer is shown in Figure 7.1, where it is compared with a multi-rate observer in the absence of measurement delays with the same design parameters. Figure 7.1(a) shows that the estimate from the multi-rate multi-delay observer has approximately the same convergence rate as that from the multi-rate design. Figures 7.1(b)-(f) show the evolution of estimated outputs obtained from inter-sample predictors and in this way, the inter-sample behavior can be reconstructed under nonuniform sampling schedule. When a sampled and delayed measurement arrives, dead time compensation is performed by integrating Equation (7.9) from sampling time to current time and therefore the estimates will get updated, which explains the impulsive behavior. The multi-rate multi-delay observer design (7.9)&(7.10) provides reliable estimation results. In the presence of multiple measurements, the reduced-order observer formulation is preferred because the dimension would be significantly lower than the full-order formulation.

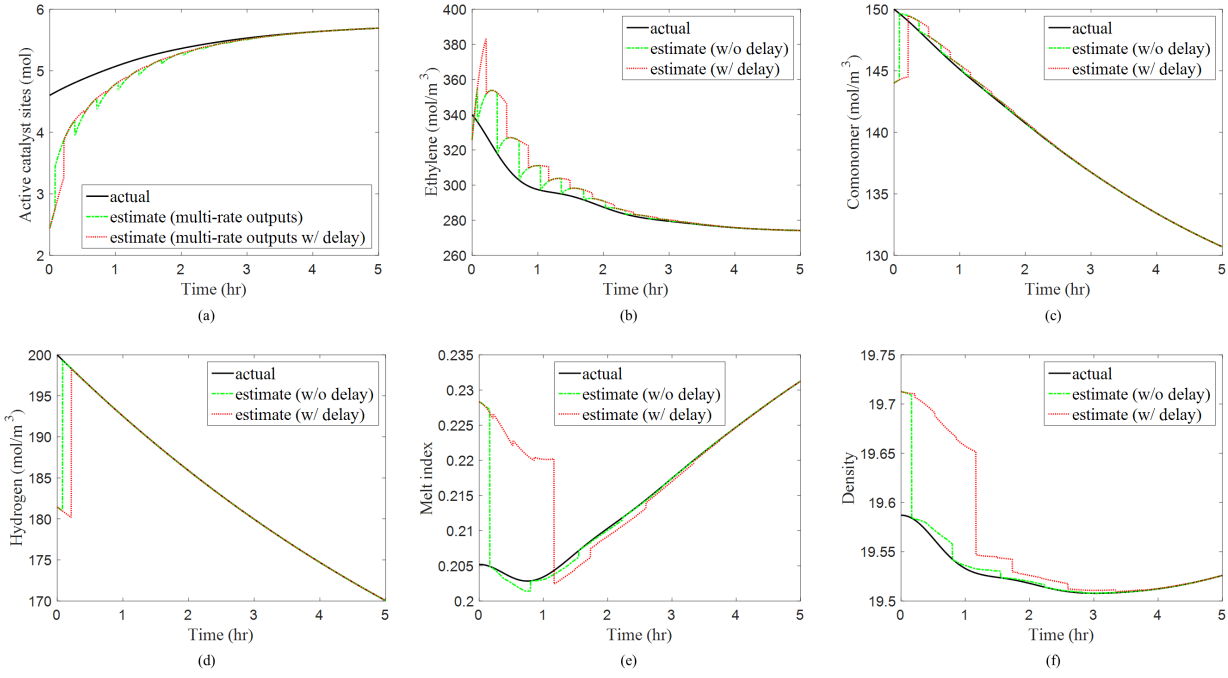

Figure 7.1: Comparison of the multi-rate multi-delay observer (red) and the multi-rate observer in the absence of measurement delay (green) in the nonlinear gas-phase polyethylene reactor example.

7.4 Conclusions

The present chapter proposes a design method for multi-rate multi-delay observers in nonlinear systems. It is based on an available multi-rate observer design combined with dead time compensation, where asynchronous and sampled measurements, in the presence of possible measurement delays, are accounted for. The estimation process has two steps: (i) dead time compensation when a delayed measurement becomes available and the current estimates are updated; (ii) inter-sample prediction in the time interval between consecutive delayed measurements. Two attractive features of the proposed observer are that it inherits the stability property from a delay-free multi-rate observer and it can handle nonconstant and arbitrarily large delays, in the absence of measurement errors. Unlike the chain observers in the literature where a high dimensionality may be required in the case of large delays, the proposed observer has the same dimension as a multi-rate observer for a delay-free system. From the case study, we see that the multi-rate multi-delay observer can provide reliable estimation results. The presence of delays in the measurements inevitably slows down convergence of the observer.

8. CONCLUSIONS AND FUTURE RESEARCH DIRECTIONS

State observer design is a vast and rapidly growing research field with potential applications to process monitoring, controller synthesis, and fault detection and identification. While this dissertation focuses on only a subset of the theory and applications of observer design, it accomplishes a goal of furthering the algorithms and applicability of observer design by enabling the utilization of all available on-line measurements and demonstrates its usefulness in a polymerization reactor context. Motivated by practical needs of monitoring chemical processes, this dissertation addressed the problem of multi-rate multi-delay observer design in linear and nonlinear systems and stability analysis was carried out based on Lyapunov's stability theory and the vector small-gain theorem, respectively.

Chapter 2 presented an application of a nonlinear observer for monitoring degree of polymerization in a series of PET polycondensation reactors in the presence of a continuous measurement and a sampled, delayed measurement. By exploiting the special LBT structure of the system, the complexity of the state dependence of the observer gains was reduced. Inter-sample prediction and dead time compensation were used to handle the sampled, delayed measurement. From simulation, it was shown that the observer can provide good estimates in the presence of sensor noise. But the problem of multi-rate observer design was bypassed because the discrete measurement was not an input for the continuous-time observer.

Chapter 3 developed a design method for multi-rate observers in linear multi-output systems, considering both continuous and discrete measurements with asynchronous sampling. It was based on an available continuous-time Luenberger observer design coupled with inter-sample predictors for the sampled measurements. The stability analysis was carried out based on Lyapunov's second method and it was concluded that the error dynamics of the multi-rate observer will be exponential stable as long as the sampling period is sufficiently small. Sufficient and explicit conditions were provided, in terms of maximum sampling period, to guarantee exponential stability, irrespective of perturbations in the sampling schedule. A gas-phase polyethylene reactor example demonstrated

the applicability of the proposed method in a linear context.

Another important characteristic of the process outputs is time delay which was accounted for in Chapter 4. A design method of multi-rate multi-delay observers in linear systems was developed based on an available multi-rate observer design proposed in Chapter 3 combined with dead time compensation. Two attractive features of the observer are that it inherits stability from a delay-free multi-rate observer and it can handle nonconstant, arbitrarily large measurement delays. The two case studies of Chapter 3 were reconsidered in the presence of delays and it can be seen that the multi-rate multi-delay observer provided reliable estimation results.

The previous chapters focused on the problem of incorporating different types of measurements in the observer design, for prescribed eigenvalues of the error dynamics. In Chapter 5, a rigorous approach for observer gain selection was developed so that a compromise can be reached between the effect of modeling error on the accuracy of state estimates and the effect of measurement error on the accuracy of state estimates, by optimizing a performance index. The effects of modeling error and measurement error were evaluated by studying the response of the observer error dynamics to a unit impulse function. This approach was demonstrated through two classes of linear systems with single-rate measurements and with fast and slow measurements, respectively. It is possible to generalize the optimal observer design to a broader class of multi-rate systems.

Chapter 6 presented a design method for multi-rate observers in nonlinear systems under asynchronous sampling. It was based on an available continuous-time design coupled with inter-sample predictors for the sampled measurements. The input-to-output stability was established for the estimation/prediction errors with respect to measurement errors using the vector small-gain theorem. Moreover, the multi-rate design provided robustness with respect to perturbations in the sampling schedule. The applicability of the proposed method was seen through various example problems.

Multi-rate multi-delay observer in nonlinear systems was studied in Chapter 7. It was based on an available multi-rate observer design combined with dead time compensation, in the same spirit as the linear multi-rate multi-delay observer in Chapter 4. It inherited the stability property from a delay-free multi-rate observer in the absence of measurement errors. The gas-phase polyethylene

reactor example was reconsidered in the presence of measurement delays where reliable estimation results were demonstrated through simulation.

To this extent, this dissertation presents developments in the field of state estimation by providing the theoretical advances in multi-rate multi-delay state observer design, and several simulation examples with focus on polymerization reactors. It is the author's hope that the multi-rate observer framework may assist in the implementation of state observers for process monitoring in the future. In particular, some key areas for future work will be discussed to conclude this dissertation, as they flow naturally out of the specific developments explored to this point.

8.1 Future Work

The theoretical developments of multi-rate observers in linear and nonlinear systems provided sufficient stability conditions in terms of maximum sampling period, which were shown to be very conservative. It is desirable to find a tighter bound which would help to select appropriate sensors for particular systems and predetermine the nominal sampling rate for each sensor. Other stability tools may be required in the analysis.

Optimal multi-rate observer design was studied in linear systems in Chapter 5, along the same line as optimal feedback controller tuning. Future research efforts may focus on optimal multi-rate observer design in nonlinear systems. A systematic approach for the optimal selection of controller parameters was proposed in [336], in the sense of minimizing a performance index calculated as a function of the controller parameters by solving Zubov's PDE. Standard optimization techniques were then employed to find the optimal values of the controller parameters. There is clearly potential to extend the methodology to the optimal selection of design parameters in nonlinear multi-rate observer.

It was assumed in this dissertation that a perfect model is always available in the development of multi-rate multi-delay observers. In practice, model and parameter uncertainties are very common even in a well-developed process model. It is desirable to study the response of multi-rate observer affected by model and parameter uncertainties, both from a theory and application perspective. In addition, it is of great interest to test the multi-rate multi-delay observer on a meaningful lab-scale

process with experimental data. In this way, observer performance can be evaluated in the presence of measurement errors, model and parameter uncertainties, and disturbances.

This dissertation investigated the model-based approach for process monitoring where the measurements considered are functions of the state variables. However, a large amount of data recorded in the process industry cannot be represented in terms of state variables of a first-principle model. For example, visual appearance is an important feature in the quality assessment of chemical and pharmaceutical products. An image contains essential information on product morphology, shape, size and color. It would be beneficial to incorporate this kind of information into the process monitoring scheme by developing automatic machine-based image analysis systems. It is believed that the hybrid approach would overcome the limitations from a standalone model-based or data-driven approach.

In Chapter 7, the proposed multi-rate sampled-data observer was developed for an autonomous nonlinear system. A multi-rate observer design method for non-autonomous systems may be considered as a future research direction, where the input variable enters the system's equations in an explicit way. In such a case, a new set of sufficient conditions for the solution of the above problem should be developed.

Finally, another interesting future research direction might be devoted to the study of coupling the proposed nonlinear multi-rate observer with a state feedback controller, and to study the resulting closed-loop properties. Separation principle does not hold any longer in nonlinear systems (at least very restrictive) and thus, the design of state feedback and the design of state observer cannot be performed independently. This problem is of considerable theoretical and practical merits.

REFERENCES

[1] "Webbing Market Size, Share, Global Industry Trends Report, 2018-2025." Web, May 2018.

[2] "GBI: The Polyethylene Terephthalate (PET) Market to 2020." Web, July 2010.

[3] O. Kammona, E. G. Chatzi, and C. Kiparissides, "Recent developments in hardware sensors for the on-line monitoring of polymerization reactions," *Journal of Macromolecular Science. Reviews in Macromolecular Chemistry and Physics*, vol. 39, no. 1, pp. 57–134, 1999.

[4] N. Kazantzis, C. Kravaris, and R. A. Wright, "Nonlinear observer design for process monitoring," *Industrial & Engineering Chemistry Research*, vol. 39, no. 2, pp. 408–419, 2000.

[5] M. Soroush, "State and parameter estimations and their applications in process control," *Computers & Chemical Engineering*, vol. 23, no. 2, pp. 229–245, 1998.

[6] W. H. Ray, "Polymerization reactor control," *IEEE Control Systems Magazine*, vol. 6, no. 4, pp. 3–8, 1986.

[7] J. R. Richards and J. P. Congalidis, "Measurement and control of polymerization reactors," *Computers & Chemical Engineering*, vol. 30, no. 10-12, pp. 1447–1463, 2006.

[8] D. C. H. Chien and A. Penlidis, "On-line sensors for polymerization reactors," *Journal of Macromolecular Science. Reviews in Macromolecular Chemistry and Physics*, vol. 30, no. 1, pp. 1–42, 1990.

[9] J. E. Eldridge and J. D. Ferry, "Studies of the cross-linking process in gelatin gels. III. Dependence of melting point on concentration and molecular weight," *The Journal of Physical Chemistry*, vol. 58, no. 11, pp. 992–995, 1954.

[10] R. B. Beevers and E. F. T. White, "Physical properties of vinyl polymers. Part 1.-Dependence of the glass-transition temperature of polymethylmethacrylate on molecular weight," *Transactions of the Faraday Society*, vol. 56, pp. 744–752, 1960.

[11] T. D. Fornes, P. J. Yoon, H. Keskkula, and D. R. Paul, "Nylon 6 nanocomposites: the effect of matrix molecular weight," *Polymer*, vol. 42, no. 25, pp. 9929–9940, 2001.

[12] G. Capaccio, T. A. Crompton, and I. M. Ward, "The drawing behavior of linear polyethylene. I. Rate of drawing as a function of polymer molecular weight and initial thermal treatment," *Journal of Polymer Science: Polymer Physics Edition*, vol. 14, no. 9, pp. 1641–1658, 1976.

[13] M. E. Fowler, J. W. Barlow, and D. R. Paul, "Effect of copolymer composition on the miscibility of blends of styrene-acrylonitrile copolymers with poly(methyl methacrylate)," *Polymer*, vol. 28, no. 7, pp. 1177–1184, 1987.

[14] G. Perego, G. D. Cella, and C. Bastioli, "Effect of molecular weight and crystallinity on poly(lactic acid) mechanical properties," *Journal of Applied Polymer Science*, vol. 59, no. 1, pp. 37–43, 1996.

[15] H. W. McCormick, F. M. Brower, and L. Kin, "The effect of molecular weight distribution on the physical properties of polystyrene," *Journal of Polymer Science*, vol. 39, no. 135, pp. 87–100, 1959.

[16] W. H. Ray, "On the mathematical modeling of polymerization reactors," *Journal of Macromolecular Science. Reviews in Macromolecular Chemistry*, vol. 8, no. 1, pp. 1–56, 1972.

[17] C. Kiparissides, "Polymerization reactor modeling: a review of recent developments and future directions," *Chemical Engineering Science*, vol. 51, no. 10, pp. 1637–1659, 1996.

[18] A. Penlidis, S. R. Ponnuswamy, C. Kiparissides, and K. F. O'Driscoll, "Polymer reaction engineering: modelling considerations for control studies," *The Chemical Engineering Journal*, vol. 50, no. 2, pp. 95–107, 1992.

[19] M. E. Sacks, S.-I. Lee, and J. A. Biesenberger, "Effect of temperature variations on molecular weight distributions: batch, chain addition polymerizations," *Chemical Engineering Science*, vol. 28, no. 1, pp. 241–257, 1973.

[20] J. H. Jo and S. G. Bankoff, "Digital monitoring and estimation of polymerization reactors," *AIChE Journal*, vol. 22, no. 2, pp. 361–369, 1976.

[21] S.-A. Chen and W.-F. Jeng, "Minimum end time policies for batchwise radical chain polymerization," *Chemical Engineering Science*, vol. 33, no. 6, pp. 735–743, 1978.

[22] S.-A. Chen and K.-F. Lin, "Minimum end time policies for batchwise radical chain polymerization II. A two-stage process for styrene polymerization," *Chemical Engineering Science*, vol. 35, no. 11, pp. 2325–2335, 1980.

[23] S.-A. Chen and K.-Y. Hsu, "Minimum end time policies for batchwise radical chain polymerization IV: Consideration of chain transfer effects in isothermal operation with one-charge of initiator," *Chemical Engineering Science*, vol. 39, no. 1, pp. 177–179, 1984.

[24] I. M. Thomas and C. Kiparissides, "Computation of the near-optimal temperature and initiator policies for a batch polymerization reactor," *The Canadian Journal of Chemical Engineering*, vol. 62, no. 2, pp. 284–291, 1984.

[25] G. E. Eliçabe and G. R. Meira, "Estimation and control in polymerization reactors. A review," *Polymer Engineering & Science*, vol. 28, no. 3, pp. 121–135, 1988.

[26] M. Embiruçu, E. L. Lima, and J. C. Pinto, "A survey of advanced control of polymerization reactors," *Polymer Engineering & Science*, vol. 36, no. 4, pp. 433–447, 1996.

[27] J. P. Congalidis and J. R. Richards, "Process control of polymerization reactors: An industrial perspective," *Polymer Reaction Engineering*, vol. 6, no. 2, pp. 71–111, 1998.

[28] M. Ohshima and M. Tanigaki, "Quality control of polymer production processes," *Journal of Process Control*, vol. 10, no. 2-3, pp. 135–148, 2000.

[29] K. J. Kim and K. Y. Choi, "On-line estimation and control of a continuous stirred tank polymerization reactor," *Journal of Process Control*, vol. 1, no. 2, pp. 96–110, 1991.

[30] J. Dimitratos, C. Georgakis, M. S. El-Aasser, and A. Klein, "Dynamic modeling and state estimation for an emulsion copolymerization reactor," *Computers & Chemical Engineering*, vol. 13, no. 1-2, pp. 21–33, 1989.

[31] M. F. Ellis, T. W. Taylor, and K. F. Jensen, "On-line molecular weight distribution estimation and control in batch polymerization," *AIChE Journal*, vol. 40, no. 3, pp. 445–462, 1994.

[32] D. J. Kozub and J. F. MacGregor, "State estimation for semi-batch polymerization reactors," *Chemical Engineering Science*, vol. 47, no. 5, pp. 1047–1062, 1992.

[33] V. Liotta, C. Georgakis, and M. S. El-Aasser, "Real-time estimation and control of particle size in semi-batch emulsion polymerization," in *Proceedings of the American Control Conference*, pp. 1172–1176, IEEE, 1997.

[34] R. K. Mutha, W. R. Cluett, and A. Penlidis, "On-line nonlinear model-based estimation and control of a polymer reactor," *AIChE Journal*, vol. 43, no. 11, pp. 3042–3058, 1997.

[35] T. J. Crowley and K. Y. Choi, "Experimental studies on optimal molecular weight distribution control in a batch-free radical polymerization process," *Chemical Engineering Science*, vol. 53, no. 15, pp. 2769–2790, 1998.

[36] D. K. Adebekun and F. J. Schork, "Continuous solution polymerization reactor control. 2. Estimation and nonlinear reference control during methyl methacrylate polymerization," *Industrial & Engineering Chemistry Research*, vol. 28, no. 12, pp. 1846–1861, 1989.

[37] C. Scali, M. Morretta, and D. Semino, "Control of the quality of polymer products in continuous reactors: comparison of performance of state estimators with and without updating of parameters," *Journal of Process Control*, vol. 7, no. 5, pp. 357–369, 1997.

[38] C. Gentric, F. Pla, M. A. Latifi, and J. P. Corriou, "Optimization and non-linear control of a batch emulsion polymerization reactor," *Chemical Engineering Journal*, vol. 75, no. 1, pp. 31–46, 1999.

[39] M.-J. Park, S.-M. Hur, and H.-K. Rhee, "Online estimation and control of polymer quality in a copolymerization reactor," *AIChE Journal*, vol. 48, no. 5, pp. 1013–1021, 2002.

[40] J. M. R. Fontoura, A. F. Santos, F. M. Silva, M. K. Lenzi, E. L. Lima, and J. C. Pinto, "Monitoring and control of styrene solution polymerization using NIR spectroscopy," *Journal of Applied Polymer Science*, vol. 90, no. 5, pp. 1273–1289, 2003.

[41] R. Li, A. B. Corripio, M. A. Henson, and M. J. Kurtz, "On-line state and parameter estimation of EPDM polymerization reactors using a hierarchical extended Kalman filter," *Journal of Process Control*, vol. 14, no. 8, pp. 837–852, 2004.

[42] E. L. Haseltine and J. B. Rawlings, "Critical evaluation of extended Kalman filtering and moving-horizon estimation," *Industrial & Engineering Chemistry Research*, vol. 44, no. 8, pp. 2451–2460, 2005.

[43] D. Dochain and A. Pauss, "On-line estimation of microbial specific growth-rates: An illustrative case study," *The Canadian Journal of Chemical Engineering*, vol. 66, no. 4, pp. 626–631, 1988.

[44] S. Valluri and M. Soroush, "Nonlinear state estimation in the presence of multiple steady states," *Industrial & Engineering Chemistry Research*, vol. 35, no. 8, pp. 2645–2659, 1996.

[45] M. Vicente, S. BenAmor, L. M. Gugliotta, J. R. Leiza, and J. M. Asua, "Control of molecular weight distribution in emulsion polymerization using on-line reaction calorimetry," *Industrial & Engineering Chemistry Research*, vol. 40, no. 1, pp. 218–227, 2001.

[46] N. Sheibat-Othman, D. Peycelon, S. Othman, J.-M. Suau, and G. Févotte, "Nonlinear observers for parameter estimation in a solution polymerization process using infrared spectroscopy," *Chemical Engineering Journal*, vol. 140, no. 1-3, pp. 529–538, 2008.

[47] D. Edouard, N. Sheibat-Othman, and H. Hammouri, "Observer design for particle size distribution in emulsion polymerization," *AIChE Journal*, vol. 51, no. 12, pp. 3167–3185, 2005.

[48] C.-M. Astorga, N. Sheibat-Othman, S. Othman, H. Hammouri, and T.-F. McKenna, "Nonlinear continuous-discrete observers: application to emulsion polymerization reactors," *Control Engineering Practice*, vol. 10, no. 1, pp. 3–13, 2002.

[49] S. Tatiraju and M. Soroush, "Nonlinear state estimation in a polymerization reactor," *Industrial & Engineering Chemistry Research*, vol. 36, no. 7, pp. 2679–2690, 1997.

[50] M. Van Dootingh, F. Viel, D. Rakotopara, J.-P. Gauthier, and P. Hobbes, "Nonlinear deterministic observer for state estimation: Application to a continuous free radical polymerization reactor," *Computers & Chemical Engineering*, vol. 16, no. 8, pp. 777–791, 1992.

[51] F. Viel, E. Busvelle, and J.-P. Gauthier, "Stability of polymerization reactors using I/O linearization and a high-gain observer," *Automatica*, vol. 31, no. 7, pp. 971–984, 1995.

[52] C. Ling and C. Kravaris, "Multi-rate observer design for process monitoring using asynchronous inter-sample output predictions," *AIChE Journal*, vol. 63, no. 8, pp. 3384–3394, 2017.

[53] R. E. Kalman, "A new approach to linear filtering and prediction problems," *Journal of Basic Engineering*, vol. 82, no. 1, pp. 35–45, 1960.

[54] R. E. Kalman and R. S. Bucy, "New results in linear filtering and prediction theory," *Journal of Basic Engineering*, vol. 83, no. 1, pp. 95–108, 1961.

[55] D. G. Luenberger, "Observing the state of a linear system," *IEEE Transactions on Military Electronics*, vol. 8, no. 2, pp. 74–80, 1964.

[56] D. G. Luenberger, "Observers for multivariable systems," *IEEE Transactions on Automatic Control*, vol. 11, no. 2, pp. 190–197, 1966.

[57] D. G. Luenberger, "An introduction to observers," *IEEE Transactions on Automatic Control*, vol. 16, no. 6, pp. 596–602, 1971.

[58] C.-T. Chen, *Linear System Theory and Design*. New York, NY, USA: Oxford University Press, Inc., 1998.

[59] M. S. Arulampalam, S. Maskell, N. Gordon, and T. Clapp, "A tutorial on particle filters for online nonlinear/non-gaussian Bayesian tracking," *IEEE Transactions on Signal Processing*, vol. 50, no. 2, pp. 174–188, 2002.

[60] J. D. Schutter, J. D. Geeter, T. Lefebvre, and H. Bruyninckx, "Kalman filters: A tutorial," 10 1999.

[61] G. Welch and G. Bishop, "An introduction to the Kalman filter," tech. rep., University of North Carolina at Chapel Hill, Chapel Hill, NC, USA, 1995.

[62] S. F. Schmidt, "The Kalman filter: Its recognition and development for aerospace applications," *Journal of Guidance, Control, and Dynamics*, vol. 4, no. 1, pp. 4–7, 1981.

[63] G. Bastin and D. Dochain, *On-line Estimation and Adaptive Control of Bioreactors*. New York, NY, USA: Elsevier, 1990.

[64] J. C. Kantor, "A finite dimensional nonlinear observer for an exothermic stirred-tank reactor," *Chemical Engineering Science*, vol. 44, no. 7, pp. 1503–1510, 1989.

[65] D. Dochain, "State and parameter estimation in chemical and biochemical processes: a tutorial," *Journal of Process Control*, vol. 13, no. 8, pp. 801–818, 2003.

[66] M. J. Kurtz and M. A. Henson, "State and disturbance estimation for nonlinear systems affine in the unmeasured variables," *Computers & Chemical Engineering*, vol. 22, no. 10, pp. 1441–1459, 1998.

[67] S. Rajaraman, J. Hahn, and M. S. Mannan, "A methodology for fault detection, isolation, and identification for nonlinear processes with parametric uncertainties," *Industrial & Engineering Chemistry Research*, vol. 43, no. 21, pp. 6774–6786, 2004.

[68] S. Rajaraman, J. Hahn, and M. S. Mannan, "Sensor fault diagnosis for nonlinear processes with parametric uncertainties," *Journal of Hazardous Materials*, vol. 130, no. 1-2, pp. 1–8, 2006.

[69] A. K. Singh and J. Hahn, "State estimation for high-dimensional chemical processes," *Computers & Chemical Engineering*, vol. 29, no. 11-12, pp. 2326–2334, 2005.

[70] M. Soroush, "Nonlinear state-observer design with application to reactors," *Chemical Engineering Science*, vol. 52, no. 3, pp. 387–404, 1997.

[71] A. Gelb, *Applied Optimal Estimation*. Cambridge, MA, USA: MIT press, 1974.

[72] A. H. Jazwinski, *Stochastic Processes and Filtering Theory*. Mineola, NY, USA: Dover Publications, Inc., 2007.

[73] J. Albiol, J. Robusté, C. Casas, and M. Poch, "Biomass estimation in plant cell cultures using an extended Kalman filter," *Biotechnology Progress*, vol. 9, no. 2, pp. 174–178, 1993.

[74] J. H. Lee and N. L. Ricker, "Extended Kalman filter based nonlinear model predictive control," *Industrial & Engineering Chemistry Research*, vol. 33, no. 6, pp. 1530–1541, 1994.

[75] N. L. Ricker and J. H. Lee, "Nonlinear modeling and state estimation for the Tennessee Eastman challenge process," *Computers & Chemical Engineering*, vol. 19, no. 9, pp. 983–1005, 1995.

[76] L. F. M. Zorzetto and J. A. Wilson, "Monitoring bioprocesses using hybrid models and an extended Kalman filter," *Computers & Chemical Engineering*, vol. 20, pp. S689–S694, 1996.

[77] D. I. Wilson, M. Agarwal, and D. W. T. Rippin, "Experiences implementing the extended Kalman filter on an industrial batch reactor," *Computers & Chemical Engineering*, vol. 22, no. 11, pp. 1653–1672, 1998.

[78] S.-M. Ahn, M.-J. Park, and H.-K. Rhee, "Extended Kalman filter-based nonlinear model predictive control for a continuous MMA polymerization reactor," *Industrial & Engineering Chemistry Research*, vol. 38, no. 10, pp. 3942–3949, 1999.

[79] R. M. Oisiovici and S. L. Cruz, "State estimation of batch distillation columns using an extended Kalman filter," *Chemical Engineering Science*, vol. 55, no. 20, pp. 4667–4680, 2000.

[80] V. Prasad, M. Schley, L. P. Russo, and B. W. Bequette, "Product property and production rate control of styrene polymerization," *Journal of Process Control*, vol. 12, no. 3, pp. 353–372, 2002.

[81] V. M. Becerra, P. D. Roberts, and G. W. Griffiths, "Applying the extended Kalman filter to systems described by nonlinear differential-algebraic equations," *Control Engineering Practice*, vol. 9, no. 3, pp. 267–281, 2001.

[82] H. Khodadadi and H. Jazayeri-Rad, "Applying a dual extended Kalman filter for the nonlinear state and parameter estimations of a continuous stirred tank reactor," *Computers & Chemical Engineering*, vol. 35, no. 11, pp. 2426–2436, 2011.

[83] G. Leu and R. Baratti, "An extended Kalman filtering approach with a criterion to set its tuning parameters; application to a catalytic reactor," *Computers & Chemical Engineering*, vol. 23, no. 11-12, pp. 1839–1849, 2000.

[84] M. J. Olanrewaju and M. A. Al-Arfaj, "Estimator-based control of reactive distillation system: Application of an extended Kalman filtering," *Chemical Engineering Science*, vol. 61, no. 10, pp. 3386–3399, 2006.

[85] R. Xiong, P. J. Wissmann, and M. A. Gallivan, "An extended Kalman filter for in situ sensing of yttria-stabilized zirconia in chemical vapor deposition," *Computers & Chemical Engineering*, vol. 30, no. 10-12, pp. 1657–1669, 2006.

[86] G. L. Plett, "Extended Kalman filtering for battery management systems of LiPB-based HEV battery packs: Part 3. State and parameter estimation," *Journal of Power Sources*, vol. 134, no. 2, pp. 277–292, 2004.

[87] A. Vasebi, M. Partovibakhsh, and S. M. T. Bathaee, "A novel combined battery model for state-of-charge estimation in lead-acid batteries based on extended Kalman filter for hybrid electric vehicle applications," *Journal of Power Sources*, vol. 174, no. 1, pp. 30–40, 2007.

[88] R. M. Oisiovici and S. L. Cruz, "Inferential control of high-purity multicomponent batch distillation columns using an extended Kalman filter," *Industrial & Engineering Chemistry Research*, vol. 40, no. 12, pp. 2628–2639, 2001.

[89] E. A. Wan and R. van der Merwe, "The unscented Kalman filter for nonlinear estimation," in *Proceedings of the IEEE 2000 Adaptive Systems for Signal Processing, Communications, and Control Symposium.*, pp. 153–158, IEEE, 2000.

[90] S. J. Julier and J. K. Uhlmann, "New extension of the Kalman filter to nonlinear systems," in *Proceedings of SPIE 3068, Signal Processing, Sensor Fusion, and Target Recognition VI*, vol. 3068, pp. 182–194, International Society for Optics and Photonics, 1997.

[91] S. J. Julier, J. K. Uhlmann, and H. F. Durrant-Whyte, "A new method for the nonlinear transformation of means and covariances in filters and estimators," *IEEE Transactions on Automatic Control*, vol. 45, no. 3, pp. 477–482, 2000.

[92] S. J. Julier and J. K. Uhlmann, "Unscented filtering and nonlinear estimation," *Proceedings of the IEEE*, vol. 92, no. 3, pp. 401–422, 2004.

[93] A. Romanenko and J. A. A. M. Castro, "The unscented filter as an alternative to the EKF for nonlinear state estimation: a simulation case study," *Computers & Chemical Engineering*, vol. 28, no. 3, pp. 347–355, 2004.

[94] R. Kandepu, B. Foss, and L. Imsland, "Applying the unscented Kalman filter for nonlinear state estimation," *Journal of Process Control*, vol. 18, no. 7-8, pp. 753–768, 2008.

[95] S. Kolås, B. A. Foss, and T. S. Schei, "Constrained nonlinear state estimation based on the UKF approach," *Computers & Chemical Engineering*, vol. 33, no. 8, pp. 1386–1401, 2009.

[96] C. C. Qu and J. Hahn, "Process monitoring and parameter estimation via unscented Kalman filtering," *Journal of Loss Prevention in the Process Industries*, vol. 22, no. 6, pp. 703–709, 2009.

[97] A. Romanenko, L. O. Santos, and P. A. F. N. A. Afonso, "Unscented Kalman filtering of a simulated pH system," *Industrial & Engineering Chemistry Research*, vol. 43, no. 23, pp. 7531–7538, 2004.

[98] N. C. Jacob and R. Dhib, "Unscented Kalman filter based nonlinear model predictive control of a LDPE autoclave reactor," *Journal of Process Control*, vol. 21, no. 9, pp. 1332–1344, 2011.

[99] W. Zhang, W. Shi, and Z. Ma, "Adaptive unscented Kalman filter based state of energy and power capability estimation approach for lithium-ion battery," *Journal of Power Sources*, vol. 289, pp. 50–62, 2015.

[100] J. Wang, L. Zhao, and T. Yu, "On-line estimation in fed-batch fermentation process using state space model and unscented Kalman filter," *Chinese Journal of Chemical Engineering*, vol. 18, no. 2, pp. 258–264, 2010.

[101] J. H. Kotecha and P. M. Djurić, "Gaussian particle filtering," *IEEE Transactions on Signal Processing*, vol. 51, no. 10, pp. 2592–2601, 2003.

[102] N. J. Gordon, D. J. Salmond, and A. F. M. Smith, "Novel approach to nonlinear/non-Gaussian Bayesian state estimation," *IEE Proceedings F - Radar and Signal Processing*, vol. 140, no. 2, pp. 107–113, 1993.

[103] A. Doucet, S. Godsill, and C. Andrieu, "On sequential Monte Carlo sampling methods for Bayesian filtering," *Statistics and Computing*, vol. 10, no. 3, pp. 197–208, 2000.

[104] A. Doucet, N. de Freitas, and N. Gordon, "An introduction to sequential Monte Carlo methods," in *Sequential Monte Carlo Methods in Practice*, pp. 3–14, Springer, 2001.

[105] A. Doucet and A. M. Johansen, "A tutorial on particle filtering and smoothing: Fifteen years later," in *The Oxford Handbook of Nonlinear Filtering*, pp. 656–704, Oxford University Press, 2009.

[106] S. Gillijns, O. Barrero Mendoza, J. Chandrasekar, B. L. R. De Moor, D. S. Bernstein, and A. Ridley, "What is the ensemble Kalman filter and how well does it work," in *Proceedings of the American Control Conference*, IEEE, 2006.

[107] G. Evensen, "The ensemble Kalman filter for combined state and parameter estimation," *IEEE Control Systems*, vol. 29, no. 3, pp. 83–104, 2009.

[108] G. Evensen, "Advanced data assimilation for strongly nonlinear dynamics," *Monthly Weather Review*, vol. 125, no. 6, pp. 1342–1354, 1997.

[109] S. I. Aanonsen, G. Nævdal, D. S. Oliver, A. C. Reynolds, and B. Vallès, "The ensemble Kalman filter in reservoir engineering–a review," *SPE Journal*, vol. 14, no. 03, pp. 393–412, 2009.

[110] K. Ito, "Gaussian filter for nonlinear filtering problems," in *Proceedings of the 39th IEEE Conference on Decision and Control*, vol. 2, pp. 1218–1223, IEEE, 2000.

[111] I. Arasaratnam and S. Haykin, "Cubature Kalman filters," *IEEE Transactions on Automatic Control*, vol. 54, no. 6, pp. 1254–1269, 2009.

[112] H. Fang, N. Tian, Y. Wang, M. C. Zhou, and M. A. Haile, "Nonlinear Bayesian estimation: from Kalman filtering to a broader horizon," *IEEE/CAA Journal of Automatica Sinica*, vol. 5, no. 2, pp. 401–417, 2018.

[113] T. Lefebvre, H. Bruyninckx, and J. De Schutter, "Kalman filters for non-linear systems: a comparison of performance," *International Journal of Control*, vol. 77, no. 7, pp. 639–653, 2004.

[114] D. G. Robertson, J. H. Lee, and J. B. Rawlings, "A moving horizon-based approach for least-squares estimation," *AIChE Journal*, vol. 42, no. 8, pp. 2209–2224, 1996.

[115] V. M. Zavala, C. D. Laird, and L. T. Biegler, "A fast moving horizon estimation algorithm based on nonlinear programming sensitivity," *Journal of Process Control*, vol. 18, no. 9, pp. 876–884, 2008.

[116] V. M. Zavala and L. T. Biegler, "Optimization-based strategies for the operation of low-density polyethylene tubular reactors: Moving horizon estimation," *Computers & Chemical Engineering*, vol. 33, no. 1, pp. 379–390, 2009.

[117] P. Kühl, M. Diehl, T. Kraus, J. P. Schlöder, and H. G. Bock, "A real-time algorithm for moving horizon state and parameter estimation," *Computers & Chemical Engineering*, vol. 35, no. 1, pp. 71–83, 2011.

[118] F. V. Lima and J. B. Rawlings, "Nonlinear stochastic modeling to improve state estimation in process monitoring and control," *AIChE Journal*, vol. 57, no. 4, pp. 996–1007, 2011.

[119] A. Küpper, L. Wirsching, M. Diehl, J. P. Schlöder, H. G. Bock, and S. Engell, "Online identification of adsorption isotherms in SMB processes via efficient moving horizon state and parameter estimation," *Computers & Chemical Engineering*, vol. 34, no. 12, pp. 1969–1983, 2010.

[120] L. Ji and J. B. Rawlings, "Application of MHE to large-scale nonlinear processes with delayed lab measurements," *Computers & Chemical Engineering*, vol. 80, pp. 63–72, 2015.

[121] K. R. Muske, J. B. Rawlings, and J. H. Lee, "Receding horizon recursive state estimation," in *Proceedings of American Control Conference*, pp. 900–904, IEEE, 1993.

[122] K. R. Muske and J. B. Rawlings, "Nonlinear moving horizon state estimation," in *Methods of Model Based Process Control*, pp. 349–365, Springer, 1995.

[123] F. Allgöwer, T. A. Badgwell, J. S. Qin, J. B. Rawlings, and S. J. Wright, "Nonlinear predictive control and moving horizon estimation–an introductory overview," in *Advances in Control*, pp. 391–449, Springer, 1999.

[124] C. V. Rao and J. B. Rawlings, "Constrained process monitoring: Moving-horizon approach," *AIChE Journal*, vol. 48, no. 1, pp. 97–109, 2002.

[125] C. V. Rao, J. B. Rawlings, and J. H. Lee, "Constrained linear state estimation–a moving horizon approach," *Automatica*, vol. 37, no. 10, pp. 1619–1628, 2001.

[126] C. V. Rao, J. B. Rawlings, and D. Q. Mayne, "Constrained state estimation for nonlinear discrete-time systems: Stability and moving horizon approximations," *IEEE Transactions on Automatic Control*, vol. 48, no. 2, pp. 246–258, 2003.

[127] J. B. Rawlings and B. R. Bakshi, "Particle filtering and moving horizon estimation," *Computers & Chemical Engineering*, vol. 30, no. 10-12, pp. 1529–1541, 2006.

[128] X. Shao, B. Huang, and J. M. Lee, "Constrained Bayesian state estimation–A comparative study and a new particle filter based approach," *Journal of Process Control*, vol. 20, no. 2, pp. 143–157, 2010.

[129] A. Mesbah, A. E. M. Huesman, H. J. M. Kramer, and P. M. J. Van den Hof, "A comparison of nonlinear observers for output feedback model-based control of seeded batch crystallization processes," *Journal of Process Control*, vol. 21, no. 4, pp. 652–666, 2011.

[130] M. Zeitz, "The extended Luenberger observer for nonlinear systems," *Systems & Control Letters*, vol. 9, no. 2, pp. 149–156, 1987.

[131] F. Deza, E. Busvelle, J. P. Gauthier, and D. Rakotopara, "High gain estimation for nonlinear systems," *Systems & Control Letters*, vol. 18, no. 4, pp. 295–299, 1992.

[132] J. P. Gauthier, H. Hammouri, and S. Othman, "A simple observer for nonlinear systems applications to bioreactors," *IEEE Transactions on Automatic Control*, vol. 37, no. 6, pp. 875–880, 1992.

[133] J. P. Gauthier and I. A. K. Kupka, "Observability and observers for nonlinear systems," *SIAM Journal on Control and Optimization*, vol. 32, no. 4, pp. 975–994, 1994.

[134] K. Busawon, M. Farza, and H. Hammouri, "Observer design for a special class of nonlinear systems," *International Journal of Control*, vol. 71, no. 3, pp. 405–418, 1998.

[135] H. Hammouri, B. Targui, and F. Armanet, "High gain observer based on a triangular structure," *International Journal of Robust and Nonlinear Control*, vol. 12, no. 6, pp. 497–518, 2002.

[136] G. Besançon, "High-gain observation with disturbance attenuation and application to robust fault detection," *Automatica*, vol. 39, no. 6, pp. 1095–1102, 2003.

[137] H. K. Khalil and L. Praly, "High-gain observers in nonlinear feedback control," *International Journal of Robust and Nonlinear Control*, vol. 24, no. 6, pp. 993–1015, 2014.

[138] A. N. Atassi and H. K. Khalil, "A separation principle for the stabilization of a class of nonlinear systems," *IEEE Transactions on Automatic Control*, vol. 44, no. 9, pp. 1672–1687, 1999.

[139] A. N. Atassi and H. K. Khalil, "Separation results for the stabilization of nonlinear systems using different high-gain observer designs," *Systems & Control Letters*, vol. 39, no. 3, pp. 183–191, 2000.

[140] L. Praly, "Asymptotic stabilization via output feedback for lower triangular systems with output dependent incremental rate," *IEEE Transactions on Automatic Control*, vol. 48, no. 6, pp. 1103–1108, 2003.

[141] V. Andrieu, L. Praly, and A. Astolfi, "High gain observers with updated gain and homogeneous correction terms," *Automatica*, vol. 45, no. 2, pp. 422–428, 2009.

[142] L. Praly and Z.-P. Jiang, "Linear output feedback with dynamic high gain for nonlinear systems," *Systems & Control Letters*, vol. 53, no. 2, pp. 107–116, 2004.

[143] A. A. Prasov and H. K. Khalil, "A nonlinear high-gain observer for systems with measurement noise in a feedback control framework," *IEEE Transactions on Automatic Control*, vol. 58, no. 3, pp. 569–580, 2013.

[144] D. Astolfi, L. Marconi, L. Praly, and A. Teel, "Sensitivity to high-frequency measurement noise of nonlinear high-gain observers," in *Proceedings of 10th IFAC Symposium on Nonlinear Control Systems*, pp. 276–278, IFAC, 2016.

[145] L. K. Vasiljevic and H. K. Khalil, "Error bounds in differentiation of noisy signals by high-gain observers," *Systems & Control Letters*, vol. 57, no. 10, pp. 856–862, 2008.

[146] J. Tsinias, "Observer design for nonlinear systems," *Systems & Control Letters*, vol. 13, no. 2, pp. 135–142, 1989.

[147] J. Tsinias, "Further results on the observer design problem," *Systems & Control Letters*, vol. 14, no. 5, pp. 411–418, 1990.

[148] N. Kazantzis and C. Kravaris, "Nonlinear observer design using Lyapunov's auxiliary theorem," *Systems & Control Letters*, vol. 34, no. 5, pp. 241–247, 1998.

[149] C. Kravaris, V. Sotiropoulos, C. Georgiou, N. Kazantzis, M. Xiao, and A. J. Krener, "Nonlinear observer design for state and disturbance estimation," *Systems & Control Letters*, vol. 11, no. 56, pp. 730–735, 2007.

[150] C. Kravaris and G. Savoglidis, "Modular design of nonlinear observers for state and disturbance estimation," *Systems & Control Letters*, vol. 57, no. 11, pp. 946–957, 2008.

[151] V. Andrieu and L. Praly, "On the existence of a Kazantzis–Kravaris/Luenberger observer," *SIAM Journal on Control and Optimization*, vol. 45, no. 2, pp. 432–456, 2006.

[152] A. Astolfi and L. Praly, "Global complete observability and output-to-state stability imply the existence of a globally convergent observer," *Mathematics of Control, Signals and Systems*, vol. 18, no. 1, pp. 32–65, 2006.

[153] M. Guay, "Observer linearization by output-dependent time-scale transformations," *IEEE Transactions on Automatic Control*, vol. 47, no. 10, pp. 1730–1735, 2002.

[154] G. Kreisselmeier and R. Engel, "Nonlinear observers for autonomous Lipschitz continuous systems," *IEEE Transactions on Automatic Control*, vol. 48, no. 3, pp. 451–464, 2003.

[155] A. J. Krener and A. Isidori, "Linearization by output injection and nonlinear observers," *Systems & Control Letters*, vol. 3, no. 1, pp. 47–52, 1983.

[156] A. J. Krener and W. Respondek, "Nonlinear observers with linearizable error dynamics," *SIAM Journal on Control and Optimization*, vol. 23, no. 2, pp. 197–216, 1985.

[157] A. J. Krener and M. Xiao, "Nonlinear observer design in the Siegel domain," *SIAM Journal on Control and Optimization*, vol. 41, no. 3, pp. 932–953, 2002.

[158] X.-H. Xia and W.-B. Gao, "Nonlinear observer design by observer error linearization," *SIAM Journal on Control and Optimization*, vol. 27, no. 1, pp. 199–216, 1989.

[159] M. Xiao, "A direct method for the construction of nonlinear discrete-time observer with linearizable error dynamics," *IEEE Transactions on Automatic Control*, vol. 51, no. 1, pp. 128–135, 2006.

[160] W. Chen and M. Saif, "Unknown input observer design for a class of nonlinear systems: an LMI approach," in *Proceedings of American Control Conference*, pp. 834–838, IEEE, 2006.

[161] X. Pan and M. N. Karim, "Modelling and monitoring of natural gas pipelines: New method for leak detection and localization estimation," in *Computer Aided Chemical Engineering*, vol. 37, pp. 1787–1792, Elsevier, 2015.

[162] X. Pan, W. Tang, J. P. Raftery, and M. N. Karim, "Design of an unknown input observer for leak detection under process disturbances," *Industrial & Engineering Chemistry Research*, vol. 56, no. 4, pp. 989–998, 2017.

[163] X. Pan, W. Tang, and M. N. Karim, "Detection of multiple leaks in a natural gas pipeline using observer and mixed-integer partial differential equation-constrained optimization," *Industrial & Engineering Chemistry Research*, vol. 56, no. 41, pp. 11839–11846, 2017.

[164] X. Pan, J. P. Raftery, C. Botre, M. R. DeSessa, T. Jaladi, and M. N. Karim, "Estimation of unmeasured states in a bioreactor under unknown disturbances," *Industrial & Engineering Chemistry Research*, vol. 58, no. 6, pp. 2235–2245, 2019.

[165] Y. Xiong and M. Saif, "Sliding mode observer for nonlinear uncertain systems," *IEEE Transactions on Automatic Control*, vol. 46, no. 12, pp. 2012–2017, 2001.

[166] S. Yin, S. X. Ding, X. Xie, and H. Luo, "A review on basic data-driven approaches for industrial process monitoring," *IEEE Transactions on Industrial Electronics*, vol. 61, no. 11, pp. 6418–6428, 2014.

[167] P. Kadlec, B. Gabrys, and S. Strandt, "Data-driven soft sensors in the process industry," *Computers & Chemical Engineering*, vol. 33, no. 4, pp. 795–814, 2009.

[168] P. Kadlec, R. Grbić, and B. Gabrys, "Review of adaptation mechanisms for data-driven soft sensors," *Computers & Chemical Engineering*, vol. 35, no. 1, pp. 1–24, 2011.

[169] Z. Ge, Z. Song, and F. Gao, "Review of recent research on data-based process monitoring," *Industrial & Engineering Chemistry Research*, vol. 52, no. 10, pp. 3543–3562, 2013.

[170] S. Yin, S. X. Ding, A. Haghani, H. Hao, and P. Zhang, "A comparison study of basic data-driven fault diagnosis and process monitoring methods on the benchmark Tennessee Eastman process," *Journal of Process Control*, vol. 22, no. 9, pp. 1567–1581, 2012.

[171] S. Park and C. Han, "A nonlinear soft sensor based on multivariate smoothing procedure for quality estimation in distillation columns," *Computers & Chemical Engineering*, vol. 24, no. 2-7, pp. 871–877, 2000.

[172] S. J. Qin, "Recursive PLS algorithms for adaptive data modeling," *Computers & Chemical Engineering*, vol. 22, no. 4-5, pp. 503–514, 1998.

[173] L. Chen, O. Bernard, G. Bastin, and P. Angelov, "Hybrid modelling of biotechnological processes using neural networks," *Control Engineering Practice*, vol. 8, no. 7, pp. 821–827, 2000.

[174] S. James, R. Legge, and H. Budman, "Comparative study of black-box and hybrid estimation methods in fed-batch fermentation," *Journal of Process Control*, vol. 12, no. 1, pp. 113–121, 2002.

[175] H. Hotelling, "The generalization of student's ratio," *The Annals of Mathematical Statistics*, vol. 2, no. 3, pp. 360–378, 1931.

[176] J. E. Jackson and G. S. Mudholkar, "Control procedures for residuals associated with principal component analysis," *Technometrics*, vol. 21, no. 3, pp. 341–349, 1979.

[177] J. V. Kresta, J. F. MacGregor, and T. E. Marlin, "Multivariate statistical monitoring of process operating performance," *The Canadian Journal of Chemical Engineering*, vol. 69, no. 1, pp. 35–47, 1991.

[178] J. F. MacGregor, C. Jaeckle, C. Kiparissides, and M. Koutoudi, "Process monitoring and diagnosis by multiblock PLS methods," *AIChE Journal*, vol. 40, no. 5, pp. 826–838, 1994.

[179] J. F. MacGregor and T. Kourti, "Statistical process control of multivariate processes," *Control Engineering Practice*, vol. 3, no. 3, pp. 403–414, 1995.

[180] J. Chen and K.-C. Liu, "On-line batch process monitoring using dynamic PCA and dynamic PLS models," *Chemical Engineering Science*, vol. 57, no. 1, pp. 63–75, 2002.

[181] W. Li, H. H. Yue, S. Valle-Cervantes, and S. J. Qin, "Recursive PCA for adaptive process monitoring," *Journal of Process Control*, vol. 10, no. 5, pp. 471–486, 2000.

[182] B. Schölkopf, A. Smola, and K.-R. Müller, "Nonlinear component analysis as a kernel eigenvalue problem," *Neural Computation*, vol. 10, no. 5, pp. 1299–1319, 1998.

[183] J.-M. Lee, C. Yoo, S. W. Choi, P. A. Vanrolleghem, and I.-B. Lee, "Nonlinear process monitoring using kernel principal component analysis," *Chemical Engineering Science*, vol. 59, no. 1, pp. 223–234, 2004.

[184] S. W. Choi and I.-B. Lee, "Nonlinear dynamic process monitoring based on dynamic kernel PCA," *Chemical Engineering Science*, vol. 59, no. 24, pp. 5897–5908, 2004.

[185] S. W. Choi, C. Lee, J.-M. Lee, J. H. Park, and I.-B. Lee, "Fault detection and identification of nonlinear processes based on kernel PCA," *Chemometrics and Intelligent Laboratory Systems*, vol. 75, no. 1, pp. 55–67, 2005.

[186] Y. Zhang, H. Zhou, S. J. Qin, and T. Chai, "Decentralized fault diagnosis of large-scale processes using multiblock kernel partial least squares," *IEEE Transactions on Industrial Informatics*, vol. 6, no. 1, pp. 3–10, 2010.

[187] C. Botre, M. Mansouri, M. Nounou, H. Nounou, and M. N. Karim, "Kernel PLS-based GLRT method for fault detection of chemical processes," *Journal of Loss Prevention in the Process Industries*, vol. 43, pp. 212–224, 2016.

[188] S. J. Qin, "Survey on data-driven industrial process monitoring and diagnosis," *Annual Reviews in Control*, vol. 36, no. 2, pp. 220–234, 2012.

[189] R. Dunia, S. J. Qin, T. F. Edgar, and T. J. McAvoy, "Identification of faulty sensors using principal component analysis," *AIChE Journal*, vol. 42, no. 10, pp. 2797–2812, 1996.

[190] R. Dunia and S. J. Qin, "Subspace approach to multidimensional fault identification and reconstruction," *AIChE Journal*, vol. 44, no. 8, pp. 1813–1831, 1998.

[191] H. H. Yue and S. J. Qin, "Reconstruction-based fault identification using a combined index," *Industrial & Engineering Chemistry Research*, vol. 40, no. 20, pp. 4403–4414, 2001.

[192] B. Lin, B. Recke, J. K. Knudsen, and S. B. Jørgensen, "A systematic approach for soft sensor development," *Computers & Chemical Engineering*, vol. 31, no. 5-6, pp. 419–425, 2007.

[193] H. Zhang and B. Lennox, "Integrated condition monitoring and control of fed-batch fermentation processes," *Journal of Process Control*, vol. 14, no. 1, pp. 41–50, 2004.

[194] O. Marjanovic, B. Lennox, D. Sandoz, K. Smith, and M. Crofts, "Real-time monitoring of an industrial batch process," *Computers & Chemical Engineering*, vol. 30, no. 10-12, pp. 1476–1481, 2006.

[195] N. Sheibat-Othman, N. Laouti, J.-P. Valour, and S. Othman, "Support vector machines combined to observers for fault diagnosis in chemical reactors," *The Canadian Journal of Chemical Engineering*, vol. 92, no. 4, pp. 685–695, 2014.

[196] K. Ravindranath and R. A. Mashelkar, "Modeling of poly(ethylene terephthalate) reactors. I. A semibatch ester interchange reactor," *Journal of Applied Polymer Science*, vol. 26, no. 10, pp. 3179–3204, 1981.

[197] K. Ravindranath and R. A. Mashelkar, "Modeling of poly(ethylene terephthalate) reactors. II. A continuous transesterification process," *Journal of Applied Polymer Science*, vol. 27, no. 2, pp. 471–487, 1982.

[198] J. Shin, Y. Lee, and S. Park, "Optimization of the pre-polymerization step of polyethylene terephthalate (PET) production in a semi-batch reactor," *Chemical Engineering Journal*, vol. 75, no. 1, pp. 47–55, 1999.

[199] K. Ravindranath and R. A. Mashelkar, "Modelling of poly(ethylene terephthalate) reactors. III. A semibatch prepolymerization process," *Journal of Applied Polymer Science*, vol. 27, no. 7, pp. 2625–2652, 1982.

[200] K. Ravindranath and R. A. Mashelkar, "Modeling of poly(ethylene terephthalate) reactors: 5. A continuous prepolymerization process," *Polymer Engineering & Science*, vol. 22, no. 10, pp. 619–627, 1982.

[201] K. Ravindranath and R. A. Mashelkar, "Modeling of poly(ethylene terephthalate) reactors: 6. A continuous process for final stages of polycondensation," *Polymer Engineering & Science*, vol. 22, no. 10, pp. 628–636, 1982.

[202] C. Laubriet, B. LeCorre, and K. Y. Choi, "Two-phase model for continuous final stage melt polycondensation of poly(ethylene terephthalate). 1. Steady-state analysis," *Industrial & Engineering Chemistry Research*, vol. 30, no. 1, pp. 2–12, 1991.

[203] I. Devotta and R. A. Mashelkar, "Modelling of polyethylene terephthalate reactors–X. A comprehensive model for solid-state polycondensation process," *Chemical Engineering Science*, vol. 48, no. 10, pp. 1859–1867, 1993.

[204] K. Tomita, "Studies on the formation of poly(ethylene terephthalate): 1. Propagation and degradation reactions in the polycondensation of bis(2-hydroxyethyl) terephthalate," *Polymer*, vol. 14, no. 2, pp. 50–54, 1973.

[205] W. Zhong, W. Wang, Z. Shao, Y. Zhang, and J. Qian, "Optimization of an industrial batch polycondensation reactor," in *Proceedings of the American Control Conference*, vol. 1, pp. 368–373, IEEE, 2001.

[206] G. Rafler, G. Reinisch, E. Bonatz, H. Versaumer, H. Gajewski, H.-D. Sparing, K. Stein, and C. Mühlhaus, "Kinetics of mass transfer in the melt polycondensation of poly(ethylene terephthalate)," *Journal of Macromolecular Science–Chemistry*, vol. 22, no. 10, pp. 1413–1427, 1985.

[207] T. E. Nowlin, *Business and Technology of the Global Polyethylene Industry*. Beverly, MA, USA: John Wiley & Sons, 2014.

[208] D. Yan, W.-J. Wang, and S. Zhu, "Effect of long chain branching on rheological properties of metallocene polyethylene," *Polymer*, vol. 40, no. 7, pp. 1737–1744, 1999.

[209] P. M. Wood-Adams, J. M. Dealy, A. W. deGroot, and O. D. Redwine, "Effect of molecular structure on the linear viscoelastic behavior of polyethylene," *Macromolecules*, vol. 33, no. 20, pp. 7489–7499, 2000.

[210] P. M. Wood-Adams and S. Costeux, "Thermorheological behavior of polyethylene: effects of microstructure and long chain branching," *Macromolecules*, vol. 34, no. 18, pp. 6281–6290, 2001.

[211] F. J. Stadler, J. Kaschta, and H. Münstedt, "Thermorheological behavior of various long-chain branched polyethylenes," *Macromolecules*, vol. 41, no. 4, pp. 1328–1333, 2008.

[212] H. A. Khonakdar, S. H. Jafari, U. Wagenknecht, and D. Jehnichen, "Effect of electron-irradiation on cross-link density and crystalline structure of low- and high-density polyethylene," *Radiation Physics and Chemistry*, vol. 75, no. 1, pp. 78–86, 2006.

[213] X. Zhang, S. Elkoun, A. Ajji, and M. A. Huneault, "Oriented structure and anisotropy properties of polymer blown films: HDPE, LLDPE and LDPE," *Polymer*, vol. 45, no. 1, pp. 217–229, 2004.

[214] T. Xie, K. B. McAuley, J. C. C. Hsu, and D. W. Bacon, "Gas phase ethylene polymerization: Production processes, polymer properties, and reactor modeling," *Industrial & Engineering Chemistry Research*, vol. 33, no. 3, pp. 449–479, 1994.

[215] K. B. McAuley, J. P. Talbot, and T. J. Harris, "A comparison of two-phase and well-mixed models for fluidized-bed polyethylene reactors," *Chemical Engineering Science*, vol. 49, no. 13, pp. 2035–2045, 1994.

[216] P. S. Chum and K. W. Swogger, "Olefin polymer technologies–History and recent progress at The Dow Chemical Company," *Progress in Polymer Science*, vol. 33, no. 8, pp. 797–819, 2008.

[217] K.-Y. Choi and W. H. Ray, "The dynamic behaviour of fluidized bed reactors for solid catalysed gas phase olefin polymerization," *Chemical Engineering Science*, vol. 40, no. 12, pp. 2261–2279, 1985.

[218] K. B. McAuley, J. F. MacGregor, and A. E. Hamielec, "A kinetic model for industrial gas-phase ethylene copolymerization," *AIChE Journal*, vol. 36, no. 6, pp. 837–850, 1990.

[219] K. B. McAuley, D. A. Macdonald, and P. J. McLellan, "Effects of operating conditions on stability of gas-phase polyethylene reactors," *AIChE Journal*, vol. 41, no. 4, pp. 868–879, 1995.

[220] F. A. N. Fernandes and L. M. F. Lona, "Heterogeneous modeling for fluidized-bed polymerization reactor," *Chemical Engineering Science*, vol. 56, no. 3, pp. 963–969, 2001.

[221] A. Kiashemshaki, N. Mostoufi, and R. Sotudeh-Gharebagh, "Two-phase modeling of a gas phase polyethylene fluidized bed reactor," *Chemical Engineering Science*, vol. 61, no. 12, pp. 3997–4006, 2006.

[222] K. B. McAuley and J. F. MacGregor, "On-line inference of polymer properties in an industrial polyethylene reactor," *AIChE Journal*, vol. 37, no. 6, pp. 825–835, 1991.

[223] K. B. McAuley and J. F. MacGregor, "Optimal grade transitions in a gas phase polyethylene reactor," *AIChE Journal*, vol. 38, no. 10, pp. 1564–1576, 1992.

[224] K. B. McAuley and J. F. MacGregor, "Nonlinear product property control in industrial gas-phase polyethylene reactors," *AIChE Journal*, vol. 39, no. 5, pp. 855–866, 1993.

[225] S. A. Dadebo, M. L. Bell, P. J. McLellan, and K. B. McAuley, "Temperature control of industrial gas phase polyethylene reactors," *Journal of Process Control*, vol. 7, no. 2, pp. 83–95, 1997.

[226] C. Sato, T. Ohtani, and H. Nishitani, "Modeling, simulation and nonlinear control of a gas-phase polymerization process," *Computers & Chemical Engineering*, vol. 24, no. 2-7, pp. 945–951, 2000.

[227] E. Ali, K. Al-Humaizi, and A. Ajbar, "Multivariable control of a simulated industrial gas-phase polyethylene reactor," *Industrial & Engineering Chemistry Research*, vol. 42, no. 11, pp. 2349–2364, 2003.

[228] A. Gani, P. Mhaskar, and P. D. Christofides, "Fault-tolerant control of a polyethylene reactor," *Journal of Process Control*, vol. 17, no. 5, pp. 439–451, 2007.

[229] P. Mhaskar, A. Gani, C. McFall, P. D. Christofides, and J. F. Davis, "Fault-tolerant control of nonlinear process systems subject to sensor faults," *AIChE Journal*, vol. 53, no. 3, pp. 654–668, 2007.

[230] B. J. Ohran, D. Muñoz de la Peña, P. D. Christofides, and J. F. Davis, "Enhancing data-based fault isolation through nonlinear control," *AIChE Journal*, vol. 54, no. 1, pp. 223–241, 2008.

[231] A. Shamiri, M. A. Hussain, F. S. Mjalli, N. Mostoufi, and S. Hajimolana, "Dynamics and predictive control of gas phase propylene polymerization in fluidized bed reactors," *Chinese Journal of Chemical Engineering*, vol. 21, no. 9, pp. 1015–1029, 2013.

[232] C. Chatzidoukas, J. D. Perkins, E. N. Pistikopoulos, and C. Kiparissides, "Optimal grade transition and selection of closed-loop controllers in a gas-phase olefin polymerization fluidized bed reactor," *Chemical Engineering Science*, vol. 58, no. 16, pp. 3643–3658, 2003.

[233] C. Kiparissides, G. Verros, and J. F. MacGregor, "Mathematical modeling, optimization, and quality control of high-pressure ethylene polymerization reactors," *Journal of Macromolecular Science, Part C: Polymer Reviews*, vol. 33, no. 4, pp. 437–527, 1993.

[234] J. Liu, "On-line soft sensor for polyethylene process with multiple production grades," *Control Engineering Practice*, vol. 15, no. 7, pp. 769–778, 2007.

[235] V. M. Zavala and L. T. Biegler, "Large-scale parameter estimation in low-density polyethylene tubular reactors," *Industrial & Engineering Chemistry Research*, vol. 45, no. 23, pp. 7867–7881, 2006.

[236] C. Kiparissides, G. Verros, A. Pertsinidis, and I. Goossens, "On-line parameter estimation in a high-pressure low-density polyethylene tubular reactor," *AIChE Journal*, vol. 42, no. 2, pp. 440–454, 1996.

[237] H. Jiang, Z. Yan, and X. Liu, "Melt index prediction using optimized least squares support vector machines based on hybrid particle swarm optimization algorithm," *Neurocomputing*, vol. 119, pp. 469–477, 2013.

[238] W. Wang and X. Liu, "Melt index prediction by least squares support vector machines with an adaptive mutation fruit fly optimization algorithm," *Chemometrics and Intelligent Laboratory Systems*, vol. 141, pp. 79–87, 2015.

[239] J. Li and X. Liu, "Melt index prediction by RBF neural network optimized with an MPSO-SA hybrid algorithm," *Neurocomputing*, vol. 74, no. 5, pp. 735–740, 2011.

[240] B. Kou, K. B. McAuley, C. C. Hsu, D. W. Bacon, and K. Z. Yao, "Mathematical model and parameter estimation for gas-phase ethylene homopolymerization with supported metallocene catalyst," *Industrial & Engineering Chemistry Research*, vol. 44, no. 8, pp. 2428–2442, 2005.

[241] C. Ling and C. Kravaris, "State observer design for monitoring the degree of polymerization in a series of melt polycondensation reactors," *Processes*, vol. 4, no. 1, p. 4, 2016.

[242] R. Janssen, H. Ruysschaert, and R. Vroom, "The determination of the diethylene glycol incorporated in poly(ethylene terephthalate)," *Die Makromolekulare Chemie: Macromolecular Chemistry and Physics*, vol. 77, no. 1, pp. 153–158, 1964.

[243] J.-M. Besnoin and K. Y. Choi, "Identification and characterization of reaction byproducts in the polymerization of polyethylene terephthalate," *Journal of Macromolecular Science. Reviews in Macromolecular Chemistry and Physics*, vol. 29, no. 1, pp. 55–81, 1989.

[244] H. Zimmerman and N. T. Kim, "Investigations on thermal and hydrolytic degradation of poly(ethylene terephthalate)," *Polymer Engineering & Science*, vol. 20, no. 10, pp. 680–683, 1980.

[245] T. J. Crowley and K.-Y. Choi, "On-line monitoring and control of a batch polymerization reactor," *Journal of Process Control*, vol. 6, no. 2-3, pp. 119–127, 1996.

[246] S. Tatiraju, M. Soroush, and B. A. Ogunnaike, "Multirate nonlinear state estimation with application to a polymerization reactor," *AIChE Journal*, vol. 45, no. 4, pp. 769–780, 1999.

[247] K.-Y. Choi and A. A. Khan, "Optimal state estimation in the transesterification stage of a continuous polyethylene terephthalate condensation polymerization process," *Chemical Engineering Science*, vol. 43, no. 4, pp. 749–762, 1988.

[248] P. Appelhaus and S. Engell, "Design and implementation of an extended observer for the polymerization of polyethylenterephthalate," *Chemical Engineering Science*, vol. 51, no. 10, pp. 1919–1926, 1996.

[249] T. Yamada, Y. Imamura, O. Makimura, and H. Kamatani, "A mathematical model for computer simulation of the direct continuous esterification process between terephthalic acid and ethylene glycol. part II: Reaction rate constants," *Polymer Engineering & Science*, vol. 26, no. 10, pp. 708–716, 1986.

[250] I. Karafyllis and C. Kravaris, "From continuous-time design to sampled-data design of observers," *IEEE Transactions on Automatic Control*, vol. 54, no. 9, pp. 2169–2174, 2009.

[251] N. Kazantzis, *Lie and Lyapunov Methods in the Analysis and Synthesis of Nonlinear Process Control Systems*. PhD thesis, University of Michigan, Ann Arbor, MI, USA, 1997.

[252] C. D. de Gooijer, W. A. M. Bakker, H. H. Beeftink, and J. Tramper, "Bioreactors in series: An overview of design procedures and practical applications," *Enzyme and Microbial Technology*, vol. 18, no. 3, pp. 202–219, 1996.

[253] K. Boe and I. Angelidaki, "Serial CSTR digester configuration for improving biogas production from manure," *Water Research*, vol. 43, no. 1, pp. 166–172, 2009.

[254] D. Thoenes, *Chemical Reactor Development: From Laboratory Synthesis to Industrial Production*. Dordrecht, The Netherlands: Kluwer Academic Publishers, 1994.

[255] L. Cao and H. Yue, "Modelling and control of molecular weight distribution for a polycondensation process," in *Proceedings of the 2004 IEEE International Symposium on Intelligent Control*, pp. 137–142, IEEE, 2004.

[256] Y. Kim, "Two phase mass transfer model for the semibatch melt polymerization process of polycarbonate," *Korean Journal of Chemical Engineering*, vol. 15, no. 6, pp. 671–677, 1998.

[257] T. E. Daubert and R. P. Danner, *Physical and Thermodynamic Properties of Pure Chemicals: Data Compilation*. New York, NY, USA: Hemisphere Publishing Corporation, 1989.

[258] K. Ravindranath and R. A. Mashelkar, "Finishing stages of PET synthesis: a comprehensive model," *AIChE Journal*, vol. 30, no. 3, pp. 415–422, 1984.

[259] I. S. Kim, B. G. Woo, K. Y. Choi, and C. Kiang, "Two-phase model for continuous final-stage melt polycondensation of poly(ethylene terephthalate). III. Modeling of multiple reactors with multiple reaction zones," *Journal of Applied Polymer Science*, vol. 90, no. 4, pp. 1088–1095, 2003.

[260] V. Bhaskar, S. K. Gupta, and A. K. Ray, "Modeling of an industrial wiped film poly(ethylene terephthalate) reactor," *Polymer Reaction Engineering*, vol. 9, no. 2, pp. 71–99, 2001.

[261] H. A. Pohl, "Determination of carboxyl end groups in a polyester, polyethylene terephthalate," *Analytical Chemistry*, vol. 26, no. 10, pp. 1614–1616, 1954.

[262] C. Kravaris, J. Hahn, and Y. Chu, "Advances and selected recent developments in state and parameter estimation," *Computers & Chemical Engineering*, vol. 51, pp. 111–123, 2013.

[263] J. M. Ali, N. H. Hoang, M. A. Hussain, and D. Dochain, "Review and classification of recent observers applied in chemical process systems," *Computers & Chemical Engineering*, vol. 76, pp. 27–41, 2015.

[264] H. Michalska and D. Q. Mayne, "Moving horizon observers and observer-based control," *IEEE Transactions on Automatic Control*, vol. 40, no. 6, pp. 995–1006, 1995.

[265] M. F. Ellis, T. W. Taylor, V. Gonzalez, and K. F. Jensen, "Estimation of the molecular weight distribution in batch polymerization," *AIChE Journal*, vol. 34, no. 8, pp. 1341–1353, 1988.

[266] R. D. Gudi, S. L. Shah, and M. R. Gray, "Adaptive multirate state and parameter estimation strategies with application to a bioreactor," *AIChE Journal*, vol. 41, no. 11, pp. 2451–2464, 1995.

[267] R. K. Mutha, W. R. Cluett, and A. Penlidis, "A new multirate-measurement-based estimator: Emulsion copolymerization batch reactor case study," *Industrial & Engineering Chemistry Research*, vol. 36, no. 4, pp. 1036–1047, 1997.

[268] N. Zambare, M. Soroush, and M. C. Grady, "Real-time multirate state estimation in a pilot-scale polymerization reactor," *AIChE Journal*, vol. 48, no. 5, pp. 1022–1033, 2002.

[269] R. López-Negrete and L. T. Biegler, "A Moving Horizon Estimator for processes with multi-rate measurements: A Nonlinear Programming sensitivity approach," *Journal of Process Control*, vol. 22, no. 4, pp. 677–688, 2012.

[270] S. Krämer and R. Gesthuisen, "Multirate state estimation using moving horizon estimation," in *Proceedings of the 16th IFAC World Conference*, pp. 1–6, IFAC, 2005.

[271] S. Krämer, R. Gesthuisen, and S. Engell, "Fixed structure multirate state estimation," in *Proceedings of the American Control Conference*, pp. 4613–4618, IEEE, 2005.

[272] A. Liu, W. Zhang, L. Yu, and J. Chen, "Moving horizon estimation for multi-rate systems," in *Proceedings of the 54th IEEE Conference on Decision and Control*, pp. 6850–6855, IEEE, 2015.

[273] M. Nadri and H. Hammouri, "Design of a continuous-discrete observer for state affine systems," *Applied Mathematics Letters*, vol. 16, no. 6, pp. 967–974, 2003.

[274] M. Nadri, H. Hammouri, and C. Astorga, "Observer design for continuous-discrete time state affine systems up to output injection," *European Journal of Control*, vol. 10, no. 3, pp. 252–263, 2004.

[275] H. Hammouri, M. Nadri, and R. Mota, "Constant gain observer for continuous-discrete time uniformly observable systems," in *Proceedings of the 45th IEEE Conference on Decision and Control*, pp. 5406–5411, IEEE, 2006.

[276] M. Nadri, H. Hammouri, and R. M. Grajales, "Observer design for uniformly observable systems with sampled measurements," *IEEE Transactions on Automatic Control*, vol. 58, no. 3, pp. 757–762, 2013.

[277] T. Raff, M. Kögel, and F. Allgöwer, "Observer with sample-and-hold updating for Lipschitz nonlinear systems with nonuniformly sampled measurements," in *Proceedings of the American Control Conference*, pp. 5254–5257, IEEE, 2008.

[278] F. Ferrante, F. Gouaisbaut, R. G. Sanfelice, and S. Tarbouriech, "A hybrid observer with a continuous intersample injection in the presence of sporadic measurements," in *Proceedings of the 54th IEEE Conference on Decision and Control*, pp. 5654–5659, IEEE, 2015.

[279] T. Ahmed-Ali, I. Karafyllis, and F. Lamnabhi-Lagarrigue, "Global exponential sampled-data observers for nonlinear systems with delayed measurements," *Systems & Control Letters*, vol. 62, no. 7, pp. 539–549, 2013.

[280] M. Moarref and L. Rodrigues, "Observer design for linear multi-rate sampled-data systems," in *Proceedings of the American Control Conference*, pp. 5319–5324, IEEE, 2014.

[281] G. C. Walsh, H. Ye, and L. G. Bushnell, "Stability analysis of networked control systems," *IEEE Transactions on Control Systems Technology*, vol. 10, no. 3, pp. 438–446, 2002.

[282] H. K. Khalil, *Nonlinear Systems*. Upper Saddle River, NJ, USA: Prentice Hall, 2002.

[283] T. Raff and F. Allgöwer, "Observers with impulsive dynamical behavior for linear and nonlinear continuous-time systems," in *Proceedings of the 46th IEEE Conference on Decision and Control*, pp. 4287–4292, IEEE, 2007.

[284] T. H. Gronwall, "Note on the derivatives with respect to a parameter of the solutions of a system of differential equations," *Annals of Mathematics*, vol. 20, pp. 292–296, 1919.

[285] R. Bellman, "The stability of solutions of linear differential equations," *Duke Mathematical Journal*, vol. 10, no. 4, pp. 643–647, 1943.

[286] K. B. McAuley, *Modelling, Estimation and Control of Product Properties in a Gas Phase Polyethylene Reactor*. PhD thesis, McMaster University, Hamilton, Ontario, Canada, 1991.

[287] C. Ling and C. Kravaris, "A dead time compensation approach for multirate observer design with large measurement delays," *AIChE Journal*, vol. 65, no. 2, pp. 562–570, 2019.

[288] A. Germani, C. Manes, and P. Pepe, "A new approach to state observation of nonlinear systems with delayed output," *IEEE Transactions on Automatic Control*, vol. 47, no. 1, pp. 96–101, 2002.

[289] N. Kazantzis and R. A. Wright, "Nonlinear observer design in the presence of delayed output measurements," *Systems & Control Letters*, vol. 54, no. 9, pp. 877–886, 2005.

[290] T. Ahmed-Ali, E. Cherrier, and F. Lamnabhi-Lagarrigue, "Cascade high gain predictors for a class of nonlinear systems," *IEEE Transactions on Automatic Control*, vol. 57, no. 1, pp. 224–229, 2012.

[291] M. Farza, M. M'Saad, T. Ménard, M. L. Fall, O. Gehan, and E. Pigeon, "Simple cascade observer for a class of nonlinear systems with long output delays," *IEEE Transactions on Automatic Control*, vol. 60, no. 12, pp. 3338–3343, 2015.

[292] K. Subbarao and P. C. Muralidhar, "A state observer for LTI systems with delayed outputs: Time-varying delay," in *Proceedings of the American Control Conference*, pp. 3029–3033, IEEE, 2008.

[293] F. Cacace, A. Germani, and C. Manes, "An observer for a class of nonlinear systems with time varying observation delay," *Systems & Control Letters*, vol. 59, no. 5, pp. 305–312, 2010.

[294] M. Kahelras, T. Ahmed-Ali, F. Giri, and F. Lamnabhi-Lagarrigue, "Sampled-data chain-observer design for a class of delayed nonlinear systems," *International Journal of Control*, vol. 91, no. 5, pp. 1076–1090, 2018.

[295] T. Ahmed-Ali, V. Van Assche, J.-F. Massieu, and P. Dorléans, "Continuous-discrete observer for state affine systems with sampled and delayed measurements," *IEEE Transactions on Automatic Control*, vol. 58, no. 4, pp. 1085–1091, 2013.

[296] N. Zambare, M. Soroush, and B. A. Ogunnaike, "A method of robust multi-rate state estimation," *Journal of Process Control*, vol. 13, no. 4, pp. 337–355, 2003.

[297] A. Gopalakrishnan, N. S. Kaisare, and S. Narasimhan, "Incorporating delayed and infrequent measurements in Extended Kalman Filter based nonlinear state estimation," *Journal of Process Control*, vol. 21, no. 1, pp. 119–129, 2011.

[298] A. Fatehi and B. Huang, "Kalman filtering approach to multi-rate information fusion in the presence of irregular sampling rate and variable measurement delay," *Journal of Process Control*, vol. 53, pp. 15–25, 2017.

[299] C. Antoniades and P. D. Christofides, "Feedback control of nonlinear differential difference equation systems," *Chemical Engineering Science*, vol. 54, no. 23, pp. 5677–5709, 1999.

[300] J. Liu, D. Muñoz de la Peña, P. D. Christofides, and J. F. Davis, "Lyapunov-based model predictive control of nonlinear systems subject to time-varying measurement delays," *International Journal of Adaptive Control and Signal Processing*, vol. 23, no. 8, pp. 788–807, 2009.

[301] J. Liu, D. Muñoz de la Peña, and P. D. Christofides, "Distributed model predictive control of nonlinear systems subject to asynchronous and delayed measurements," *Automatica*, vol. 46, no. 1, pp. 52–61, 2010.

[302] J. Liu, X. Chen, D. Muñoz de la Peña, and P. D. Christofides, "Iterative distributed model predictive control of nonlinear systems: Handling asynchronous, delayed measurements," *IEEE Transactions on Automatic Control*, vol. 57, no. 2, pp. 528–534, 2012.

[303] M. Ellis and P. D. Christofides, "Economic model predictive control of nonlinear time-delay systems: Closed-loop stability and delay compensation," *AIChE Journal*, vol. 61, no. 12, pp. 4152–4165, 2015.

[304] I. Karafyllis and Z.-P. Jiang, "A vector small-gain theorem for general non-linear control systems," *IMA Journal of Mathematical Control and Information*, vol. 28, no. 3, pp. 309–344, 2011.

[305] O. J. M. Smith, "Closer control of loops with time delays," *Chemical Engineering Progress*, vol. 53, pp. 216–219, 1957.

[306] M. Krstic, "Lyapunov stability of linear predictor feedback for time-varying input delay," *IEEE Transactions on Automatic Control*, vol. 55, no. 2, pp. 554–559, 2010.

[307] A. Echevarría, J. R. Leiza, J. C. de la Cal, and J. M. Asua, "Molecular-weight distribution control in emulsion polymerization," *AIChE Journal*, vol. 44, no. 7, pp. 1667–1679, 1998.

[308] D. S. Bernstein and W. So, "Some explicit formulas for the matrix exponential," *IEEE Transactions on Automatic Control*, vol. 38, no. 8, pp. 1228–1232, 1993.

[309] C. Ling and C. Kravaris, "Multi-rate sampled-data observers based on a continuous-time design," in *Proceedings of the 56th IEEE Conference on Decision and Control*, pp. 3664–3669, IEEE, 2017.

[310] T. Ahmed-Ali, R. Postoyan, and F. Lamnabhi-Lagarrigue, "Continuous-discrete adaptive observers for state affine systems," *Automatica*, vol. 45, no. 12, pp. 2986–2990, 2009.

[311] M. Farza, M. M'Saad, M. L. Fall, E. Pigeon, O. Gehan, and K. Busawon, "Continuous-discrete time observers for a class of MIMO nonlinear systems," *IEEE Transactions on Automatic Control*, vol. 59, no. 4, pp. 1060–1065, 2014.

[312] M. Farza, I. Bouraoui, T. Ménard, R. B. Abdennour, and M. M'Saad, "Adaptive observers for a class of uniformly observable systems with nonlinear parametrization and sampled outputs," *Automatica*, vol. 50, no. 11, pp. 2951–2960, 2014.

[313] V. Andrieu, M. Nadri, U. Serres, and J.-C. Vivalda, "Self-triggered continuous-discrete observer with updated sampling period," *Automatica*, vol. 62, pp. 106–113, 2015.

[314] T. N. Dinh, V. Andrieu, M. Nadri, and U. Serres, "Continuous-discrete time observer design for Lipschitz systems with sampled measurements," *IEEE Transactions on Automatic Control*, vol. 60, no. 3, pp. 787–792, 2015.

[315] H. Beikzadeh and H. J. Marquez, "Multirate observers for nonlinear sampled-data systems using input-to-state stability and discrete-time approximation," *IEEE Transactions on Automatic Control*, vol. 59, no. 9, pp. 2469–2474, 2014.

[316] H. Beikzadeh and H. J. Marquez, "Sampled-data observer for one-sided Lipschitz systems: Single-rate and multirate cases," in *Proceedings of the American Control Conference*, pp. 3386–3391, IEEE, 2015.

[317] Y. Shen, D. Zhang, and X. Xia, "Continuous observer design for a class of multi-output nonlinear systems with multi-rate sampled and delayed output measurements," *Automatica*, vol. 75, pp. 127–132, 2017.

[318] E. D. Sontag and Y. Wang, "Notions of input to output stability," *Systems & Control Letters*, vol. 38, no. 4-5, pp. 235–248, 1999.

[319] I. Karafyllis, "A system-theoretic framework for a wide class of systems I: Applications to numerical analysis," *Journal of Mathematical Analysis and Applications*, vol. 328, no. 2, pp. 876–899, 2007.

[320] I. Karafyllis, "A system-theoretic framework for a wide class of systems II: Input-to-output stability," *Journal of Mathematical Analysis and Applications*, vol. 328, no. 1, pp. 466–486, 2007.

[321] I. Karafyllis and Z.-P. Jiang, "A small-gain theorem for a wide class of feedback systems with control applications," *SIAM Journal on Control and Optimization*, vol. 46, no. 4, pp. 1483–1517, 2007.

[322] L. Hong, "Multiresolutional filtering using wavelet transform," *IEEE Transactions on Aerospace and Electronic Systems*, vol. 29, no. 4, pp. 1244–1251, 1993.

[323] L. Hong and T. Scaggs, "Real-time optimal multiresolutional sensor/data fusion," in *Proceedings of IEEE International Conference on Robotics and Automation*, pp. 117–122, IEEE, 1993.

[324] L. Hong, "Multiresolutional distributed filtering," *IEEE Transactions on Automatic Control*, vol. 39, no. 4, pp. 853–856, 1994.

[325] L. Yan, B. Liu, and D. Zhou, "Asynchronous multirate multisensor information fusion algorithm," *IEEE Transactions on Aerospace and Electronic Systems*, vol. 43, no. 3, pp. 1135–1146, 2007.

[326] J. Ma, H. Lin, and S. Sun, "Distributed fusion filter for asynchronous multi-rate multi-sensor non-uniform sampling systems," in *Proceedings of the 15th International Conference on Information Fusion*, pp. 1645–1652, IEEE, 2012.

[327] A. T. Alouani, J. E. Gray, and D. H. McCabe, "Theory of distributed estimation using multiple asynchronous sensors," *IEEE Transactions on Aerospace and Electronic Systems*, vol. 41, no. 2, pp. 717–722, 2005.

[328] Y. Hu, Z. Duan, and D. Zhou, "Estimation fusion with general asynchronous multi-rate sensors," *IEEE Transactions on Aerospace and Electronic Systems*, vol. 46, no. 4, pp. 2090–2102, 2010.

[329] W.-A. Zhang, S. Liu, and L. Yu, "Fusion estimation for sensor networks with nonuniform estimation rates," *IEEE Transactions on Circuits and Systems I: Regular Papers*, vol. 61, no. 5, pp. 1485–1498, 2014.

[330] H. Lin and S. Sun, "Distributed fusion estimator for multisensor multirate systems with correlated noises," *IEEE Transactions on Systems, Man, and Cybernetics: Systems*, vol. 48, no. 7, pp. 1131–1139, 2018.

[331] D. Angeli and E. D. Sontag, "Forward completeness, unboundedness observability, and their Lyapunov characterizations," *Systems & Control Letters*, vol. 38, no. 4-5, pp. 209–217, 1999.

[332] S. N. Dashkovskiy, B. S. Rüffer, and F. R. Wirth, "An ISS small gain theorem for general networks," *Mathematics of Control, Signals, and Systems*, vol. 19, no. 2, pp. 93–122, 2007.

[333] S. N. Dashkovskiy, B. S. Rüffer, and F. R. Wirth, "Small gain theorems for large scale systems and construction of ISS Lyapunov functions," *SIAM Journal on Control and Optimization*, vol. 48, no. 6, pp. 4089–4118, 2010.

[334] Z.-P. Jiang and Y. Wang, "A generalization of the nonlinear small-gain theorem for large-scale complex systems," in *Proceedings of the 7th World Congress on Intelligent Control and Automation*, pp. 1188–1193, IEEE, 2008.

[335] T. Liu, D. J. Hill, and Z.-P. Jiang, "Lyapunov formulation of ISS cyclic-small-gain in continuous-time dynamical networks," *Automatica*, vol. 47, no. 9, pp. 2088–2093, 2011.

[336] N. Kazantzis, C. Kravaris, C. Tseronis, and R. A. Wright, "Optimal controller tuning for nonlinear processes," *Automatica*, vol. 41, no. 1, pp. 79–86, 2005.